



HAL
open science

Role of the clathrin adaptor AP-1 in the virulence and the biogenesis process of secretory vesicles in the plant-pathogenic fungus *Botrytis cinerea*

Glen Calvar

► **To cite this version:**

Glen Calvar. Role of the clathrin adaptor AP-1 in the virulence and the biogenesis process of secretory vesicles in the plant-pathogenic fungus *Botrytis cinerea*. Microbiology and Parasitology. INSA de Lyon, 2022. English. NNT : 2022ISAL0113 . tel-04142230

HAL Id: tel-04142230

<https://theses.hal.science/tel-04142230v1>

Submitted on 26 Jun 2023

HAL is a multi-disciplinary open access archive for the deposit and dissemination of scientific research documents, whether they are published or not. The documents may come from teaching and research institutions in France or abroad, or from public or private research centers.

L'archive ouverte pluridisciplinaire **HAL**, est destinée au dépôt et à la diffusion de documents scientifiques de niveau recherche, publiés ou non, émanant des établissements d'enseignement et de recherche français ou étrangers, des laboratoires publics ou privés.



N°d'ordre NNT : 2022ISAL0113

**THESE de DOCTORAT DE L'INSA LYON,
membre de l'Université de Lyon**

**Ecole Doctorale N° 341
Evolution, Ecosystèmes, Microbiologie, Modélisation**

Spécialité/ discipline de doctorat : Microbiologie

Soutenue publiquement le 14/12/2022, par :

Glen Calvar

**Role of the clathrin adaptor AP-1 in the virulence and
the biogenesis process of secretory vesicles in the
plant-pathogenic fungus *Botrytis cinerea***

Devant le jury composé de :

Godiard Laurence	Chargé de Recherche HDR	INRAe	Rapporteure
Hahn Matthias	Professeur des Universités	TUK	Rapporteur
Le Borgne Roland	Directeur de Recherche	CNRS	Rapporteur
Zaidman-Rémy Anna	Maître de Conférences HDR	INSA Lyon	Examinatrice
Poussereau Nathalie	Maître de Conférences HDR	UCBL1	Directrice de thèse
Rahbé Yvan	Directeur de Recherche	INRAe	Co-directeur de thèse

Département FEDORA – INSA Lyon - Ecoles Doctorales

SIGLE	ECOLE DOCTORALE	NOM ET COORDONNEES DU RESPONSABLE
CHIMIE	<u>CHIMIE DE LYON</u> https://www.edchimie-lyon.fr Sec. : Renée EL MELHEM Bât. Blaise PASCAL, 3e étage secretariat@edchimie-lyon.fr	M. Stéphane DANIELE C2P2-CPE LYON-UMR 5265 Bâtiment F308, BP 2077 43 Boulevard du 11 novembre 1918 69616 Villeurbanne directeur@edchimie-lyon.fr
E.E.A.	<u>ÉLECTRONIQUE, ÉLECTROTECHNIQUE, AUTOMATIQUE</u> https://edeea.universite-lyon.fr Sec. : Stéphanie CAUVIN Bâtiment Direction INSA Lyon Tél : 04.72.43.71.70 secretariat.edeea@insa-lyon.fr	M. Philippe DELACHARTRE INSA LYON Laboratoire CREATIS Bâtiment Blaise Pascal, 7 avenue Jean Capelle 69621 Villeurbanne CEDEX Tél : 04.72.43.88.63 philippe.delachartre@insa-lyon.fr
E2M2	<u>ÉVOLUTION, ÉCOSYSTÈME, MICROBIOLOGIE, MODÉLISATION</u> http://e2m2.universite-lyon.fr Sec. : Bénédicte LANZA Bât. Atrium, UCB Lyon 1 Tél : 04.72.44.83.62 secretariat.e2m2@univ-lyon1.fr	Mme Sandrine CHARLES Université Claude Bernard Lyon 1 UFR Biosciences Bâtiment Mendel 43, boulevard du 11 Novembre 1918 69622 Villeurbanne CEDEX sandrine.charles@univ-lyon1.fr
EDISS	<u>INTERDISCIPLINAIRE SCIENCES-SANTÉ</u> http://ediss.universite-lyon.fr Sec. : Bénédicte LANZA Bât. Atrium, UCB Lyon 1 Tél : 04.72.44.83.62 secretariat.ediss@univ-lyon1.fr	Mme Sylvie RICARD-BLUM Institut de Chimie et Biochimie Moléculaires et Supramoléculaires (ICBMS) - UMR 5246 CNRS - Université Lyon 1 Bâtiment Raulin - 2ème étage Nord 43 Boulevard du 11 novembre 1918 69622 Villeurbanne Cedex Tél : +33(0)4 72 44 82 32 sylvie.ricard-blum@univ-lyon1.fr
INFOMATHS	<u>INFORMATIQUE ET MATHÉMATIQUES</u> http://edinfomaths.universite-lyon.fr Sec. : Renée EL MELHEM Bât. Blaise PASCAL, 3e étage Tél : 04.72.43.80.46 infomaths@univ-lyon1.fr	M. Hamamache KHEDDOUCI Université Claude Bernard Lyon 1 Bât. Nautibus 43, Boulevard du 11 novembre 1918 69 622 Villeurbanne Cedex France Tél : 04.72.44.83.69 hamamache.kheddouci@univ-lyon1.fr
Matériaux	<u>MATÉRIAUX DE LYON</u> http://ed34.universite-lyon.fr Sec. : Yann DE ORDENANA Tél : 04.72.18.62.44 yann.de-ordenana@ec-lyon.fr	M. Stéphane BENAYOUN Ecole Centrale de Lyon Laboratoire LTDS 36 avenue Guy de Collongue 69134 Ecully CEDEX Tél : 04.72.18.64.37 stephane.benayoun@ec-lyon.fr
MEGA	<u>MÉCANIQUE, ÉNERGÉTIQUE, GÉNIE CIVIL, ACOUSTIQUE</u> http://edmega.universite-lyon.fr Sec. : Stéphanie CAUVIN Tél : 04.72.43.71.70 Bâtiment Direction INSA Lyon mega@insa-lyon.fr	M. Jocelyn BONJOUR INSA Lyon Laboratoire CETHIL Bâtiment Sadi-Carnot 9, rue de la Physique 69621 Villeurbanne CEDEX jocelyn.bonjour@insa-lyon.fr
ScSo	<u>ScSo*</u> https://edsciencesociales.universite-lyon.fr Sec. : Mélina FAVETON INSA : J.Y. TOUSSAINT Tél : 04.78.69.77.79 melina.faveton@univ-lyon2.fr	M. Bruno MILLY Université Lumière Lyon 2 86 Rue Pasteur 69365 Lyon CEDEX 07 bruno.milly@univ-lyon2.fr

*ScSo : Histoire, Géographie, Aménagement, Urbanisme, Archéologie, Science politique, Sociologie, Anthropologie

Acknowledgements / Remerciements

J'exprime ma gratitude envers les membres du jury de thèse Laurence Godiard, Matthias Hahn, Roland Le Borgne et Anna Zaidman-Rémy pour avoir accepté d'évaluer le travail effectué lors de cette thèse. Je tiens aussi à remercier Nathalie Poussereau, Yvan Rahbé et Christophe Bruel pour m'avoir fait confiance et pour leur participation au projet de thèse.

Je remercie particulièrement Nathalie, pour son soutien, ses conseils avisés et sa disponibilité tout au long de ces trois années.

Je remercie également Sylvie Reverchon et Yvan Rahbé sans qui je n'aurais pas pu faire cette thèse.

Je tiens aussi à remercier chaleureusement Amélie de Vallée et Christine Rasclé pour leur soutien technique, et leurs efforts pour le maintien d'une vie de laboratoire saine. Merci aussi à Mathias Choquer et Christophe Bruel pour leurs échanges scientifiques et leurs recommandations.

Je remercie également Bastien Malbert pour son aide sur la co-immunoprécipitation et François-Xavier Gillet pour avoir permis la collaboration avec la plateforme de microscopie électronique de Grenoble.

Je remercie aussi les doctorants du laboratoire Mélanie Crumière, Matthieu Blandenet et Adrien Hamandjian. Un grand merci à vous pour nos discussions scientifiques existentielles et personnelles. Adrien, j'ai adoré travailler avec toi ces deux années. Tes conseils et réponses à mes innombrables questions m'ont été d'une aide précieuse. Tu resteras une personne modèle pour moi.

Enfin, je remercie ma famille et mes amis pour m'avoir soutenu durant ces trois années. Je tiens particulièrement à remercier Romain pour m'avoir encouragé et supporté dans les moments de doutes. Je n'y serais pas arrivé sans toi.

Résumé

Les champignons phytopathogènes représentent une menace croissante pour la sécurité alimentaire mondiale qui est amplifiée par le dérèglement climatique. La compréhension des mécanismes de pathogénie est donc essentielle à la limitation du développement de maladies fongiques des plantes. La virulence de ces champignons repose en grande partie sur la sécrétion de diverses protéines capables de dégrader les constituants de la plante-hôte. Avant d'être libérées dans le milieu extracellulaire, ces protéines transitent par le réticulum endoplasmique, l'appareil de Golgi et parfois l'endosome, et sont transportées d'un compartiment cellulaire à l'autre à l'intérieur de vésicules intracellulaires. Aujourd'hui, les mécanismes de sécrétion, et plus particulièrement de la biogénèse de ces vésicules sont très peu connus chez les champignons, alors qu'ils sont essentiels à la compréhension du processus de pathogénie. Pour mieux comprendre ces mécanismes, nous avons créé un mutant de sous-expression d'un gène codant pour une sous-unité de l'adaptateur de clathrine AP-1 chez le champignon nécrotrophe *Botrytis cinerea*. Cet adaptateur est connu pour être impliqué dans la biogénèse des granules de sécrétion chez la drosophile et l'humain. La caractérisation du mutant AP-1 a révélé que le complexe était impliqué dans la croissance polarisée, la synthèse de la paroi fongique, et la sécrétion d'enzymes hydrolytiques essentielles à la nutrition et à la virulence du champignon. Afin de mieux comprendre le rôle supposé de cet adaptateur dans la biogénèse de vésicules, nous avons aussi entrepris l'enrichissement de vésicules intracellulaires et proposons une stratégie pour isoler les vésicules de sécrétion. Notre étude montre pour la première fois l'importance de l'adaptateur de clathrine AP-1 dans les mécanismes de sécrétion chez un champignon phytopathogène.

Abstract

Plant pathogenic fungi represent an increasing threat to global food security which is increased by climate change. Understanding the mechanisms of pathogenesis is therefore essential to limit the development of fungal diseases in plants. The virulence of these fungi is largely based on the secretion of various proteins capable of degrading the host plant's constituents. Before being released into the extracellular environment, these proteins pass through the endoplasmic reticulum, the Golgi apparatus and sometimes the endosome, and are transported from one cellular compartment to another in intracellular vesicles. Today, the mechanisms of secretion, and more particularly of the biogenesis of these vesicles, are very little studied in fungi, despite being essential for the comprehension of pathogenesis. To better understand these mechanisms, we have created an under-expression mutant of a gene encoding for a subunit of the clathrin adaptor AP-1 in the necrotrophic fungus *Botrytis cinerea*. This adaptor is involved in the biogenesis of secretory granules in *Drosophila* and humans. Characterization of the AP-1 mutant revealed that the complex was involved in polarized growth, fungal cell-wall synthesis, and the secretion of hydrolytic enzymes essential for fungal nutrition and virulence. To better understand the putative role of this adaptor in vesicle biogenesis, we also undertook the enrichment of intracellular vesicles, and we propose a strategy to isolate secretory vesicles. Our study shows for the first time the importance of the clathrin adaptor AP-1 in secretion mechanisms in a plant pathogenic fungus.

Résumé de thèse détaillé

Les champignons phytopathogènes représentent une menace croissante pour la sécurité alimentaire mondiale qui est amplifiée par le dérèglement climatique^{1,2}. La compréhension des mécanismes de pathogénie est donc essentielle à la limitation du développement de maladies fongiques des plantes. La virulence de ces champignons repose en grande partie sur la sécrétion de diverses protéines capables de dégrader les constituants de la plante-hôte³. Avant d'être libérées dans le milieu extracellulaire, ces protéines transitent par le réticulum endoplasmique, l'appareil de Golgi et parfois l'endosome, et sont transportées d'un compartiment cellulaire à l'autre à l'intérieur de vésicules intracellulaires. Chez de nombreux champignons filamenteux, les vésicules de sécrétion s'accumulent à l'apex de l'hyphes fongique et forment le Spitzenkörper avant de libérer leur contenu par exocytose⁴. Le Spitzenkörper est une structure organisée qui regroupe des vésicules de différentes tailles ; les micro-vésicules (30-50 nm) et les macro-vésicules (100-150 nm). Aujourd'hui, les mécanismes de sécrétion et les mécanismes de biogénèse de ces vésicules sont très peu connus chez les champignons, alors qu'ils sont essentiels à la compréhension du processus de pathogénie.

Au laboratoire, de précédents travaux ont été portés sur rôle la clathrine dans la biologie du champignon phytopathogène nécrotrophe *Botrytis cinerea*. Chez de nombreux organismes eucaryotes, la clathrine est connue pour être impliquée dans la biogénèse de vésicules de l'endocytose et de l'exocytose⁵. Or, l'étude de cette protéine chez *B. cinerea* a révélé que la clathrine était peu impliquée dans le processus d'endocytose⁶. Au contraire, chez ce champignon, la clathrine est importante à la délivrance de facteurs de virulence sécrétés dans le milieu extracellulaire⁶, ce qui nous a conduit à supposer que la clathrine serait impliquée dans la biogénèse de vésicules de sécrétion chez *B. cinerea*. Cette hypothèse est consolidée par des découvertes faites chez d'autres organismes. En effet, la clathrine est impliquée dans la biogénèse de vésicules de sécrétion chez la levure *Saccharomyces cerevisiae*⁷. Chez la drosophile *Drosophila melanogaster* et les cellules cancéreuses de souris AtT20, la clathrine participe à la formation de granules de sécrétion^{8,9}. Un autre complexe protéique, en interaction avec la clathrine, est impliquée dans la biogénèse de vésicules. Il s'agit de l'adaptateur de clathrine AP-1, localisé à l'appareil de Golgi et à l'endosome, qui est formé de quatre sous-unités : σ , μ , β et γ . Les sous-unités σ , μ sélectionnent des protéines transmembranaires de manière spécifique via la reconnaissance de motifs présents dans les régions cytosoliques de protéines transmembranaires. La sous-unité β , elle, est impliquée dans le recrutement de la

clathrine¹⁰. Pour mieux comprendre le rôle de la machinerie AP-1/Clathrine dans la biogénèse des vésicules intracellulaires chez *B. cinerea*, nous avons créé un mutant de sous-expression d'un gène (*bcap1b*) codant pour la sous-unité β de l'adaptateur de clathrine AP-1. Nous avons envisagé de produire un mutant de délétion du gène *bcap1b*, mais aucune souche homocaryotique n'a pu être obtenue. Ceci est probablement dû au caractère essentiel du gène, comme constaté chez le champignon filamenteux *Aspergillus nidulans*¹¹. La caractérisation du mutant de sous-expression de AP-1 a révélé que le complexe était impliqué dans la croissance polarisée et la synthèse de la paroi fongique. Le défaut de paroi, et plus particulièrement, la diminution du contenu en chitine pourrait s'expliquer par une perturbation du trafic des chitines synthèses chez le mutant AP-1. En effet, la chitine synthase de classe III BcCHSIIIa est mal-localisée chez le mutant AP-1 où elle se retrouve accumulée dans des puncta dans les régions sub-apicales, alors qu'elle est normalement localisée à l'apex de l'hyphe fongique, au niveau du Spitzenkörper. En plus du défaut de croissance et de paroi, le mutant AP-1 semble être impliqué dans les mécanismes de stratégies d'infection nécrotrophe employée par *B. cinerea*. En effet, le mutant AP-1 ne peut pas produire de structures de pénétration comme le coussin d'infection, est entravé dans le processus d'acidification du milieu extracellulaire, et est sévèrement impacté dans la capacité à sécréter des enzymes hydrolytiques essentielles à la nutrition et à la virulence du champignon. L'ensemble de ces phénotypes pourrait expliquer le défaut de virulence observé chez ce mutant. Au cours de cette thèse, nous avons démontré que AP-1 était un élément clé de la virulence chez le champignon nécrotrophe *B. cinerea*. Cette étude est donc la première à démontrer que AP-1 est important pour la virulence de champignons phytopathogènes. De plus, le fait que AP-1 est impliqué dans le processus de pathogénie des parasites eucaryotes humains comme *Toxoplasma gondii*¹², *Trypanosoma cruzi*¹³ et *Leishmania maculans*¹⁴, pourrait suggérer que AP-1 est un élément de virulence important pour un grand nombre d'organismes eucaryotes pathogènes.

Puisque AP-1 est connu pour être impliqué dans la sélection de cargos transmembranaires, nous avons voulu identifier quelles étaient les protéines cargos sélectionnées par AP-1 chez *B. cinerea*. Pour réaliser cette étude préliminaire globale, nous avons utilisé une approche interactomique. Le but était de capturer les protéines interagissant avec la sous-unité μ du complexe AP-1, qui est impliquée dans la sélection des cargos transmembranaires possédant un motif tyrosine Yxx[FILMV] dans leur régions

cytosoliques. Pour cela, nous avons ajouté une étiquette 3xHA à cette sous-unité (BcAPM1) et récupéré les interactants par immunoprécipitation. Ces interactants ont ensuite été identifiés par spectrométrie de masse. L'analyse protéomique a permis de retrouver les éléments du complexe AP-1 et quelques protéines impliquées dans la biogénèse des vésicules de clathrine, cependant la clathrine n'a pas été significativement enrichie dans notre jeu de données. De plus, aucune protéine transmembranaire connue pour interagir avec AP-1 chez d'autres organismes n'a pu être retrouvée. Ceci s'explique probablement par les conditions d'extraction des protéines ou les conditions de lavages qui auraient pu être trop stringentes pour pouvoir récupérer l'intégralité du complexe AP-1 interagissant avec d'autres protéines. Cependant, nous avons, au cours de cette étude préliminaire, identifiés trois protéines sécrétées qui pourraient interagir indirectement avec AP-1 via des récepteurs de cargos solubles. En effet, ces trois protéines sécrétées étaient très sous-accumulées dans le sécrétome du mutant AP-1, ce qui suggère que leur trafic pourrait être AP-1 dépendant. D'autres approches comme le double-hybride, la co-localisation ou encore l'immuno-précipitation par affinité en tandem sont à mettre au point pour approfondir cette première étude préliminaire et identifier les cargos sélectionnés AP-1 chez *B. cinerea*.

Afin de mieux comprendre le rôle supposé de cet adaptateur dans la biogénèse de vésicules, nous avons aussi entrepris l'enrichissement de vésicules intracellulaires par différentes techniques. La première approche visait à enrichir les vésicules intracellulaires par chromatographie taille exclusion. Cependant, des observations en microscopie électronique des échantillons obtenues après passage sur colonne de chromatographie ont révélé qu'aucune vésicule ne pouvait être enrichie dans les conditions utilisées. Nous avons alors exploré une autre approche, basée sur des centrifugations différentielles et gradient de densité pour enrichir les vésicules intracellulaires. Les premiers échantillons obtenus avec cette approche montrent que nous parvenons à enrichir des vésicules intracellulaires de tailles différentes. La caractérisation de la taille, du contenu protéique et du contenu lipidique de ces vésicules sera poursuivie au laboratoire par Adrien Hamandjian. L'objectif sera d'isoler les vésicules chez la souche parentale, le mutant AP-1 et le mutant clathrine afin de comparer les éventuelles différences de contenu et de taille retrouvées dans les vésicules intracellulaires. Associé à un sécrétome comparatif entre ces trois souches, le protéome comparatif des vésicules intracellulaires permettra peut-être d'identifier quelles sont les protéines transportées par des vésicules AP-1/Clathrine. En plus de cela, nous proposons une approche pour l'isolement de vésicules de sécrétion

localisées au Spitzenkörper, qui est basée sur l'enrichissement de vésicules intracellulaires par gradient de densité, couplée à une approche d'immunocapture. Cette approche permettra d'isoler des populations de vésicules de sécrétion spécifiques, avec peu de vésicules intracellulaires contaminantes. Cette méthode pourra aussi être appliquée à la souche parentale, au mutant AP-1 et au mutant clathrine pour mieux comprendre le rôle de la machinerie AP-1/Clathrine dans la biogénèse de vésicules de sécrétion chez *B. cinerea*.

Références

1. Anderson, W., Lane, R. & Korbie, D. Observations of tunable resistive pulse sensing for exosome analysis: improving system sensitivity and stability. *6577–6587* (2015).
2. Shaw, M. W. & Osborne, T. M. Geographic distribution of plant pathogens in response to climate change. *Plant Pathology* **60**, 31–43 (2011).
3. Bradshaw, M. J. et al. Delivering the goods: Fungal secretion modulates virulence during host–pathogen interactions. *Fungal Biology Reviews* **36**, 76–86 (2021).
4. Steinberg, G., Penalva, M., Riquelme, M., Wösten, H. & Harris, S. Cell biology of hyphal growth. *Microbial Spectrum* **5**, 231–265 (2017).
5. Briant, K., Redlingshöfer, L. & Brodsky, F. M. Clathrin's life beyond 40: Connecting biochemistry with physiology and disease. *Current Opinion in Cell Biology* **65**, 141–149 (2020).
6. Souibgui, E. et al. Clathrin Is Important for Virulence Factors Delivery in the Necrotrophic Fungus *Botrytis cinerea*. *Front. Plant Sci.* **12**, 668937 (2021).
7. Gurunathan, S., David, D. & Gerst, J. E. Dynamin and clathrin are required for the biogenesis of a distinct class of secretory vesicles in yeast. *EMBO J* **21**, 602–614 (2002).
8. Burgess, J. et al. AP-1 and clathrin are essential for secretory granule biogenesis in *Drosophila*. 2094–2105 (2011).
9. Bonnemaïson, M. et al. AP-1A Controls Secretory Granule Biogenesis and Trafficking of Membrane Secretory Granule Proteins. *Traffic* **15**, 1099–1121 (2014).
10. Robinson, M. S. Adaptable adaptors for coated vesicles. *Trends in Cell Biology* **14**, 167–174 (2004).
11. Martzoukou, O., Diallinas, G. & Amillis, S. Secretory vesicle polar sorting, endosome recycling and cytoskeleton organisation require the AP-1 complex in *Aspergillus nidulans*. **209**, 1121–1138 (2018).
12. Venugopal, K. et al. Dual role of the *Toxoplasma gondii* clathrin adaptor AP1 in the sorting of rhoptry and microneme proteins and in parasite division. *PLoS Pathog* **13**, e1006331 (2017).
13. Moreira, C. M. do N. et al. Knockout of the gamma subunit of the AP-1 adaptor complex in the human parasite *Trypanosoma cruzi* impairs infectivity and differentiation and prevents the maturation and targeting of the major protease cruzipain. *PLoS ONE* **12**, e0179615 (2017).
14. Vince, J. E. et al. *Leishmania* Adaptor Protein-1 Subunits Are Required for Normal Lysosome Traffic, Flagellum Biogenesis, Lipid Homeostasis, and Adaptation to Temperatures Encountered in the Mammalian Host. *Eukaryotic Cell* **7**, 1256–1267 (2008).

List of Abbreviations

ABA : Acid abscisic

A. nidulans: *Aspergillus nidulans*

AP: Adaptor Protein

Arf: ADP-ribosylation Factor

Arl: ADP-ribosylation Factor Like GTPase

AtMT: *Agrobacterium tumefaciens*-mediated Transformation

AVC: Apical vesicular crescent

BAR: Bin-Amphiphysin-Rys

B. cinerea: *Botrytis cinerea*

BFA: Brefeldin A

BSA: Bovine Serum Albumin

CAZy: Carbohydrate Active enZYmes

CCV: Clathrin-coated vesicle

CDIP: Cell-death-inducing protein

CHC: Clathrin heavy chain

CHS: Chitin synthases

Cle: Clathrin light chain

CME: Clathrin mediated endocytosis

COP: Coat Protein Complex

CPS: Conventional Protein Secretion

CPP: Cerrato-platanin protein

Da: Dalton

D. melanogaster: *Drosophila melanogaster*

DNA: Desoxyribonucleic acid

DnfA: Aminophospholipid flippase A

DnfB: Aminophospholipid flippase B

Dpi: Days post-inoculation

eGFP: enhanced Green Fluorescent Protein

ENTH: Epsin N-terminal Homology

ER: Endoplasmic Reticulum

ERAD: Endoplasmic Reticulum associated degradation

ERV25; Endoplasmic Reticulum vesicle protein 25

EVs: Extracellular Vesicles

FCHo: Fer/Cip4 homology domain only

GDP: Guanosine Di-Phosphate
GGA: Golgi-localized, Gamma ear containing ADP-ribosylation factor binding
GS: Glucan synthase
GTP: Guanosine Tri-Phosphate
HA: Hemagglutinin
HDSV: High density secretory vesicles
HMSV: Hooking Myosin to SVs
HR: Hypersensitive Response
Hsc70: Heat shock cognate 71 kDa protein
Hsp70: Heat Shock Protein 70
IC: Infection cushion
IPCC: Intergovernmental Panel on Climate Change
ISG: Immature secretory granule
KHC: Kinesin Heavy Chain
KLC: Kinesin Light Chain
LDL: Low density lipoprotein
LDSV: Low density secretory vesicles
MMII: minimal medium 2
M6PR: Mannose 6 Phosphate Receptor
mRNA: messenger RNA
MS/MS: mass spectrometry
MVB: Multi-vesicular bodies
N. crassa: Neurospora crassa
NIP: Necrotic Inducing Protein
Nm: Nanometer
NMDA: N-methyl-D-aspartate
OD: Optical density
OSR: Oxidative Stress Response
PAMPs: Pathogen associated molecular patterns
PCR: Polymerase Chain Reaction
PCWDE: Plant Cell Wall Degrading Enzymes
PH: Pleckstrin Homology
PI: Phosphoinositide
PI4P: Phosphatidylinositol 4-phosphate
PM: Plasma Membrane

pNiaD: nitrate reductase promoter
PtInsP: Phosphatidylinositol phosphates
qRT-PCR: quantitative Real-Time Polymerase Chain Reaction
RLK: Receptor-like kinases
RLP: Receptor-like proteins
RNA: Ribonucleic acid
ROS: Reactive Oxygen Species
S. cerevisiae: *Saccharomyces cerevisiae*
SP: Signal peptide
Spk: Spitzenkörper
SNARE: Soluble N-éthylmaleimide sensitive factor Attachment protein REceptor
sRNA: small RNA
SRP: Signal Recognition Particle
SV: Secretory vesicle
T. cruzi: *Trypanosoma cruzi*
T. gondi: *Toxoplasma gondi*
TGN: Trans-Golgi Network
TM: Transmembrane
t-SNARE: target-SNARE
TfR: Transferrin Receptor
UapA: Uric acid/xanthine H⁺ symporter
UPS: Unconventional Protein Secretion
UPR: Unfolded Protein Response
VPS1: Vacuolar Protein Sorting protein 1
VSC: Vesicle Supply Center
v-SNARE: vesicular-SNARE
YPT: Yeast Protein Transport protein

Introduction

1	<i>Plant pathogenic Fungi</i>	20
1.1	Fungi: some characteristics	20
1.2	Fungal pathogenicity, climate change and human activities	20
1.3	<i>Botrytis cinerea: a necrotrophic model</i>	23
1.3.1	Necrotrophy versus biotrophy and hemibiotrophy	23
1.3.2	<i>Botrytis cinerea</i> , a broad host range plant pathogenic fungus.....	23
1.3.3	The infectious cycle	23
1.3.4	Secreted molecules required for host invasion	25
1.3.4.1	ROS production	25
1.3.4.2	Organic acids production	25
1.3.4.3	Phytotoxins production	26
1.3.4.4	Secretion of hydrolytic enzymes.....	26
1.3.4.5	Secretion of effectors	27
2	<i>Fungal secretory vesicles: putative origins and traffic</i>	29
2.1	Two secretory pathways	29
2.1.1	Conventional secretory pathway.....	29
2.1.1.1	Polypeptide translocation in the endoplasmic reticulum	29
2.1.1.2	Unfolded protein response.....	30
2.1.1.3	Endoplasmic-reticulum exit	30
2.1.1.4	The Golgi apparatus in fungi	31
2.1.1.5	Golgi maturation in fungi.....	32
2.1.1.6	Example of proteins undergoing CPS	34
2.1.2	Unconventional secretory pathway.....	36
2.1.2.1	Extracellular vesicles (EVs).....	36
2.1.2.2	Cell-wall synthases	38
2.1.2.3	Protein effectors and hydrolytic enzymes.....	38
2.1.2.4	Transporters in <i>Aspergillus nidulans</i>	39
2.2	Vesicle biogenesis in the conventional secretory pathway	41
2.2.1	Two distinct ways: clathrin-dependent vs clathrin-independent biogenesis of secretory vesicles	41
2.2.2	Clathrin coated vesicles biogenesis.....	42
2.2.2.1	Clathrin structure	42
2.2.2.2	Size of clathrin-coated vesicles.....	43
2.2.2.3	Clathrin localization	44
2.2.2.4	Clathrin-coated vesicles biogenesis.....	44
2.2.2.5	Clathrin-cage uncoating	49
2.3	Secretory vesicles transport	51
2.3.1	Microtubules dependent transport.....	51
2.3.2	Actin dependent transport.....	52
2.4	Exocytosis in fungal hyphae	53
2.4.1	Apex directed exocytosis	53
2.4.1.1	The Spitzenkörper: a conserved fungal structure made of micro- and macro-vesicles	53
2.4.1.2	Stratification of the Spitzenkörper	54
2.4.1.3	Spitzenkörper and cytoskeleton organization	57
2.4.1.4	The vesicle supply center model.....	59
2.4.1.5	Exocytosis	60
2.4.2	Non-apex directed exocytosis.....	63
3	<i>Thesis project</i>	64

Chapter 1 – Role of the clathrin adaptor AP-1 in the biology of *Botrytis cinerea*

Part 1. Secretion of hydrolytic enzymes and delivery of the chitin synthase CHSIIIa depend on the AP-1 clathrin adaptor in the plant-pathogen *Botrytis cinerea*

1	Introduction.....	85
2	Results.....	88
2.1	Construction of a mutant reduced in the expression of <i>Bcap1b</i>	88
2.2	<i>Bcap1b</i> , a gene involved in hyphal elongation	88
2.3	<i>Bcap1b</i> contributes to cell wall integrity maintenance	90
2.4	<i>Bcap1b</i> is involved in differentiation programs.....	92
2.5	<i>Bcap1b</i> is involved in protein secretion.....	94
2.6	<i>Bcap1b</i> is critical for pathogenicity	96
3	Discussion	99
3.1	AP-1 is essential in filamentous fungi	99
3.2	AP-1 is implicated in cell-wall integrity maintenance and the traffic of a chitin synthase	99
3.3	The AP-1 mutant is characterized by hypersecretion and a loss of polarity.....	101
3.4	AP-1 is involved in the conventional secretion of hydrolytic enzymes required for nutrition and virulence.....	101
3.5	AP-1 is a virulence determinant in plant-pathogenic fungi.....	102
3.6	Conclusion.....	103
4	Material and methods.....	104
4.1	Fungal strains and culture conditions	104
4.2	Mutants construction in <i>Botrytis cinerea</i>	104
4.3	RNA extraction and RT-qPCR.....	104
4.4	Growth measurement in non-agitated liquid media in inducible or repressive conditions.....	105
4.5	Transmission Electron Microscopy (TEM)	105
4.6	Determination of susceptibility to osmotic and parietal stresses	106
4.7	Chitin quantification.....	107
4.8	Aniline blue fluorescence quantification.....	107
4.9	General microscopy techniques and image acquisition	107
4.10	Activities of secreted enzymes	108

4.11	Proteomic Analysis	109
4.12	pH measurement	110
4.13	Pathogenicity assays	110
5	References	112
6	Supplementary data	115
6.1	Figures	115
6.2	Appendix S1	121
6.3	Table S1	126
6.4	Table S2	127

Part 2. Preliminary-work: Identification of putative proteins interacting with the clathrin adaptor AP-1

1	Introduction.....	136
2	Results and discussion	137
2.1	Construction of the BcAPM1:3×HA strain and validation of the immunoprecipitation technique.....	137
2.2	Identification of proteins involved in vesicular trafficking potentially interacting with AP-1	137
2.3	Identification of putative AP-1 transmembrane cargos	139
2.4	Identification of putative AP-1 soluble cargos	143
2.5	Limitations of the immunocapture-based method and perspectives ...	143
3	Materials and methods.....	147
3.1	Strains and culture conditions	147
3.2	Molecular biology	147
3.3	Transformation of <i>Botrytis cinerea</i>	147
3.4	Immunoprecipitation.....	147
3.1	SDS-PAGE and western blot	148
3.2	Sample preparation for proteomics.....	148
3.3	Mass spectrometry analysis	148
3.4	Database search and results processing.....	149
3.5	Label-Free Quantitative Data Analysis.....	149
4	References.....	150
5	Supplementary data	153

Chapter 2 - Strategies to isolate fungal secretory vesicles

1	<i>Introduction</i>	189
2	<i>Results</i>	192
2.1	Enrichment of intracellular vesicles by Size-Exclusion Chromatography	192
2.2	Enrichment of intracellular vesicles by density-gradient centrifugation.....	194
2.1	Proposed isolation procedure for the isolation of BcCHSIIIa-GFP SVs	198
3	<i>Discussion</i>	202
3.1	Size exclusion chromatography is not suitable for IVs isolation.....	202
3.2	IVs can be enriched using density-gradient centrifugation	202
3.3	Immuno-isolation is a promising technique for SVs isolation but needs further improvements.....	203
4	<i>Materials and methods</i>	205
4.1	Culture media	205
4.2	Strains and culture conditions.....	205
4.3	Cell fractionation	205
4.4	Size-exclusion chromatography.....	206
4.5	Density gradient.....	206
4.6	SDS-PAGE and western blots	206
4.7	Detection of pectin-hydrolase activity	207
4.8	Transmission electron microscopy.....	207
5	<i>Supplementary data</i>	208
6	<i>References</i>	210
	Discussion and perspectives	212
	Appendix	223

Introduction

Introduction

1	<i>Plant pathogenic Fungi</i>	20
1.1	Fungi: some characteristics	20
1.2	Fungal pathogenicity, climate change and human activities	20
1.3	<i>Botrytis cinerea: a necrotrophic model</i>	23
1.3.1	Necrotrophy versus biotrophy and hemibiotrophy	23
1.3.2	<i>Botrytis cinerea</i> , a broad host range plant pathogenic fungus.....	23
1.3.3	The infectious cycle	23
1.3.4	Secreted molecules required for host invasion.....	25
1.3.4.1	ROS production	25
1.3.4.2	Organic acids production	25
1.3.4.3	Phytotoxins production	26
1.3.4.4	Secretion of hydrolytic enzymes.....	26
1.3.4.5	Secretion of effectors	27
2	<i>Fungal secretory vesicles: putative origins and traffic</i>	29
2.1	Two secretory pathways	29
2.1.1	Conventional secretory pathway.....	29
2.1.1.1	Polypeptide translocation in the endoplasmic reticulum	29
2.1.1.2	Unfolded protein response.....	30
2.1.1.3	Endoplasmic-reticulum exit	30
2.1.1.4	The Golgi apparatus in fungi	31
2.1.1.5	Golgi maturation in fungi.....	32
2.1.1.6	Example of proteins undergoing CPS.....	34
2.1.2	Unconventional secretory pathway.....	36
2.1.2.1	Extracellular vesicles (EVs).....	36
2.1.2.2	Cell-wall synthases	38
2.1.2.3	Protein effectors and hydrolytic enzymes.....	38
2.1.2.4	Transporters in <i>Aspergillus nidulans</i>	39
2.2	Vesicle biogenesis in the conventional secretory pathway	41
2.2.1	Two distinct ways: clathrin-dependent vs clathrin-independent biogenesis of secretory vesicles.....	41
2.2.2	Clathrin coated vesicles biogenesis.....	42
2.2.2.1	Clathrin structure	42
2.2.2.2	Size of clathrin-coated vesicles.....	43
2.2.2.3	Clathrin localization	44
2.2.2.4	Clathrin-coated vesicles biogenesis.....	44
2.2.2.5	Clathrin-cage uncoating	49
2.3	Secretory vesicles transport	51
2.3.1	Microtubules dependent transport.....	51
2.3.2	Actin dependent transport.....	52
2.4	Exocytosis in fungal hyphae	53
2.4.1	Apex directed exocytosis	53
2.4.1.1	The Spitzenkörper: a conserved fungal structure made of micro- and macro-vesicles	53
2.4.1.2	Stratification of the Spitzenkörper	54
2.4.1.3	Spitzenkörper and cytoskeleton organization	57
2.4.1.4	The vesicle supply center model.....	59
2.4.1.5	Exocytosis	60
2.4.2	Non-apex directed exocytosis.....	63
3	<i>Thesis project</i>	64

1 Plant pathogenic Fungi

1.1 Fungi: some characteristics

The fungal kingdom includes a very high diversity of organisms with various ecologies and lifestyles. Some species have developed evolved relationships with plants and animals, ranging from symbiotic relationships to parasitism, including opportunistic behaviors^{1,2}. The number of fungal species is estimated to range between 2.2 and 3.8 million, with 120 000 described species in 2017³.

Fungal cells are characterized by the presence of a cell wall, which protects the organism from environmental stresses like changes in osmolarity or mechanical stresses. The fungal cell wall contains many polysaccharides like chitin, a rigid polymer, and glucans such as 1,3- β -glucan. Fungi are heterotrophic eukaryotes and feed on decaying organic matter. They secrete hydrolytic enzymes to degrade external macromolecules into smaller molecules that can be taken up for nutrition. They can be divided in two groups: unicellular fungi commonly called “yeasts” and multicellular fungi. Multicellular fungi, sometimes called “molds” or “filamentous fungi”, produce hypha that have a tubular-like shape. Fungal hypha branches and constitutes a network of hypha called the mycelium. Some yeasts are referred as dimorphic fungi since they can produce hyphae. *Candida albicans* is a good example of these microorganisms able to change their morphology.

1.2 Fungal pathogenicity, climate change and human activities

Some fungal species pose a global threat to human health, biodiversity, and food security. These threats are becoming increasingly important because of climate change which causes an increase in fungal disease worldwide^{4,5}. Indeed, global warming increases the spread of pathogens and their vectors to new geographical areas⁶.

Over 600 human pathogens have been identified so far, resulting in the death of 1.6 million people each year^{7,8}. *Aspergillus*, *Cryptococcus*, *Candida*, *Pneumocystis*, *Coccidioides* and *Histoplasma* species are responsible for 90% of human deaths due to fungal infections^{7,9,10}. However, there is a growing concern on two relatively new human yeast-pathogens that have spread across continents in recent years: *Candida auris* and *Cryptococcus deuterogatii*. *Candida auris* was first identified in Japan in 2009 and is now found on every continent¹¹. The pathogen is currently under high surveillance because the number of human

infections rises, and the yeast is resistant to many antifungals¹⁰. *Cryptococcus deuterogatti* is another example of a human-yeast pathogen which has spread to new areas in recent years¹². Human activities such as construction, forestry activity, together with climate change are responsible for the spread of the pathogen^{13,14}.

Fungal species threatening biodiversity have also recently emerged because of global warming. The chytridiomycete *Batrachochytrium dendrobatidis* is responsible for chytridiomycosis, a disease emerging worldwide, causing amphibian extinctions¹⁵. The Intergovernmental Panel on Climate Change (IPCC) forecast that the pathogen will spread to northern regions of the globe¹⁶. Moreover, a recent study focusing on the impact of amphibian larvae exposition to microplastics revealed that the larvae were more susceptible to get infected by *B. dendrobatidis*¹⁷. Thus, in addition to global warming, the pollution generated by humans participates in the spread and emergence of fungal disease. Other reports of a fungal species threatening biodiversity because of climate change have been reported. The introduction of *Pseudodymnoascus destructans* to North-America, a mold causing the white-nose syndrome in hibernating bats, has resulted in the collapse of the bat population in this region¹⁸. Trees are not spared by the increase in fungal infection related to global warming. The myrtle rust *Austropuccinia psidii* is spreading around the world, and could infect other Myrtaceae species, like tea trees and eucalyptus^{15,19,20}.

So far, more than 10 000 plant pathogenic species have been identified²¹. These organisms damage crops and causes severe losses in food production and agriculture²². The problem is of growing concern. Indeed, in recent years, the misuse of crop protection solutions led to the emergence of new crop-pathogens as explained by Fisher *et al.*¹⁰; “Modern agricultural intensification practices, in particular, have heightened the challenge, as the planting of vast swathes of genetically uniform crops, guarded by one or two inbred resistance genes, and use of single-target antifungals have accelerated the emergence of new virulent and fungicide-resistant strains.” (Figure 1).

Wheat, is one of the five global calorie crops (maize, oil palm, rice, soybean and wheat)¹⁰. So far, two wheat pathogens: *Fusarium graminearum* and the rust fungus *Puccinia striiformis* are suggested to have evolved in response to climate change⁶. *Fusarium graminearum*, responsible for the fusarium head blight disease, has overtaken the less aggressive *Fusarium culmorum* in temperate regions²³, resulting in higher yield loss⁶.

Puccinia striiformis f. sp. tritici behaves similarly: the fungus, which normally prefers cool regions has started to invade warmer regions²⁴. Another important wheat pathogen, *Magnaporthe oryzae* pathotype Triticum (MoT), responsible for the wheat blast disease, is another example of a fungal pathogen spreading across the globe. It was first discovered in Brazil in 1985, has spread in other south-american countries during the nineties and has now reached Bangladesh in Asia^{10,25}. The pathogen was imported from Brazil to Bangladesh via rotten wheat¹⁰.

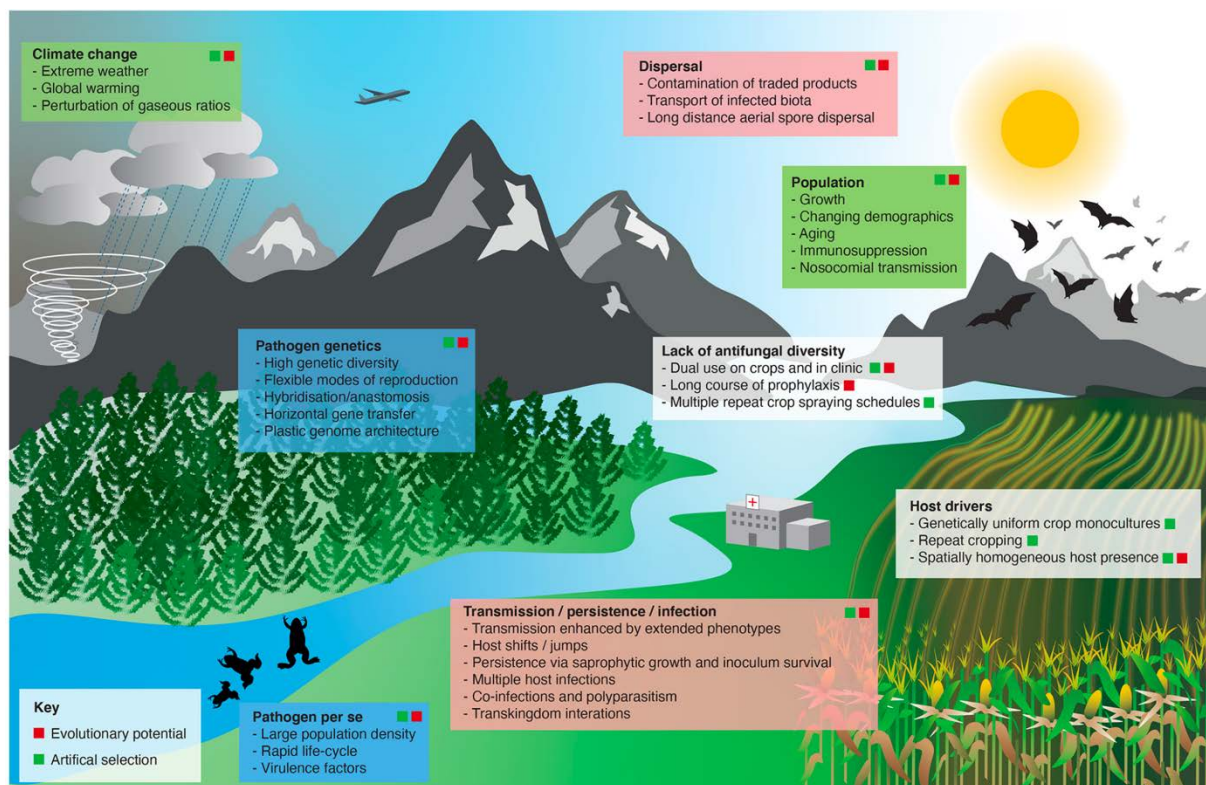


Figure 1 – Drivers of emerging fungal threats to plants and animals.

(Modified from Fisher *et al.*, 2020, ¹⁰)

Thus, climate change and human activities increase the threat posed by fungal pathogens on biodiversity, human-health, and crops. It is becoming imperative to understand the biological processes underlying fungal pathogenicity to prevent and reduce ecological and economic loss while adapting our behavior for a sustainable world.

1.3 *Botrytis cinerea*: a necrotrophic model

1.3.1 Necrotrophy versus biotrophy and hemibiotrophy

Among the five calorie crops (maize, oil palm, rice, soybean and wheat), rice and maize are the sources of over 18 % of human calorie intake²⁶. Therefore, fungal plant pathogens can represent a major threat to food security²⁷. Crop pathogens have developed three different infectious strategies: biotrophy, hemibiotrophy and necrotrophy. Each strategy is characterized by a different type of interaction between the fungus and its host.

Biotrophy is characterized by an exchange of nutrients between the fungus and the living plant hosts²⁸. Hemibiotrophy, on the other hand, can be distinguished by two distinct phases: Hemibiotrophic fungi initiate a biotrophic-phase, and then, switch to a necrotrophic-phase and secrete toxins and enzymes to induce necrosis²⁹. Contrary to hemibiotrophs, the current dogma for necrotrophs is that they do not start the infectious process with a biotrophic phase. Instead, they immediately induce plant-necrosis and feed only on dead plant-tissues²⁹.

1.3.2 *Botrytis cinerea*, a broad host range plant pathogenic fungus

Botrytis cinerea, which refers to the haploidic anamorph (asexual stage) of the ascomycete *Botryotinia fuckeliana* (teleomorphic form)³⁰ was found to cause disease on more than 586 genera of vascular plants (tracheophytes)³¹. The majority of recorded *Botrytis* spp. originate from economic hosts grown in cool- and warm-temperate zones, including extremely cold, desert, temperate, tropical, and sub-tropical regions on either the northern or the southern globe³². According to Elad *et al.*,³¹ no specific correlation between the occurrence of *Botrytis* spp. with the phylogeny of Plantae can be observed. They seem more related to the presence of soft and tender tissues rather than a specific clade of plants.

The fungus can infect many plant parts, from the leaf to petals, including fruits. Each year, the fungus is responsible for 10-100 billion US dollar losses worldwide³³.

1.3.3 The infectious cycle

The *Botrytis cinerea* infectious cycle (Figure 2) starts with plant surface adhesion. Usually, a conidium originated from conidiophores attaches the plant and germinates. The germinated spore extends to form a germinative tube that later differentiates to produce an appressorium that can pierce the plant cell wall. Hyphae can also produce infection

cushions (ICs – Figure 3), another penetration structure dedicated to the secretion of proteins required for virulence^{34,35}. During the colonization of plant tissues, the fungus secretes metabolites and many proteins including hydrolytic enzymes like plant cell-wall degrading enzymes (PCWDEs) and metabolites to induce cell death and necrosis. Once plant tissues are necrotized, the fungus can uptake nutrients and colonize dead tissues. When necrosis has affected the whole plant, *Botrytis* produces conidiophores, releases conidia that can be transported by either the wind or the rain³⁶, and make the infection of another plant possible.

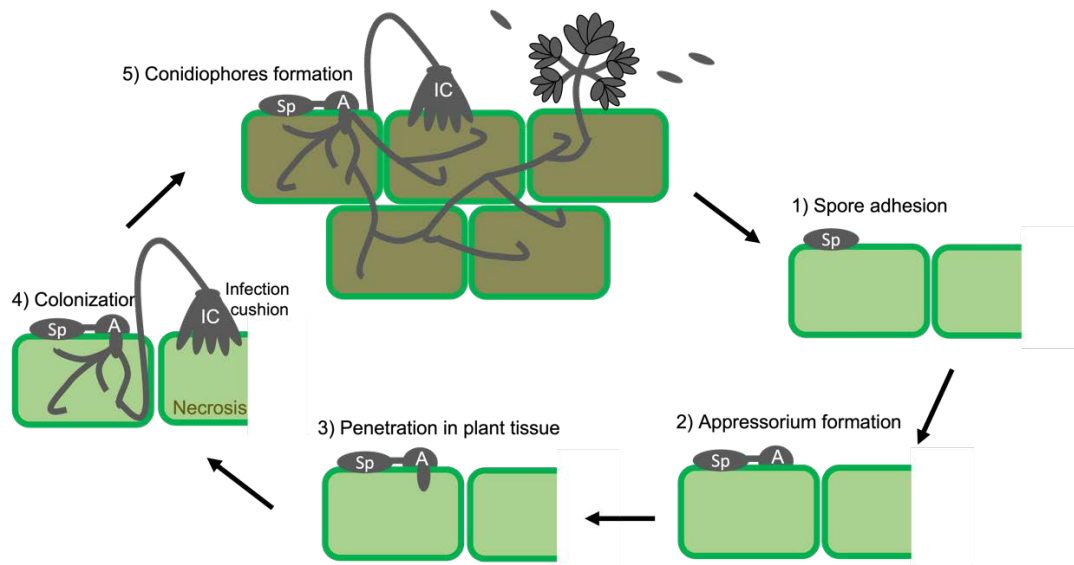


Figure 2 – *Botrytis cinerea* infectious cycle

Main steps of the infectious cycle of *Botrytis cinerea* – spore (Sp) ; appressorium (A), infection cushion (IC)



Figure 3 – *Botrytis cinerea* Infection cushion

Scanning electron microscopy of *Botrytis cinerea* infection cushion (From Choquer *et al.*, 2021 - ³⁵)

1.3.4 Secreted molecules required for host invasion

Botrytis cinerea has a typical necrotrophic lifestyle by causing plant cells death apoptosis and necrosis. To do so, the fungus needs to secrete a broad set of molecules, including reactive oxygen species (ROS), organic acids, toxins, cell-death inducing proteins (CDIP) and hydrolytic enzymes.

1.3.4.1 ROS production

During the early stage of infection, the pathogen produces pathogen associated molecular patterns (PAMPs) that are recognized by the plant. The recognition of PAMPs by receptor-like kinases (RLKs) and receptor-like proteins (RLPs) triggers plant defenses: the plant produces an oxidative burst³⁷ that can induce the plant hypersensitive response (HR). HR promotes the apoptosis of infected plant cells and prevents the spread of the pathogen³⁸. However, *B. cinerea*, like other necrotrophs, takes advantage of the oxidative burst and even produces its own ROS during the infection process³⁹. Govrin and Levine 2000⁴⁰ have shown that the virulence of *B. cinerea* was reduced in HR-deficient *Arabidopsis thaliana* mutants. *B. cinerea* produces ROS not only during the early stages of the disease around the attachment site of the conidium^{39,41,42}, but also at later stages. Indeed, ROS accumulate inside infection tissues, leading to the death of plant-cells providing a source of nutrients for the pathogen⁴².

B. cinerea has developed an Oxidative Stress Response (OSR) to circumvent the molecular damages produced by ROS. The fungus secretes several enzymes such as super oxidase dismutase, catalase, peroxiredoxins, and peroxidase to scavenge ROS⁴³. *B. cinerea* also uses the thioredoxin system made of the enzymes thioreoxin and thioredoxin reductase to maintain a balanced redox status⁴⁴.

1.3.4.2 Organic acids production

Besides ROS production, pH modulation of plant tissues by *B. cinerea* is critical for virulence. *B. cinerea* modifies the ambient pH during plant-infection and can infect plant tissues with various pH⁴⁵. It can produce organic acids such as oxalic acid, citric acid and succinic acid to acidify the environment, or alkalinize it with the production of ammonia⁴⁶. When acidifying a plant tissue, *B. cinerea* produces succinic and citric acids first, and then secretes oxalic acid⁴⁶.

1.3.4.3 *Phytotoxins production*

In addition to ROS and organic acids, the phytotoxins produced by *B. cinerea* also play a significant role in pathogenesis (reviewed by Collado and Viaud 2016⁴⁷). *B. cinerea* produces at least two class of secondary metabolites: terpenes and polyketides.

Two secondary metabolites belonging to the terpenes may play a role in the virulence of *B. cinerea*: botrydial and acid abscisic (ABA)^{48–50}. Botrydial has a phytotoxic activity⁵¹ and was found in many of *B. cinerea* hosts, two days post-inoculation. It may promote plant cell death⁴⁷. Indeed, botrydial induces the hypersensitive response (HR) in *Arabidopsis thaliana*⁵². However, the cellular target of botrydial remains unknown⁴⁷. As proposed by Collado and Viaud⁴⁷, “botrydial could act as a weapon to kill the cells of a large range of hosts to allow the pathogen to feed on dead tissues.”. ABA, another interesting terpene produced by *B. cinerea*, is also produced in plants, and known as a plant hormone. In plants, ABA down-regulates plant defense-genes⁵³. Therefore, ABA could be produced by *B. cinerea* to shape host-defense mechanism⁴⁷.

The most characterized phytotoxin belonging to the polyketides class produced by *B. cinerea* is botcinic acid. In the 1990s, Cutler *et al.*,^{54,55} demonstrated that botcinic acid induced necrosis in plants. In 2011, Dalmais *et al.*⁵⁶, proved that botrydial and botcinic acid have a redundant role in the virulence of *B. cinerea*.

1.3.4.4 *Secretion of hydrolytic enzymes*

The first barrier that *B. cinerea* needs to remove for plant infection is the cuticula. This layer is usually made of cutin and hydroxylated polyesters. The digestion of the cuticula is usually processed by the release of extracellular enzymes such as cutinases and lipases.

Once the cuticula has been degraded, *B. cinerea* needs to digest the plant cell wall to pursue infection. This defensive barrier contains cellulose, hemicellulose (xylan), and pectin.

Fourteen enzymes potentially involved in the degradation of cellulose have been identified in the secretome of *B. cinerea*, while only eight hemicellulases such as xylanase were found⁵⁷. The last activity required for cell wall degradation is pectinase. Pectin is mainly composed of two polymers: homogalacturonans and rhamnogalacturonans. Three different activities are required to degrade pectin. First, pectin methylesterases demethylate pectin, facilitating pectin degradation by the two depolymerizing enzymes:

endopolygalacturonases and rhamnogalacturonases⁵⁷. These enzymes are usually encoded by multigenic families, and their expression is somehow related to both the environment and the host⁵⁸.

Proteases are another family of hydrolytic enzymes secreted by *B. cinerea*. They are the most abundant hydrolytic enzymes family found in secretomes: 34 proteases have been found in extracellular media⁵⁷. However, their role in *B. cinerea* virulence is unclear. Proteases are supposed to be important for fungal nutrition, the digestion plant cell-wall proteins, and the degradation of plant defenses proteins⁵⁷.

1.3.4.5 Secretion of effectors

Effectors are molecules secreted by plant-pathogens that manipulate the plant to facilitate disease establishment and progression⁵⁹. The understanding of role of effectors produced by necrotrophs during plant-infection remains limited⁵⁹. Until recently, the dogma excluded that necrotrophs could produce effectors. Necrotrophs were thought to kill plants only by secreting PCWDEs, ROS, organic acids, and toxins⁵⁹.

However, studies from the 2010s demonstrated that *B. cinerea* secretes two-types of protein effectors: cell-death-inducing proteins (CDIPs), previously called necrosis-inducing proteins (NIPs)⁶⁰; and cerato-platanin proteins (CPPs). So far, most of the 15 CDIPs described in *B. cinerea* are PCWDEs^{59,60}, however the effector capacity of these proteins is not related to their enzymatic activity⁶¹. These CDIPs include the xylanases BcXyn11A^{62,63}, BcXyl1⁶⁴, the xyloglucanase BcXYG1⁶⁵, and the glucan 1,4- α -glucosidase BcGS1⁶⁶. All these CDIPs induce plant cell death and most of them are recognized by plant receptors and elicit plant defenses⁶⁰. BcGS1, BcXYN11A and BcXyl1 also induce ROS production^{63,64,66}. Furthermore, three CDIPs that are not classified as PCWDEs have been described in *B. cinerea*: BcIEB1 (IgE binding domain protein)⁶⁷, BcCrh1 (congo-red hypersensitivity transglycosylase)⁶⁸ and BcSSP2 (unknown domain)⁶⁹. The deletion of 10 CDIPs in a single *B. cinerea* mutant revealed that their role in virulence is host-dependent. Indeed, this mutant displayed a 40% loss of virulence on apple fruits, but no virulence defect on tomatoes.

To date, only one CPP effector has been described in *B. cinerea*: BcSpl1. This protein induces plant cell death and an oxidative burst⁷⁰.

A few years ago, other non-protein associated secreted molecules were reported to be involved in pathogenesis and to act like effectors in *B. cinerea*. Exported RNAs able to suppress host defense mechanisms have been identified in this organism⁷¹. They target key component of the plant responses: signal transduction pathways and immune responses⁵⁹. Recently, small RNAs produced during the early stages of *B. cinerea* and tomato interaction were sequenced and 7042 sRNA were predicted to target 3185 mRNAs in tomato. However, even if the deletion of genes involved in sRNAs production (dicer-like genes *Bcdcl1* and *Bcdlc2*) strongly reduced (> 99%) the production of transposon-derived sRNAs, no virulence defect could be observed in these mutants. Thus, this study suggests that sRNA might not play a role in the virulence of *B. cinerea* when infecting tomato⁷².

2 Fungal secretory vesicles: putative origins and traffic

Secretory pathways deliver proteins and lipids to the plasma membrane, supporting growth, virulence, or symbiosis. Two secretory pathways have been described so far: the conventional and the unconventional secretory pathways.

2.1 Two secretory pathways

2.1.1 Conventional secretory pathway

The conventional secretory pathway, also named *conventional protein secretion* (CPS) refers to endoplasmic reticulum (ER) to Golgi-dependent protein secretion. In the 1980s, Randy Schekman generated secretory “*sec*” mutants in the yeast *Saccharomyces cerevisiae*. These mutants were unable to secrete invertase⁷³ and were used to unravel the molecular mechanisms underlying fungal secretion. In 2013, Randy Schekman together with James Rothman and Thomas Südhof, won the Nobel Prize in Physiology and Medicine, "for their discoveries of machinery regulating vesicle traffic, a major transport system in cells."⁷⁴. Thus, they uncovered the molecular mechanisms governing vesicular transport⁷⁵ in the conventional secretory pathway.

2.1.1.1 Polypeptide translocation in the endoplasmic reticulum

After, and sometimes during translation, proteins containing an N-terminal signal peptide (SP) and/or transmembrane domain are translocated to protein transporter complexes on the ER membrane. Two translocation processes called cotranslational and posttranslational processes exist. In the cotranslational process, the signal recognition particle (SRP) recognizes the SP, stops translation and directs the translational complex (ribosome, mRNA, peptide ternary complex) on the ER membrane, to the translocon which is made of several proteins (Figure 4). Once attached, translation starts again, and the forming polypeptide is further translocated into the ER lumen. During posttranslational translocation, synthesized polypeptides precursors interact with chaperones, such as HSP70, and a heterotetrameric membrane proteins-constituted complex recognizes the SP, directing the polypeptide to the translocon. Polypeptide chain translocation is facilitated by the ER chaperone complex Bip/Kar2p and, later, a signal peptidase cleaves the signal sequence and release the polypeptide in the ER lumen⁷⁶ (Figure 4).

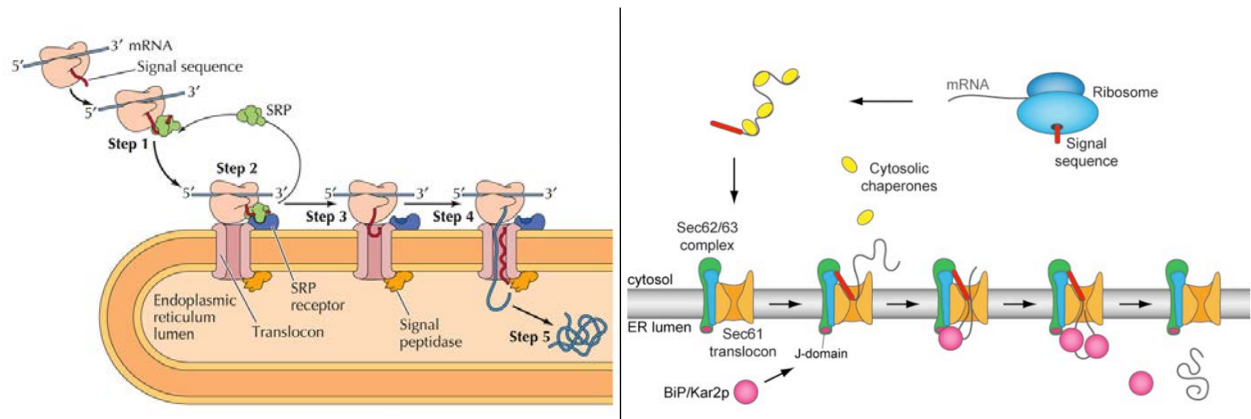


Figure 4 - Polypeptide translocation in ER

Left: Cotranslational translocation

The signal recognition particle (SRP) recognizes the N-terminal signal-sequence (step 1) and directs the translation complex to the ER membrane and stops translation (step 2). Once attached to the translocon, translation pursues (step 3) producing the polypeptide (step 5). THE CELL, Fourth Edition © 2006 ASM Press and Sinauer Associates, Inc.

Right: Posttranslational translocation

After mRNA translation, chaperones attach to the polypeptide and direct it to the complexes b (Sec62/63 complex and Sec61 translocon). Sec63 J-domain recruits Bip/Kar2p complex that facilitates the polypeptide chain translocation. Then, the polypeptide chain is released by signal sequence's cleavage performed by the signal peptidase. (Modified from Reithinger, 2013 - 77)

Once in the ER lumen, these proteins undergo many modifications, such as glycosylation. Carbohydrates are attached to many proteins via either asparagine N-glycosylation or threonine/serine O-glycosylation. In fungi, protein-O-mannosyltransferases (PMTs), catalyzes O-linked glycosylation⁷⁸. Other post-translational modifications occur at the ER, such as disulfur bridge formation, phosphorylation, folding by chaperones, and subunit assembly.

2.1.1.2 Unfolded protein response

Environmental perturbations can lead to a secretory stress that disturbs protein folding. When unfolded proteins accumulate in ER lumen, the unfolded protein response (UPR) is triggered⁷⁹. UPR induces transcription of chaperone encoding genes and ER expansion related genes. UPR also restructures cellular transport processes such as ER to Golgi transport. UPR is also related to the degradation of irreversibly misfolded proteins through the endoplasmic reticulum associated degradation (ERAD)⁸⁰⁻⁸³. The misfolded proteins are delivered to vacuoles⁸⁴⁻⁸⁶ or to the cytosol to be degraded by proteasomes⁸⁷. Thus, the ER can be regarded as a protein quality control center.

2.1.1.3 Endoplasmic-reticulum exit

ER proteins are then transported to the Golgi apparatus through anterograde transport into Coat-protein complex II (COPII)-coated vesicles. COPII-vesicles bud off at ER-exit sites for further modifications such as glycosylation and peptide processing in Golgi^{88 89}. Retrograde transport from the Golgi to the ER, performed by Coat-protein complex I

(COPI)-coated vesicles also happens when ER proteins such as cargo receptors need to be recycled. COPI and COPII vesicles fuse at targeted organelles through the interaction between vesicular Soluble-N-ethylmaleimide-sensitive-factor proteins (v-SNAREs) and target SNARE proteins (t-SNARE) (Figure 5).

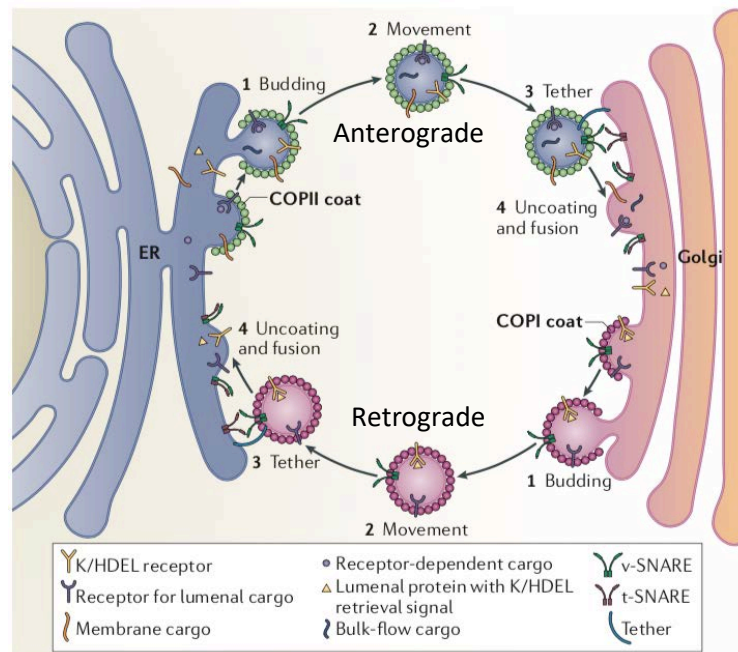


Figure 5 – Bidirectional transport between ER and Golgi

Secretory cargos are transported by either coat protein complex II (COPII) for anterograde transport or coat protein complex I (COPI) for retrograde transport between ER and Golgi. K/HDEL receptors recognize luminal proteins with K/HDEL retrieval signals. SNAREs proteins mediate vesicle fusion. (Modified from Brandizzi *et al.*, 2013 - ⁹⁰)

2.1.1.4 The Golgi apparatus in fungi

In fungi, the Golgi apparatus does not consist of several Golgi stacks, as observed in mammalian cells⁹¹. Indeed, in *Saccharomyces cerevisiae*, and the filamentous fungi *Aspergillus nidulans* and *Neurospora crassa*, Golgi can be regarded as membrane-bound structures^{92,93} (Figure 6). Fluorescence microscopy revealed that Golgi apparatus was made of a dynamic network ring-shaped cisterna, sometimes bound to tubular structures^{94–96}. Moreover, the apical accumulation of Golgi structures could suggest its central role in the dominant secretion at the apex⁹⁷.

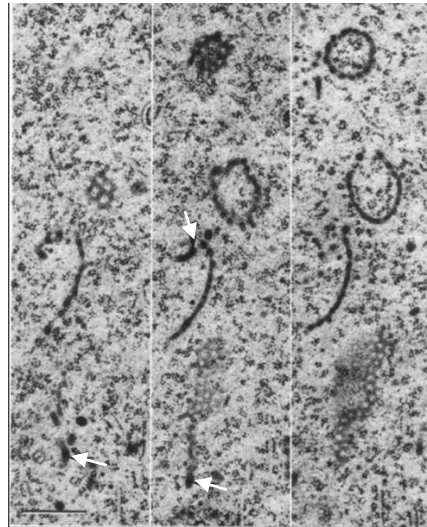


Figure 6 – Golgi structures in filamentous fungi

Golgi cisternae in *Fusarium acuminatum* seen as tubules or sheets belong to the same organelle, as suggested from electron micrographs of adjacent, serial, thin sections of freeze-substituted cells. Some cisternae are hollow spheres. The white arrows indicate tubular elements that exhibit continuity with Golgi sheets and tubules but are wider and more electron dense. Bar = 500 nm. Images are reproduced from Howard RJ. (1981) - ⁹⁸ . (Modified from Pantazopoulou, 2016 – ⁹³)

2.1.1.5 Golgi maturation in fungi

In filamentous fungi, the Golgi apparatus likely matures via the cisternal maturation model. The early-cisternae, fed continuously by COPII vesicles, change its lipid and protein composition to produce the late Golgi. Even if the passage of ER-derived cargos across Golgi remains unknown, one explanation could be that cargos traffic through cisternal maturation, rather than vesicle-mediated connections between the early-cisternae and the late Golgi⁹¹. Recent work has focused on the Golgi maturation process. It is thought that the early cisternae are the result of COPII vesicle fusion (stage I of Golgi maturation, Figure 7) and that glycosylation occurs at the early stages of Golgi maturation (stage II, Figure 7). In maturing Golgi cisterna, glycosylation enzymes such as glycosidases and glycosyltransferases are recycled to the early cisterna by COPI anterograde transport. In the meantime, enriched cargos cisterna acquires late Golgi related markers such as the pleckstrin homology domain of the human oxysterol binding PH^{OSBP} ⁹⁶. Later, cargo-enriched cisternae acquire a composition that enables them to generate anterograde cargos destined to either the plasma membrane or endosomes⁹¹ (stage III, Figure 7). However, this acquisition makes COPI retrograde traffic impossible. According to Steinberg *et al.*, 2017⁹¹, traffic from late Golgi to endosomes is mediated by clathrin-coated vesicles (CCVs). Appropriate cargos are sorted into CCVs by adaptor

proteins such as AP-1, GGA (Golgi-localized gamma adaptin ear-containing, ARF-binding) and epsin.

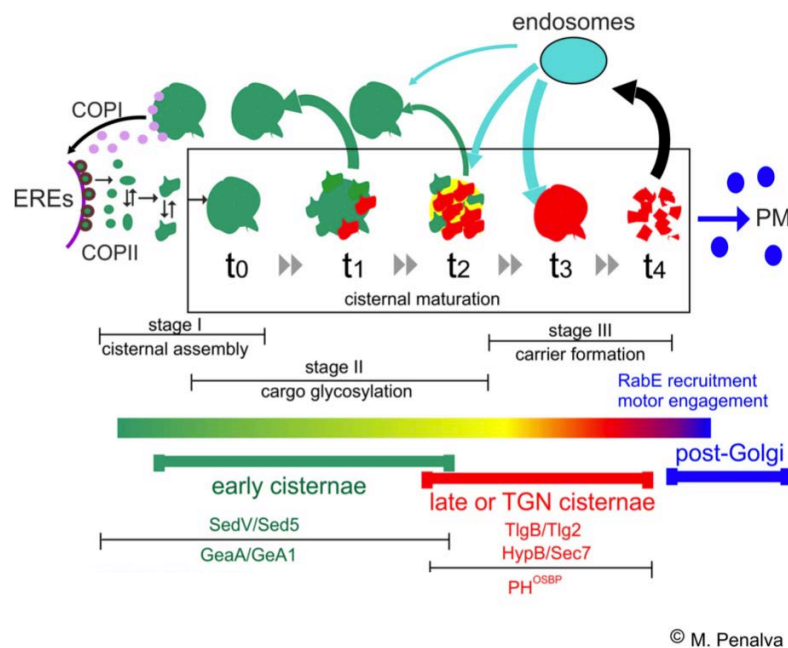


Figure 7 - Golgi maturation model in *Aspergillus nidulans*

ER budded COPII vesicles (green) merge to produce the early cisternae (marked with SedV and GeaA), equipped with cargo glycosylation enzymes (t0). Cargo receptors that require recycling are directed to the ER by COPI transport (purple vesicles). Later, the enriched cargo cisternae resemble the late Golgi (PH^{OSBP}, TlgB and HypB markers accumulate). Golgi glycosylation enzymes are thought to be transported back to early cisterna by COPI mediated retrograde transport (t1 and t2). Cargo-enriched cisterna produces vesicles destined for the plasma membrane (PM) and endosomes (t3 – t4). Late Golgi cisterna also receives traffic from endosomes. The Rab GTPase RabE^{Rab11} is involved in the transition from Late to Post Golgi-identity. Specific stages proteins are indicated. Green refers to early Golgi, while red refers to Late Golgi. (Steinberg *et al.*, 2017 - ⁹¹ – Modified from Penalva)

This model suggests the differentiation of late Golgi into post-Golgi vesicles, destined to the apical plasma membrane. Cisternal membranes lose late Golgi markers such as PH^{OSBP} and become enriched in the Rab GTPase RabE^{RAB11} ⁹⁹. RabE^{RAB11} fluorescently labeled post-Golgi vesicles were found to be directed to the hyphal tip, to the Spitzenkörper⁹⁹ (Figure 8).

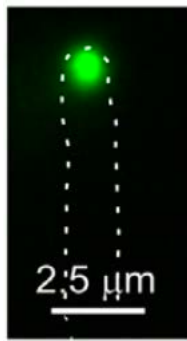


Figure 8 – RabE^{Rab11} localization at the Spitzenkörper in *Aspergillus nidulans*

Fluorescently tagged RabE^{Rab11} in *Aspergillus nidulans* (Modified from Pinar, et al. 2022 - ¹⁰⁰)

2.1.1.6 Example of proteins undergoing CPS

In *Aspergillus nidulans*, apical cargos such as the chitin synthase ChsB and the SNARE synaptobrevin SynA are located at the fungal apex (Figure 9). These apical cargos displayed a clear dependence on early and late-Golgi/TGN and post-Golgi secretory routes in *Aspergillus nidulans*. Indeed, the localization of ChsB and SynA at the hyphal tip was very disrupted when RabE^{Rab11} and AP-1 encoding genes, which encode for two proteins involved in post-Golgi vesicles biogenesis, were downregulated¹⁰¹.

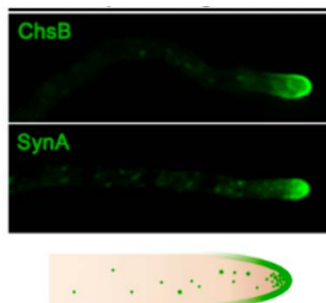


Figure 9 – Localization of apical cargos in *Aspergillus nidulans*

Localization of GFP functionally-tagged chitin synthase ChsB and synaptobrevin SynA. (Modified from Dimou et al, 2020 - ¹⁰²)

Previous studies have highlighted the importance of the conventional secretory pathway for fungal pathogenesis. CPS secretes many proteins involved not only in growth but also in pathogenicity¹⁰³. In the human pathogen *A. fumigatus*, 6.1% of the proteome, which represents 90% of the secreted proteins is secreted by the conventional secretory pathway¹⁰⁴.

In plant-pathogenic fungi, the current dogma is that most of the secreted proteins undergo the conventional secretory pathway^{105,106}.

In *B. cinerea*, a lot of secreted hydrolytic enzymes are predicted to be secreted via the conventional secretory pathway. Indeed, more than 320 hydrolytic enzymes (proteases, PCWDE, lipases) found in the secretome are predicted to have a signal peptide³⁴. The lysin domain effector (LysM) which mediates virulence by binding fungal chitin, thus preventing the triggering of plant defenses¹⁰⁷, is also predicted to be secreted via the conventional secretory pathway in plant-pathogenic fungi.

So far, evidence of effectors undergoing CPS has only been described in *Magnaporthe oryzae*. The apoplastic effectors Slp1 and Bas113, which are virulence determinants required for tissue invasion, are secreted through the conventional secretory pathway¹⁰⁶. Indeed, secretion of Slp1:GFP and Bas113:GFP was blocked when the brefeldin A (BFA) was added to the culture medium. BFA is drug that blocks conventional protein secretion. The drug impairs the formation of coat protein complex I (COPI) and AP-1 derived vesicles by inhibiting guanine-nucleotide exchange factors for Arf GTPases¹⁰⁸. If the secretion of a protein is not disrupted by BFA, then the protein undergoes the unconventional secretory pathway.

Only a few studies focused on the secretion mechanisms of effectors and hydrolytic enzymes in plant-pathogenic fungi. So far, most of the data available on proteins undergoing CPS is solely based on the prediction of a signal peptide. The study of the secretion mechanisms involved in the secretion of hydrolytic enzymes closely linked to virulence has been neglected¹⁰⁹.

2.1.2 Unconventional secretory pathway

Contrary to the conventional secretory pathway, the unconventional secretory pathway, also named *unconventional protein secretion* (UPS) relates to the secretory mechanisms where secreted proteins enter the endoplasmic reticulum but bypass the Golgi apparatus¹¹⁰. UPS also refers to cargos without a signal peptide or a transmembrane domain that can translocate across the plasma membrane¹¹⁰.

2.1.2.1 Extracellular vesicles (EVs)

A few examples of UPS have been described in fungi. Extracellular vesicles (EVs) are an example of the unconventional secretory pathway. EVs are found across all kingdoms of life^{111–114} and have been isolated in several fungal species such as the pathogenic yeasts *Candida albicans*, *Cryptococcus neoformans*, *Histoplasma capsulatum*, *Cryptococcus gattii*^{115–118}. In filamentous fungi, EVs were first discovered in *Alternaria infectoria*¹¹⁹, a ubiquitous fungus that spoils food crops and causes human infections. Since 2014, EVs have been identified in a growing list of filamentous fungi: *Aspergillus fumigatus*, *Trichoderma reesei*¹²², *Penicillium chrysogenum*¹²³ and the hemibiotrophs *Fusarium oxysporum*¹²⁴, *Fusarium graminearum*¹²⁵, *Zymoseptoria tritici*¹²⁶, *Ustilago maydis*¹²⁷, *Colletotrichum higginsianum*¹²⁸.

EVs are bilayer-lipid vesicles containing proteins, nucleic acids and polysaccharides¹²⁹ (Figure 10). These vesicles with a diameter ranging from 50-1000 nm deliver virulence-associated-molecules, including some virulence factors, such as *Cryptococcus neoformans* glucuronoxylomannan (GXM)¹¹⁷. Proteins involved in fungal virulence were also found in the pathogenic filamentous fungus *A. fumigatus*¹³⁰. In plant-pathogenic fungi, EVs from *Fusarium oxysporum* induced a phytotoxic response in cotton leaves¹²⁴. More recently, protein effectors were found in *F. graminearum* EVs during corn infection¹²⁵. EVs found in phytopathogenic fungi also carry hydrolytic enzymes required for plant cell wall degradation^{119,122,124,126}. These recent findings suggest EVs play a very important role in fungal virulence.

Involvement of EVs in cell wall remodeling¹³¹ is another interesting component of EVs role in fungal biology. In *A. fumigatus*, proteins related to the biosynthesis of the cell wall as well as monosaccharides required for the production of the extracellular matrix were found in EVs¹³².

Cell-wall related proteins were also found in EVs from *Alternaria infectoria*¹¹⁹, *Fusarium graminearum*¹²⁵, *Colletotrichum higginsianum*¹²⁸ and *B. cinerea* (de Vallée *et al.*, 2023 submitted).

Recently, it was shown that *Ustilago maydis* EVs carry mRNAs. Among these mRNAs, some encoded effectors and other proteins linked to virulence¹²⁷. Kwon *et al.*¹²⁷, proposed that EV-associated mRNAs may participate in plant-pathogens interactions.

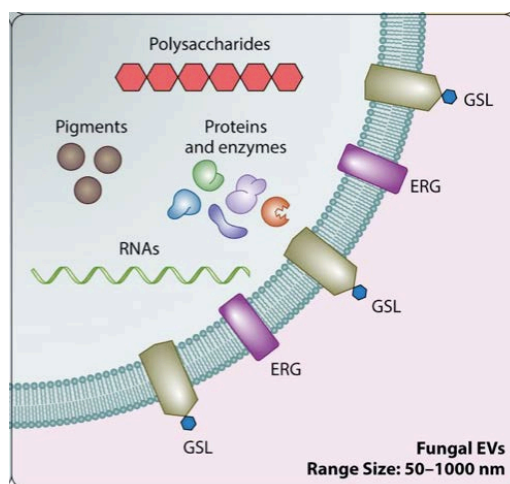


Figure 10 – Fungal EVs content

GSL: glycosphingolipids ; ERG: ergosterol (Modified from Joffe *et al.*, 2016 -¹³³)

Fungal EVs secretion and biogenesis is poorly understood¹³¹, but depends on Golgi- and endosome-related proteins¹³⁴. The endosomal sorting complex required for transport (ESCRT) machinery is critical for biogenesis of mammalian exosomes (an EVs subtype)^{129,135} and has also been found to be involved in the production of EVs in *Saccharomyces cerevisiae* and *Candida albicans*^{131,136}. In fungi, strong evidence suggests that EVs are produced in multivesicular bodies (MVBs) - late-endosome equivalent – before MVBs fusion at the plasma membrane (Figure 11). The involvement of MVB in the production of *Cryptococcus neoformans* EVs has been demonstrated¹¹⁶. Moreover, some plant pathogenic fungi, such as the powdery mildew: *Golovinomyces orontii* and the necrotroph *B. cinerea* may utilize similar MVB-mediated extracellular vesicle secretion for effector secretion^{137,138}(de Vallée *et al.*, 2023 – submitted). Potential involvement of Golgi-related proteins in EVs biogenesis makes the classification of EVs in UPS debatable.

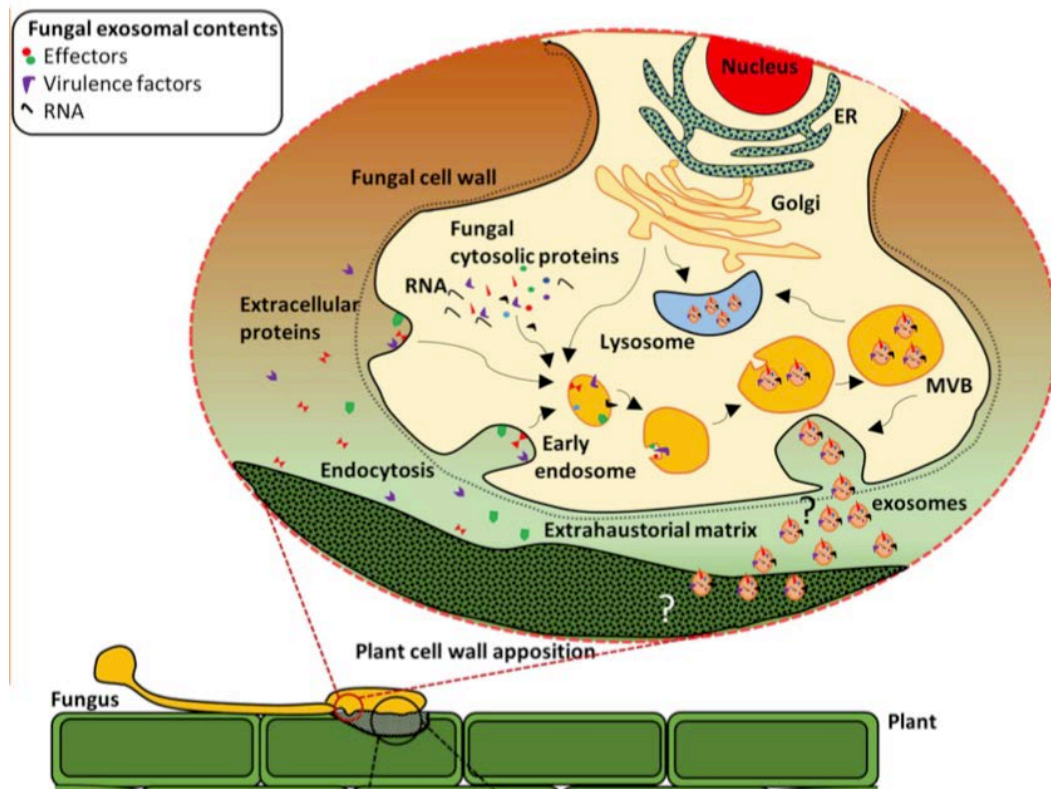


Figure 11 - Speculative EVs (exosomes) production in a plant-pathogenic fungus at the plant-fungal interface

Early endosomes mature into multivesicular bodies (MVBs). Membrane invagination within MVBs results in the formation of intraluminal vesicles containing RNAs and proteins. Then MVBs are either directed to lysosomes for degradation or to the plasma membrane for exosomes release. (Modified from Samuel *et al.*, 2015 – 139)

2.1.2.2 Cell-wall synthases

BFA-insensitive protein secretion has been found in various filamentous fungi. In *Neurospora crassa*, the fungal cell wall enzymes chitin synthases CHS-1, CHS-3 and CHS-6 transport to the Spitzenkörper was not impaired by BFA, suggesting that some CHS were secreted by UPS^{140, 141}. However, chitin synthases traffic remains unclear. Indeed, in *Aspergillus nidulans*, the chitin synthase ChsB (Class III, *N. crassa* CHS-1 ortholog) is localized at the Late Golgi¹⁴² and traffics *via* the conventional protein secretion pathway^{101,102}.

2.1.2.3 Protein effectors and hydrolytic enzymes

There are a few examples of protein effectors undergoing UPS in fungi. In *Magnaporthe oryzae*, the secretion of the cytoplasmic effector PWL2 at subapical regions was not impaired by BFA¹⁰⁶. In *Ustilago maydis*, Stock, Sarkari and Kreibich¹⁴³ found that the protein effector Cts1, an endochitinase, was secreted via a novel unconventional route. To

demonstrate this, they used a Gus reporter assay developed in tobacco¹⁴⁴. When Gus is conventionally secreted, it becomes inactive due to a N-glycosylation. If Gus undergoes UPS, it is not N-glycosylated and is therefore active. In *Ustilago maydis*, when Gus was fused to the signal peptide of a secreted invertase, no Gus activity could be found in culture supernatants. However, when Gus was fused to the amino terminus of Cts1, they observed active Gus in culture supernatants, proving that Cts1 undergoes UPS¹⁴³.

To date, there is only one example of hydrolytic enzyme secretion through UPS in fungi. In *Termitomyces clypeatus*, an agaric fungus, cellobiase was still secreted after BFA treatment¹⁴⁵.

2.1.2.4 Transporters in *Aspergillus nidulans*

In *Aspergillus nidulans*, transporters are localized in a non-polar pattern. Indeed, transporters can be found homogeneously along the plasma membrane (Figure 12)¹⁰².

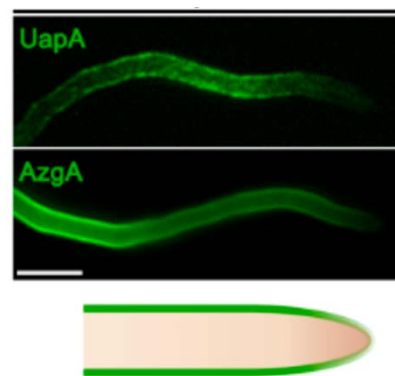


Figure 12 – Localization of transporters in *Aspergillus nidulans*

Localization of GFP functionnally-tagged UapA and AzgA transporters
(Modified from Dimou et al, 2020 - ¹⁰²)

Based on these different localization patterns, it seems possible that transporters reach the plasma membrane in a different way than apical cargos. Recently, Dimou et al. (2020) revealed that nutrients transporter traffic bypassed the Golgi apparatus in *Aspergillus nidulans*. They demonstrated that *de novo* UapA^{Uap1} transport depends on post-ER COPII-vesicles and the clathrin heavy chain and actin polymerization¹⁴⁶. However, UapA does not co-localize with Golgi markers (SedV^{Sed5}, GeaA^{Gea1}, HypB^{Sec7} and PH^{OSBP}), and the transport of UapA to the plasma membrane is not impaired in mutant underexpressing several genes encoding for proteins involved in conventional protein secretion such as RabE^{Rab11} (TGN/post-Golgi traffic), AP-1 (post-Golgi secretion) or ClaH (clathrin heavy chain/post-Golgi secretion). Similar results were also obtained for distinct transporter

families: AzgA (purines) and FurA (allantoin) which suggest that the transport of transporters relies on unconventional protein secretion.

2.2 Vesicle biogenesis in the conventional secretory pathway

A very few laboratories have studied the components of the secretory machinery in filamentous fungi. As a consequence, there is few information on vesicle biogenesis and traffic¹⁴⁷. However, the eukaryotic model *Saccharomyces cerevisiae* has been widely used to study the molecular mechanisms underlying fungal secretion.

2.2.1 Two distinct ways: clathrin-dependent vs clathrin-independent biogenesis of secretory vesicles

In 1995, Harsay and Bretscher⁷⁰ identified two class of secretory vesicles in *Saccharomyces cerevisiae* *sec* and *snc* mutants. These mutants, deficient in Golgi and plasma membrane (PM) transport, accumulate late secretory vesicles, that do not differ in size (100 nm) but in densities. They found that high-density secretory vesicles (HDSVs) carry enzymes such as invertase, acid phosphatase and exoglucanase, while low-density secretory vesicles (LDSVs) transport the plasma membrane H⁺-ATPase (Pma1). Thus, they demonstrated that exocytic cargos were transported by at least two routes. A few years later, it was shown that the clathrin heavy chain CHC1, PEP12, a t-SNARE mediating all Golgi to pre-vacuolar compartment) and VPS1, a dynamin related protein are involved in the biogenesis of HDSVs, but not LDSVs (Figure 13). Moreover, they also proposed that HDSVs could transit through the endosome before reaching the plasma membrane, while LDSVs would bypass endosome and directly fuse to the plasma membrane.

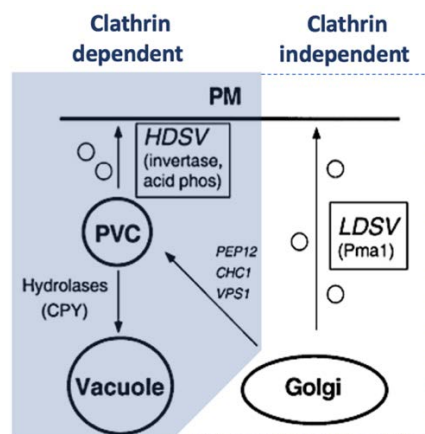


Figure 13 - Secretory vesicle biogenesis model in yeast

Proteins destined to the plasma membrane (PM) traffic from Golgi to the cell surface by either low-density secretory vesicles (LDSVs) carrying the H⁺-ATPase Pma1, or high-density secretory vesicles (HDSVs) that carry invertase and acid phosphatase. The biogenesis of HDSVs requires either PEP12, CHC1, or VPS1 and HDSVs transit via the endosome (PVC). The biogenesis of LDSVs is CHC1, VPS1 and PEP12 independent and LDSVs bypass the endosome. (Modified from Gurunathan *et al.*, 2002¹⁴⁹)

Recent findings in *Botrytis cinerea* proved that clathrin was involved in the secretion of virulence factors¹⁵⁰. Souibgui *et al.*¹⁵⁰, proposed that clathrin may be involved in the biogenesis process of vesicles transporting hydrolytic enzymes and cell death inducing proteins. In *Cryptococcus neoformans*, a human pathogenic yeast, production of virulence factors was also impaired in clathrin mutants¹⁵¹. To date, only two studies focused on the role of clathrin in fungal secretion.

2.2.2 Clathrin coated vesicles biogenesis

To date, there is no information on the biogenesis process of the LDSVs (clathrin independent) described by Harsay and Bretscher. On the contrary, the biogenesis process of clathrin-coated vesicles has been extensively studied, although most of the knowledge originates from the study of endocytic vesicles.

2.2.2.1 Clathrin structure

Clathrin was first observed and named in 1975 by Barbara Pearse when she purified coated vesicles from brain, adrenal medulla and non-secreting lymphoma cell. Coated vesicles of various size were found and coats were made of variable numbers of clathrin subunits, arranged in closed networks of hexagons and pentagons¹⁵². In 1981, Unanue *et al.*¹⁵³, isolated clathrin-coated vesicles (CCVs) from bovine brain and depolymerized clathrin coats. They found that non-assembled clathrin resembled triskelion, and proposed that it was made of three copies of clathrin, with three other copies of a smaller protein¹⁵³. Now, it is widely accepted that the clathrin triskelion is made of three clathrin heavy chains (180 kDa), and three clathrin light chains (35 kDa), that assembles to form clathrin-coat (or clathrin-cages) structures (Figure 14).

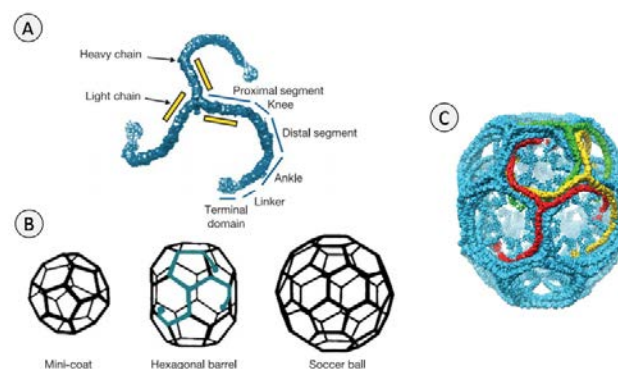


Figure 14 - 3D structure of a clathrin triskelion and clathrin coats

Clathrin triskelion made of three clathrin heavy chain (blue) and three clathrin chains (yellow). Segments of the heavy chain are labelled. **B)** *in-vitro* clathrin coats structures of several coat shapes. Schematic representation of a clathrin triskelion (in blue) within the hexagonal barrel. **C)** Image reconstruction of a hexagonal barrel made of 36 clathrin triskelions (Modified from Fotin *et al.*, 2004 - ¹⁵⁴)

In human, the clathrin heavy chain (CHC) is divided in several domains: the terminal domain (N-terminal), the linker, the ankle, and distal proximal segments which contain a trimerization domain. The CHC C-terminal region interacts with regulatory proteins enabling clathrin recruitment, while the distal segment and the proximal segment are involved in clathrin cages assembly. Clathrin triskelion is stabilized by clathrin light chain (CLC), which interacts with the proximal segment of clathrin heavy chain, avoiding random CHC assembly¹⁵⁵.

2.2.2.2 Size of clathrin-coated vesicles

Clathrin coats can adopt two different configurations, either pentagonal or hexagonal (Figure 14B) and various sizes. It has been shown that CCVs diameter can be dependent on cargos¹⁵⁶ and that it can vary between different cell types within the same species: CCVs with a diameter of 70-90 nm have been found in mouse brain¹⁵⁷, while larger CCVs (120-150 nm) were observed in mouse epithelial cells¹⁵⁸. CCVs diameter also varies between species. CCVs can be as small as 36 nm in *Saccharomyces cerevisiae*¹⁵⁹, while CCVs diameter can exceed 200 nm during virus uptake in mammalian cells¹⁶⁰ (Figure 15). In the filamentous fungus *Neurospora crassa*, the size CCVs is also relatively small (42 nm)¹⁶¹. Yet, it is important to keep in mind that the diameter of the vesicles contained in a clathrin cage is a lot smaller. Brain-derived CCVs have external diameters of 70-90 nm while internal vesicle diameter ranges between 34 nm and 45 nm¹⁶². Based on these observations, McMahon and Boucrot (2011) suggested that, in yeast or plants, where CCVs have an external diameter of 35-60 nm, the internal vesicle would measure 15-25 nm, which would be too small to package large cargos or a large number of cargos.

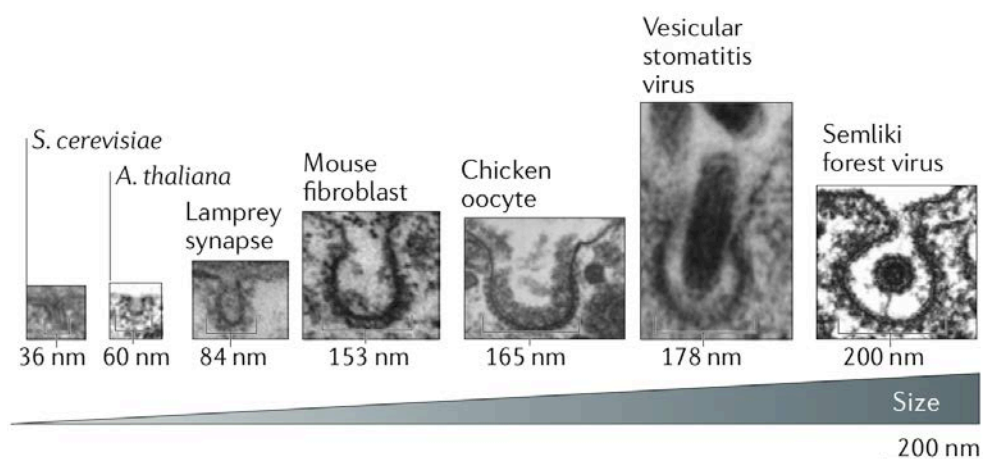


Figure 15 - Electron micrograph of clathrin-coated vesicles in various species

(from McMahon and Boucrot, 2011)

2.2.2.3 Clathrin localization

In animals, clathrin has been localized at the Golgi apparatus, the plasma membrane and endosomes. A similar localization of clathrin has been observed in the filamentous fungus *Aspergillus nidulans*, where clathrin was associated to the late Golgi, the endocytic collar and small, rapidly moving puncta that were seen trafficking long distances in nearly all hyphal compartments¹⁶³.

2.2.2.4 Clathrin-coated vesicles biogenesis

The formation of clathrin-coated vesicles can be divided in four steps. First, cargos are selected before clathrin assembly and membrane invagination. Then, the vesicle buds and, finally, the clathrin coat disassembles and is later recycled to induce the formation of new CCVs (Figure 16).

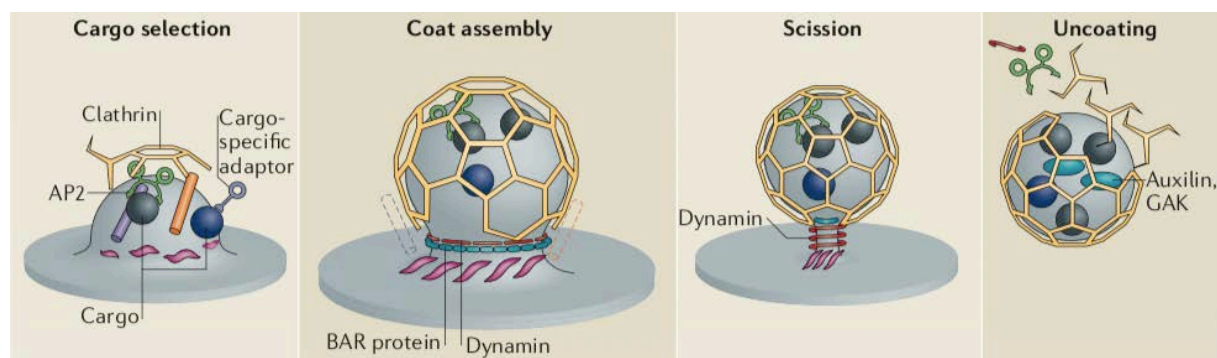


Figure 16 - Formation of clathrin coated vesicles

Schema of the four main steps of clathrin-coated vesicles formation.
(Modified from McMahon and Boucrot, 2011 - ¹⁵⁷)

The initiation of CCV formation starts with the recruitment of cargo adaptors such as adaptor proteins (APs) at the donor membrane. Adaptor proteins are also recruited by other proteins such as the GTPase Arf1. Once activated by the guanine exchange factor Big1/2, Arf1 associates with the donor membrane, and together with the cytoplasmic domain of the cargo, recruit APs¹⁶⁴. Then, adaptor proteins directly interact with clathrin¹⁶⁵ and the triskelion assembles, facilitating membrane invagination.

These cargo adaptors are also very important for the loading of cargos - the proteins carried by vesicles - into the nascent vesicle.

Cargo adaptors can be divided into distinct families: multimeric adaptor proteins including the adaptor protein family (APs), and monomeric adaptors, such as the Golgi localized γ ear-containing Arf binding proteins (GGAs) (Figure 17).

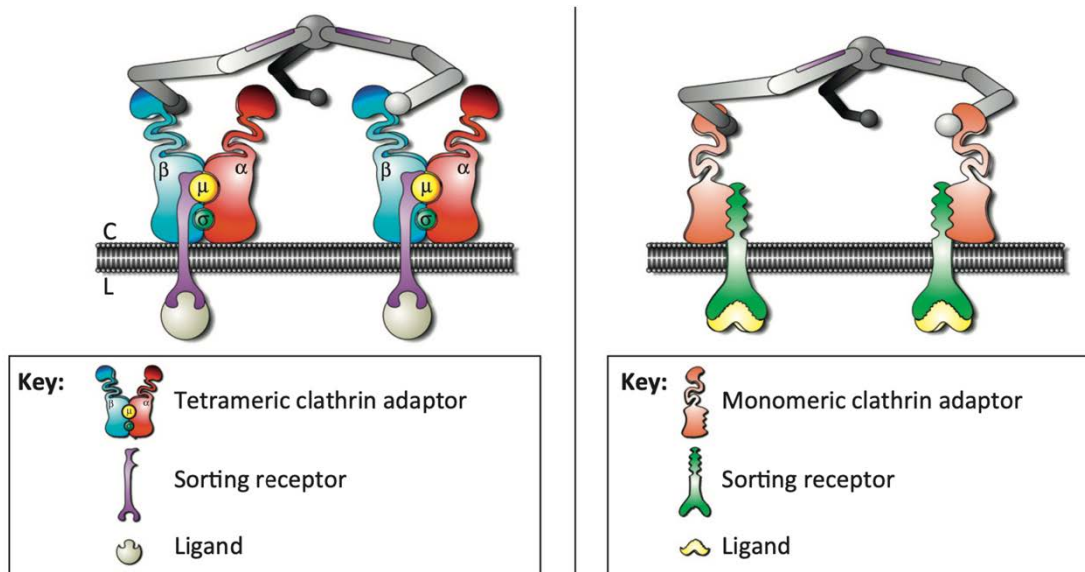


Figure 17 – Multimeric and monomeric clathrin adaptor proteins.

Adaptor proteins located in the cytoplasm (C) select transmembrane cargos and sorting receptors located in Golgi/Endosomes lumen. (Modified from Robinson and Pimpl, 2014 - 166)

APs are heterotetrameric proteins which stimulates clathrin lattice assembly. They are made of four subunits, one small (σ , ~20 kDa), one medium (μ , ~50 kDa), and two large subunits (α , γ , δ , ϵ , ζ ; and $\beta 1-5$ - ~100 kDa each). They interact with clathrin through the N-terminal domain of the clathrin heavy chain via the clathrin box consensus: “L Φ [D/E/N] Φ [D/E]” where Φ represents any bulky hydrophobic residue, localized in protein sequence of the β -subunit¹⁶⁷.

Adaptor proteins select cargos via recognizing specific motifs, called “sorting signals” located at cytoplasmic domains of transmembrane cargos. Two sorting signals are particularly well studied: the tyrosine-based (YXX Φ - where Φ can be either I, L, M, F or V ; X any amino acid) and the dileucine-based [DE]XXXL[LI]. The C-terminal domain of the μ -subunit of all adaptor proteins (except AP-5) recognizes the tyrosine-based motif. On the other hand, the dileucine-based motif is recognized by APs hemicomplexes: γ - σ^1 for AP-1, α - σ^2 for AP-2 and δ - σ^3 for AP-3^{168,169}.

Of the five APs found in animal cells, only three are localized at the Golgi apparatus: AP-1, AP-3, and AP-4, but only AP-1 can be associated with CCVs. Evidence shows that AP-1 is involved in bidirectional trafficking between the TGN and endosomes¹⁷⁰. In mammals, two AP-1 μ -subunit isoforms exist in epithelial cells. AP-1A isoform μA is the isoform associated with the TGN, while AP-1B, is localized at recycling endosomes^{171,172}. The former is involved in the polar sorting of cargos such as N-methyl-D-aspartate (NMDA)

Receptors, transferrin receptor (TfR), and also coxsackievirus and adenovirus receptor¹⁷³. In yeasts, AP-1 sorts the chitin synthase Chs3p¹⁷⁴.

A lot of research has been carried out on multimeric adaptor proteins. However, the monomeric adaptors GGAs, are less studied¹⁷⁰. Their biological functions remain elusive, and they probably have redundant functions¹⁷⁰. Mammalian cells have three GGAs (GGA1-GGA3), while the yeast *Saccharomyces cerevisiae* has only two GGAs. Like APs, they select cargos and bind to clathrin. They regulate the traffic of cargos such as sortilin and Mannose 6-phosphate Receptors (MPRs) from the TGN to endosomes^{175,176}. It is suggested they regulate anterograde trafficking from the TGN in coordination with AP-1.

Some accessory proteins, such as Epsins, control membrane curvature. Epsins are monomeric adaptors and contain the epsin N-terminal homology (ENTH) domain. This domain of roughly 150 amino acids binds to the phospholipid phosphoinositide (PI) and helps membrane invagination^{177,178}. Epsins recognize clathrin via multiple binding sites at the C-terminus and connect clathrin to the vesicle membrane.

Membrane trafficking is initiated by activated small protein G ADP ribosylation factor proteins (Arf). Once they have been activated by Guanine nucleotide exchange factors (GEFs), Arf associate with the membrane and recruit cargo adaptors^{179,180}. Arf can also induce the conformational change of cytoplasmic APs. Adaptor proteins need to open their conformation to recognize cargos¹⁸¹ (Figure 18).

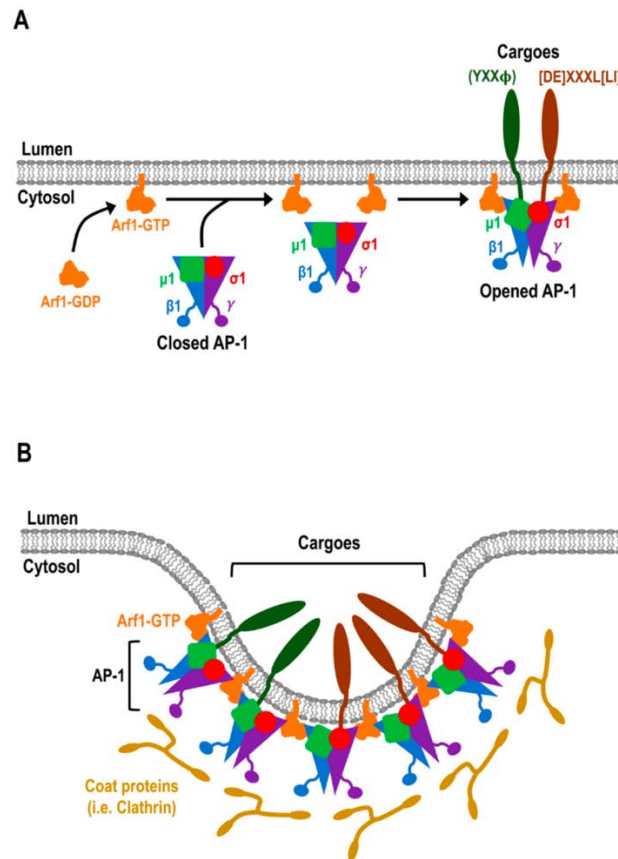


Figure 18 – Cargo sorting at the TGN

A) Activated Arf1 opens the conformation of AP-1. Opened AP-1 is then able to recognize sorting signals and sort cargos at the TGN. B) Recruited AP-1s recruit clathrin via the hinge-ear on the β -subunit - (Modified from Anson Tan and Gleeson, 2019 - 170)

With Arf, the phospholipid phosphatidylinositol 4-phosphate (PI4P), which is specifically enriched in TGN membranes, also contributes to the recruitment of cargo adaptors^{182,183}.

Once the adaptor proteins have recruited clathrin, other proteins proceed to the invagination of the membrane. Molecular actors have been described for vesicles deriving from clathrin-mediated endocytosis. Proteins with BAR (Bin-Amphiphysin-Rvs) and F-BAR domain are a class of cytosolic proteins with membrane-deforming properties. F-BAR domain proteins such as FCHo proteins interact with the donor membrane phospholipids. They form a curved structure by dimerizing themselves and sculpt the membrane¹⁸⁴. Amphiphysin, another F-BAR domain protein, interacts with clathrin and accentuate membrane curvature¹⁸⁵. BAR and F-BAR proteins also induce tubular invaginations of the plasma membrane by disrupting the actin cytoskeleton¹⁸⁶.

Clathrin-coated vesicle scission is mediated by the GTPase: Dynamin, which is recruited by amphiphysin. Dynamin induces the constriction of the donor membrane. Dynamin comprises a N—terminal G-domain which is connected to an α -helix which is involved in dynamin dimerization. Dynamin has also a pleckstrin homology (PH) domain that interacts with membranes phosphatidylinositol. G domains promotes the interaction between dynamin dimers and lead to their assembly into helical polymers at the neck of budding vesicles. Then GTP hydrolysis of dynamin results in membrane constriction (Figure 19). However, constriction of the vesicle neck by dynamin might not be sufficient for scission¹⁸⁷, and the vesicle detachment mechanism remains unclear¹⁸⁸.

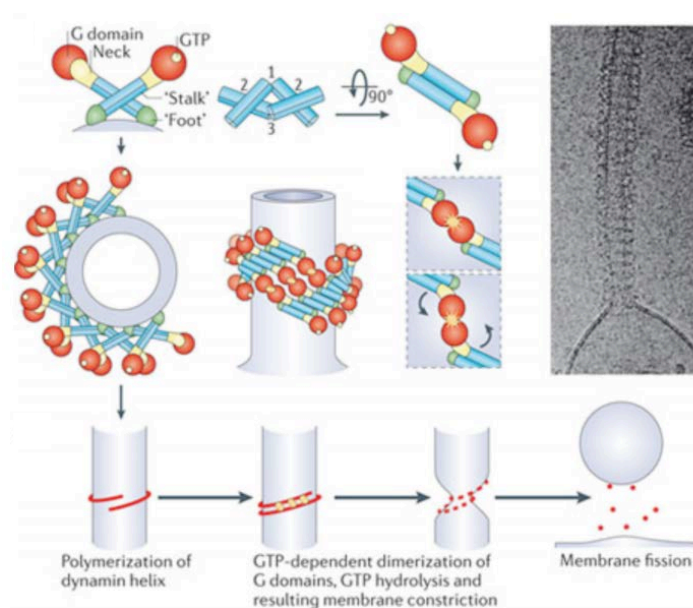


Figure 19 - Dynamin involvement in vesicle scission

Representation of dynamin dimers and the polymerization process leading to vesicle scission. The electron micrograph shows *in-vitro* dynamin polymerization which lead to the formation of a tubular structure on a liposome (from Ferguson and Camilli, 2012 - ¹⁸⁸)

Actin and molecular motors are likely to play a major role in vesicle scission during endocytosis. Myosin VI, which move towards the actin (-) end, attaches to clathrin-coated vesicles through the accessory protein Dab2 and PI(4,5)P₂¹⁸⁹. Moreover, myosin 1E, which move towards the actin (+) end, attaches to dynamin¹⁹⁰. Though, according to Ungewickell and Hinrichsen (2007), this suggests that myosin 1E might pull the dynamin ring toward the plasma membrane while myosin VI pulls the bud into the cytoplasm (Figure 20). Recently, it was shown that the interaction between myosin VI_{long} and clathrin-light chain CLCa was needed to generate the force that leads to invagination and fission of clathrin-coated pits at the apical surface of highly polarized cells¹⁹¹.

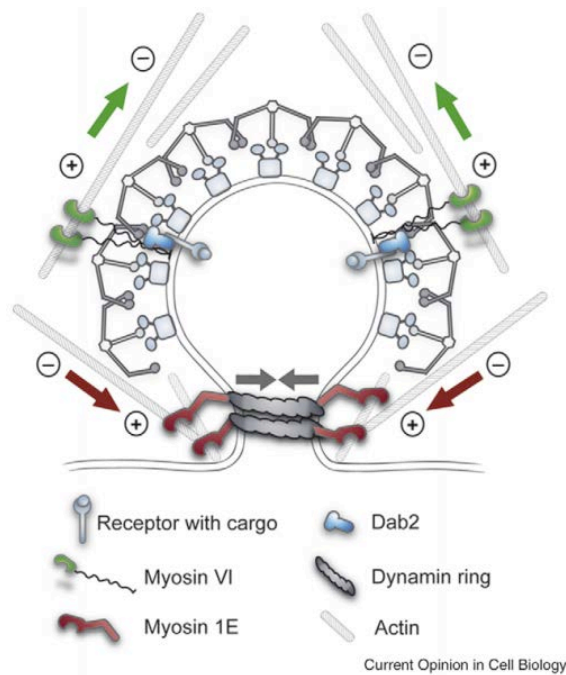


Figure 20 - Proposed model of the role of actin and molecular motors in clathrin-coated vesicle scission

The (+)-end motor myosin 1E, which attaches to Clathrin through Dab2, pulls the dynamin ring in the direction of the cell surface while the (-)-end motor myosin VI pulls the coated bud into the cytoplasm. (from Ungewickell and Hinrichsen, 2007 - ¹⁹²)

2.2.2.5 Clathrin-cage uncoating

Once the clathrin-coated vesicle has detached from the donor membrane, the protein coat is rapidly removed and recycled before the vesicle fuse to the acceptor membrane. The uncoating process involves two proteins: the DnaJ co-factor auxilin and the chaperone Hsc70. The first model was proposed by Ungewickell *et al.*, in 1995. Auxilin interacts with the C-terminal domain of the clathrin heavy chain which is involved in triskelion formation. Auxilin then recruits Hsc70:ATP. ATP hydrolysis of Hsc70:ATP promotes the binding of a second Hsc70:ATP and a third Hsc70:ATP is further recruited and hydrolysed. Hsc70:ADP has a higher affinity for clathrin than that of auxilin, and therefore produces clathrin-cage disassembly (Figure 21)¹⁹³.

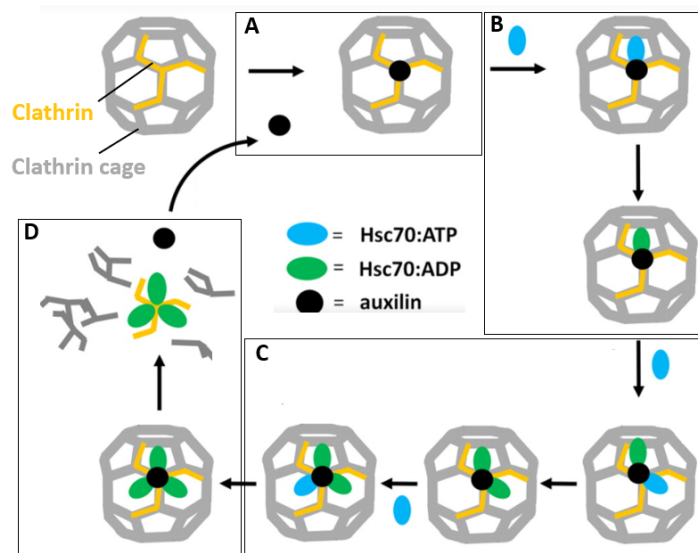


Figure 21 – Schematisation of clathrin coat uncoating

A) Auxilin interacts with clathrin heavy chain, B) Recruitment of Hsc70:ATP and interaction of Hsc70:ATP with auxilin. C) Recruitment of two additional Hsc70:ATP, D) Dissociation of clathrin triskelion and uncoating. (Modified from Rothnie *et al.*, 2011 - 193)

2.3 Secretory vesicles transport

Once secretory vesicles are formed, they are transported by the cytoskeleton to different exocytosis sites. In eukaryotic cells, the cytoskeleton is principally made of microtubules and actin.

2.3.1 Microtubules dependent transport

Microtubules are long and rigid structures composed of tubulin, a heterodimer of α - and β -tubulin (~ 50 KDa). Tubulin dimers polymerize and arrange to form a 25 nm hollow core. Microtubules have distinctive ends: a minus-end and a growing plus-end. These polarized ends determine the direction of travel of either proteins or organelles along microtubule tracks¹⁹⁴.

Long-range transport of organelles and secretory vesicles along microtubules relies on kinesin molecular motors. Kinesins are involved in the movement towards the plus-end (anterograde transport). Kinesin proteins vary in shape. Kinesin-1, is made of two kinesin heavy chain (KHC) and two kinesin light chain (KLC). The component that will be transported attaches to and is recognized by the light chain. Thus, kinesins transport only specific vesicles. In filamentous fungi, genomes encode between 10 to 12 kinesins^{195,196}. Dyneins transport material towards the minus-end (retrograde transport, Figure 22). Dyneins structure is more complex. They made of two identical heavy chains, and intermediate light chains. Filamentous fungi encode only one dynein^{195,196}. ATP hydrolysis drives the movement of kinesins and dyneins along microtubules.

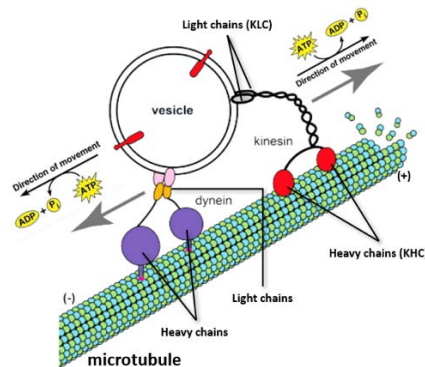


Figure 22 – Microtubule transport of vesicles

Kinesins mediate the transport of vesicles along microtubule toward the (+) end, while dyneins transport vesicles toward the (-) end. (Modified from Hey et al., 2022 - ¹⁹⁷)

In filamentous fungi, only a few studies report that SVs can be transported toward the hyphal tip using microtubule-based transport^{198–200}. In *Neurospora crassa* and *Aspergillus nidulans*, kinesin-1 mutants displayed a reduced delivery of extracellular enzymes and an impaired hyphal growth^{200–203}, suggesting that some SVs are transported along microtubules in filamentous fungi. In 2017, Penalva *et al.*,¹⁹⁹ identified a specific population of SVs that are transported along microtubules in *Aspergillus nidulans*. Indeed, they found that post-Golgi RAB11 secretory vesicles (sometimes referred as AP-1/RAB11 SVs) transport depends on kinesin-1.

2.3.2 Actin dependent transport

The actin cytoskeleton comprises G-actin proteins (43 kDa) which assemble to form two helicoidal filaments (F-actin)²⁰⁴. Like microtubules, actin filaments are polarized with a minus- and a plus-end. Actin filaments extend at the plus-end, while the minus end is less stable and prone to depolymerization.

Entities transported on F-actin are conveyed by myosin molecular motors. For example, myosin I and V are involved in the transport of vesicles toward the plus-end while myosin VI is implicated in retrograde transport towards the minus-end^{205,206}.

In filamentous fungi, F-actin has different structures: patches, cables, and rings, each associated with a specific function^{200,207–209}. Patches of actin can be found at the subapical-collar, approximately 5 μm behind the hyphal tip. Here, actin is associated with endocytosis^{200,208,210–212} where plasma membrane and polar cargos recycling takes place. There are also some reports of actin rings involved in septum formation^{200,213,214}. F-actin cables can also be found along hyphae and are involved in the transport of secretory vesicles, Golgi and/or endosomes across the cell²⁰⁰. In *Aspergillus nidulans*, when Rab11-secretory vesicles reach the hyphal tip, they are transferred to myosin 5 MyoE, and form the HUM complex made of the “hooking myosin to SVs” HMSV protein, the Rab11 effector UDS1 and MyoE¹⁰⁰ (Figure 23).

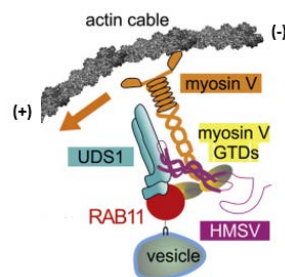


Figure 23 – Actin transport of Rab11-vesicles

The molecular motor myosin V conveys Rab11-secretory vesicles toward the (+) end of actin filaments and forms the HUM complex (HMSV, the rab11 effector UTS1, and MyoE). (Modified from Pinar *et al.*, 2022 - ¹⁰⁰)

2.4 Exocytosis in fungal hyphae

2.4.1 Apex directed exocytosis

2.4.1.1 *The Spitzenkörper: a conserved fungal structure made of micro- and macro-vesicles*

In Ascomycota and Basidiomycota, prior to exocytosis, secretory vesicles aggregate to form the so-called Spitzenkörper (Spk). This apical structure can be observed in mature growing hyphal apex, but not at the germling apex²¹⁵. The Spk was first identified in 1924 in *Coprinus* spp. and later observed in other fungal species through phase-contrast microscopy^{216–218}. In Zygomycete, no Spk can be observed. Instead, at the hyphal apex, vesicles accumulate just beneath the plasma membrane and form a crescent called the apical vesicular crescent (AVC). Both Spk and AVC are made of secretory vesicles that can vary in size (Figure 24).

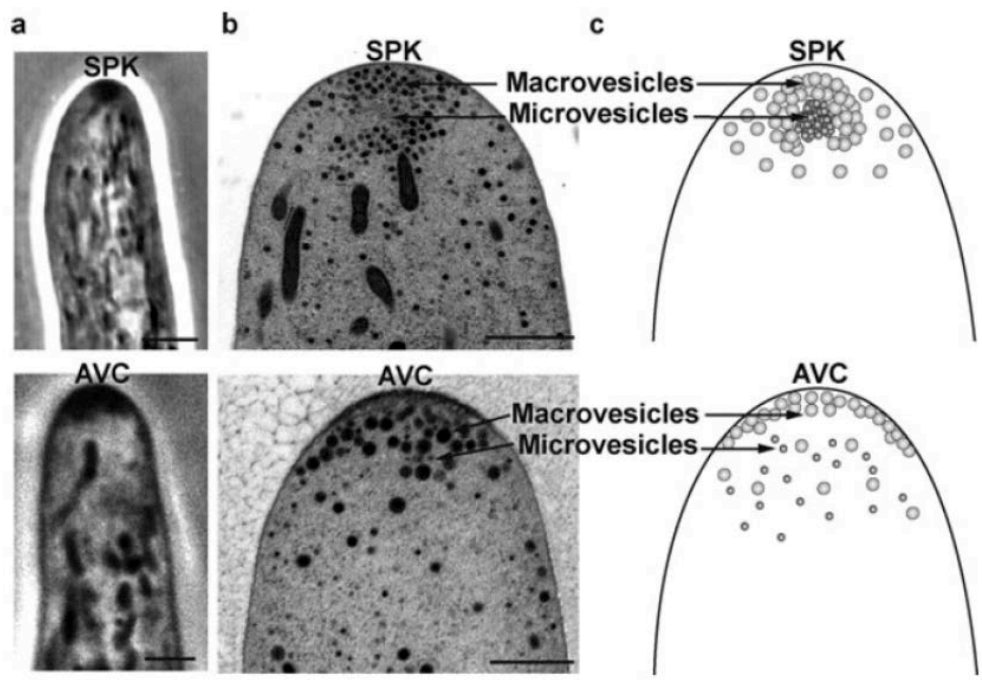


Figure 24 - The Spitzenkörper (Spk) and the apical vesicle crescent (AVC) at hyphal tip

Top panels: *Neurospora crassa* – bottom: *Mucor indicus* - **a**) Phase-contrast microscopy (scale bar, top: 3 μm , bottom : 1 μm) ; **b**) transmission electron microscopy (scale bars 1 μm) ; **c**) Spk and AVC organization (Modified from Riquelme *et al.*, 2016 - ²¹⁹)

In 2000, Fischer-Patron managed to stain the Spk of different species, including *Botrytis cinerea*, using FM4-64²²⁰, a lipophilic dye endocytosed at the plasma membrane.

The Spitzenkörper is made of secretory vesicles, microtubules, ribosomes and unidentified amorphous material^{217,221}. Despite its identification in several fungal species the Spk has only been well characterized in *Neurospora crassa*.

In *N. crassa*, the Spk is made of macrovesicles and microvesicles. This pattern has also been observed in *Botrytis cinerea* and *Aspergillus nidulans* where macro- and microvesicles, as well as other Spk components such as microfilaments were identified^{222,223} (Figure 25). In *Botrytis cinerea*, macrovesicles have a diameter: of 100 to 150 nm , while microvesicles are twice smaller (30 to 50 nm)²²⁴.

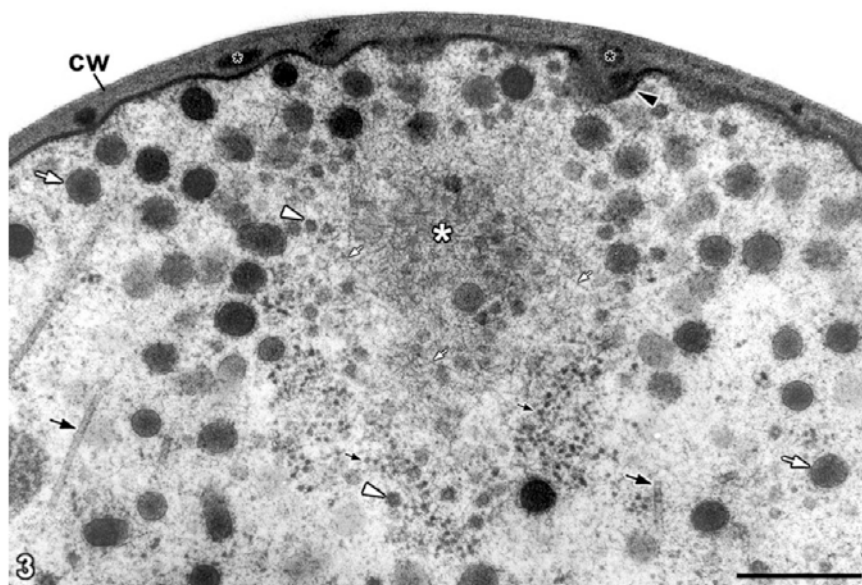


Figure 25 - The Spitzenkörper of *Botrytis cinerea* visualized by transmission electron microscopy

Apical vesicles (white arrows); microvesicles (white arrowheads); central core (asterisk); Microtubules (black arrows), Actin microfilaments (small black arrows); plasma membrane at sites of exocytosis (black arrowheads); ribosomes (small white arrows); cell wall (CW); cell wall inclusions (black asterisks). Scale bar, 200 nm (Modified from Roberson *et al.*, 2010 - ²²²)

2.4.1.2 Stratification of the Spitzenkörper

In the 1960s and 1970s, Bartnicki-Garcia and Bracker started to regard the Spk as a structure potentially involved in cell wall assembly. Several arguments suggested this hypothesis. First, the fact that hyphal growth occurs at the hyphal tip in filamentous fungi had been demonstrated for a hundred years ²²⁵. Secondly, the chitin monomer N-acetyl-D-glucosamine was found to be accumulated in *Mucor indicus* apex²²⁶. Finally, chitin was produced in small vesicles (chitosomes), *in-vitro*²²⁷. Indeed, Bracker, Ruiz-Herrera and Bartnicki-Garcia²²⁷ observed the formation of a coiled microfibril of chitin inside

chitosomes when the substrate (N-acetyl-D-glucosamine) and the acid protease rennilase were added to a purified fraction of chitosomes in *Mucor rouxii*.

When molecular tools and confocal microscopy emerged as powerful tools for the understanding of fungal biology, the team of Marixtell Riquelme decided to fluorescently tag a chitin synthase (CHS-1) and a glucan synthase associated protein (GS-1) to explore the hypothesis.

The localization of fluorescently tagged CHS-1 and GS-1 revealed a stratification of the Spk in *N. crassa*¹⁶⁰ (Figure 26). Indeed, CHS-1 was associated with the Spk core, which is made of microvesicles (30 to 50 nm diameter), while GS containing vesicles were associated to peripheral Spk macrovesicles²²⁸ (Figure 26), with a diameter ranging from 70 to 100 nm. In 2015, Sanchez-Leon and Riquelme further supported this finding: the GFP-tagged glucan synthase FKS1 accumulated at the outer layer of the Spk. Later, chitin synthases CHS-1, CHS-2, CHS-3, CHS-4, CHS-5 and CHS-6 were all found to localize at the Spk core in *N. crassa*^{140,229}.

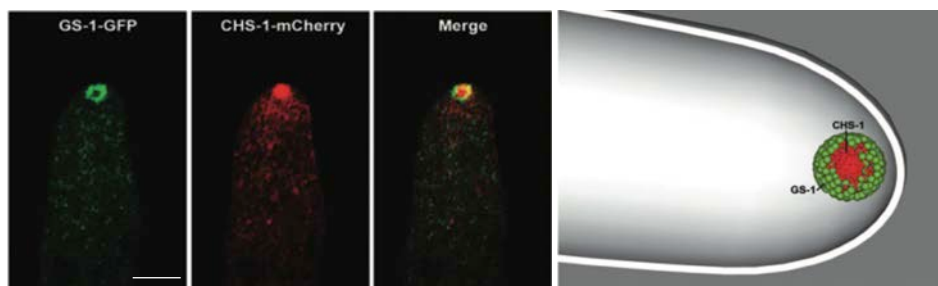


Figure 26 - Spk vesicles is made with GS containing macrovesicles and chitosomes

GS-1-GFP and CHS-1-mCherry spatial relationship. GS-1 is located at the peripheral Spk while CHS-1 is mainly located in the Spk core - scale bar = 5 μ m. (Modified from Verdin *et al.*, 2009 - ²²⁸)

Besides a Spk stratification based on CHS and GS localization, Rab GTPases also confirmed this characteristic of the Spk in *N. crassa*. Rab GTPases act as signaling molecules ensuring the arrival of the vesicles to the specific downstream compartment^{230,231}. The highly conserved small GTPases regulate vesicular trafficking through the action of guanine exchange factors (GEFs) and GTPases activating proteins (GAPs). In *N. crassa*, the Ypt31 ortholog YPT-31 was localized at the Spk peripheral layer (macrovesicles), so did SEC-4 (Sec4 ortholog) – (Figure 27). These findings suggest a potential role of YPT-1 in the regulation of chitosomes reaching the Spk in *N. crassa*²²⁹.

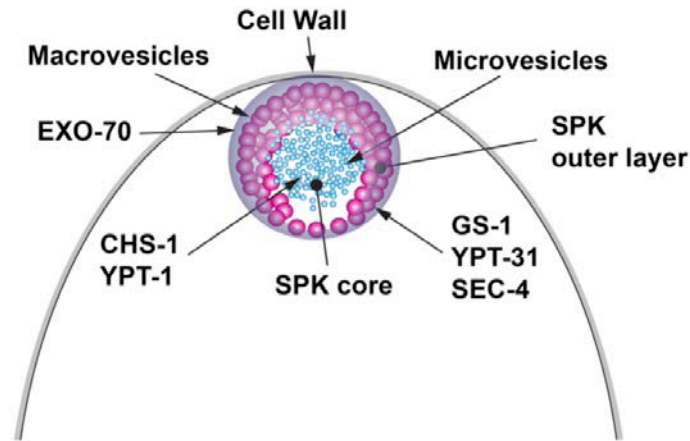


Figure 27 - RabGTPases localization in the Spitzenkörper in *Neurospora crassa*

Distribution of Rab GTPases at the Spk. Macrovesicles are shown in pink and are presumably associated the glucan synthase GS-1, two Rab GTPases: YPT-31 and SEC-4. The chitin synthase CHS-1 and the Rab GTPase YPT-1 were found in microvesicles (blue). Note that YPT-1 was also found in CHS pull downs experiments (CHS-1, CHS-4 and CHS-5). (Modified from Sanchez-Léon *et al.*, 2015 - ²³²)

Table 2 – Rab GTPases involved in anterograde transport

<i>S. cerevisiae</i>	Mammalian	<i>N. crassa</i>	<i>A. nidulans</i>	<i>B. cinerea</i>
Ypt1	Rab1	YPT-1	RabO	ND
Ypt31/32	Rab11	YPT-31	RabE	ND
Sec4	Rab8	SEC-4	ND	BcSAS1

Despite numerous observations made with fluorescent proteins, no one has suggested a stratification of the Spk similar to *N. crassa* in *A. nidulans*²³³ or any other filamentous fungi. In *A. nidulans*, RabO (Ypt1 ortholog) was also found at the Spk, but not at a specific layer, contrary to *N. crassa*, where YPT-1 was found at the Spk core. Moreover, the chitin synthase ChsB (CHS-1 ortholog in *N. crassa*) was also found at the Spk²³⁴, but not in any Spk layer (macro- or microvesicles) in *Aspergillus nidulans*. However, some observations support a stratification of the Spitzenkörper in *Aspergillus nidulans* based on flippase localization studies. These transmembrane lipid transporter proteins, belong to the ABC transporter family. Based on a H⁺ATPase activity, they catalyze the movement of phospholipid molecules between the two leaflets of the plasma membrane. A specific yet distinct localization of two flippases was reported by Penalva *et al.*, in 2015²³³. The flippases DnfA is localized at the Spk peripheral layer while DnfB at the core. They proposed that DnfA could be associated with macrovesicles and DnfB to microvesicles, further supporting the existence of different vesicles populations at the Spk (Figure 28).

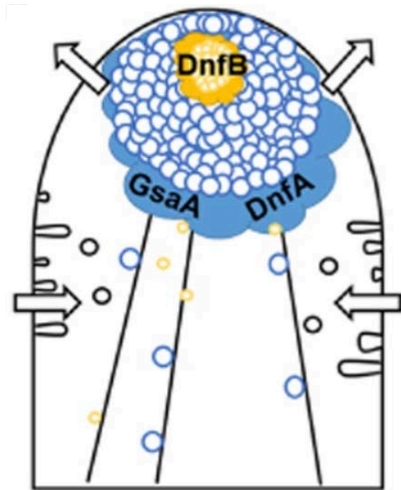


Figure 28 – Stratification of the Spk in *Aspergillus nidulans*

Model of Spk organization. Secretory vesicles (blue and yellow circles) travel to the fungal apex along microtubules (black lines). DnfA and glucan synthase subunit GsaA vesicles (blue) accumulate at the periphery of the Spitzenkörper, while DnfB vesicles (gold) accumulate at the Spk core. Arrows represent membrane flow out of (exocytosis) and into (endocytosis) the cell. (Modified from Schultzhaus, Yan and Shaw, 2015 - ²³⁵)

Recent findings highlight the fact that delivery of cell wall synthesizing enzymes in different vesicles population, as observed in *N. crassa*,^{141,228,229,236} might not be a general secretion mechanism. Experiments carried on the basidiomycete *Ustilago maydis* and the ascomycete *Zymoseptoria tritici* by Schuster et al.,^{237,238} challenged the dogma proposed by Riquelme. First, they fluorescently tagged the glucan synthase and chitin synthases. Then, they studied their localization using confocal microscopy and performed immunogold-labeling on enriched vesicles. They found that the class V chitin synthase Mcs1, the class VII chitin synthase Chs6 are transported with the glucan synthase Gsc1 in the same microvesicle (35 nm) in *Ustilago maydis*²³⁹. Similar results were also obtained in the ascomycete *Zymoseptoria tritici* where the class V chitin synthase ZtChs5 and the glucan synthase ZtGsc1 were also found to be transported in the same microvesicles (32 nm)²³⁷.

2.4.1.3 Spitzenkörper and cytoskeleton organization

According to Bartnicki-Garcia (2002)²⁴⁰ and Harris *et al.* (2005)²⁴¹, the Spitzenkörper can be regarded as a transfer station from microtubules to actin microfilaments (Figure 29).

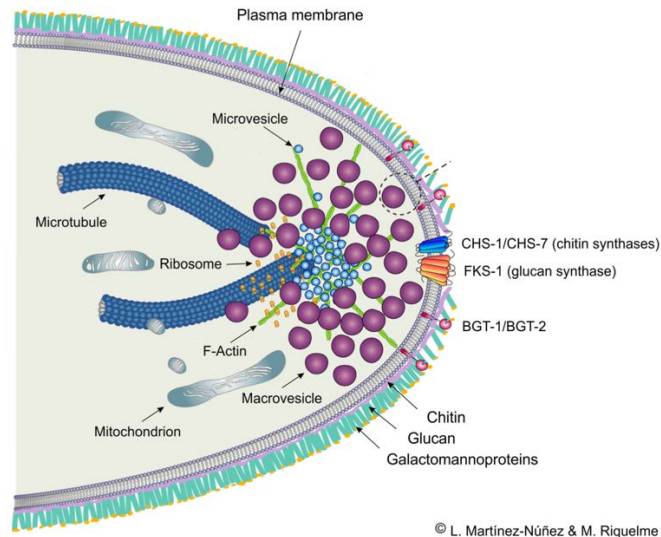


Figure 29 – *Neurospora crassa* hyphal tip and Spitzenkörper organization
(Modified from Steinberg *et al.*, 2017 - 91)

Cytoplasmic microtubules reaching the Spk are involved in long-distance traffic and are important for Spk stability, hyphal morphology and fast growth rates, but seem dispensable for vesicles to reach the Spk^{242,243}. However, in *Ustilago maydis*, long-range delivery of the class V chitin synthase depends on microtubules²⁴⁴. In *N. crassa*, the motor protein kinesin-1 KIN-1 is required for vesicular transport²⁴⁵. Surprisingly, in $\Delta kin-1$ mutants, , CHS-1 accumulated at the Spk but was not maintained on-axis²⁴⁶.

In filamentous fungi, actin is found at the Spk core^{208,210} and the endocytic collar^{208,210,247-251} and is thought to mediate vesicles flow to and from the Spk^{208,210}. When *N. crassa* was exposed to actin inhibitors such as Cytochalasin A or Latrunculin A, a mis-localization of several fungal cell wall enzymes such as CHS-1, CHS-4, β -1,3 endoglucanase BGT-1 and BGT-2, and the glucan synthase GS-1 was observed^{141,228,236,252,253}. Moreover, correct localization of class V and VII CHSs (containing a MMD) in *Ustilago maydis* (Mcs1) and *Aspergillus nidulans* (CsmA, CsmB) were also dependent on actin cytoskeleton^{244,254,255}.

Thus, generally, both actin and microtubules seem to be involved in tipwards motility of secretory vesicles.

2.4.1.4 The vesicle supply center model

In 1989, Bartnicki Garcia, Hergert and Gierz proposed a mathematical model explaining how a tubular shoe can be generated by a tip growing cell, based on three assumptions: 1) the cell surface expands from materials discharged by wall-destined vesicles, 2) that vesicles were released at the apex from a vesicle supply center (VSC), and 3) vesicles move from the VSC to the surface in any random direction²⁵⁶. The typical fungal hyphae shape was obtained when the VSC was moving towards a linear direction. The VSC position in the model corresponded to the Spk location in living hyphae, and therefore supported the idea that the Spk was essential for hyphal morphogenesis (Figure 30)²⁵⁶. Thus, according to the VSC model, the Spk act as a vesicle supply center where vesicles containing cell wall synthesis material aggregate before releasing their content to the apical plasma membrane through exocytosis. In other words, the Spk likely act as an exocytic regulatory structure which is able to receive and to distribute secretory vesicles^{256,257}.

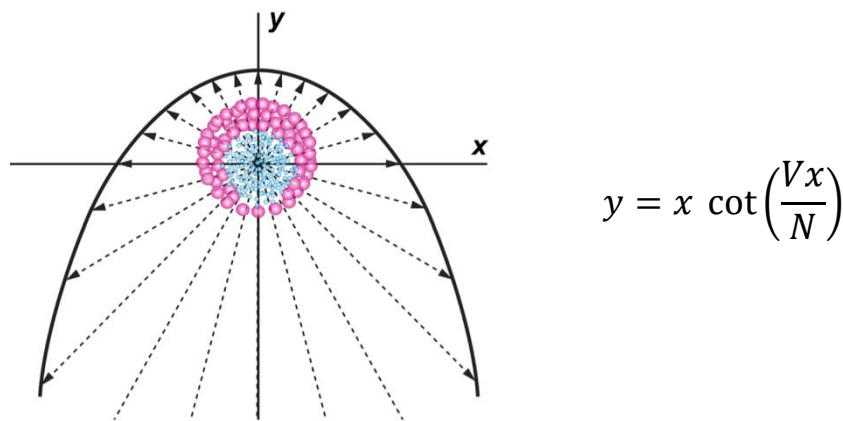


Figure 30 - Vesicle supply center (VSC) model

VSC model proposed by Bartnicki-Garcia *et al.* 1989. Pink vesicles: macrovesicles; blue vesicles: microvesicles (Modified from Sanchez-Léon *et al.*, 2015 - ²³²)

Equation defining both the shape and diameter of hyphae with V the rate of linear displacement of the VSC and N the number of wall-destined vesicles released from the VSC.

Surprisingly, in the plant-pathogenic fungus *Zymoseptoria tritici*, where chitin synthase ZtChs5 co-travels with glucan synthase ZtGsc1 in microvesicles, Schuster *et al.*, (2020) have shown that, these microvesicles do not transit in the Spitzenkörper, but directly fuse at the plasma membrane. Therefore, in slow growing fungi such as *Zymoseptoria tritici*, hyphae may not require a « distribution depot »²³⁸.

2.4.1.5 Exocytosis

Cargos transported by secretory vesicles are delivered to the plasma membrane or the extracellular medium through regulated exocytosis. This final step of the secretory pathway, is characterized by the fusion of secretory vesicles at a specific location, also allows the maintenance of lipids and proteins at the plasma membrane. In fungi, exocytosis is essential for polar growth, morphogenesis but also host-pathogen relationships and virulence¹⁻⁴. This process requires the exocyst which is a conserved multiprotein complex, made of 8 proteins: Sec3p, Sec5p, Sec6p, Sec8p, Sec10p, Sec15p, Exo70p and Exo84p²⁶¹⁻²⁶³. In the yeast *Saccharomyces cerevisiae*, the exocyst assembly is controlled by a number of RAB GTPases and directs the docking and the tethering of secretory vesicles to specific sites at the plasma membrane for the SNARE (soluble NSF-attachment protein receptor)-mediated fusion event^{261,264}. In yeast, the exocyst is divided in two subcomplexes; the Exo70 subcomplex, which is associated to secretory vesicles, and the Sec3 subcomplex, bound to the plasma membrane (Figure 31)²⁶⁵.

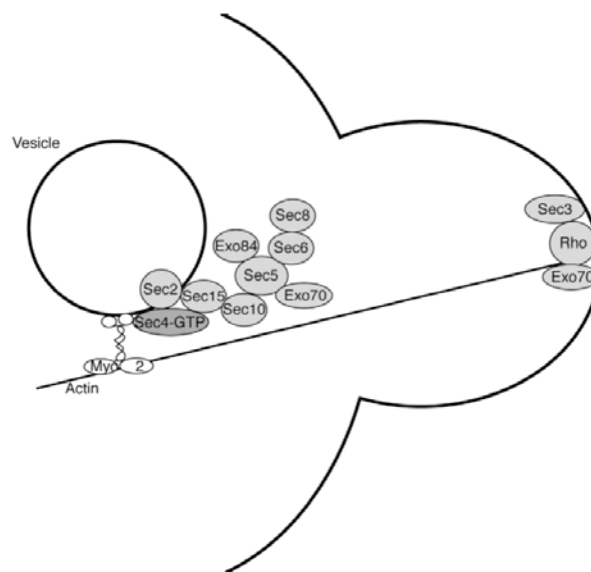


Figure 31 - *Saccharomyces cerevisiae* exocyst is divided in two sub-complexes

Most of the exocyst subunits associate with secretory vesicles before Sec3p binding at the bud tip. Exo70p ride vesicles to the sites of exocytosis and interacts with Rho3p at the bud tip. (Modified from Boyd *et al.*, 2004 - ²⁶⁵)

The exocyst components have been identified in numerous filamentous fungi: *Aspergillus nidulans*²⁰⁷, *Aspergillus niger*²⁶⁶, *Ashbya gossypii*²⁶⁷, *Aspergillus oryzae*²⁶⁸, *Magnaporthe oryzae*¹⁰⁶ and *Neurospora crassa*²⁵⁷ and each exocyst proteins are encoded by a single gene. In *N. crassa*, immunoaffinity purification of single exocyst proteins: SEC3, SEC5, SEC6, SEC8, EXO70 and EXO84 yielded the complete exocyst complex. The absence of RAB

GTPases involved in the exocyst regulation might be due to either dynamic or weak interactions between the exocyst and its regulators²⁵⁷.

Studies on filamentous fungi show that most of exocyst components are essential, and for those who are dispensable, mutations lead to important growth, morphology and virulence defects^{257,266,267,269,270}. After regrouping at the vesicle supply center, secretory vesicles are assumed to be further docked by the exocyst complex to the apical plasma membrane along actin microfilaments before exocytosis¹⁴⁷ - (Figure 32). However, exocyst assembly, localization and action appear to vary among different fungal groups and might be dependent on growth rates in some fungal species²⁷¹.

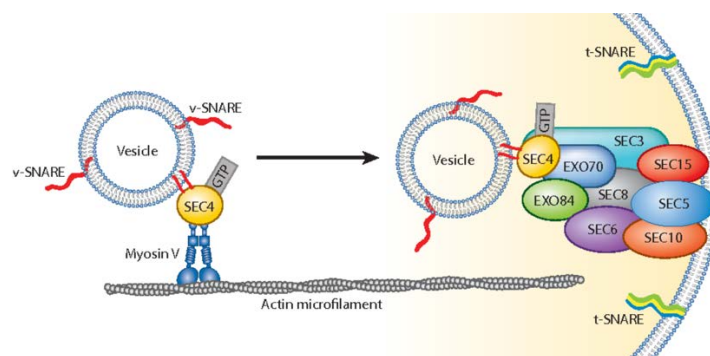


Figure 32 – The exocyst complex in *Neurospora crassa*

At the subapical region, secretory vesicles associate with the Rab GTPase SEC4 and travel along actin filaments via Myosin V. At the Spitzenkörper, the exocyst complex mediates vesicles docking to the plasma membrane, where v-SNAREs and t-SNAREs interact to promote vesicle fusion. (from Riquelme, 2013 - 147)

In *Ashiba gossypi*, when the growth rate is slow, the exocyst components AgExo70, AgSec3, and AgSec5 co-localize and form a “cortical cap” at the apex, whereas, when the growth rate is higher, this cap expands to form a sphere (Figure 33)²⁶⁷. However, in *N. crassa*, no correlation was observed between the localization pattern of EXO70 and the tip growth rate²⁵⁷. Despite, EXO70 and EXO84 were found at the peripheral layer of the Spitzenkörper, which is associated to macrovesicles. Other exocyst components SEC-5, -6, -8 and -15 formed a crescent at the apical plasma membrane. Interestingly, SEC-6 and EXO-70 localizations depend on actin and microtubule cytoskeletons, respectively. Moreover, an intact exocyst complex is necessary for organization of the Spitzenkörper, in *sec-5*⁽⁷⁻⁹⁾ mutant, macrovesicles accumulated and contained a more diverse content, ranging from electron dense to translucent with varying degrees of granularity²⁵⁷.

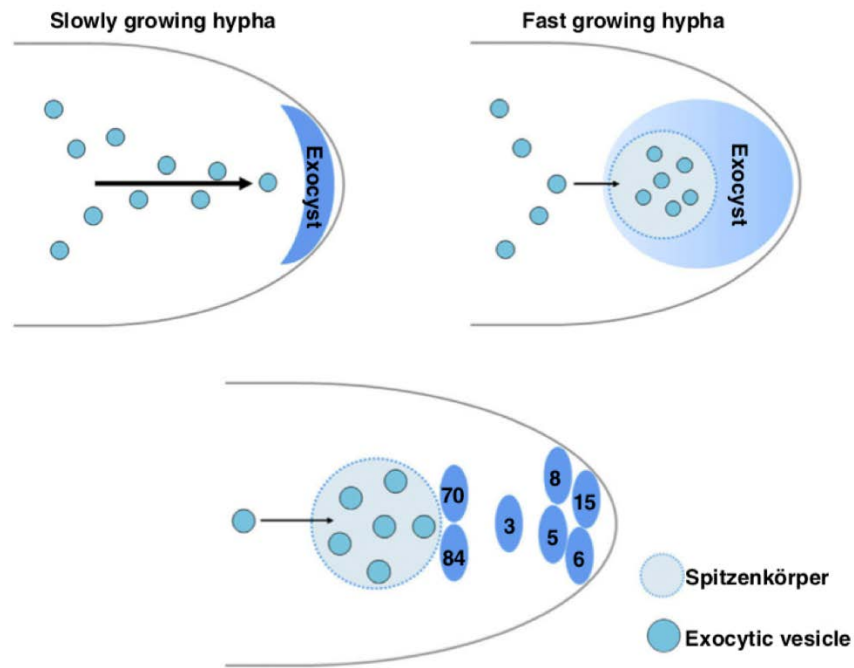


Figure 33 - Exocyst localization in two filamentous fungi

Top: *Ashbya gossypi* exocyst forms a crescentic cap at the slowly growing tip, and this accumulation pattern will be expanded to the Spitzenkörper at fast-growing hyphal tip. Bottom: in *Neurospora crassa*, EXO70 and EXO84 localize at the Spitzenkörper peripheral layer, while SEC5, SEC6, SEC8 and SEC15 are localized at the apical plasma membrane. SEC3 is somewhere in between. (Modified from Chen et al., 2015-²⁷¹)

Despite an essential role in fungal growth, the exocyst complex is anticipated to be a crucial component in fungal pathogenesis²⁷¹. In *M. oryzae*, the deletion of either *Sec5* or *Exo70* impaired the secretion of PWL2, a cytoplasmic effector which is secreted by UPS and lead to a significant loss in virulence. Surprisingly, the secretion of BAS4, an apoplasmic effector, secreted by CPS was not obviously block¹⁰⁶. In *Botrytis cinerea*, the homolog of the exocyst regulator Sec4 is involved in filamentous growth, conidiation and virulence²⁷⁰, further supporting the potential importance of the exocyst in fungal virulence. Surprisingly, the viability of Sec4 mutants in various filamentous fungi suggest the existence of extra secretory routes and/or unknown regulatory mechanisms that do not exist in yeasts²⁵⁷.

2.4.2 Non-apex directed exocytosis

In 1965, Robertson proposed the following dogma: ‘the key to the fungal hypha lies in the apex’²⁷². Mycologists have widely accepted this dogma for many years. Indeed, plenty of studies showed that the hyphal apex is the primary site of exocytosis of extracellular enzymes^{273,274}. However, this dogma is currently being questioned.

Localization of both the v-SNARE (SNC1) and the t-SNARE (SSO1) at the plasma membrane in subapical regions in the filamentous fungus *Trichoderma reesei* suggested that secretion could also occur in subapical regions²⁷⁵.

In 2011, Sanchez-Leon *et al.* demonstrated the exocytotic delivery of chitin synthases at septa in *Neurospora crassa*¹⁴¹, and now there is evidence that some hydrolytic enzymes can also be secreted from other hyphal regions, such as septa^{276,277}. In 2011, Hayakawa *et al.* were the first to show that the α -amylase AmyB accumulates in the Spitzenkörper at growing hyphal tips as well as septal periplasm in *Aspergillus oryzae* (Figure 34). More recently, similar results were obtained in the banana wilt fungal pathogen *Fusarium odoratissimum*, where the α -amylase AmyB was also found at septa²⁷⁷.

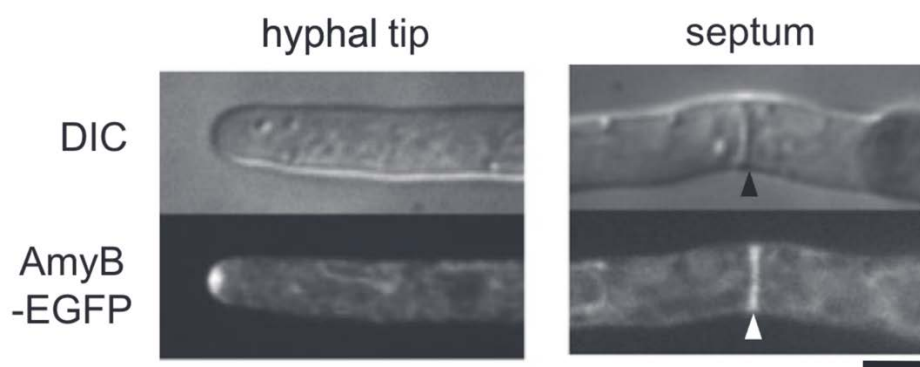


Figure 34 – Localization of the amylase AmyB in *Aspergillus oryzae*
The secreted α -amylase AmyB localizes at the hyphal tip and septa in *Aspergillus oryzae*.
Scale bar = 3 μ m. (Modified from Hayakawa *et al.*, 2011 - ²⁷⁶)

3 Thesis project

In many filamentous fungi, secretory vesicles accumulate at the hyphal apex of fast-growing hyphae and form the Spitzenkörper (Spk), an organized structure made of small vesicles at the Spk core, and larger vesicles at the periphery²⁰⁰. These vesicles are implicated in hyphal growth and nutrition via the transport of lipids, cell-wall synthases²²⁸, hydrolytic enzymes^{268,277}, and are thought to transport virulence factors in pathogenic filamentous fungi. While being important in the biology of filamentous fungi, the biogenesis process of secretory vesicles remains unclear.

In the laboratory a previous study identified clathrin, a protein involved in the biogenesis process of endocytic and exocytic vesicles in eukaryotes, as important for the delivery of hydrolytic enzymes and virulence factors in *B. cinerea*¹⁵⁰. Contrary to the current dogma in animals, in our necrotrophic model, clathrin seems to be more important to the exocytosis process rather than the endocytosis process. In *A. nidulans*, another filamentous fungi, Schultzhaus *et al.*²⁷⁸ found that the role of clathrin in endocytosis was also minor. These discoveries suggest that clathrin could play an important role in the biogenesis process of secretory vesicles in filamentous fungi.

In many eukaryotic organisms, clathrin interacts with the clathrin adaptor AP-1 at the Golgi apparatus and endosomes. AP-1 is a protein complex made of four subunits involved in the recognition and loading of specific transmembrane cargos into nascent vesicles. It has been previously shown that AP-1 is required for the biogenesis of secretory granules in the fruit fly *Drosophila melanogaster*²⁷⁹ and in mouse corticotrope tumor cells²⁸⁰. In the protist pathogen *Toxoplasma gondii*, AP-1 mediates the biogenesis of the Rhoptry secretory organelle²⁸¹. Finally, in the filamentous fungus *A. nidulans*, AP-1 is thought to sort secretory vesicles¹⁰¹.

So far, only a few studies focused on the role of AP-1 in the infectious strategies employed by eukaryotic pathogens. AP-1 is a virulence determinant in the protists *Toxoplasma gondii*²⁸², *Trypanosoma cruzi*²⁸³ and *Leishmania*²⁸⁴. In *T. cruzi*, AP-1 is required for the loading of cruzipain into vesicles, a secreted protease important for nutrition, virulence, and differentiation²⁸³. In plant-pathogenic fungi, the role of AP-1 has not been described so far.

In this thesis, we aimed at precisising the role of the clathrin adaptor AP-1 in the development, the virulence, and the biogenesis process of secretory vesicles in the plant-pathogenic fungus *B. cinerea*,

To decipher the role of AP-1 in the biology of *B. cinerea* and determine whether AP-1 was also involved in biological processes similar to those of clathrin, we performed a functional study of the gene encoding for $\beta 1$, one of the four subunits that constitutes the AP-1 complex. In order to identify protein cargos carried by the AP-1/Clathrin vesicles, we attempted an interactomic approach. At the same time, we explored different strategies for isolating intracellular vesicles. The development of this approach will also contribute to precise whether the AP-1/Clathrin machinery is involved in the biogenesis process of one of the two populations of vesicles forming the Spitzenkörper.

References

1. Treseder, K. & Lennon, J. Fungal Traits That Drive Ecosystem Dynamics on Land. (2015) doi:doi:10.1128/MMBR.00001-15.
2. Pappas, P. G. Opportunistic fungi: a view to the future. *Am. J. Med. Sci.* **340**, 253–257 (2010).
3. Hawksworth, D. & Lücking, R. Fungal Diversity Revisited: 2.2 to 3.8 Million Species. *Microbial Spectrum* **5**, (2017).
4. Anderson, P. K. *et al.* Emerging infectious diseases of plants: pathogen pollution, climate change and agrotechnology drivers. *Trends Ecol. Evol. (Amst.)* **19**, 535–544 (2004).
5. Shaw, M. W. & Osborne, T. M. Geographic distribution of plant pathogens in response to climate change. *Plant Pathology* **60**, 31–43 (2011).
6. Nnadi, N. E. & Carter, D. A. Climate change and the emergence of fungal pathogens. *PLoS Pathog* **17**, e1009503 (2021).
7. Brown, G. D. *et al.* Hidden killers: human fungal infections. *Sci Transl Med* **4**, 165rv13 (2012).
8. Life. <http://www.life-worldwide.org/media-centre/article/the-burden-of-fungal-disease-new-evidence-to-show-the-scale-of-the-problem>.
9. Brown, G., Denning, D. & Levitz, S. Tackling Human Fungal Infections. *Science* **336**, 647 (2012).
10. Fisher, M. C. *et al.* Threats Posed by the Fungal Kingdom to Humans, Wildlife, and Agriculture. *mBio* **11**, e00449-20 (2020).
11. Peleg, A., Hogan, D. & Mylonakis, E. Medically important bacterial-fungal interactions. *Nat Rev Microbiol* **8**, 340–349 (2010).
12. Datta, K. *et al.* Spread of *Cryptococcus gattii* into Pacific Northwest Region of the United States. *Emerg. Infect. Dis.* **15**, 1185–1191 (2009).
13. Bartlett, K. H., Kidd, S. E. & Kronstad, J. W. The emergence of *Cryptococcus gattii* in British Columbia and the Pacific Northwest. *Curr Infect Dis Rep* **10**, 58–65 (2008).
14. Greer, A., Ng, V. & Fisman, D. Climate change and infectious diseases in North America: the road ahead. *CMAJ* **178**, 715–722 (2008).
15. Fisher, M., Pasmans, F. & Martel, A. Virulence and Pathogenicity of Chytrid Fungi Causing Amphibian Extinctions. *Annual Review of Microbiology* **75**, 673–693 (2021).
16. Xie, G. Y., Olson, D. H. & Blaustein, A. R. Projecting the Global Distribution of the Emerging Amphibian Fungal Pathogen, *Batrachochytrium dendrobatidis*, Based on IPCC Climate Futures. *PLoS ONE* **11**, e0160746 (2016).
17. Bosch, J. *et al.* Microplastics increase susceptibility of amphibian larvae to the chytrid fungus *Batrachochytrium dendrobatidis*. *Sci Rep* **11**, 22438 (2021).
18. Hoyt, J. R., Kilpatrick, A. M. & Langwig, K. E. Ecology and impacts of white-nose syndrome on bats. *Nat Rev Microbiol* **19**, 196–210 (2021).
19. Berthon, K., Esperon-Rodriguez, M., Beaumont, L. J., Carnegie, A. J. & Leishman, M. R. Assessment and prioritisation of plant species at risk from myrtle rust (*Austropuccinia psidii*) under current and future climates in Australia. *Biological Conservation* **218**, 154–162 (2018).
20. Narouei-Khandan, H. A., Worner, S. P., Viljanen, S. L. H., Bruggen, A. H. C. & Jones, E. E. Projecting the suitability of global and local habitats for myrtle rust (*Austropuccinia psidii*) using model consensus. *Plant Pathol* **69**, 17–27 (2020).
21. *Plant Pathology*. (Elsevier, 1988). doi:10.1016/C2012-0-01423-8.
22. Savary, S. *et al.* The global burden of pathogens and pests on major food crops. *Nature Ecology & Evolution* **3**, 430–439.
23. Goertz, A. *et al.* Fusarium species and mycotoxin profiles on commercial maize hybrids in Germany. *Eur J Plant Pathol* **128**, 101–111 (2010).
24. Milus, E. A., Seyran, E. & McNew, R. Aggressiveness of *Puccinia striiformis* f. sp. *tritici* Isolates in the South-Central United States. *Plant Disease* **90**, 847–852 (2006).
25. Islam, M. T. *et al.* Emergence of wheat blast in Bangladesh was caused by a South

- American lineage of *Magnaporthe oryzae*. *BMC Biol* **14**, 84 (2016).
26. FAOSTAT. <http://www.fao.org/faostat/en/#home>.
 27. Fisher, M. C. *et al.* Emerging fungal threats to animal, plant and ecosystem health. *Nature* **484**, 186–194 (2012).
 28. Spanu, P. & Kämper, J. Genomics of biotrophy in fungi and oomycetes--emerging patterns. *Curr. Opin. Plant Biol.* **13**, 409–414 (2010).
 29. Doehlemann, G., Ökmen, B., Zhu, W. & Sharon, A. Plant Pathogenic Fungi. *Microbiology Spectrum* vol. 5 (2017).
 30. Faretra, F., Antonacci, E. & Pollastro, S. Sexual Behaviour and Mating System of *Botryotinia fuckeliana*, Teleomorph of *Botrytis cinerea*. *Microbiology*, **134**, 2543–2550 (1988).
 31. Elad, Y., Pertot, I., Cotes Prado, A. & Stewart, A. Chapitre 20 Plant Hosts of *Botrytis* spp. in *Botrytis - The Fungus the Pathogen and its Management in Agricultural Systems* 486 (2016).
 32. Elad, Y., Pertot, I., Cotes Prado, A. M. & Stewart, A. Plant Hosts of *Botrytis* spp. in *Botrytis – the Fungus, the Pathogen and its Management in Agricultural Systems* (eds. Fillinger, S. & Elad, Y.) 413–486 (Springer International Publishing, 2016). doi:10.1007/978-3-319-23371-0_20.
 33. Hua, L. *et al.* Pathogenic mechanisms and control strategies of *Botrytis cinerea* causing post-harvest decay in fruits and vegetables. *Food Qual Saf* **2**, 111–119 (2018).
 34. de Vallée, A. *et al.* A Similar Secretome Disturbance as a Hallmark of Non-pathogenic *Botrytis cinerea* ATMT-Mutants? *Front. Microbiol.* **10**, (2019).
 35. Choquer, M. *et al.* The infection cushion of *Botrytis cinerea*

48. Collado, I., Aleu, J., Hernandez-Galan, R. & Duran-Patron, R. Botrytis Species: An Intriguing Source of Metabolites with a Wide Range of Biological Activities. Structure, Chemistry and Bioactivity of Metabolites Isolated from Botrytis Species. *COC* **4**, 1261–1286 (2000).
49. Collado, I. G., Sánchez, A. J. M. & Hanson, J. R. Fungal terpene metabolites: biosynthetic relationships and the control of the phytopathogenic fungus *Botrytis cinerea*. *Nat. Prod. Rep.* **24**, 674 (2007).
50. Shiina, I. & Fukui, H. Chemistry and structural determination of botcinolides, botcinins, and botcinic acids. *Chem. Commun.* 385–400 (2009) doi:10.1039/B814375G.
51. Rebordinos, L., Cantoral, J. M., Prieto, M. V., Hanson, J. R. & Collado, I. G. The phytotoxic activity of some metabolites of *Botrytis cinerea*. *Phytochemistry* **42**, 383–387 (1996).
52. Rossi, F. R. *et al.* The Sesquiterpene Botrydial Produced by *Botrytis cinerea* Induces the Hypersensitive Response on Plant Tissues and Its Action Is Modulated by Salicylic Acid and Jasmonic Acid Signaling. *MPMI* **24**, 888–896 (2011).
53. Mauch-Mani, B. & Mauch, F. The role of abscisic acid in plant–pathogen interactions. *Current Opinion in Plant Biology* **8**, 409–414 (2005).
54. Cutler, H. G. *et al.* Botcinolide: A Biologically Active Natural Product from *Botrytis cinerea*. *Bioscience, Biotechnology, and Biochemistry* **57**, 1980–1982 (1993).
55. Cutler, H., Parker, S., Ross, S., Crumley, F. & Schreiner, P. Homobotcinolide: a biological active natural homolog of botcinolide from *Botrytis cinerea*. *Biosci Biotech Biochem* **60**, 656–658 (1996).
56. Dalmais, B. *et al.* The *Botrytis cinerea* phytotoxin botcinic acid requires two polyketide synthases for production and has a redundant role in virulence with botrydial. *Mol. Plant Pathol.* **12**, 564–579 (2011).
57. González, C., Brito, N. & Sharon, A. Chapter 12 - Infection Process and Fungal Virulence Factors. in *Botrytis - the Fungus, the Pathogen and its Management in Agricultural Systems* 486 (2016).
58. Wubben, J. P., Mulder, W., ten Have, A., van Kan, J. A. L. & Visser, J. Cloning and Partial Characterization of Endopolygalacturonase Genes from *Botrytis cinerea*. *Appl Environ Microbiol* **65**, 1596–1602 (1999).
59. Shao, D., Smith, D. L., Kabbage, M. & Roth, M. G. Effectors of Plant Necrotrophic Fungi. *Front. Plant Sci.* **12**, 687713 (2021).
60. Bi, K., Liang, Y., Mengiste, T. & Sharon, A. Killing softly: a roadmap of *Botrytis cinerea* pathogenicity. *Trends in Plant Science* S136013852200245X (2022) doi:10.1016/j.tplants.2022.08.024.
61. Kars, I. *et al.* Necrotizing activity of five *Botrytis cinerea* endopolygalacturonases produced in *Pichia pastoris*: Necrotizing activity of BcPGs. *The Plant Journal* **43**, 213–225 (2005).
62. Noda, J., Brito, N. & González, C. The *Botrytis cinerea* xylanase Xyn11A contributes to virulence with its necrotizing activity, not with its catalytic activity. *BMC Plant Biol* **10**, 38 (2010).
63. Frías, M., González, M., González, C. & Brito, N. A 25-Residue Peptide From *Botrytis cinerea* Xylanase BcXyn11A Elicits Plant Defenses. *Front. Plant Sci.* **10**, 474 (2019).
64. Yang, Y., Yang, X., Dong, Y. & Qiu, D. The *Botrytis cinerea* Xylanase BcXyl1 Modulates Plant Immunity. *Front. Microbiol.* **9**, 2535 (2018).
65. Zhu, W. *et al.* BcXYG1, a Secreted Xyloglucanase from *Botrytis cinerea*, Triggers Both Cell Death and Plant Immune Responses. *Plant Physiol.* **175**, 438–456 (2017).
66. Zhang, Y. *et al.* BcGs1, a glycoprotein from *Botrytis cinerea*, elicits defence response and improves disease resistance in host plants. *Biochemical and Biophysical Research Communications* **457**, 627–634 (2015).
67. Frías, M., González, M., González, C. & Brito, N. BcIEB1, a *Botrytis cinerea* secreted protein, elicits a defense response in plants. *Plant Science* **250**, 115–124 (2016).
68. Bi, K. *et al.* The *Botrytis cinerea* Crh1 transglycosylase is a cytoplasmic effector triggering plant cell death and defense response. *Nat Commun* **12**, 2166 (2021).
69. Zhu, W. *et al.* *Botrytis cinerea* BcSSP2 protein is a late infection phase, cytotoxic

- effector. *Environmental Microbiology* (2022) doi:<https://doi.org/10.1111/1462-2920.15919>.
70. Frías, M., González, C. & Brito, N. BcSpl1, a cerato-platanin family protein, contributes to *Botrytis cinerea* virulence and elicits the hypersensitive response in the host. *New Phytologist* **192**, 483–495 (2011).
 71. Weiberg, A. *et al.* Fungal small RNAs suppress plant immunity by hijacking host RNA interference pathways. *Science* **342**, 118–123 (2013).
 72. Qin, S. *et al.* Molecular characterization reveals no functional evidence for naturally occurring cross-kingdom RNA interference in the early stages of *Botrytis cinerea* –tomato interaction. *Molecular Plant Pathology* mpp.13269 (2022) doi:10.1111/mpp.13269.
 73. Novick, P., Field, C. & Schekman, R. Identification of 23 complementation groups required for post-translational events in the yeast secretory pathway. *Cell* **21**, 205–215 (1980).
 74. The Nobel Prize in Physiology or Medicine 2013. *NobelPrize.org*. vol. Nobel Prize Outreach AB 2022.
 75. Mellman, I. & Emr, S. D. A Nobel Prize for membrane traffic: Vesicles find their journey's end. *Journal of Cell Biology* **203**, 559–561 (2013).
 76. Cross, B. C. S., Sinning, I., Luirink, J. & High, S. Delivering proteins for export from the cytosol. *Nat. Rev. Mol. Cell Biol.* **10**, 255–264 (2009).
 77. Reithinger, J. Membrane protein biogenesis in *Saccharomyces cerevisiae*. (Department of Biochemistry and Biophysics, Stockholm University, 2013).
 78. Lommel, M. & Strahl, S. Protein O-mannosylation: conserved from bacteria to humans. *Glycobiology* **19**, 816–828 (2009).
 79. Heimel, K. Unfolded protein response in filamentous fungi-implications in biotechnology. *Appl. Microbiol. Biotechnol.* **99**, 121–132 (2015).
 80. Chen, C., Bonifacino, J. S., Yuan, L. C. & Klausner, R. D. Selective degradation of T cell antigen receptor chains retained in a pre-Golgi compartment. *J. Cell Biol.* **107**, 2149–2161 (1988).
 81. Amara, J. F., Lederkremer, G. & Lodish, H. F. Intracellular degradation of unassembled asialoglycoprotein receptor subunits: a pre-Golgi, nonlysosomal endoproteolytic cleavage. *J. Cell Biol.* **109**, 3315–3324 (1989).
 82. Ng, D. T., Spear, E. D. & Walter, P. The unfolded protein response regulates multiple aspects of secretory and membrane protein biogenesis and endoplasmic reticulum quality control. *J. Cell Biol.* **150**, 77–88 (2000).
 83. Travers, K. J. *et al.* Functional and genomic analyses reveal an essential coordination between the unfolded protein response and ER-associated degradation. *Cell* **101**, 249–258 (2000).
 84. Hong, E., Davidson, A. R. & Kaiser, C. A. A pathway for targeting soluble misfolded proteins to the yeast vacuole. *J. Cell Biol.* **135**, 623–633 (1996).
 85. Coughlan, C. M., Walker, J. L., Cochran, J. C., Wittrup, K. D. & Brodsky, J. L. Degradation of mutated bovine pancreatic trypsin inhibitor in the yeast vacuole suggests post-endoplasmic reticulum protein quality control. *J. Biol. Chem.* **279**, 15289–15297 (2004).
 86. Kruse, K. B., Brodsky, J. L. & McCracken, A. A. Characterization of an ERAD gene as VPS30/ATG6 reveals two alternative and functionally distinct protein quality control pathways: one for soluble Z variant of human alpha-1 proteinase inhibitor (A1PiZ) and another for aggregates of A1PiZ. *Mol. Biol. Cell* **17**, 203–212 (2006).
 87. Hampton, R. Y. ER-associated degradation in protein quality control and cellular regulation. *Current Opinion in Cell Biology* **14**, 476–482 (2002).
 88. Barlowe, C. *et al.* COPII: A membrane coat formed by Sec proteins that drive vesicle budding from the endoplasmic reticulum. *Cell* **77**, 895–907 (1994).
 89. Conesa, A., Punt, P. J., van Luijk, N. & van den Hondel, C. A. M. J. J. The Secretion Pathway in Filamentous Fungi: A Biotechnological View. *Fungal Genetics and Biology* **33**, 155–171 (2001).
 90. Brandizzi, F. & Barlowe, C. Organization of the ER–Golgi interface for membrane traffic control. *Nature Reviews Molecular Cell Biology* **14**, 382–392 (2013).
 91. Steinberg, G., Penalva, M., Riquelme, M., Wösten, H. & Harris, S. Cell biology of hyphal growth. *Microbial Spectrum* **5**, 231–265 (2017).

92. Klumperman, J. Architecture of the mammalian Golgi. *Cold Spring Harb Perspect Biol* **3**, (2011).
93. Pantazopoulou, A. The Golgi apparatus: insights from filamentous fungi. *Mycologia* **108**, 603–622 (2016).
94. Pantazopoulou, A. & Peñalva, M. A. Characterization of *Aspergillus nidulans* RabC/Rab6. *Traffic* **12**, 386–406 (2011).
95. Breakspear, A., Langford, K. J., Momany, M. & Assinder, S. J. CopA:GFP localizes to putative Golgi equivalents in *Aspergillus nidulans*. *FEMS Microbiol. Lett.* **277**, 90–97 (2007).
96. Pantazopoulou, A. & Peñalva, M. A. Organization and dynamics of the *Aspergillus nidulans* Golgi during apical extension and mitosis. *Mol. Biol. Cell* **20**, 4335–4347 (2009).
97. Shoji, J., Arioka, M. & Kitamoto, K. Dissecting cellular components of the secretory pathway in filamentous fungi: insights into their application for protein production. *Biotechnol Lett* **30**, 7–14 (2008).
98. Howard, R. J. Ultrastructural analysis of hyphal tip cell growth in fungi: Spitzenkörper, cytoskeleton and endomembranes after freeze-substitution. *J Cell Sci* **48**, 89–103 (1981).
99. Pantazopoulou, A., Pinar, M., Xiang, X. & Penalva, M. Maturation of late Golgi cisternae into RabERab11 exocytic post-Golgi carriers visualized in vivo. 2428–2443 (2014).
100. Pinar, M. *et al.* The type V myosin-containing complex HUM is a RAB11 effector powering movement of secretory vesicles. *iScience* **25**, 104514 (2022).
101. Martzoukou, O., Diallinas, G. & Amillis, S. Secretory vesicle polar sorting, endosome recycling and cytoskeleton organisation require the AP-1 complex in *Aspergillus nidulans*. **209**, 1121–1138 (2018).
102. Dimou, S. & Diallinas, G. Life and Death of Fungal Transporters under the Challenge of Polarity. *IJMS* **21**, 5376 (2020).
103. Sorgo, A. G., Heilmann, C. J., Brul, S., de Koster, C. G. & Klis, F. M. Beyond the wall: *Candida albicans* secret(e)s to survive. *FEMS Microbiol. Lett.* **338**, 10–17 (2013).
104. Vivek-Ananth, R. P. *et al.* Comparative systems analysis of the secretome of the opportunistic pathogen *Aspergillus fumigatus* and other *Aspergillus* species. *Sci Rep* **8**, 6617 (2018).
105. Agrawal, G. K., Jwa, N.-S., Lebrun, M.-H., Job, D. & Rakwal, R. Plant secretome: Unlocking secrets of the secreted proteins. *Proteomics* **10**, 799–827 (2010).
106. Giraldo, M. C. *et al.* Two distinct secretion systems facilitate tissue invasion by the rice blast fungus *Magnaporthe oryzae*. *Nat Commun* **4**, 1996 (2013).
107. Miya, A. *et al.* CERK1, a LysM receptor kinase, is essential for chitin elicitor signaling in *Arabidopsis*. *Proc. Natl. Acad. Sci. U.S.A.* **104**, 19613–19618 (2007).
108. Peyroche, A. *et al.* Brefeldin A acts to stabilize an abortive ARF-GDP-Sec7 domain protein complex: involvement of specific residues of the Sec7 domain. *3* 275–285 (1999).
109. Kubicek, C. P., Starr, T. L. & Glass, N. L. Plant cell wall-degrading enzymes and their secretion in plant-pathogenic fungi. *Annu Rev Phytopathol* **52**, 427–451 (2014).
110. Rabouille, C. Pathways of Unconventional Protein Secretion. *Trends in Cell Biology* **27**, 230–240 (2017).
111. Pathirana, R. D. & Kaparakis-Liaskos, M. Bacterial membrane vesicles: Biogenesis, immune regulation and pathogenesis. *Cell. Microbiol.* **18**, 1518–1524 (2016).
112. Maas, S. L. N., Breakefield, X. O. & Weaver, A. M. Extracellular Vesicles: Unique Intercellular Delivery Vehicles. *Trends Cell Biol.* **27**, 172–188 (2017).
113. Bielska, E. & May, R. C. Extracellular vesicles of human pathogenic fungi. *Current Opinion in Microbiology* **52**, 90–99 (2019).
114. Rybak, K. & Robatzek, S. Functions of Extracellular Vesicles in Immunity and Virulence[OPEN]. *Plant Physiol* **179**, 1236–1247 (2019).
115. Albuquerque, P. C. *et al.* Vesicular transport in *Histoplasma capsulatum*: an effective mechanism for trans-cell wall transfer of proteins and lipids in ascomycetes. *Cell. Microbiol.* **10**, 1695–1710 (2008).
116. Rodrigues, M. L. *et al.* Vesicular polysaccharide export in *Cryptococcus neoformans* is a eukaryotic solution to the problem of fungal trans-cell wall transport. *Eukaryotic Cell* **6**, 48–

- 59 (2007).
117. Rodrigues, M. L. *et al.* Extracellular Vesicles Produced by *Cryptococcus neoformans* Contain Protein Components Associated with Virulence. *Eukaryot Cell* **7**, 58–67 (2008).
 118. Reis, F. C. G. *et al.* A Novel Protocol for the Isolation of Fungal Extracellular Vesicles Reveals the Participation of a Putative Scramblase in Polysaccharide Export and Capsule Construction in *Cryptococcus gattii*. *mSphere* **4**, (2019).
 119. Silva, B. M. A. *et al.* Characterization of *Alternaria infectoria* extracellular vesicles. *Med Mycol* **52**, 202–210 (2014).
 120. Bitencourt, T. A. *et al.* Extracellular Vesicles From the Dermatophyte *Trichophyton interdigitale* Modulate Macrophage and Keratinocyte Functions. *Front Immunol* **9**, 2343 (2018).
 121. Liu, M., Bruni, G. O., Taylor, C. M., Zhang, Z. & Wang, P. Comparative genome-wide analysis of extracellular small RNAs from the mucormycosis pathogen *Rhizopus delemar*. *Scientific Reports* **8**, 1–10 (2018).
 122. de Paula, R. G. *et al.* Extracellular vesicles carry cellulases in the industrial fungus *Trichoderma reesei*. *Biotechnol Biofuels* **12**, 146 (2019).
 123. Samuel, A. Z. *et al.* Raman Microspectroscopy Imaging Analysis of Extracellular Vesicles Biogenesis by Filamentous Fungus *Penicillium chrysogenum*. *Advanced Biology* **6**, 2101322 (2022).
 124. Bleackley, M. R. *et al.* Extracellular Vesicles From the Cotton Pathogen *Fusarium oxysporum* f. sp. *vasinfectum* Induce a Phytotoxic Response in Plants. *Frontiers in Plant Science* **10**, 1610 (2020).
 125. Garcia-Ceron, D. *et al.* Extracellular Vesicles from *Fusarium graminearum* Contain Protein Effectors Expressed during Infection of Corn. *JoF* **7**, 977 (2021).
 126. Hill, E. H. & Solomon, P. S. Extracellular vesicles from the apoplastic fungal wheat pathogen *Zymoseptoria tritici*. *Fungal Biol Biotechnol* **7**, 13 (2020).
 127. Kwon, S. *et al.* mRNA Inventory of Extracellular Vesicles from *Ustilago maydis*. *JoF* **7**, 562 (2021).
 128. Rutter, B. D. *et al.* The development of extracellular vesicle markers for the fungal phytopathogen *Colletotrichum higginsianum*. *J of Extracellular Vesicle* **11**, (2022).
 129. Colombo, M., Raposo, G. & Théry, C. Biogenesis, secretion, and intercellular interactions of exosomes and other extracellular vesicles. *Annu. Rev. Cell Dev. Biol.* **30**, 255–289 (2014).
 130. Souza, J. A. M. *et al.* Characterization of *Aspergillus fumigatus* Extracellular Vesicles and Their Effects on Macrophages and Neutrophils Functions. *Front. Microbiol.* **10**, 2008 (2019).
 131. Zhao, K. *et al.* Extracellular vesicles secreted by *Saccharomyces cerevisiae* are involved in cell wall remodelling. *Communications Biology* **2**, 1–13 (2019).
 132. Rizzo, J., Rodrigues, M. L. & Janbon, G. Extracellular Vesicles in Fungi: Past, Present, and Future Perspectives. *Front. Cell. Infect. Microbiol.* **10**, 346 (2020).
 133. Joffe, L. S., Nimrichter, L., Rodrigues, M. L. & Poeta, M. D. Potential Roles of Fungal Extracellular Vesicles during Infection. *mSphere* **1**, (2016).
 134. Shoji, J., Kikuma, T. & Kitamoto, K. Vesicle trafficking, organelle functions, and unconventional secretion in fungal physiology and pathogenicity. *Curr. Opin. Microbiol.* **20**, 1–9 (2014).
 135. Hurley, J. H. ESCRT complexes and the biogenesis of multivesicular bodies. *Curr. Opin. Cell Biol.* **20**, 4–11 (2008).
 136. Zarnowski, R. *et al.* *Candida albicans* biofilm-induced vesicles confer drug resistance through matrix biogenesis. *PLOS Biology* **16**, e2006872 (2018).
 137. Yi, M. & Valent, B. Communication between filamentous pathogens and plants at the biotrophic interface. *Annu Rev Phytopathol* **51**, 587–611 (2013).
 138. Micali, C. O., Neumann, U., Grunewald, D., Panstruga, R. & O’Connell, R. Biogenesis of a specialized plant-fungal interface during host cell internalization of *Golovinomyces orontii* haustoria. *Cell. Microbiol.* **13**, 210–226 (2011).
 139. Samuel, M., Bleackley, M., Anderson, M. & Mathivanan, S. Extracellular vesicles

including exosomes in cross kingdom regulation: a viewpoint from plant-fungal interactions. *Front. Plant Sci.* **6**, (2015).

140. Riquelme, M. *et al.* Spitzenkörper localization and intracellular traffic of green fluorescent protein-labeled CHS-3 and CHS-6 chitin synthases in living hyphae of *Neurospora crassa*. **6**, 1853–1864 (2007).

141. Sánchez-León, E. *et al.* Traffic of Chitin Synthase 1 (CHS-1) to the Spitzenkörper and Developing Septa in Hyphae of *Neurospora crassa*: Actin Dependence and Evidence of Distinct Microvesicle Populations. *Eukaryotic cell* **10**, 683–95 (2011).

142. Hernández-González, M. *et al.* Endocytic recycling via the TGN underlies the polarized hyphal mode of life. *PLoS Genet* **14**, e1007291 (2018).

143. Stock, P. *et al.* Applying unconventional secretion of the endochitinase Cts1 to export heterologous proteins in *Ustilago maydis*. *J Biotechnol* 80–91 (2012).

144. Iturriaga, G., Jefferson, R. & Bevan, M. Endoplasmic Reticulum Targeting and Glycosylation of Hybrid Proteins in Transgenic Tobacco. *The Plant Cell* **1**, 381–390 (1989).

145. Banik, S., Pal, S., Chowdhury, S., Ghorai, S. & Khowala, S. Evidence of an alternative route of cellobiase secretion in the presence of brefeldin A in the filamentous fungus *Termitomyces clypeatus*. 412–420 (2011).

146. Dimou, S. *et al.* Translocation of nutrient transporters to cell membrane via Golgi bypass in *Aspergillus nidulans*. *EMBO Reports* **21**, (2020).

147. Riquelme, M. Tip growth in filamentous fungi: a road trip to the apex. *Annu. Rev. Microbiol.* **67**, 587–609 (2013).

148. Harsay, E. & Bretscher, A. Parallel secretory pathways to the cell surface in yeast. *The Journal of Cell Biology* **131**, 297–310 (1995).

149. Gurunathan, S., David, D. & Gerst, J. E. Dynamin and clathrin are required for the biogenesis of a distinct class of secretory vesicles in yeast. *EMBO J* **21**, 602–614 (2002).

150. Souibgui, E. *et al.* Clathrin Is Important for Virulence Factors Delivery in the Necrotrophic Fungus *Botrytis cinerea*. *Front. Plant Sci.* **12**, 668937 (2021).

151. Bairwa, G., Caza, M., Horianopoulos, L., Hu, G. & Kronstad, J. Role of clathrin-mediated endocytosis in the use of heme and hemoglobin by the fungal pathogen *Cryptococcus neoformans*. *Cellular Microbiology* **21**, e12961 (2019).

152. Pearse, B. M. Clathrin: a unique protein associated with intracellular transfer of membrane by coated vesicles. *Proc Natl Acad Sci U S A* **73**, 1255–1259 (1976).

153. Unanue, E. R., Ungewickell, E. & Branton, D. The binding of clathrin triskelions to membranes from coated vesicles. *Cell* **26**, 439–446 (1981).

154. Fotin, A. *et al.* Molecular model for a complete clathrin lattice from electron cryomicroscopy. *Nature* **432**, 573–579 (2004).

155. Kirchhausen, T., Owen, D. & Harrison, S. C. Molecular Structure, Function, and Dynamics of Clathrin-Mediated Membrane Traffic. *Cold Spring Harb Perspect Biol* **6**, (2014).

156. Ehrlich, M. *et al.* Endocytosis by Random Initiation and Stabilization of Clathrin-Coated Pits. *Cell* **118**, 591–605 (2004).

157. McMahon, H. T. & Boucrot, E. Molecular mechanism and physiological functions of clathrin-mediated endocytosis. *Nature Reviews Molecular Cell Biology* **12**, 517–533 (2011).

158. Bretscher, M. S., Thomson, J. N. & Pearse, B. M. Coated pits act as molecular filters. *Proc Natl Acad Sci U S A* **77**, 4156–4159 (1980).

159. Dhonukshe, P. *et al.* Clathrin-Mediated Constitutive Endocytosis of PIN Auxin Efflux Carriers in *Arabidopsis*. *Current Biology* **17**, 520–527 (2007).

160. Cureton, D. K., Massol, R. H., Saffarian, S., Kirchhausen, T. L. & Whelan, S. P. J. Vesicular Stomatitis Virus Enters Cells through Vesicles Incompletely Coated with Clathrin That Depend upon Actin for Internalization. *PLoS Pathog* **5**, (2009).

161. Rosa, A. & Maccioni, H. Clathrin coated vesicles in *Neurospora crassa*. *Mol Cell Biochem* **77**, 63–70 (1987).

162. Cheng, Y., Boll, W., Kirchhausen, T., Harrison, S. C. & Walz, T. Cryo-electron Tomography of Clathrin-coated Vesicles: Structural Implications for Coat Assembly. *Journal of Molecular Biology* **365**, 892–899 (2007).

163. Schultzhau, Z., Johnson, T. B. & Shaw, B. D. Clathrin localization and dynamics in

- Aspergillus nidulans*. *Molecular Microbiology* **103**, 299–318 (2017).
164. Borgne, R. L., Griffiths, G. & Hoflack, B. Mannose 6-Phosphate Receptors and ADP-ribosylation Factors Cooperate for High Affinity Interaction of the AP-1 Golgi Assembly Proteins with Membranes. *J. Biol. Chem.* **271**, 2162–2170 (1996).
165. Robinson, M. S. The role of clathrin, adaptors and dynamin in endocytosis. *Current Opinion in Cell Biology* **6**, 538–544 (1994).
166. Robinson, D. G. & Pimpl, P. Clathrin and post-Golgi trafficking: a very complicated issue. *Trends in Plant Science* **19**, 134–139 (2014).
167. Sanger, A., Hirst, J., Davies, A. K. & Robinson, M. S. Adaptor protein complexes and disease at a glance. *J Cell Sci* **132**, jcs222992 (2019).
168. Bonifacino, J. S. & Traub, L. M. Signals for Sorting of Transmembrane Proteins to Endosomes and Lysosomes. *Annu. Rev. Biochem.* **72**, 395–447 (2003).
169. Park, S. Y. & Guo, X. Adaptor protein complexes and intracellular transport. *Bioscience Reports* **34**, e00123 (2014).
170. Tan, J. Z. A. & Gleeson, P. A. Cargo Sorting at the trans-Golgi Network for Shunting into Specific Transport Routes: Role of Arf Small G Proteins and Adaptor Complexes. *Cells* **8**, (2019).
171. Fölsch, H., Pypaert, M., Schu, P. & Mellman, I. Distribution and Function of AP-1 Clathrin Adaptor Complexes in Polarized Epithelial Cells. *The Journal of Cell Biology* **152**, 595–606 (2001).
172. Fölsch, H., Pypaert, M., Maday, S., Pelletier, L. & Mellman, I. The AP-1A and AP-1B clathrin adaptor complexes define biochemically and functionally distinct membrane domains. *Journal of Cell Biology* **163**, 351–362 (2003).
173. Bonifacino, J. S. Adaptor proteins involved in polarized sorting. *Journal of Cell Biology* **204**, 7–17 (2014).
174. Starr, T. L., Pagant, S., Wang, C.-W. & Schekman, R. Sorting Signals That Mediate Traffic of Chitin Synthase III between the TGN/Endosomes and to the Plasma Membrane in Yeast. *PLoS One* **7**, (2012).
175. Puertollano, R., Randazzo, P. A., Presley, J. F., Hartnell, L. M. & Bonifacino, J. S. The GGAs Promote ARF-Dependent Recruitment of Clathrin to the TGN. *Cell* **105**, 93–102 (2001).
176. Nielsen, M. S. The sortilin cytoplasmic tail conveys Golgi-endosome transport and binds the VHS domain of the GGA2 sorting protein. *The EMBO Journal* **20**, 2180–2190 (2001).
177. Ford, M. G. J. *et al.* Curvature of clathrin-coated pits driven by epsin. *Nature* **419**, 361–366 (2002).
178. Miller, S. E., Collins, B. M., McCoy, A. J., Robinson, M. S. & Owen, D. J. A SNARE–adaptor interaction is a new mode of cargo recognition in clathrin-coated vesicles. *Nature* **450**, 570–574 (2007).
179. Donaldson, J. G. & Jackson, C. L. ARF family G proteins and their regulators: roles in membrane transport, development and disease. *Nat Rev Mol Cell Biol* **12**, 362–375 (2011).
180. Gillingham, A. K. & Munro, S. The Small G Proteins of the Arf Family and Their Regulators. *Annu. Rev. Cell Dev. Biol.* **23**, 579–611 (2007).
181. Ren, X., Farías, G. G., Canagarajah, B. J., Bonifacino, J. S. & Hurley, J. H. Structural Basis for Recruitment and Activation of the AP-1 Clathrin Adaptor Complex by Arf1. *Cell* **152**, 755–767 (2013).
182. Wang, Y. J. *et al.* Phosphatidylinositol 4 Phosphate Regulates Targeting of Clathrin Adaptor AP-1 Complexes to the Golgi. *Cell* **114**, 299–310 (2003).
183. Wang, J. *et al.* PI4P Promotes the Recruitment of the GGA Adaptor Proteins to the Trans -Golgi Network and Regulates Their Recognition of the Ubiquitin Sorting Signal. *MBoC* **18**, 2646–2655 (2007).
184. Henne, W. M. *et al.* FCHo Proteins are Nucleators of Clathrin-Mediated Endocytosis. *Science* **328**, 1281–1284 (2010).
185. Takei, K., Slepnev, V. I., Haucke, V. & De Camilli, P. Functional partnership between amphiphysin and dynamin in clathrin-mediated endocytosis. *Nat Cell Biol* **1**, 33–39 (1999).
186. Itoh, T. *et al.* Dynamin and the Actin Cytoskeleton Cooperatively Regulate Plasma Membrane Invagination by BAR and F-BAR Proteins. *Developmental Cell* **9**, 791–804 (2005).

187. Roux, A., Uyhazi, K., Frost, A. & De Camilli, P. GTP-dependent twisting of dynamin implicates constriction and tension in membrane fission. *Nature* **441**, 528–531 (2006).
188. Ferguson, S. M. & De Camilli, P. Dynamin, a membrane remodelling GTPase. *Nat Rev Mol Cell Biol* **13**, 75–88 (2012).
189. Spudich, G. *et al.* Myosin VI targeting to clathrin-coated structures and dimerisation is mediated by binding to Disabled-2 and PtdIns(4,5)P₂. *Nat Cell Biol* **9**, 176–183 (2007).
190. Krendel, M., Osterweil, E. K. & Mooseker, M. S. Myosin 1E interacts with synaptojanin-1 and dynamin via its SH3 domain. *FEBS Lett* **581**, 644–650 (2007).
191. Biancospino, M. *et al.* Clathrin light chain A drives selective myosin VI recruitment to clathrin-coated pits under membrane tension. *Nat Commun* **10**, (2019).
192. Ungewickell, E. J. & Hinrichsen, L. Endocytosis: clathrin-mediated membrane budding. *Current Opinion in Cell Biology* **19**, 417–425 (2007).
193. Rothnie, A., Clarke, A. R., Kuzmic, P., Cameron, A. & Smith, C. J. A sequential mechanism for clathrin cage disassembly by 70-kDa heat-shock cognate protein (Hsc70) and auxilin. *Proc Natl Acad Sci U S A* **108**, 6927–6932 (2011).
194. Cooper, G. Microtubules. in *The Cell: A Molecular Approach* (Sinauer Associates, 2000).
195. Schoch, C. L., Aist, J. R., Yoder, O. C. & Gillian Turgeon, B. A complete inventory of fungal kinesins in representative filamentous ascomycetes. *Fungal Genetics and Biology* **39**, 1–15 (2003).
196. Takeshita, N. & Fischer, R. The Cytoskeleton and Polarity Markers During Polarized Growth of Filamentous Fungi. in *Biology of the Fungal Cell* (eds. Hoffmeister, D. & Gressler, M.) 43–62 (Springer International Publishing, 2019). doi:10.1007/978-3-030-05448-9_3.
197. Hey, S., Ratt, A. & Linder, S. There and back again: Intracellular trafficking, release and recycling of matrix metalloproteinases. *Biochimica et Biophysica Acta (BBA) - Molecular Cell Research* **1869**, 119189 (2022).
198. Zhou, L. *et al.* Superresolution and pulse-chase imaging reveal the role of vesicle transport in polar growth of fungal cells. *Sci. Adv.* **4**, e1701798 (2018).
199. Penalva, M., Zhang, J., Xiang, X. & Pantazopoulou, A. transport of fungal RAB11 secretory vesicles involves myosin-5n dynein/dynactin/p25, and kinesin-1 and is independent of kinesin-3. 947–961 (2017).
200. Riquelme, M. *et al.* Fungal Morphogenesis, from the Polarized Growth of Hyphae to Complex Reproduction and Infection Structures. *Microbiol. Mol. Biol. Rev.* **82**, (2018).
201. Takeshita, N. *et al.* Transportation of *Aspergillus nidulans* Class III and V Chitin Synthases to the Hyphal Tips Depends on Conventional Kinesin. *PLoS ONE* **10**, 10(5): e0125937 (2015).
202. Requena, N. *et al.* Genetic evidence for a microtubule-destabilizing effect of conventional kinesin and analysis of its consequences for the control of nuclear distribution in *Aspergillus nidulans*: Conventional kinesin in *A. nidulans*. *Molecular Microbiology* **42**, 121–132 (2008).
203. Seiler, S., Plamann, M. & Schliwa, M. Kinesin and dynein mutants provide novel insights into the roles of vesicle traffic during cell morphogenesis in *Neurospora*. *Current Biology* **9**, 779-S1 (1999).
204. Hanson, J. & Lowy, J. The structure of F-actin and of actin filaments isolated from muscle. *Journal of Molecular Biology* **6**, 46-IN5 (1963).
205. Sellers, J. R. & Veigel, C. Walking with myosin V. *Current Opinion in Cell Biology* **18**, 68–73 (2006).
206. Buss, F. & Kendrick-Jones, J. How are the cellular functions of myosin VI regulated within the cell? *Biochemical and Biophysical Research Communications* **369**, 165–175 (2008).
207. Taheri-Talesh, N. *et al.* The Tip Growth Apparatus of *Aspergillus nidulans*. *Mol Biol Cell* **19**, 1439–1449 (2008).
208. Delgado-Alvarez, D. L. *et al.* Visualization of F-actin localization and dynamics with live cell markers in *Neurospora crassa*. *Fungal Genet. Biol.* **47**, 573–586 (2010).
209. Moseley, J. B. & Goode, B. L. The Yeast Actin Cytoskeleton: from Cellular Function to Biochemical Mechanism. *Microbiol Mol Biol Rev* **70**, 605–645 (2006).
210. Berepiki, A., Lichius, A., Shoji, J.-Y., Tilsner, J. & Read, N. D. F-Actin Dynamics in

- Neurospora crassa. *Eukaryot Cell* **9**, 547–557 (2010).
211. Wang, C. L. & Shaw, B. D. F-actin localization dynamics during appressorium formation in *Colletotrichum graminicola*. *Mycologia* **108**, 506–514 (2016).
212. Schultzhau, Z., Quintanilla, L., Hilton, A. & Shaw, B. D. Live Cell Imaging of Actin Dynamics in the Filamentous Fungus *Aspergillus nidulans*. *Microsc Microanal* **22**, 264–274 (2016).
213. Delgado-Álvarez, D. L., Bartnicki-García, S., Seiler, S. & Mouriño-Pérez, R. R. Septum Development in *Neurospora crassa*: The Septal Actomyosin Tangle. *PLoS ONE* **9**, e96744 (2014).
214. Bezanilla, M. & Pollard, T. D. Myosin-II Tails Confer Unique Functions in *Schizosaccharomyces pombe*: Characterization of a Novel Myosin-II Tail. *MBoC* **11**, 79–91 (2000).
215. Araujo-Palomares, C. L., Castro-Longoria, E. & Riquelme, M. Ontogeny of the Spitzenkörper in germlings of *Neurospora crassa*. *Fungal Genet. Biol.* **44**, 492–503 (2007).
216. Girbardt, M. Die Ultrastruktur der Apikalregion von Pilzhypphen. *Protoplasma* **67**, 413–441 (1969).
217. Grove, S. N. & Bracker, C. E. Protoplasmic organization of hyphal tips among fungi: vesicles and Spitzenkörper. *J. Bacteriol.* **104**, 989–1009 (1970).
218. López-Franco, R. & Bracker, C. E. Diversity and dynamics of the Spitzenkörper in growing hyphal tips of higher fungi. *Protoplasma* (2005) doi:10.1007/BF01279189.
219. Riquelme, M., Roberson, R. & Sánchez-León, E. 3 hyphal tip growth in filamentous fungi. in *Growth, Differentiation and Sexuality* vol. 1 47–66 (Wendland J., 2016).
220. Fischer-Parton, S. *et al.* Confocal microscopy of FM4-64 as a tool for analysing endocytosis and vesicle trafficking in living fungal hyphae. *Journal of Microscopy* **198**, 246–259 (2000).
221. Bourett, T. M. & Howard, R. J. Ultrastructural immunolocalization of actin in a fungus. *Protoplasma* **163**, 199–202 (1991).
222. Roberson, R. W. *et al.* Hyphal Structure. *Cellular and Molecular Biology of Filamentous Fungi* 8–24 (2010) doi:10.1128/9781555816636.ch2.
223. Hohmann-Marriott, M. F. *et al.* Application of electron tomography to fungal ultrastructure studies. *New Phytol.* **172**, 208–220 (2006).
224. Weber, R., Gavin, E., Pitt, W. & Pitt, D. Histochemical and ultrastructural characterization of vacuoles and spherosomes as components of the lytic system in hyphae of the fungus *Botrytis cinerea*. *The Histochemical Journal* **31**, 293–301 (1999).
225. Reinhardt, M. Das Wachstum von Pilzhypphen. *Jahrb Wiss Bot* **23**, 479–566 (1892).
226. Bartnicki-Garcia, S. & Lippman, E. Fungal morphogenesis: cell wall construction in *Mucor rouxii*. *Science* **165**, 302–304 (1969).
227. Bracker, C. E., Ruiz-Herrera, J. & Bartnicki-Garcia, S. Structure and transformation of chitin synthetase particles (chitosomes) during microfibril synthesis in vitro. *Proc Natl Acad Sci U S A* **73**, 4570–4574 (1976).
228. Verdín, J., Bartnicki-Garcia, S. & Riquelme, M. Functional stratification of the Spitzenkörper of *Neurospora crassa*. *Molecular Microbiology* **74**, 1044–1053 (2009).
229. Fajardo-Somera, R. A. *et al.* Dissecting the function of the different chitin synthases in vegetative growth and sexual development in *Neurospora crassa*. *Fungal Genet. Biol.* **75**, 30–45 (2015).
230. Jin, Y. *et al.* Myosin V transports secretory vesicles via a Rab GTPase cascade and interaction with the exocyst complex. *Dev. Cell* **21**, 1156–1170 (2011).
231. Hervé, J. C. & Bourmeyster, N. Rab GTPases, master controllers of eukaryotic trafficking. *Small GTPases* **9**, 1–4 (2018).
232. Sánchez-León, E. *et al.* The Rab GTPase YPT-1 associates with Golgi cisternae and Spitzenkörper microvesicles in *Neurospora crassa*. *Molecular Microbiology* **95**, 472–490 (2015).
233. Peñalva, M. A. A lipid-managing program maintains a stout Spitzenkörper. *Mol. Microbiol.* **97**, 1–6 (2015).
234. Fukuda, K. *et al.* Class III Chitin Synthase ChsB of *Aspergillus nidulans* Localizes at the Sites of Polarized Cell Wall Synthesis and Is Required for Conidial Development. *Eukaryot*

Cell **8**, 945–956 (2009).

235. Schultzhaus, Z., Yan, H. & Shaw, B. D. Aspergillus nidulans flippase DnfA is cargo of the endocytic collar and plays complementary roles in growth and phosphatidylserine asymmetry with another flippase, DnfB. *Mol. Microbiol.* **97**, 18–32 (2015).
236. Sánchez-León, E. & Riquelme, M. Live imaging of β -1,3-glucan synthase FKS-1 in Neurospora crassa hyphae. *Fungal Genetics and Biology* **82**, 104–107 (2015).
237. Schuster, M. *et al.* Co-delivery of cell-wall-forming enzymes in the same vesicle for coordinated fungal cell wall formation. *Nature Microbiology* **1**, (2016).
238. Schuster, M., Guiu-Aragones, C. & Steinberg, G. Class V chitin synthase and β (1,3)-glucan synthase co-travel in the same vesicle in Zymoseptoria tritici. *Fungal Genetics and Biology* **135**, (2020).
239. Lehmler, C. *et al.* Identification of a motor protein required for filamentous growth in Ustilago maydis. *EMBO J.* **16**, 3464–3473 (1997).
240. Bartnicki-Garcia, S. Hyphal Tip Growth Outstanding Questions. in *Molecular Biology of Fungal Development* (ed. Osiewacz, H.) (CRC Press, 2002). doi:10.1201/9780203910719.ch2.
241. Harris, S. *et al.* Polarisome meets sptzenkörper: microscopy, genetics, and genomics coverage. *4* 225–229 (2005).
242. Horio, T. & Oakley, B. R. The role of microtubules in rapid hyphal tip growth of Aspergillus nidulans. *Mol. Biol. Cell* **16**, 918–926 (2005).
243. Riquelme, M., Gierz, G. & Bartnicki-García, S. Dynein and dynactin deficiencies affect the formation and function of the Spitzenkörper and distort hyphal morphogenesis of Neurospora crassa. *Microbiology (Reading, Engl.)* **146 (Pt 7)**, 1743–1752 (2000).
244. Treitschke, S., Doehlemann, G., Schuster, M. & Steinberg, G. The Myosin Motor Domain of Fungal Chitin Synthase V Is Dispensable for Vesicle Motility but Required for Virulence of the Maize Pathogen Ustilago maydis[W]. *Plant Cell* **22**, 2476–2494 (2010).
245. Seiler, S., Nargang, F. E., Steinberg, G. & Schliwa, M. Kinesin is essential for cell morphogenesis and polarized secretion in Neurospora crassa. *EMBO J* **16**, 3025–3034 (1997).
246. Mouriño-Pérez, R. R., Riquelme, M., Callejas-Negrete, O. A. & Galván-Mendoza, J. I. Microtubules and associated molecular motors in Neurospora crassa. *Mycologia* **108**, 515–527 (2016).
247. Araujo-Bazán, L., Peñalva, M. A. & Espeso, E. A. Preferential localization of the endocytic internalization machinery to hyphal tips underlies polarization of the actin cytoskeleton in Aspergillus nidulans. *Mol. Microbiol.* **67**, 891–905 (2008).
248. Echaurren-Espinosa, R. O., Callejas-Negrete, O. A., Roberson, R. W., Bartnicki-García, S. & Mouriño-Pérez, R. R. Coronin Is a Component of the Endocytic Collar of Hyphae of Neurospora crassa and Is Necessary for Normal Growth and Morphogenesis. *PLoS One* **7**, (2012).
249. Roberson, R. W. The Actin Cytoskeleton in Hyphal Cells of Sclerotium Rolfsii. *Mycologia* **84**, 41–51 (1992).
250. Srinivasan, S., Vargas, M. M. & Roberson, R. W. Functional, organizational, and biochemical analysis of actin in hyphal tip cells of Allomyces macrogynus. *Mycologia* **88**, 57–70 (1996).
251. Upadhyay, S. & Shaw, B. D. The role of actin, fimbrin and endocytosis in growth of hyphae in Aspergillus nidulans. *Mol. Microbiol.* **68**, 690–705 (2008).
252. Martínez-Núñez, L. & Riquelme, M. Role of BGT-1 and BGT-2, two predicted GPI-anchored glycoside hydrolases/glycosyltransferases, in cell wall remodeling in Neurospora crassa. *Fungal Genet. Biol.* **85**, 58–70 (2015).
253. Rico-Ramírez, A. M., Roberson, R. W. & Riquelme, M. Imaging the secretory compartments involved in the intracellular traffic of CHS-4, a class IV chitin synthase, in Neurospora crassa. *Fungal Genetics and Biology* **117**, 30–42 (2018).
254. Tsuizaki, M., Takeshita, N., Ohta, A. & Horiuchi, H. Myosin motor-like domain of the class VI chitin synthase CsmB is essential to its functions in Aspergillus nidulans. *Biosci. Biotechnol. Biochem.* **73**, 1163–1167 (2009).
255. Takeshita, N., Ohta, A. & Horiuchi, H. CsmA, a Class V Chitin Synthase with a Myosin Motor-like Domain, Is Localized through Direct Interaction with the Actin Cytoskeleton in

- Aspergillus nidulans*. *Mol Biol Cell* **16**, 1961–1970 (2005).
256. Bartnicki-Garcia, S., Hergert, F. & Gierz, G. Computer simulation of fungal morphogenesis and the mathematical basis for hyphal (tip) growth. *Protoplasma* **153**, 46–57 (1989).
257. Riquelme, M. *et al.* The *Neurospora crassa* exocyst complex tethers Spitzenkörper vesicles to the apical plasma membrane during polarized growth. *Mol. Biol. Cell* **25**, 1312–1326 (2014).
258. Heider, M. R. & Munson, M. Exorcising the Exocyst Complex. *Traffic* **13**, 898–907 (2012).
259. Wang, D. & Dong, X. A Highway for War and Peace: The Secretory Pathway in Plant–Microbe Interactions. *Molecular Plant* **4**, 581–587 (2011).
260. Hückelhoven, R. Transport and secretion in plant–microbe interactions. *Current Opinion in Plant Biology* **10**, 573–579 (2007).
261. TerBush, D. R., Maurice, T., Roth, D. & Novick, P. The Exocyst is a multiprotein complex required for exocytosis in *Saccharomyces cerevisiae*. *EMBO J* **15**, 6483–6494 (1996).
262. Guo, W., Roth, D., Walch-Solimena, C. & Novick, P. The exocyst is an effector for Sec4p, targeting secretory vesicles to sites of exocytosis. *EMBO J* **18**, 1071–1080 (1999).
263. Guo, W., Grant, A. & Novick, P. Exo84p Is an Exocyst Protein Essential for Secretion. *J. Biol. Chem.* **274**, 23558–23564 (1999).
264. Wu, H., Rossi, G. & Brennwald, P. The ghost in the machine: small GTPases as spatial regulators of exocytosis. *Trends Cell Biol* **18**, 397–404 (2008).
265. Boyd, C., Hughes, T., Pypaert, M. & Novick, P. Vesicles carry most exocyst subunits to exocytic sites marked by the remaining two subunits, Sec3p and Exo70p. *J Cell Biol* **167**, 889–901 (2004).
266. Kwon, M. *et al.* Molecular Genetic Analysis of Vesicular Transport in *Aspergillus Niger* Reveals Partial Conservation of the Molecular Mechanism of Exocytosis in Fungi. *Microbiology* **160**, 316–329 (2014).
267. Kohli, M., Galati, V., Boudier, K., Roberson, R. W. & Philippsen, P. Growth-speed-correlated localization of exocyst and polarisome components in growth zones of *Ashbya gossypii* hyphal tips. *Journal of Cell Science* **121**, 3878–3889 (2008).
268. Hayakawa, Y., Ishikawa, E., Shoji, J., Nakano, H. & Kitamoto, K. Septum-directed secretion in the filamentous fungus *Aspergillus oryzae*. 40–55 (2011).
269. Li, C.-R., Lee, R. T.-H., Wang, Y.-M., Zheng, X.-D. & Wang, Y. *Candida albicans* hyphal morphogenesis occurs in Sec3p-independent and Sec3p-dependent phases separated by septin ring formation. *Journal of Cell Science* **120**, 1898–1907 (2007).
270. Zhang, Z., Qin, G., Li, B. & Tian, S. Knocking out *Bcsas1* in *Botrytis cinerea* impacts growth, development, and secretion of extracellular proteins, which decreases virulence. *Mol. Plant Microbe Interact.* **27**, 590–600 (2014).
271. Chen, X., Ebbole, D. J. & Wang, Z. The exocyst complex: delivery hub for morphogenesis and pathogenesis in filamentous fungi. *Current Opinion in Plant Biology* **28**, 48–54 (2015).
272. Robertson, N. F. The fungal hypha. **48**, 1–8 (1965).
273. Wösten, H. A., Moukha, S. M., Sietsma, J. H. & Wessels, J. G. Localization of growth and secretion of proteins in *Aspergillus niger*. *J. Gen. Microbiol.* **137**, 2017–2023 (1991).
274. Moukha, S. M., Wösten, H. A., Asther, M. & Wessels, G. H. In situ localization of the secretion of lignin peroxidases in colonies of *Phanerochaete chrysosporium* using a sandwiched mode of culture. *J Gen Microbiol* **139**, 969–978 (1993).
275. Valkonen, M. *et al.* Spatially segregated SNARE protein interactions in living fungal cells. 22775–22785 (2007).
276. Hayakawa, Y., Ishikawa, E., Shoji, J., Nakano, H. & Kitamoto, K. Septum-directed secretion in the filamentous fungus *Aspergillus oryzae*. *Molecular Microbiology* **81**, 40–55 (2011).
277. Yang, S. *et al.* The exocyst regulates hydrolytic enzyme secretion at hyphal tips and septa in banana *Fusarium wilt* fungus, *Fusarium odoratissimum*. *Appl Environ Microbiol* (2021) doi:10.1128/AEM.03088-20.
278. Schultzhaus, Z., Johnson, T. & Shaw, B. Clathrin localization and dynamics in

- Apergillus nidlans. *Mol Microbiol* **103**, 299–318 (2017).
279. Burgess, J. *et al.* AP-1 and clathrin are essential for secretory granule biogenesis in *Drosophila*. 2094–2105 (2011).
280. Bonnemaïson, M. *et al.* AP-1A Controls Secretory Granule Biogenesis and Trafficking of Membrane Secretory Granule Proteins. *Traffic* **15**, 1099–1121 (2014).
281. Ngô, H. M. *et al.* AP-1 in *Toxoplasma gondii* Mediates Biogenesis of the Rhoptry Secretory Organelle from a Post-Golgi Compartment. *Journal of Biological Chemistry* **278**, 5343–5352 (2003).
282. Venugopal, K. *et al.* Dual role of the *Toxoplasma gondii* clathrin adaptor AP1 in the sorting of rhoptry and microneme proteins and in parasite division. *PLoS Pathog* **13**, e1006331 (2017).
283. Moreira, C. M. do N. *et al.* Knockout of the gamma subunit of the AP-1 adaptor complex in the human parasite *Trypanosoma cruzi* impairs infectivity and differentiation and prevents the maturation and targeting of the major protease cruzipain. *PLoS ONE* **12**, e0179615 (2017).
284. Vince, J. E. *et al.* Leishmania Adaptor Protein-1 Subunits Are Required for Normal Lysosome Traffic, Flagellum Biogenesis, Lipid Homeostasis, and Adaptation to Temperatures Encountered in the Mammalian Host. *Eukaryotic Cell* **7**, 1256–1267 (2008).

Chapter 1 – Role of the clathrin adaptor AP-1 in the biology of *Botrytis cinerea*

Part 1. Secretion of hydrolytic enzymes and delivery of the
chitin synthase CHSIIIa depend on the AP-1 clathrin
adaptor in the plant-pathogen
Botrytis cinerea

1	Introduction.....	85
2	Results	88
2.1	Construction of a mutant reduced in the expression of <i>Bcap1b</i>	88
2.2	<i>Bcap1b</i> , a gene involved in hyphal elongation	88
2.3	<i>Bcap1b</i> contributes to cell wall integrity maintenance	90
2.4	<i>Bcap1b</i> is involved in differentiation programs.....	92
2.5	<i>Bcap1b</i> is involved in protein secretion.....	94
2.6	<i>Bcap1b</i> is critical for pathogenicity.....	96
3	Discussion	99
3.1	AP-1 is essential in filamentous fungi	99
3.2	AP-1 is implicated in cell-wall integrity maintenance and the traffic of a chitin synthase.....	99
3.3	The AP-1 mutant is characterized by hypersecretion and a loss of polarity	101
3.4	AP-1 is involved in the conventional secretion of hydrolytic enzymes required for nutrition and virulence	101
3.5	AP-1 is a virulence determinant in plant-pathogenic fungi.....	102
3.6	Conclusion.....	103
4	Material and methods.....	104
4.1	Fungal strains and culture conditions.....	104
4.2	Mutants construction in <i>Botrytis cinerea</i>	104
4.3	RNA extraction and RT-qPCR.....	104
4.4	Growth measurement in non-agitated liquid media in inducible or repressive conditions.....	105
4.5	Transmission Electron Microscopy (TEM)	105
4.6	Determination of susceptibility to osmotic and parietal stresses	106
4.7	Chitin quantification.....	107
4.8	Aniline blue fluorescence quantification.....	107
4.9	General microscopy techniques and image acquisition	107
4.10	Activities of secreted enzymes	108
4.11	Proteomic Analysis.....	109
4.12	pH measurement	110
4.13	Pathogenicity assays.....	110
5	References	112
6	Supplementary data	115
6.1	Figures	115

6.2	Appendix S1	121
6.3	Table S1.....	126
6.4	Table S2.....	127

Secretion of hydrolytic enzymes and delivery of the chitin synthase CHSIIIa depend on the AP-1 clathrin adaptor in the plant-pathogen *Botrytis cinerea*

Glen Calvar¹, Adrien Hamandjian¹, Mélanie Crumière¹, Jean-William Dupuy², Christine Moriscot³, Benoit Gallet³, François-Xavier Gillet¹, Amélie de Vallée¹, Christine Rascle¹, Mathias Choquer^{1#}, Christophe Bruel^{1#}, Nathalie Poussereau^{1#*}

¹ Microbiologie, Adaptation, Pathogénie, UMR5240, Univ Lyon, Université Lyon 1, CNRS, INSA, Bayer SAS, Lyon, France.

² Plateforme protéome, Centre de Génomique Fonctionnelle, Université de Bordeaux, Bordeaux, France.

³ Integrated Structural Biology Grenoble (ISBG), Campus EPN / Bâtiment Institut de Biologie Structurale, Grenoble, France.

*** Correspondance:** Nathalie Poussereau – nathalie.poussereau@univ-lyon1.fr
These authors contributed equally

Keywords: Adaptor protein 1, AP-1, growth, polarity, cell wall, secretion, clathrin, vesicles.

Abstract

The secretory pathway plays a key role in the polarized growth and the infectious strategy of pathogenic filamentous fungi through the delivery of enzymes transported in vesicles and participating to cell wall synthesis, fungal nutrition, and virulence. In metazoa and yeast, the formation of several secretory vesicles occurs at the Golgi apparatus and endosomes through a complex and partially characterized machinery involving clathrin and adaptor proteins such as AP-1. This adaptor protein is known to recruit clathrin and to sort cargo proteins. In filamentous fungi, data on the molecular mechanisms controlling the secretion process are still scarce. Using a mutant underexpressing the clathrin heavy chain encoding gene, we have previously demonstrated the essential role of clathrin in the secretion of proteins contributing to the virulence of the phytopathogenic fungus *Botrytis cinerea*. Due to the several roles of clathrin in the biology of the cell, these observations needed to be further addressed to ensure that they were related to a disruption of secretory vesicles biogenesis. A conditional mutant of the β -subunit of the heterotetrameric AP-1 clathrin adaptor complex was therefore constructed. Characterization of the mutant revealed a strong alteration in radial growth, hyphal morphology, and a chitin content defect associated with a mis-localization of the chitin synthase BcCHSIIIa. Finally, this AP-1 mutant is affected in plant-penetration, infection cushions formation, acidification and secretion of hydrolytic enzymes leading to a defect in pathogenicity. This study demonstrates the essential role of the clathrin adaptor AP-1 in both cell wall integrity maintenance and the infectious process of the plant-pathogen *B. cinerea*. It confirms the importance of the AP1/clathrin machinery in the secretory pathway of *B. cinerea*.

1 Introduction

Efficient host-colonization by plant-pathogenic fungi relies on three main biological processes that are nutrient acquisition, hyphal growth and secretion of virulence factors facilitating pathogen invasion. Moreover, hyphal growth is linked to the establishment of a functional cell wall which protects the fungus from external environment stresses and particularly from the plant response. The establishment of these biological processes relies on the production of secretory vesicles (SVs) and an efficient vesicular trafficking.

The hyphal tip is considered as the major site of exocytosis in filamentous fungi. SVs accumulate at the hyphal apex and fuse with the plasma membrane, delivering the lipids and the cell wall material required for polarized-cell elongation. These apical vesicles transport fungal cell wall enzymes (FCWE) such as chitin synthases and the 1,3- β -glucan synthase and are therefore essential for cell wall biogenesis^{1,2}. The hyphal tip is also the major site of exocytosis of hydrolytic enzymes. For example, the xylanase XYNII a Plant Cell Wall Degrading Enzyme (PCWDE) of *Trichoderma reesei*³, and a glucoamylase of *Aspergillus niger*⁴ are secreted at the fungal apex. Therefore, it is highly suspected that hyphal tip SVs could transport hydrolytic enzymes and virulence factors such as Cell Death Inducing Proteins (CDIP), in addition to FCWE. This hypothesis is supported by several studies which demonstrated that the α -amylase *amyB* localizes in hyphal tip vesicles in several plant-pathogenic fungi^{5,6}. In addition, virulence factors such as Cell Death Inducing Proteins (CDIP) are suspected to be secreted via SVs^{5,6}. SVs could therefore be considered as a cornerstone of fungal virulence and yet very little is known about the mechanisms leading to their biogenesis.

Clathrin, a protein complex conserved in eukaryotes, is involved in the biogenesis process of intracellular vesicles, including endocytic vesicles at the plasma membrane (PM) and SVs at the *trans*-Golgi network (TGN) and endosomes⁷⁻¹⁰. Extensive studies have focused on clathrin mediated endocytosis (CME) during the last 40 years, but only a very few focused on the role of clathrin in the production of secretory vesicles. So far, little information is available in filamentous fungi about clathrin, and the machinery involved in the formation of clathrin-coated vesicles. An endocytic role for exogenous double-stranded RNA has been described in the phytopathogenic fungus *Sclerotinia sclerotiorum*¹¹, but it has been reported to be minor in the endocytosis process in *Botrytis cinerea*, another plant necrotroph, and in the saprophyte *Aspergillus nidulans*^{12,13}. In

parallel, evidence supports that clathrin plays a pivotal role in the secretion process¹³. Indeed, it is critical for the secretion of virulence factors in *B. cinerea*¹³ and it is mainly localized at the Late Golgi apparatus in *A. nidulans*^{14,15}, comforting its putative role in SVs biogenesis.

Clathrin is a self-assembling protein complex made of heavy and light-chain subunits forming clathrin 'triskelions'. These triskelions are recruited to membranes by adaptor proteins (APs) and assemble to form a clathrin-coat around nascent vesicles. The association of APs with the triskelions likely contributes to the membrane deformation required for vesicle biogenesis¹⁶. After scission from the donor membrane, the clathrin/adaptor complex detaches from the vesicle during an uncoating process¹⁷.

APs are made of four subunits: one small subunit σ (~20 kDa), one medium subunit μ (~50 kDa) and two large subunits β_{1-5} and either α , γ , δ , ϵ , ζ (~100 kDa each). Subunits μ , and σ sort transmembrane cargos by recognizing specific motifs located in their cytoplasmic tails. The β -subunit recruits coat proteins such as clathrin¹⁸. Up to five different APs (AP-1 to AP-5) have been found in animals and plants. Each AP is associated with vesicles formation at specific subcellular locations^{18,19} and provides the specificity determining which cargo is selected. AP-1 is involved in forming clathrin-coated vesicles trafficking between the TGN and early endosomes (EE). AP-2 is implicated in clathrin-mediated endocytosis via its role in forming clathrin-endocytic vesicles at the plasma membrane. AP-3 could be involved in clathrin-independent biogenesis of vesicles addressed to endosomes, lysosomes or vacuoles, at the TGN^{7,18,20}. Finally, AP-4 and AP-5 do not interact with clathrin for vesicle biogenesis. AP-4 is implicated in the traffic between the TGN and specialized compartments whereas AP-5 is involved in the traffic between late endosomes and the TGN²¹. In ascomycetes and basidiomycetes, only AP-1, AP-2, and AP-3 homolog complexes have been reported to be conserved¹².

Only a few functional studies have focused on APs in filamentous fungi. In *A. nidulans*, AP-1 was shown to be involved in SVs polar sorting and to co-localize with clathrin at the Golgi apparatus¹⁵. The disruption of any AP-1 subunit has been reported to inactivate the function of the whole adaptor complex^{7,18} and the knock-out of AP-1 small subunit (s) is lethal in *A. nidulans*¹². In the same fungus, AP-2 was found to be involved in endocytosis, but in a clathrin-independent manner¹². Finally, in *Neurospora crassa*, a significant increase in lignocellulase secretion associates with the absence of the AP-3 μ subunit²².

Even though our previous work highlighted the role of clathrin in the secretion process of virulence factors in *Botrytis cinerea*¹³, clathrin is also involved in the formation of non-secretory vesicles at multiple subcellular locations. Therefore, more work is required to precise the potential role of clathrin in the biogenesis process of SVs. So far, AP-1 is the only AP complex interacting with clathrin reported to localize at the Golgi apparatus in filamentous fungi. Thus, we studied the functions of AP-1, to decipher the role of the AP-1/clathrin machinery in the biogenesis process of SVs and virulence in *B. cinerea*. Here we propose the first study focusing on AP-1 in a plant-pathogenic fungus.

The disruption of any AP-1 subunit has been reported to inactivate the function of the whole adaptor complex^{7,18}. In *A. nidulans*, the knock-out of AP-1 small subunit (σ) is lethal¹². Therefore, we studied the functions of AP-1 using a “conditional” mutant. The gene encoding for the β subunit of the AP-1 complex (*Bcap1b*) was chosen due to its critical role in clathrin recruitment and was placed under the control of the inducible nitrate reductase promoter *pNiaD* promoter. We showed that AP-1 is involved in fungal elongation, cell wall integrity maintenance, secretion of hydrolytic enzymes, and pathogenicity. This study revealed the importance of the AP-1 clathrin adaptor not only in the saprophytic life of the fungus but also in the necrotrophic strategy. The importance of the AP1/clathrin machinery in the secretory pathway of *B. cinerea* is confirmed.

2 Results

2.1 Construction of a mutant reduced in the expression of *Bcap1b*

To investigate the role of the AP-1 complex in the physiology of *B. cinerea*, we constructed a null mutant carrying a deletion of *Bcap1b*, the gene encoding the β -subunit of the complex. However, heterokaryotic transformants carrying the deletion could not be purified into haploid strains suggesting the essential role of this gene (Fig. S1). Given this result, previously described in other organisms¹⁵, we constructed a strain where the *Bcap1b* gene was placed under the control of *pniaD*, the nitrate reductase promoter from *B. cinerea* (*pNiaD::Bcap1b* strain, named AP-1^{cond} mutant – Fig. S2). This promoter induces expression of the downstream gene in presence of nitrate and represses it when other nitrogen sources are added to the culture medium²³. The quantification of the expression of the *Bcap1b* gene confirmed its reduced expression in the mutant (Fig. S3A). When using the repressing condition (glutamate), *bcap1b* expression was reduced (4-fold) when compared to the parental strain. This down-regulation of *Bcap1b* resulted in extremely retarded growth in liquid medium (Fig. S3B), and severe altered morphology, as observed by confocal microscopy (Fig. S4). The alteration of the growth and morphology was maintained even after longer times of incubation. This extremely severe growth reduction compromised further phenotyping of the mutant strain in this condition.

Under the inducible condition (nitrate), *bcap1b* endogenous expression levels were not completely restored in the mutant as *bcap1b* gene expression reduced slightly (1.2-fold) compared to the parental strain. The inducible condition sufficed to down-regulate *bcap1b* without compromising growth in liquid medium (Fig. S3A and S3B). Thus, we used the inducible condition to investigate the role of *Bcap1b* in the biology of *B. cinerea*

2.2 *Bcap1b*, a gene involved in hyphal elongation

To assess the impact of the down-expression of *Bcap1b* on radial growth, the parental strain, the AP-1^{cond} mutant and the complemented AP-1^{cond}/C strain where *Bcap1b* was placed under the control of the constitutive *pOliC* promoter (Fig. S2.B), were cultivated in solid minimal medium. The parental and complemented strains produced thin and non-pigmented hyphae while the AP-1^{cond} mutant displayed severely retarded radial growth (Fig. 1A). To study the role of BcAp1b on hyphal morphology, the strains were cultivated in liquid inducible medium. Observation of mycelia using confocal

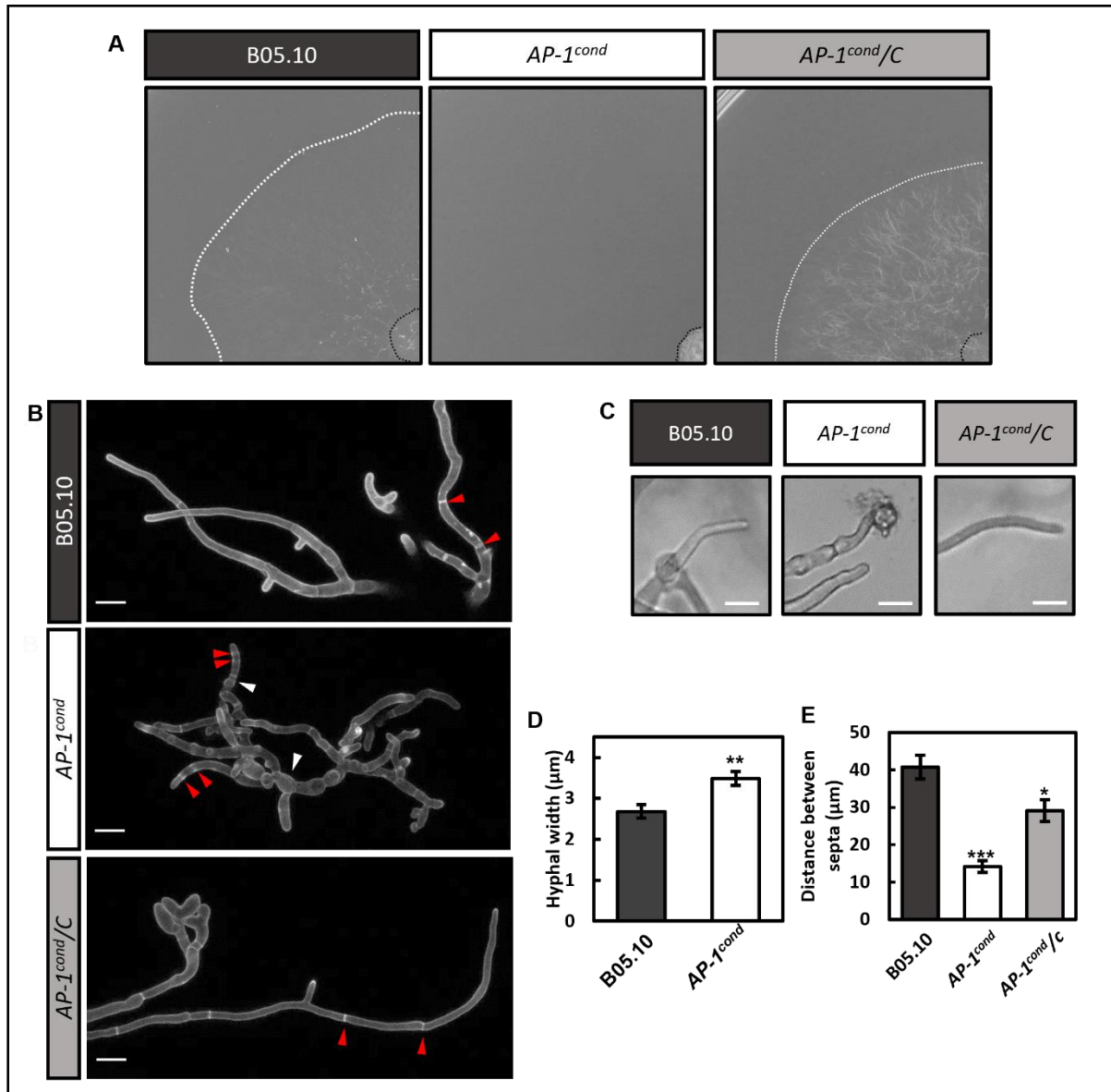


Figure 1 - BcAp1b is involved in polarized growth and hyphal morphology maintenance. **(A)** Radial growth of the parental strain B05.10, the *AP-1^{cond}* mutant, and the complemented *AP-1^{cond}/C* strain on solid inducible MMIII medium after five days of incubation. The black dotted line indicates the edge of the inoculum (10^4 conidia), while the white dotted line indicates the edge of the mycelium. **(B)** Confocal microscopy of hypha after 48h of growth under inducible conditions in liquid minimal medium. The cell wall was stained with aniline blue. Image acquisition was carried out using a 40x objective under 405nm laser excitation. Septa are indicated with red arrows and hyphal swelling with white arrows. Scale bar = 10 μm . **(C)** Hyphal tips with balloon-like structure observed under light microscopy in inducible conditions. Scale bar = 13 μm . **(D)** Hyphal width measured from transmission electron micrographs from 4 day-old liquid cultures in inducible conditions. **(E)** Distance between septa in strain B05.10, the *AP-1^{cond}* mutant, and the complemented *AP-1^{cond}/C* strain (Student *t*-test, * *p*-value < 0.05, ** *p*-value < 0.01)

microscopy revealed drastic alterations of the hyphal morphology. The AP-1^{cond} mutant displayed severe morphological defects with swelling (Fig. 1B white arrows), hyper-branching, and abnormal septa distribution (Fig. 1B red arrows). Determination of the distance between septa revealed a 2.8 –fold reduction in the mutant compared to the parental strain, (Fig. 1E) confirming the previously observed hyperseptation phenotype. Sometimes strong hyphal tip swelling could also be observed in the AP-1^{cond} mutant (Fig. 1C). When compared to the parental strain, hyphae were 60% wider in the AP-1^{cond} mutant (Fig. 1D) as illustrated by electron microscopy (Fig.2A). These altered phenotypes observed in the AP-1^{cond} mutant strain were restored in the complemented strain.

2.3 *Bcap1b* contributes to cell wall integrity maintenance

The observed morphological defects in the AP-1^{cond} mutant could be associated to a cell wall defect. To investigate the role of BcAp1b in cell wall biogenesis, we first observed the fungal cell wall under electron microscopy (Fig. 2A). In comparison with the parental strain, the cell wall along hyphae was significantly thicker (+35%) in the mutant strain (Fig. 2A and 2B). Interestingly, at septa, the cell wall appeared significantly thinner in the AP-1^{cond} mutant (Fig. 2A and 2B). Altogether these results suggested that the AP-1^{cond} mutant may exhibit an alteration of the composition and the properties of the cell wall.

To further investigate a potential difference in the cell wall of the two strains, the impact of increasing concentrations of potassium chloride on fungal growth was first monitored. KCl was chosen for its wide use in *B. cinerea* osmotic stresses studies and because it is not metabolized and less toxic to fungi than sodium ions²⁴. By using the relative half-maximal effective concentration (EC₅₀) as an indicator, the collected data showed that the AP-1^{cond} mutant was highly sensitive to KCl (EC₅₀ reduced by 1.9) when compared to the parental and complemented strain (Fig. 2C).

The higher sensitivity to osmotic stress observed in the AP-1^{cond} mutant could result from a modification of the cell wall composition. Nikkomycin-Z, a chitin synthase inhibitor, was used to stress the cell wall and explore this hypothesis (Fig. 2D). A 2.7-fold EC₅₀ decrease was measured in the AP-1^{cond} strain while, the complemented strain restored nikkomycin Z sensitivity levels similar to the parental strain (Fig. 2D).

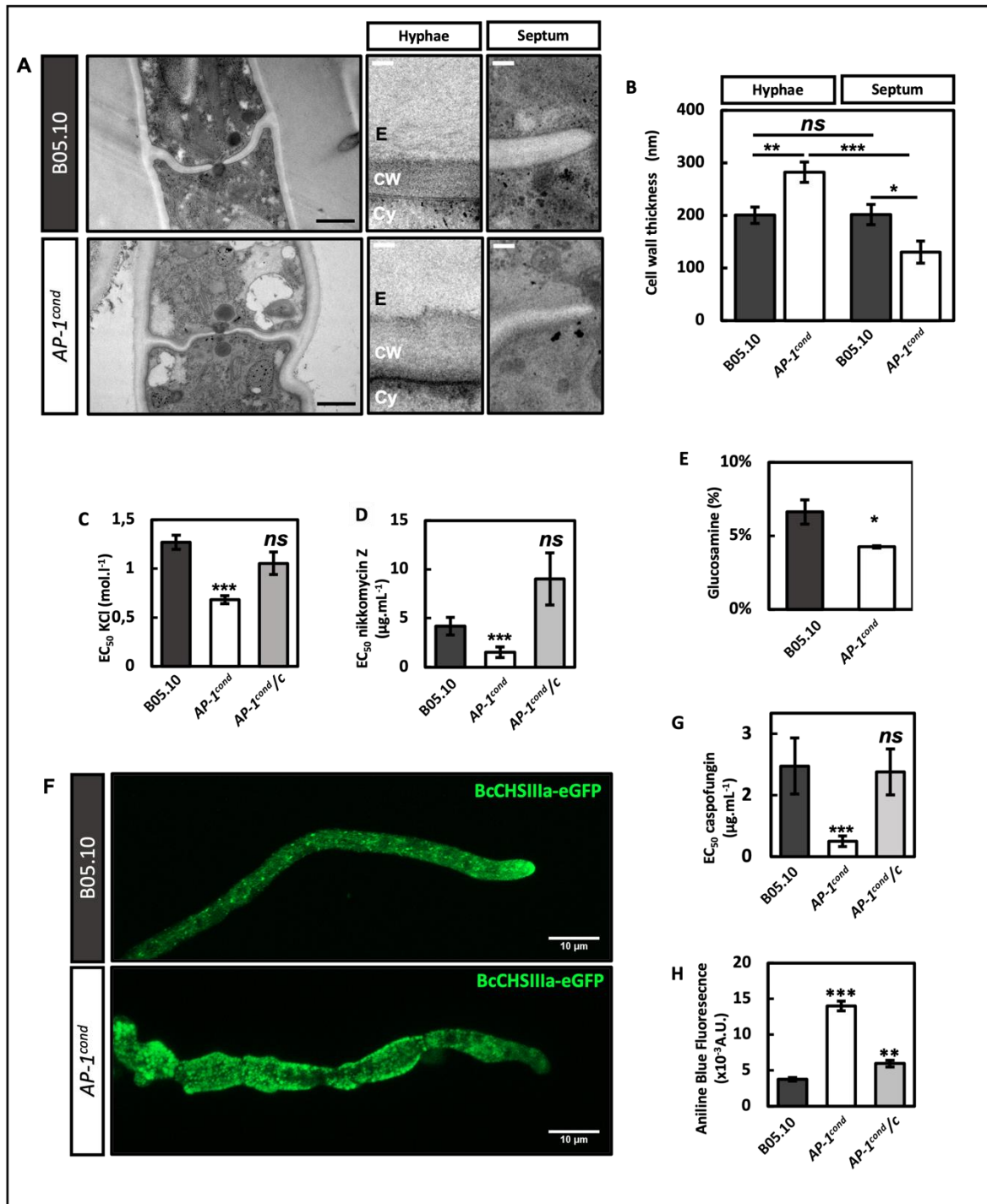


Figure 2 - BcAp1b is involved in cell wall integrity maintenance. **(A)** Representative electron micrographs of *Botrytis cinerea* cultured in liquid minimal medium (inducible condition) showing the cell wall (CW), the cytoplasm and (Cy) and the extracellular medium (E) – black scale bar = 500 nm; white scale bar = 75 nm. **(B)** Cell wall thickness was measured on electron micrographs. (Student *t*-test, ** *p*-value < 0.01) **(C)** Sensitivity to osmotic stress was investigated using KCl. Fungal growth was measured after 7 days of culture in minimal liquid media (inducible condition) supplemented with rising concentrations of KCl. To determine relative half-maximal effective concentration (EC₅₀). (F-test, *** *p*-value < 0.001). **(D)** Chitin stress induced by Nikkomycin Z after 7 days of culture in minimal liquid media (inducible condition). (F-test, *** *p*-value < 0.001). **(E)** Chitin quantification shows a reduction of 36% of total glucosamine in the AP-1^{cond} mutant compared to B0.10 (Student *t*-test, * *p*-value < 0.05). **(F)** Z-stack of chitin synthase IIIa localization in the parental strain and AP-1^{cond} mutant. In B05.10, BcCHSIIIa-eGFP polarly localizes at the fungal apex while in AP-1^{cond} mutant, BcCHSIIIa-eGFP is mainly localized in small puncta in the subapical region. **(G)** 1,3-β-glucan stress induced by Caspofungin after 7 days of culture in minimal liquid media (inducible condition). (F-test, *** *p*-value < 0.0005). **(H)** 1,3-β-glucan was quantified by measuring aniline-blue fluorescence after 7 days of culture in minimal liquid media (Inducible condition). (Student *t*-test, * *p*-value < 0.05, ** *p*-value < 0.01, *** *p*-value < 0.001)

As this increased susceptibility to chitin synthase inhibition may indicate an alteration of the chitin content, we quantified the amount of glucosamine, a derivate of the chitin monomer N-acetyl-glucosamine. Treatment with hydrochloric acid released glucosamine from chitin and quantification through the Elson and Morgan method²⁵ showed a 36% glucosamine reduction in the AP-1^{cond} strain when compared to the parental strain (Fig. 2E). To further characterize the chitin defect observed in the AP-1^{cond} mutant, we performed the localization of the class IIIa chitin synthase BcCHSIIIa-GFP (Fig. 2F). While the BcCHSIIIa-GFP accumulated in hyphal tips in the B05.10 strain, the chitin synthase was mainly localized in small puncta, just beneath the plasma membrane at sub-apical regions in the AP-1^{cond} mutant. Thus, BcAp1b is required for the proper localization of BcCHSIIIa-GFP.

We then investigated if the downregulation of *Bcap1b* affected other important cell wall polysaccharides. Therefore, we focused on 1,3- β -glucan. First, we exposed the fungus to increasing concentrations of caspofungin, a 1,3- β -glucan synthase inhibitor, to determine the relative EC₅₀. Compared to the parental strain, the relative EC₅₀ for caspofungin in the AP-1^{cond} mutant was 5.8 times lower, showing that the mutant was more sensitive to the drug (Fig. 2G). Then we aimed at quantifying β -1,3-glucan. Aniline blue was used to stain 1,3- β -glucan specifically. When excited at a 395 nm wavelength, the aniline-blue and 1,3- β -glucan complex emit fluorescence at a specific wavelength (495 nm)²⁶. This property was used to quantify 1,3- β -glucan. The aniline-blue fluorescence measured from 7-day-old cultures was 3.5 times higher in the AP-1^{cond} mutant when compared to B05.10 (Fig. 2H). The complemented strain partly restored this phenotype. This experiment shows that the AP-1^{cond} mutant accumulates 1,3- β -glucan in higher amounts and might compensate for the reduction in chitin content. Overall, these results demonstrate the significant role of Bcap1b in cell wall integrity maintenance.

2.4 *Bcap1b* is involved in differentiation programs

To evaluate macroconidia production, B05.10, AP-1^{cond} and AP-1^{cond}/C strains were cultured on Tanaka medium (inducible condition) for 14 days, at 21°C. The mutant formed irregular-edged colonies. An 8-fold reduction of counted conidia was observed in AP-1^{cond} mutant, indicating a strong impairment of asexual reproduction capacities (Fig. 3A). Longer incubation of the cultures confirmed that this defect was

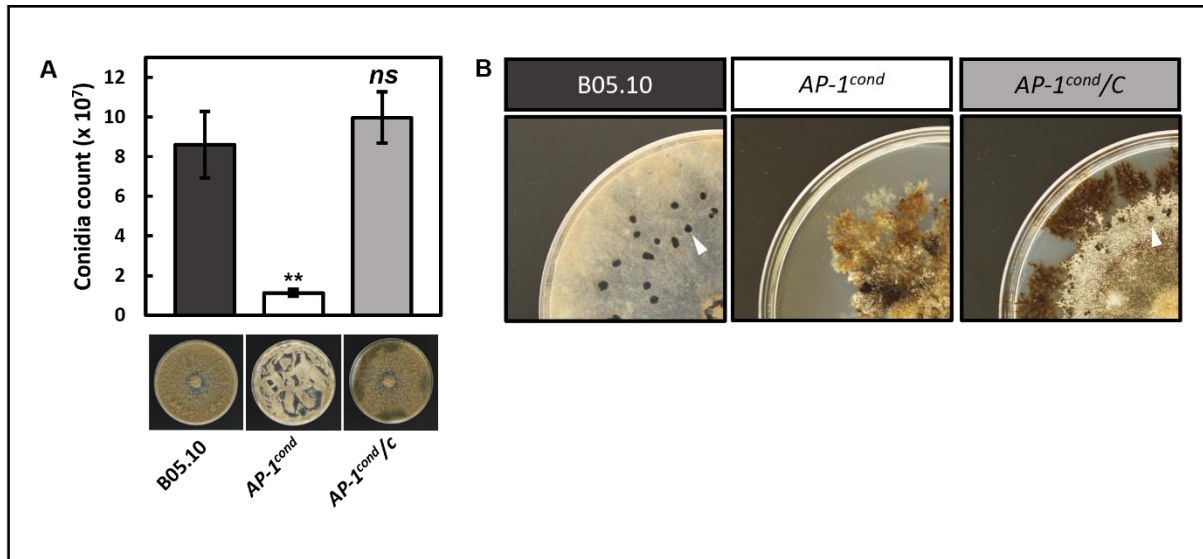


Figure 3 - The *AP-1^{cond}* mutant shows defect in differentiation programs

(A) Conidiation was quantified from 14-day-old cultures grown on modified Tanaka medium (inducible condition) under near-UV light conditions. Spores were collected and counted under a microscope. Data were collected from three biological replicates. Standard deviations are indicated, and statistics were obtained using a Student's T-test. Asterisks indicate significant differences compared to the B05.10 strain (***p*-value < 0.01). **(B)** Sclerotium formation was observed after 29 days of culture on solid Tanaka medium maintained in the dark.

quantitative and not due to a delay in conidial differentiation. Sclerotium differentiation was also investigated after 24 days of growth on solid Tanaka medium in the dark. The AP-1^{cond} mutant failed to produce sclerotia (Fig. 3B). However, the complemented strain produced a similar number of conidia compared to the B05.10 strain and produced some sclerotia.

2.5 *Bcap1b* is involved in protein secretion

In a previous study, we highlighted the important role of clathrin in the secretion process of virulence factors and hydrolytic enzymes in *B. cinerea*¹³. This work suggested that clathrin could be involved in the biogenesis of secretory vesicles in plant-pathogenic fungi. As AP-1 is known to act together with clathrin in the biogenesis process of secretory granules in the fruit fly *D. melanogaster*¹⁰, we investigated the role of AP-1 in protein secretion in *B. cinerea*.

To test the impact of the downregulation of the β -subunit of the clathrin adaptor AP-1 on protein secretion, the parental and AP-1^{cond} strains were cultured in minimal liquid medium to perform a comparative shotgun proteomic analysis of the secreted extracellular proteins. Noticeably, the AP-1^{cond} mutant accumulated more total extracellular proteins than the parental strain in its culture medium (1.8-fold – Fig. S5), suggesting an alteration of the secretion process. In 4 biological replicates, 343 proteins identified with a minimum of 2 unique and specific peptides were detected in both the parental and mutant strains. Most of these proteins (54% - 185 proteins – Table S2) were predicted as secreted by the conventional secretory pathway, based on the detection of a signal peptide and no transmembrane domain. Surprisingly, 74% of the 185 proteins containing a signal peptide (137 proteins) were down-accumulated in the mutant exoproteome when compared to the parental strain (Fig. 4A) suggesting a crucial role of BcAp1b in the conventional secretory pathway. Functional classification of the differentially accumulated proteins highlighted 10 different categories impacted in the AP-1^{cond} mutant (Fig. 4B). One of them was the fungal cell wall related enzymes (FCWE), with 14 members down-accumulated (up to 167-fold) and 8 members up-accumulated (up to 16.4-fold). Protein degradation represented the most altered functional category, with 21 proteases down-accumulated, only 4 up-accumulated and the acid protease BcAP8 (Bcin12p02040.1) being one of the most down-accumulated proteins (500-fold) found in the mutant exoproteome. The plant cell wall degrading enzymes category (PCWDEs) was also much altered, with 31 proteins down-accumulated, among which 14 pectin-associated enzymes

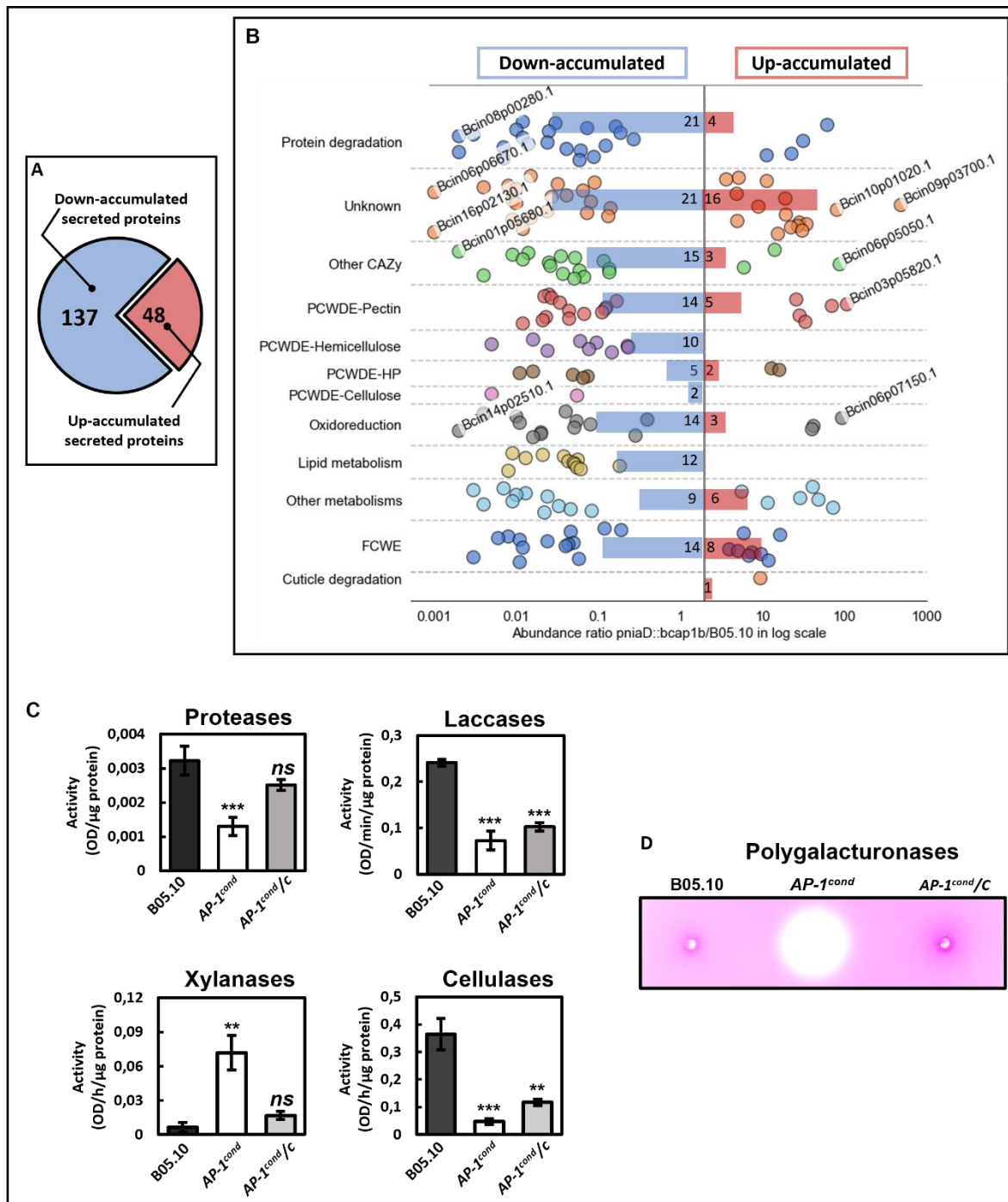


Figure 4 - BcAp1b is involved in the secretion of hydrolytic enzymes. **(A)** Up- and down-accumulated proteins with a predicted signal peptide identified in the exoproteome. **(B)** Functional categories classification of predicted secreted proteins [SPs but no TM] that are up- or down-accumulated in comparison to the parental strain B05.10 (fold change > 2 ; see Supplementary Table 2 for details). Exoproteome analyses were performed after 4 days of growth in liquid minimal medium (inducible condition, four independent biological experiments). The protein accession numbers correspond to the five most up- and down-accumulated proteins. CAZy, carbohydrate active enzymes; PCWDE, plant cell wall degrading enzymes; FCWE, fungal cell wall enzymes; HP, Hemicellulose-Pectin **(C)** Enzymatic activities measured in the supernatants of liquid cultures in minimal liquid medium (inducible condition) at 4 days post-inoculation for the B05.10, AP-1^{cond} and AP-1^{cond}/C strains. Three independent biological replicates were performed. Means with standard deviations are indicated Student *t*-test, * *p*-value < 0,05 ** *p*-value < 0.01, *** *p*-value < 0.001). **(D)** Visualized detection of polygalacturonase on pectate, in which four-day old culture supernatants from the B05.10, AP-1^{cond} and AP-1^{cond}/C strains were inoculated.

that include the virulence factor BcPG2²⁷ (Bcin14p00610.1 - 48-fold down) and the pectin-methyl esterase BcPME2 (Bcin03p03830.1 - 6-fold down). Five pectin-related proteins strongly up-accumulated, including the pectate-lyase Bcin03p05820.1 (107-fold up) and the virulence factor BcPGA1²⁸ (Bcin14p00850.1 - 33-fold up). Finally, hemicellulose, hemicellulose-pectin (HP) and cellulose related PCWDEs were also strongly down-accumulated, except for the endo- α -1,5-arabinase Bcin04p06990.1 and the sialidase Bcin02p08380.1 which up-accumulated 16-fold, and 13-fold respectively. Another impacted category was 'other CAZy' with 16 members down-accumulated, among which the mannosidase (Bcin01p05680.1- 500-fold down), and 3 members up-accumulated, among which the α -glycosidase (Bcin11p06440.1 - 100-fold up). Finally, 'oxidoreduction' and 'lipid metabolism' were the last 2 categories much altered by the mutation. All 12 proteins related to lipid metabolism and 14 of the 17 proteins related to oxidoreduction were down-accumulated, with a strong negative ratio for the laccases BcLCC8 (Bcin01p00800.1 - 25-fold down) and BcLCC2 (Bcin14p02510.1 - 500-fold down).

To validate the proteomic data, proteases, laccases, xylanases and cellulases activity assays were therefore performed (Fig. 4C). When compared to the parental strain, these activities were reduced to: 2.5, 3, and 7.4-fold respectively. However, xylanases activities were up to 7.2-fold in the AP-1^{cond} mutant. Polygalacturonase activities were detected using pectin-agar plates²⁹ (Fig. 4D). When compared to the parental strain, AP-1^{cond} mutant exhibited high pectin-hydrolase activities (white halo) while no pectin-methyl-esterase activity (dark halo) could be observed. The complemented strain AP-1^{cond}/C fully restored the phenotypes associated with proteases, xylanases and polygalacturonases activities and partially restored cellulases activities. However, the complemented strain failed to restore the parental laccase phenotype. The results indicate that Bcap1b is important for the secretion of some hydrolytic enzymes such as cellulases and proteases, while the secretion process of some polygalacturonases and xylanases seems to be AP-1 independent.

2.6 *Bcap1b* is critical for pathogenicity

French bean leaves were confronted to a conidial suspension of the parental, AP-1^{cond} and complemented strains. At 7 days post-inoculation, leaves infected by either the parental or complemented strain showed important tissue maceration. In contrast, only small

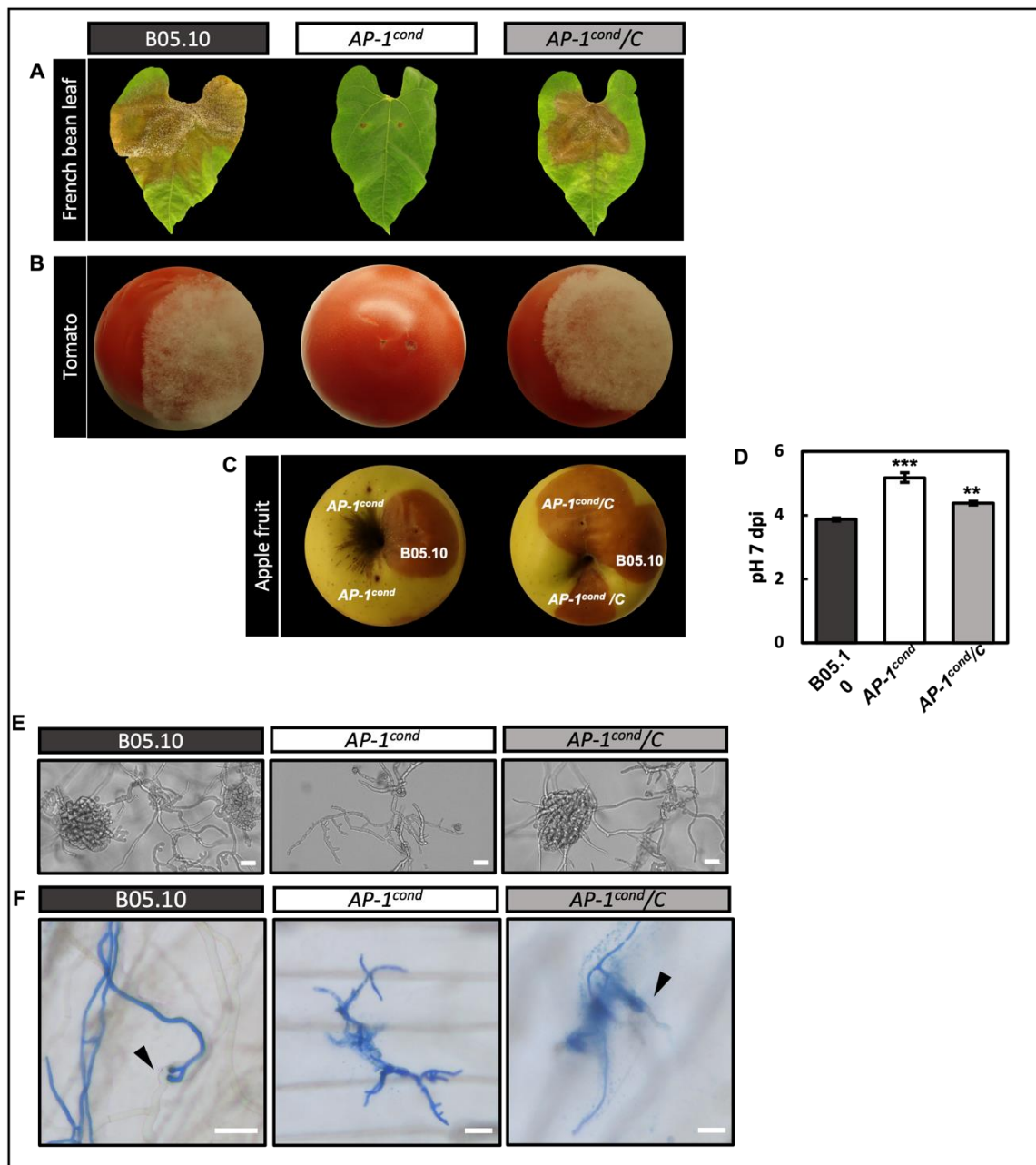


Figure 5 - BcAp1b is important for pathogenicity. Virulence of B05.10, AP-1^{cond} and AP-1^{cond}/C strains on French bean leaves (A), tomatoes (B) and apple fruits (C), 14 days old conidia were used for inoculation. Pictures were taken seven days post-inoculation. (D) Conidia from B05.10, AP-1^{cond} and AP-1^{cond}/C were cultured for seven days in liquid minimal medium (inducible condition) adjusted to pH 6. Acidification of the medium was measured 7 days post-inoculation. Student's *t*-test, * *p*-value < 0,05 ** *p*-value < 0.01, *** *p*-value < 0.001 (E) Infection cushions were observed by inverted microscopy 3 days after inoculation in inducible liquid media on glass surfaces (scale bar 25 μ m). (F) Penetration on onion epidermis: pictures were taken after 48h inoculation with conidia of B05.10, AP-1^{cond} and AP-1^{cond}/C. Penetration sites are indicated with black arrows (scale bar 15 μ m).

primary lesions were detected on the leaves infected by the mutant strain (Fig. 5A). When tomatoes and apple fruits were used as host plants, identical results were obtained (Fig. 5B and 5C). Since secretion of organic acids by *B. cinerea* plays a role during plant infection³⁰, the capacity of the AP-1^{cond} mutant at acidifying its culture medium was compared to that of the parental and complemented strains. At 7 days of growth in liquid cultures adjusted to pH 6, the pH dropped by 2.1 units in the parental culture and by 0.8 unit in the mutant culture (Fig. 5D). In the complemented strain, the acidification capacity was partially restored (-1.6 units). Lastly, the differentiation processes necessary to the early steps of plant infection by *B. cinerea* were explored. Cultures on glass cover slides first showed that germ tubes of all 3 strains could form unicellular appressoria (Fig. S7). On the contrary, these cultures then showed that the AP-1^{cond} mutant did not produce infection cushions (multicellular appressoria involved in plant-penetration, colonization and necrotrophy³¹) while the parental and complemented strains did (Fig. 5E). Furthermore, when using onion epidermis, a defect in plant penetration was observed in the mutant strain. While hyphae of the parental and complemented strains penetrated the plant cells, that of the AP-1^{cond} mutant only grew on their surface (Fig. 5F).

3 Discussion

Despite being crucial for fungal growth, nutrition, and virulence, very little is known about the molecular mechanisms underlying secretory vesicles biogenesis. We have studied the clathrin adaptor AP-1, a protein complex protein involved in cargo selection and the biogenesis of post-Golgi vesicles in eukaryotes, and describe, for the first time a plant-pathogenic fungus, the important roles of AP-1.

3.1 AP-1 is essential in filamentous fungi

The disruption of any subunit has been reported to inactivate the function of the whole adaptor complex^{7,18}. We therefore focused on the β -subunit of the AP-1 complex. Attempts to create a *Bcap1b* deletion mutant did not lead to homokaryotic strains. This is consistent with the report of AP-1 complex being essential in many organisms, including the filamentous fungus *A. nidulans*¹⁵. Hence, we have performed a conditional genetic approach, using the nitrate reductase promoter a promoter frequently used in filamentous fungi and already described in *B. cinerea*^{23,32}.

In *A. nidulans*, Martzoukou *et al.*¹⁵, reported a lack of growth soon after spore germination in AP-1 null mutants, and no growth on solid media when using repressing conditions on conditional mutants. In liquid medium, they observed severely retarded growth when *ap1s* was repressed. We found similar results in *Botrytis cinerea*, where polar growth was strongly impaired in the AP-1^{cond} mutant. Interestingly, in the yeasts *S. cerevisiae* and *S. pombe*, which do not maintain polar growth, AP-1 is not essential^{33–38}. In plants, AP-1 is also not essential but required for root growth in *A. thaliana*³⁹. These elements seem to confirm the hypothesis formulated by Martzoukou *et al.*¹⁵, who proposed that AP-1 is essential in filamentous fungi because filamentous growth depends on the polarized traffic of vesicles.

3.2 AP-1 is implicated in cell-wall integrity maintenance and the traffic of a chitin synthase

The fungal cell-wall mediates the relationships between the fungus and its environment. It protects the fungus from environmental stresses (either osmotic, chemical or mechanical) and is also important for maintaining hyphal morphology and growth⁴⁰. We observed aberrant growth and morphological phenotypes in the AP-1^{cond} mutant: hyperseptation and hyperbranching, similar to what was observed in AP-1^{cond} mutants in *A. nidulans*¹⁵ and *A. niger*⁴¹. Besides, hyphal-tip swelling could sometimes be observed in

hyphae of the AP-1^{cond} mutant. Comparable structures were previously described in *A. niger* when *aplD* (AP-1 γ encoding gene) was downregulated⁴¹. Interestingly, these swelling tips were also observed in *B. cinerea* when *bcsas1* a gene encoding for a GTP-binding protein required for exocytosis (yeast Sec4 ortholog)⁴² was deleted and in AP-2 mutants in *A. nidulans*⁴³. Jin *et al.*⁴³, reported that these hyphal-tip-balloon-like structures were stained with FM4-64 (lipid staining) but not with CFW (chitin staining) or Aniline blue (1,3- β -glucan staining), indicating an alteration of the cell-wall content. Consistent with the cell-wall defects observed in these mutants, the finding of these atypical hyphal tip structures in three different mutants associated with vesicular trafficking suggests a link between hyphal tip swelling and the disruption of the traffic of cell wall synthases towards the hyphal apex, leading to the incompleteness of the cell wall at the hyphal tip. Indeed, the localization of the class III chitin synthase BcCHSIIIa-GFP in the AP-1^{cond} mutant of *B. cinerea* confirms an abnormal localization of secretory vesicles. Interestingly, the chitin synthase ChsB (BcCHSIIIa ortholog) also mis-localizes in AP-1 mutants in *A. nidulans*¹⁵. Therefore, AP-1 function in the trafficking of the class III chitin synthase towards the hyphal tip seems to be conserved in filamentous fungi. Abnormal addressing of the class III chitin synthase likely explains why we observed a reduced amount of chitin in the *B. cinerea* AP-1^{cond} mutant, and why chitin deposition is altered in AP-1^{cond} mutants of *A. nidulans*¹⁵. In yeasts, AP-1 is also involved in the traffic of the class IV chitin synthase Chs3p^{2,24,25}.

We hypothesize that the thicker cell-wall observed in the AP-1^{cond} mutant could be the result of the accumulation of 1,3- β -glucan, which might compensate the chitin defect. This hypothesis is further supported by the hypersensitivity of the AP-1^{cond} mutant to the 1,3- β -glucan synthase inhibitor: caspofungin. Thus, when this mutant is exposed to caspofungin, the production of 1,3- β -glucan is impaired, and the mutant fails to compensate for the chitin defect and becomes more sensitive to the drug. Thus, and contrary to the chitin synthase CHSIIIa, the traffic of the glucan synthase BcFKS1 towards the hyphal tip might not depend on AP-1 in *B. cinerea*. To test this hypothesis, we have tried to localize BcFKS1 in the AP-1^{cond} mutant by fusing eGFP to BcFKS1, but no transformants could be obtained (data not shown). Interestingly in the fission yeast *S. pombe*, the glucan synthase BGS1 is a cargo of AP-1³⁷. Thus, further work is required to determine if the transport of the glucan synthase FKS1 is AP-1 dependent in filamentous fungi.

3.3 The AP-1 mutant is characterized by hypersecretion and a loss of polarity

B. cinerea is a necrotrophic pathogen: it induces plant cell death and degrades macromolecules from the plant via the secretion of hydrolytic enzymes. As late secretory processes rely on AP-1 in many eukaryotes, we investigated the impact of the reduced expression of *Bcap1b* on the secretion capacity of *B. cinerea*. To our surprise, total protein quantification showed a higher amount of proteins secreted in the culture medium of the AP-1^{cond} mutant when compared to the parental strain. In *A. niger*, Cairns, *et al*⁴¹, also reported a putative increase in protein secretion when *aplD* (AP-1 γ subunit) was downregulated. They hypothesized that the possible hypersecretion phenotype would be the result of hyperbranching. We also observed this phenotype in AP-1^{cond} mutant. On the other hand, we propose that the hypersecretion phenotype observed in the AP-1^{cond} mutant could be a consequence of a shift of exocytic sites from the hyphal tip towards subapical regions, as observed with the localization of BcCHSIIIa-eGFP. This shift would be associated with an increased number of exocytic sites, resulting in a boosted secretion. This hypothesis is based on the observation of the class III chitin synthase, a protein known to localize near exocytic sites (septa and hyphal apex) in *N. crassa* and *A. nidulans*^{44,45}. In the AP-1^{cond} mutant, BcCHSIIIa-eGFP accumulated in subapical regions instead of clustering at the hyphal tip. Besides, the increased hyphal width produced by the downregulation of AP-1 could support this hypothesis. Indeed, instead of fusing at the hyphal apex, secretory vesicles, which are implicated in hyphal extension could fuse at subapical regions, extending the hyphae in a non-polar fashion. Finally, the hypersecretion phenotype might be linked to the hyperseptation observed in the AP-1^{cond} mutant. Indeed, septa are also exocytic sites for the delivery of hydrolytic enzymes such as the amylase *amyB* in *A. oryzae* and *F. odoratissimum*^{5,6}. The increased number of septa observed in the AP-1^{cond} mutant may result in an increased number of exocytosis sites. Thus, it would be interesting to localize components of the exocyst complex in the AP-1^{cond} mutant to further address this hypothesis.

3.4 AP-1 is involved in the conventional secretion of hydrolytic enzymes required for nutrition and virulence

The capacity of the AP-1^{cond} mutant to secrete hydrolytic enzymes was investigated using protein activities and secretomic approaches. Our study shows that AP-1 is involved in the secretion process of PCWDEs, proteases and oxidoreduction-related proteins. Interestingly, the secretion defect observed in the AP-1^{cond} mutant displays a similar signature to *B. cinerea* clathrin mutants¹³. Indeed, proteases, cellulases and laccases

activities are also reduced in the clathrin mutants. As a result, our findings suggest that a functional AP-1/clathrin machinery is required for the secretion process of several hydrolytic enzymes required for nutrition and virulence. Interestingly, in the protist human pathogen *Trypanozoma cruzi*, the deletion of the AP-1 γ encoding gene blocks the transport of the secreted protease cruzipain, a protease involved in nutrition, differentiation and virulence⁴⁶. Thus, the clathrin adaptor AP-1 may play a conserved role in the secretion process of enzymes required for nutrition and virulence in eukaryotic pathogens. Intriguingly, other enzymes involved in macromolecule degradation can bypass the AP-1 route: the secretion of several pectin-hydrolases seems to be AP-1 independent. The molecular actors contributing to the AP-1 independent secretion of hydrolytic enzymes remain to be discovered in plant-pathogenic fungi. Their discovery would bring a novel understanding to the general secretion mechanisms in Fungi.

3.5 AP-1 is a virulence determinant in plant-pathogenic fungi

The capacity of fungal necrotrophs to infects plants relies, for instance, on the secretion of hydrolytic enzymes, modulation of the plant pH and plant-penetration⁴⁷. Numerous plant necrotrophs produce high amounts of organic acids to modulate the pH during plant-infection. Organic acids such as oxalic acid also induce plant cell death⁴⁸ and are required for pathogenicity in *Sclerotinia sclerotiorum*⁴⁹ and *Botrytis cinerea*⁵⁰. Our data shows that AP-1 is required for ambient environment acidification. Interestingly, clathrin is also involved in ambient medium acidification in *B. cinerea*¹³. Therefore, a functional AP-1/clathrin machinery is required for ambient pH acidification. The capacity of *Botrytis cinerea* to infect plants also depends on host-penetration and the formation of Infection Cushions (ICs)^{31,51}.

The incapacity of the AP-1^{cond} mutant to penetrate onion epidermis could be the result of a defect in early-stage secretion. Indeed, unlike hemibiotrophs, the capacity of the necrotroph *B. cinerea* to penetrate plant-cells is presumed to be related to the secretion of hydrolytic enzymes such as lipases and cutinases, and the pectinase BcPG2⁵². Several lipases and the pectinase BcPG2 were strongly down-accumulated in the mutant secretome and could explain why the penetration defect observed in the AP-1^{cond} mutant. ICs are another structure produced by *B. cinerea* involved in plant-penetration, colonization and necrotrophy³¹. When grown on glass surfaces, no IC could be observed in the AP-1^{cond} mutant. Interestingly, altered IC formation has already been described for clathrin mutants¹³. Souibgui *et al.*¹³, suggested that clathrin participates in the differentiation process of IC, possibly through the formation and/or trafficking of vesicles

involved in hyphal growth, or in the transport of IC-specific actors. Our study demonstrates that the clathrin adaptor AP-1 is required, for IC formation, comforting this hypothesis.

Overall AP-1 seems to be involved in a many virulence-related biological processes: growth for host-colonization, acidification, the secretion of hydrolytic enzymes for plant-tissue degradation, host-penetration, and the establishment of a functional cell-wall which protects the fungus from plant defenses. In other eukaryotes, AP-1 has also been described as a virulence determinant in protozoan parasites such as *Trypanosoma cruzi* and *Leishmania mexicana mexicana*^{46,53}. Hence, AP-1 might be a conserved and critical virulence determinant in eukaryotic pathogens.

3.6 Conclusion

Our work demonstrates that the clathrin adaptor AP-1 is essential for biological functions such as growth, cell-wall formation, plant-penetration and secretion. These pleiotropic functions of AP-1 reveal the importance of the clathrin/AP-1 machinery in the infection process. Identifying clathrin/AP-1 secretory cargos which might be involved in fungal pathogenicity remains a challenge. This could be achieved using an interactomic approach to detect the cargo proteins selected by AP-1. An alternative method could be to isolate intracellular vesicles from AP-1 and clathrin mutants to perform comparative proteomics. Identifying critical secretory cargos and proteins involved in the biogenesis of vesicles will bring a novel understanding of the secretion processes involved in virulence in pathogenic fungi and other eukaryotic pathogens.

4 Material and methods

4.1 Fungal strains and culture conditions

Botrytis cinerea (teleomorph *Botryotinia fuckeliana* (de Bary) Whetzel) strain B05.10 was used as control and recipient for all genetic constructions.

Conidia were collected after 14 days of culture on modified Tanaka medium containing glucose (2 g.l⁻¹), NaNO₃ (2 g.l⁻¹), KH₂PO₄ (2 g.l⁻¹), MgSO₄ (0.5 g.l⁻¹), CaCl₂ (0.1 g.l⁻¹), agar (15 g.l⁻¹) and oligoelements (ZnSO₄, CuSO₄, H₃BO₃, MnSO₄ and NaMoO₄), at 21°C under near-UV light (365 nm). Spores were resuspended in sterile liquid minimal medium (MMII) containing: 20 g of glucose, 0.2 g of KH₂PO₄, 0.1g of MgSO₄·7H₂O, 0.1g of KCl, 0.002g of FeSO₄·H₂O, per liter, supplemented with NaNO₃ (2 g.l⁻¹) or glutamate (2 g.l⁻¹). Suspended spores were then counted using Thoma cell counting chambers and stored on ice before use or suspended in glycerol (20%) for conservation at -80°C. All following experiments were carried using spores from 14-day-old cultures.

Growth assays were performed by depositing 10 µL of 10⁶ spores.ml⁻¹ at the center of 90 mm-Petri dishes containing agar minimal medium (MMII supplemented with 2 g.l⁻¹ of NaNO₃ and 15 g.l⁻¹ of agarose). Sclerotium formation was observed after 29 days of culture on modified Tanaka medium at 21°C in the dark. For growth assays in non-agitated liquid minimal media, 600 spores per well were cultivated in a 96 wells TPP microplate. For IC formation, 600 spores per well were cultivated in liquid minimal media in a 96 wells glass base microplate and incubated for 3 days.

4.2 Mutants construction in *Botrytis cinerea*

$\Delta Bcap1b$, AP-1^{cond} mutant, *BcCHSIIIa-GFP*, AP-1^{cond}-*BcCHSIIIa-GFP* strains were constructed using a gene replacement strategy (Appendix S1, Fig. S1, Fig. S2, Fig. S6 and Table S1).

4.3 RNA extraction and RT-qPCR

For *Bcap1b* gene expression analysis, conidia (10⁵ sp.ml⁻¹) from the parental strain and the AP-1^{cond} mutant were first cultured in liquid minimal medium supplemented with NaNO₃ (2 g.l⁻¹) for four days (21°C, 110 rpm). Then, mycelia were filtered (50 µm), split in two and cultured for an hour in inducing conditions NaNO₃ (2 g.l⁻¹) and glutamate (2 g.l⁻¹) for repressing conditions. Next, mycelia were filtered (50 µm), deep-froze in liquid nitrogen and stored at -80°C. RNA was extracted from 25 mg of freeze-dried mycelia using the RNeasy Midi Kit (Qiagen). RT-qPCR experiments were performed as previously described by Rascle *et al.* (2018)⁵⁴ using APBI-7900 Applied Biosystems (Applied

Biosystems). At least three independent biological replicates were performed. Relative quantification was used on the $2^{-\Delta\Delta Ct}$ method⁵⁵. Genes encoding for actin (*BcactA*, Bcin16g02020), elongation factor (*Bcef1a*, Bcin09g05760) and pyruvate dehydrogenase (*Bcpda1*, Bcin16g01890) were used as normalization internal control. Primer pair 65/66 is listed in (Table S1).

4.4 Growth measurement in non-agitated liquid media in inducible or repressive conditions

Spores of the parental B05.10, AP-1^{cond} and AP-1^{cond}/C strains were cultured with 600 spores per well in a 96 wells microplate containing MMII medium supplemented 2 g.l⁻¹ of NaNO₃. The optical density at 620nm (OD₆₂₀) was measured using a *SpectraMax Plus 384 Microplate reader* at 0h and after 7 days of incubation in the dark at 21°C. OD₆₂₀ values at 7 days were normalized using the mean OD₆₂₀ of four wells containing un-inoculated media. All data shown in the results were based on the measures of 3 biological replicates with 4 technical replicates per condition. Statistical analysis was performed using Student's T-test.

4.5 Transmission Electron Microscopy (TEM)

Sample preparation- B05.10, AP-1^{cond} and AP-1^{cond}/C strains were grown in liquid minimal medium (inducible condition) for four days at 21°C, 110 rpm. Mycelia was collected from the liquid cultures and fixed in 4% Paraformaldehyde (PFA); 0.4% Glutaraldehyde (GA) in 0.1 PHEM buffer for 30 min at room temperature (RT) with gentle shaking. The buffer was discarded, and a second incubation (30°, RT) was performed in 0.1M PHEM buffer containing 2% PFA and 0.3% GA. High pressure freezing was performed as described in Mohamed, et al⁵⁶. Briefly, the mycelium was deposited on the 200- μ m side of a 3-mm type A gold plate (Leica Microsystems) covered with the flat side of a 3-mm type B aluminum plate (Leica Microsystems) and vitrified using an HPM100 system (Leica Microsystems) as follows: after 40h at -90°C in acetone with 1% OsO₄, the samples were slowly warmed to -60°C (2°/h), stored for 10h at -60°C, then the temperature was raised to -30°C (2°/h) and the samples stored for a further 10h at -30°C before an 1h incubation at 0°C and storage at -30°C until further processing (all these steps are performed automatically in a AFS2 instrument using a pre-defined program). Then, the samples were rinsed 4 times in pure acetone before being infiltrated with progressively increasing concentrations of resin (Epoxy embedding medium, Sigma) in acetone while increasing the temperature to -20°C.

At the end, pure resin was added at RT and the samples were placed at 60°C for 2 days of polymerization.

Transmission Electron Microscopy of fungal cells- 70 nm thin sections were cut from resin embedded samples from high-pressure-freezing, using a UC7 ultramicrotome (Leica Microsystems) and collected on 100 mesh Formvar carbon copper grids. The sections were post-stained 24h with 2% uranyl acetate and lead citrate (5 minutes each). Samples were observed using a Tecnai G2 Spirit BioTwin microscope (ThermoFischer Scientific) operating at 120 kV with an Orius SC100B CCD camera (Gatan).

4.6 Determination of susceptibility to osmotic and parietal stresses

Solutions of KCl ranging from 0.005M to 2M were produced in MMII medium with 2 g.l⁻¹ of NaNO₃ (inducible condition). A stock concentration of Nikkomycin Z (Sigma) was produced at 3 000 µg.ml⁻¹ in DMSO before dilution in MMII medium (inducible condition) to produce solutions from 0.04 µg.ml⁻¹ to 400 µg.ml⁻¹ of Nikkomycin Z. For caspofungin, a stock at 3 000 µg.ml⁻¹ was produced in DMSO before dilution in MMII medium (inducible condition) to obtain solutions ranging from 0.004 µg.ml⁻¹ to 120 µg.ml⁻¹. Sensitivity to KCl, Nikkomycin Z and caspofungin were investigated by culture in 96 wells microplates. For KCl, each well contained 195 µl of KCl-containing MMII and was inoculated with 5 µl of spores suspended in MMII at a concentration of 1.2 .10⁶ spores.ml⁻¹. For Nikkomycin Z and caspofungin, each well contained 50 µl of drug-containing MMII and was inoculated with 150 µl of spores suspended in MMII at a concentration of 4 .10⁴ spores.ml⁻¹ to obtain a concentration of DMSO below 1%. On each microplate, 4 technical replicates were produced for each drug concentration. For each well, the optical density (OD) at 620nm was measured at 0h and 7 days post-inoculation and was used for downstream analysis. Data analysis was performed using R studio (4.1.2). The *drc* package (3.2-0) was used for the logit analysis of OD₆₂₀ following the method of Ritz *et al.*²⁹. The fitting of the experimental data to the logistic model was investigated using the *coefstest()* and *mselect()*. Either Hill three-parameter function (LL.3) or four parameter function (LL.4) model were selected for all analysis. The half effective concentrations (EC₅₀) were determined using the *ED()* function and compared between strains using the *EDcomp()* function³⁰. Indicated p-value correspond to the output of the *EDcomp()* based of a F-test on the residual sum of squares. All data shown in the results were based on 3 biological replicates with 4 technical replicates per condition.

4.7 Chitin quantification

A total of 5.10^6 spores were cultured for three days at 21°C under 110 rpm in 50 ml of liquid MMII (inducible condition). Mycelia from liquid culture were harvested by filtration on 11 µm sterile nylon filters before deep-freezing in liquid nitrogen and storage at -80°C. Lyophilization of frozen mycelia was performed in a *CHRIST Alpha 1-2 LD Plus* at -50°C and <0.005 mbar for 3 days. Mycelia were physically ground three times using the *TissueLyser II* (QIAGEN) for 30 seconds at 30 frequencies per second. Approximately 13 mg of ground mycelia were placed in three glass test tubes per strain. The weight of mycelium per tube was precisely measured. 5 ml of HCl 6 N were added to each tube before incubation at 100°C for six hours. The acidic reaction was neutralized by placing tubes on ice and by the addition of 5 N NaOH until a pH of 6.0 to 7.0 was reached. The volume of each tube was measured. Glucosamine was quantified using the following Elson and Morgan method³¹. A volume of 100 µl of the acidic reaction was placed in a new glass test tube before the addition of 650 µl of water and 250 µl of a solution containing 1.25 N Na₂CO₃ with 4% acetylacetone. Tubes were placed at 90°C for an hour before the addition of 1.25 ml of absolute EtOH. After five minutes, 250 µl of reagent containing DMAB, HCl 12 N and EtOH was added before incubation at room temperature in the dark for an hour. A volume of 250 µl of each reaction was placed in a 96 well plate to measure of the OD₅₂₀ using a *SpectraMax Plus 384 Microplate reader* after 5 seconds of agitation. The OD₅₂₀ were normalized using the weight of mycelium used for the reaction and the volume after adjusting the pH. The OD₅₂₀ were converted to µg of D-glucosamine using a OD₅₂₀ of a standard containing D-glucosamine concentrations ranging from 0 to 30 µg.

4.8 Aniline blue fluorescence quantification

Aniline blue fluorescence was investigated by culture in 96 wells microplates. Each well contained 600 spores suspended in 200 µl of MMII (inducible condition). At 7 days post-inoculation, the culture medium was discarded and 50 µL of 0.05% aniline blue in PBS pH 9.5 (Sigma) was added. After 60 min of incubation at 21°C, aniline blue fluorescence was measured ($\lambda_{ex} = 395$ nm, $\lambda_{em} = 495$ nm) using The Infinite® M1000 (TECAN).

4.9 General microscopy techniques and image acquisition

Confocal microscopy was performed with a Zeiss LSM850 confocal microscope (Oberkochen, Germany). 1,3- β -Glucan was stained with the addition of 0.05% aniline blue in PBS pH 9.5 (Sigma). Observations were performed a hour later using 405 nm laser excitation. For BcCHSIIIa-GFP localization, 72h-old growing hyphae were imaged (GFP

excitation: 488 nm; emission 491 nm to 574 nm). Images were captured using the LSM510 software. Images were stacked to produce Z-stacks with ImageJ (version 1.8.0).

4.10 Activities of secreted enzymes

A volume of 50 ml of liquid MMII (inducible condition) was inoculated with spores (10^5 sp.ml⁻¹) and shaken (110 rpm) at 21°C in the dark for 96h. Mycelia were recovered by filtration (11 µm), freeze-dried, and weighed. Culture filtrates were centrifuged at 14 000xg for 15 minutes at +4°C, frozen in liquid nitrogen and kept at -80°C before being used as samples in the following enzymatic reactions and proteomic analysis. Protein concentration in culture supernatants was determined using the Bradford protein quantification method⁵⁷ (Pierce™ Coomassie Bradford, ThermoFisher). Bovine serum albumin was used as standard. Protein concentration was normalized with dried fungal biomass. Enzymatic activities were performed as previously described by de Vallée *et al.* (2019)⁵¹ and Souibgui *et al.* (2021)¹³. Briefly, protease activity was measured by incubating samples with 1% hemoglobin (Sigma), pH 3.5, and reactions were stopped with 25% trichloroacetic acid. After centrifugation, culture filtrates were mixed with NaOH 0.5 M and absorbance at 280 nm was recorded. Laccase activity was measured by incubating the samples and the ABTS substrate (Sigma) in 190 µl of 50 mM Na-acetate buffer, pH 4.0. Oxidation of ABTS was recorded at 405 nm (Molecular Devices Spectramax-485) during 45 min at 30°C. Xylanase and cellulase activities were recorded on a plate reader TECAN infinite M1000 using the EnzChek-Ultra-xylanase assay kit (Thermofisher) and the cellulase assay kit (Abcam), respectively, according to manufacturer's instructions. All activities were measured on three independent biological replicates. Pectin hydrolases and pectin-methyl-esterases activities were detected using pectoplates²⁹. Pectoplates were prepared with 0.1% (w/v) of apple pectin (Sigma 76282), 1% (w/v) agarose (Fisher Bioreagents BP160), 12.5 mM citric acid and 50 mM Na₂HPO₄, pH 6.5. The gel was cast into 120 mm square petri dishes (50 ml per plate) and steel cork borer were used to produce 4mm diameter wells. 60 ng of total protein in 40 µl from culture filtrates were loaded in each well. Plates were incubated at 30°C for 24 h, and stained with 0.05% (w/v) Ruthenium red for 30 min. The plates were de-stained by several washes with ultrapure water and then photographed.

4.11 Proteomic Analysis

Culture filtrates from four independent biological replicates were prepared as previously described for enzymatic analysis. After freeze-thawing overnight at +4°C, samples were centrifuged at 14 000g for an hour at +4°C to remove potential debris and extracellular polysaccharides. Proteins from culture supernatants were precipitated overnight at +4°C using trichloroacetic acid and sodium deoxycholate (15% and 0,05% final, respectively). Precipitated proteins were collected by centrifugation (14 000g, 4°C, 20 min), and washed two times with cold acetone. The pellet was air-dried for 30 minutes and resuspended in Laemlli-DTT buffer (Tris 50mM, pH 6.8; EDTA 5 mM; Glycerol 10%; SDS 1%; bromothymol blue 0.02%; DTT 50 mM). Solubilized proteins were heated (98°C, 4 min) and stored at -20°C until proteomic preparation of the samples. Proteins (5 µg) were loaded onto a 10% acrylamide SDS-PAGE gel and visualized by Colloidal Blue staining. Migration was stopped when samples had just entered the resolving gel and the unresolved region of the gel was cut into only one segment. The steps of sample preparation and protein digestion by trypsin were performed as previously described (Rasclé et al., 2018). NanoLC-MS/MS analysis were performed using an Ultimate 3000 RSLC Nano-UPHLC system (Thermo Scientific, USA) coupled to a nan-ospray Orbitrap Fusion™ Lumos™ Tribrid™ Mass Spectrometer (Thermo Fisher Scientific, California, USA). Each peptide extracts was loaded onto a 300 µm ID x 5 mm PepMap C18 pre-column (Thermo Scientific, USA) at a flow rate of 10 µL/min. After a 3 min desalting step, peptides were separated on a 50 cm EasySpray column (75 µm ID, 2 µm C18 beads, 100 Å pore size, ES903, Thermo Fisher Scientific) with a 4-40% linear gradient of solvent B (0.1% formic acid in 80% ACN) in 91 min. The separation flow rate was set at 300 nL/min. The mass spectrometer operated in positive ion mode at a 1.9 kV needle voltage. Data were acquired using Xcalibur 4.4 software in a data-dependent mode. MS scans (m/z 375-1500) were recorded at a resolution of $R = 120000$ (@ m/z 200), a standard AGC target and an injection time in automatic mode, followed by a top speed duty cycle of up to 3 seconds for MS/MS acquisition. Precursor ions (2 to 7 charge states) were isolated in the quadrupole with a mass window of 1.6 Th and fragmented with HCD@28% normalized collision energy. MS/MS data was acquired in the Orbitrap cell with a resolution of $R=30000$ (@ m/z 200), a standard AGC target and a maximum injection time in automatic mode. Selected precursors were excluded for 60 seconds. Protein identification and Label-Free Quantification (LFQ) were done in Proteome Discoverer 2.5. The MS Amanda 2.0, Sequest HT and Mascot 2.5 algorithms were used for protein identification in batch mode by searching against the ENSEMBL *B. cinerea* ASL83294v1 database (13749 entries, release

53). Two missed enzyme cleavages were allowed for trypsin. Mass tolerances in MS and MS/MS were set to 10 ppm and 0.02 Da. Oxidation (M) and acetylation (K) were searched as dynamic modifications and carbamidomethylation (C) as static modification. Peptide validation was performed using the Percolator algorithm and only “high confidence” peptides were retained, corresponding to a 1% false discovery rate at peptide level [39]. Minora feature detector node (LFQ) was used along with the feature mapper and precursor ions quantifier. The quantification parameters were selected as follows: (1) Unique peptides, (2) Precursor abundance based on intensity, (3) Normalization mode: total peptide amount, (4) Protein abundance calculation: summed abundances, (5) Protein ratio calculation: pairwise ratio based, (6) Imputation mode: Low abundance resampling and (7) Hypothesis test: t-test (background based). Quantitative data were considered for master proteins, quantified by a minimum of 2 unique peptides, a fold changes above 2 and an abundance ratio (for each biological replicate) seen 4 times with the same trend. The mass spectrometry proteomics data have been deposited to the ProteomeXchange Consortium via the PRIDE partner repository with the dataset identifier (PXD037180).

4.12 pH measurement

25 ml of minimal medium MMII (pH 6) supplemented with NaNO₃ (2 g.l⁻¹) was inoculated with spores (10⁵ sp.ml⁻¹) and shaken (110 rpm) at 21°C in the dark for seven days. Mycelia were recovered by filtration (50 µm), freeze-dried, and weighed. pH measurements were performed on three independent biological replicates.

4.13 Pathogenicity assays

Spores were resuspended in MMII (inducible condition) and counted using a Thoma counting chamber before dilution to reach a concentration of 2 .10⁵ spores.ml⁻¹. Phosphate buffer (K₂HPO₄ 1M, KH₂PO₄ 1M) was added to the spores-containing solution before inoculation to a final concentration of 1%. French bean leaves (*Phaseolus vulgaris* var Saxa) were inoculated with of two drops of 7.5 µl of spore suspension, kept in humidified plastic boxes and placed at 21°C for seven days. For pathogenicity assays on apple fruit (*Malus domestica* cultivar Golden Delicious) and tomato (*Solanum lycopersicum*), fruits were wounded and inoculated with 7.5 µl of spore suspension. Inoculated fruits were incubated at 21°C under 80% relative humidity and dark-light (16 h/8 h) condition. Symptoms were scored up to 7 days post inoculation (dpi).

Abbreviations

TEM, transmission electron microscopy; CAZy, Carbohydrate Active Enzymes; FCWE, Fungal Cell Wall Enzymes; CDIP, Cell Death Inducing Proteins, TM, Transmembrane Domains; SP, Signal Peptides; ER, Endoplasmic Reticulum

Acknowledgment

The authors are grateful to Mathieu Lays for his contribution to the measurement of secreted enzymes activities.

5 References

1. Verdin, J., Bartnicki-Garcia, S. & Riquelme, M. Functional stratification of the Spitzenkörper of *Neurospora crassa*. *Molecular Microbiology* **74**, 1044–1053 (2009).
2. Verdín, J. *et al.* Off the wall: The rhyme and reason of *Neurospora crassa* hyphal morphogenesis. *The Cell Surface* **5**, 100020 (2019).
3. Kurzaŧkowski, W. *et al.* Ultrastructural localization of cellular compartments involved in secretion of the low molecular weight, alkaline xylanase by *Trichoderma reesei*. *Arch. Microbiol.* **159**, 417–422 (1993).
4. Wösten, H. A., Moukha, S. M., Sietsma, J. H. & Wessels, J. G. Localization of growth and secretion of proteins in *Aspergillus niger*. *J. Gen. Microbiol.* **137**, 2017–2023 (1991).
5. Hayakawa, Y., Ishikawa, E., Shoji, J., Nakano, H. & Kitamoto, K. Septum-directed secretion in the filamentous fungus *Aspergillus oryzae*. *Molecular Microbiology* **81**, 40–55 (2011).
6. Yang, S. *et al.* The exocyst regulates hydrolytic enzyme secretion at hyphal tips and septa in banana Fusarium wilt fungus, *Fusarium odoratissimum*. *Appl Environ Microbiol* (2021) doi:10.1128/AEM.03088-20.
7. Robinson, M. S. Forty Years of Clathrin-coated Vesicles: Forty Years of Clathrin-coated Vesicles. *Traffic* **16**, 1210–1238 (2015).
8. Gurunathan, S., David, D. & Gerst, J. E. Dynamin and clathrin are required for the biogenesis of a distinct class of secretory vesicles in yeast. *EMBO J* **21**, 602–614 (2002).
9. Borgonovo, B., Ouwendijk, J. & Solimena, M. Biogenesis of secretory granules. *Current Opinion in Cell Biology* **18**, 365–370 (2006).
10. Burgess, J. *et al.* AP-1 and clathrin are essential for secretory granule biogenesis in *Drosophila*. *MBoC* **22**, 2094–2105 (2011).
11. Wytinck, N. *et al.* Clathrin mediated endocytosis is involved in the uptake of exogenous double-stranded RNA in the white mold phytopathogen *Sclerotinia sclerotiorum*. *Sci Rep* **10**, 12773 (2020).
12. Martzoukou, O., Amillis, S., Zervakou, A., Christoforidis, S. & Diallinas, G. The AP-2 complex has a specialized clathrin-independent role in apical endocytosis and polar growth in fungi. *eLife* **6**, e20083 (2017).
13. Souibgui, E. *et al.* Clathrin Is Important for Virulence Factors Delivery in the Necrotrophic Fungus *Botrytis cinerea*. *Front. Plant Sci.* **12**, 668937 (2021).
14. Schultzhaus, Z., Johnson, T. B. & Shaw, B. D. Clathrin localization and dynamics in *Aspergillus nidulans*. *Molecular Microbiology* **103**, 299–318 (2017).
15. Martzoukou, O., Diallinas, G. & Amillis, S. Secretory Vesicle Polar Sorting, Endosome Recycling and Cytoskeleton Organization Require the AP-1 Complex in *Aspergillus nidulans*. *Genetics* **209**, 1121–1138 (2018).
16. Makowski, S. L., Kuna, R. S. & Field, S. J. Induction of membrane curvature by proteins involved in Golgi trafficking. *Advances in Biological Regulation* **75**, 100661 (2020).
17. Kirchhausen, T., Owen, D. & Harrison, S. C. Molecular Structure, Function, and Dynamics of Clathrin-Mediated Membrane Traffic. *Cold Spring Harb Perspect Biol* **6**, (2014).
18. Robinson, M. S. Adaptable adaptors for coated vesicles. *Trends in Cell Biology* **14**, 167–174 (2004).
19. Hirst, J., Irving, C. & Borner, G. H. H. Adaptor Protein Complexes AP-4 and AP-5: New Players in Endosomal Trafficking and Progressive Spastic Paraplegia: AP-4 and AP-5: Functions and Genetic Disorders. *Traffic* **14**, 153–164 (2013).
20. Nakatsu, F., Hase, K. & Ohno, H. The Role of the Clathrin Adaptor AP-1: Polarized Sorting and Beyond. *Membranes* **4**, 747–763 (2014).
21. Sanger, A., Hirst, J., Davies, A. K. & Robinson, M. S. Adaptor protein complexes and disease at a glance. *J Cell Sci* **132**, jcs222992 (2019).
22. Pei, X. *et al.* Involvement of the adaptor protein 3 complex in lignocellulase secretion in *Neurospora crassa* revealed by comparative genomic screening. *Biotechnol Biofuels* **8**, 124 (2015).

23. Schumacher, J. Tools for *Botrytis cinerea*: New expression vectors make the gray mold fungus more accessible to cell biology approaches. *Fungal Genetics and Biology* **49**, 483–497 (2012).
24. Araújo, C. A. S. *et al.* Osmotolerance as a determinant of microbial ecology: A study of phylogenetically diverse fungi. *Fungal Biology* **124**, 273–288 (2020).
25. Schloss, B. Colorimetric Determination of Glucosamine. *Anal. Chem.* **23**, 1321–1325 (1951).
26. Wood, P. J. Specific Interaction of Aniline Blue with 1,3- β -glucan. *Carbohydrate Polymers* **4**, 49–72 (1984).
27. Kars, I. *et al.* Necrotizing activity of five *Botrytis cinerea* endopolygalacturonases produced in *Pichia pastoris*: Necrotizing activity of BcPGs. *The Plant Journal* **43**, 213–225 (2005).
28. Have, A. ten, Mulder, W., Visser, J. & van Kan, J. A. L. The Endopolygalacturonase Gene Bcpg1 Is Required for Full Virulence of *Botrytis cinerea*. *MPMI* **11**, 1009–1016 (1998).
29. Lionetti, V. PECTOPLATE: the simultaneous phenotyping of pectin methylesterases, pectinases, and oligogalacturonides in plants during biotic stresses. *Front. Plant Sci.* **6**, (2015).
30. Billon-Grand, G., Rasclé, C., Droux, M., Rollins, J. A. & Poussereau, N. pH modulation differs during sunflower cotyledon colonization by the two closely related necrotrophic fungi *Botrytis cinerea* and *Sclerotinia sclerotiorum*: *Botrytis* and *Sclerotinia* differ in pH modulation. *Molecular Plant Pathology* **13**, 568–578 (2012).
31. Choquer, M. *et al.* The infection cushion of *Botrytis cinerea*: a fungal ‘weapon’ of plant-biomass destruction. *Environ Microbiol* **23**, 2293–2314 (2021).
32. Marchegiani, E., Sidhu, Y., Haynes, K. & Lebrun, M.-H. Conditional gene expression and promoter replacement in *Zymoseptoria tritici* using fungal nitrate reductase promoters. *Fungal Genetics and Biology* **79**, 174–179 (2015).
33. Stepp, J. D., Pellicena-Palle, A., Hamilton, S. & Kirchhausen, T. A Late Golgi Sorting Function for *Saccharomyces cerevisiae* Apm1p, but not for Apm2p, a Second Yeast Clathrin AP Medium Chain-related Protein. *Molecular Biology of the Cell* **6**, 18 (1995).
34. Huang, K. M., D’Hondt, K., Riezman, H. & Lemmon, S. K. Clathrin functions in the absence of heterotetrameric adaptors and AP180-related proteins in yeast. *EMBO J* **18**, 3897–3908 (1999).
35. Valdivia, R. H., Baggott, D., Chuang, J. S. & Schekman, R. W. The Yeast Clathrin Adaptor Protein Complex 1 Is Required for the Efficient Retention of a Subset of Late Golgi Membrane Proteins. *Developmental Cell* **2**, 283–294 (2002).
36. Ma, Y., Takeuchi, M., Sugiura, R., Sio, S. O. & Kuno, T. Deletion mutants of AP-1 adaptin subunits display distinct phenotypes in fission yeast. *Genes to Cells* **14**, 1015–1028 (2009).
37. Yu, Y. *et al.* Sip1, a Conserved AP-1 Accessory Protein, Is Important for Golgi/Endosome Trafficking in Fission Yeast. *PLoS ONE* **7**, e45324 (2012).
38. Arcones, I., Sacristán, C. & Roncero, C. Maintaining protein homeostasis: early and late endosomal dual recycling for the maintenance of intracellular pools of the plasma membrane protein Chs3. *MBoC* **27**, 4021–4032 (2016).
39. Park, M. *et al.* Arabidopsis -adaptin subunit AP1M of adaptor protein complex 1 mediates late secretory and vacuolar traffic and is required for growth. *Proceedings of the National Academy of Sciences* **110**, 10318–10323 (2013).
40. Garcia-Rubio, R., de Oliveira, H. C., Rivera, J. & Trevijano-Contador, N. The Fungal Cell Wall: *Candida*, *Cryptococcus*, and *Aspergillus* Species. *Front. Microbiol.* **10**, 2993 (2020).
41. Cairns, T. C. *et al.* A quantitative image analysis pipeline for the characterization of filamentous fungal morphologies as a tool to uncover targets for morphology engineering: a case study using ap1D in *Aspergillus niger*. *Biotechnol Biofuels* **12**, 149 (2019).
42. Zhang, Z., Qin, G., Li, B. & Tian, S. Knocking out Bcsas1 in *Botrytis cinerea* impacts growth, development, and secretion of extracellular proteins, which decreases virulence. *Mol. Plant Microbe Interact.* **27**, 590–600 (2014).

43. Jin, J., Iwama, R., Takagi, K. & Horiuchi, H. AP-2 complex contributes to hyphal-tip-localization of a chitin synthase in the filamentous fungus *Aspergillus nidulans*. *Fungal Biology* S187861462100091X (2021) doi:10.1016/j.funbio.2021.05.009.
44. Sánchez-León, E. *et al.* Traffic of Chitin Synthase 1 (CHS-1) to the Spitzenkörper and Developing Septa in Hyphae of *Neurospora crassa*: Actin Dependence and Evidence of Distinct Microvesicle Populations. *Eukaryotic cell* **10**, 683–95 (2011).
45. Takeshita, N. *et al.* Transportation of *Aspergillus nidulans* Class III and V Chitin Synthases to the Hyphal Tips Depends on Conventional Kinesin. *PLoS ONE* **10**, 10(5): e0125937 (2015).
46. Moreira, C. M. do N. *et al.* Knockout of the gamma subunit of the AP-1 adaptor complex in the human parasite *Trypanosoma cruzi* impairs infectivity and differentiation and prevents the maturation and targeting of the major protease cruzipain. *PLoS ONE* **12**, e0179615 (2017).
47. Newman, T. E. & Derbyshire, M. C. The Evolutionary and Molecular Features of Broad Host-Range Necrotrophy in Plant Pathogenic Fungi. *Front. Plant Sci.* **11**, 591733 (2020).
48. Kim, K. S., Min, J.-Y. & Dickman, M. B. Oxalic Acid Is an Elicitor of Plant Programmed Cell Death during *Sclerotinia sclerotiorum* Disease Development. *MPMI* **21**, 605–612 (2008).
49. Godoy, G., Steadman, J. R., Dickman, M. B. & Dam, R. Use of mutants to demonstrate the role of oxalic acid in pathogenicity of *Sclerotinia sclerotiorum* on *Phaseolus vulgaris*. *Physiological and Molecular Plant Pathology* **37**, 179–191 (1990).
50. Verhoeff, K. *et al.* Changes in pH and the Production of Organic Acids During Colonization of Tomato Petioles by *Botrytis cinerea*. *J Phytopathol* **122**, 327–336 (1988).
51. de Vallée, A. *et al.* A Similar Secretome Disturbance as a Hallmark of Non-pathogenic *Botrytis cinerea* ATMT-Mutants? *Front. Microbiol.* **10**, (2019).
52. van Kan, J. A. L. Licensed to kill: the lifestyle of a necrotrophic plant pathogen. *Trends Plant Sci.* **11**, 247–253 (2006).
53. Vince, J. E. *et al.* Leishmania Adaptor Protein-1 Subunits Are Required for Normal Lysosome Traffic, Flagellum Biogenesis, Lipid Homeostasis, and Adaptation to Temperatures Encountered in the Mammalian Host. *Eukaryotic Cell* **7**, 1256–1267 (2008).
54. Rascle, C. *et al.* The pH regulator PacC: a host-dependent virulence factor in *Botrytis cinerea*: The pH regulator PacC. *Environmental Microbiology Reports* **10**, 555–568 (2018).
55. Livak, K. J. & Schmittgen, T. D. Analysis of Relative Gene Expression Data Using Real-Time Quantitative PCR and the 2- $\Delta\Delta$ CT Method. *Methods* **25**, 402–408 (2001).
56. Mohamed, A. M. T. *et al.* Chromosome Segregation and Peptidoglycan Remodeling Are Coordinated at a Highly Stabilized Septal Pore to Maintain Bacterial Spore Development. *Developmental Cell* **56**, 36-51.e5 (2021).
57. Bradford, M. M. A Rapid and Sensitive Method for the Quantitation of Microgram Quantities of Protein Utilizing the Principle of Protein-Dye Binding. **7**, 248–254 (1976).

6 Supplementary data

6.1 Figures

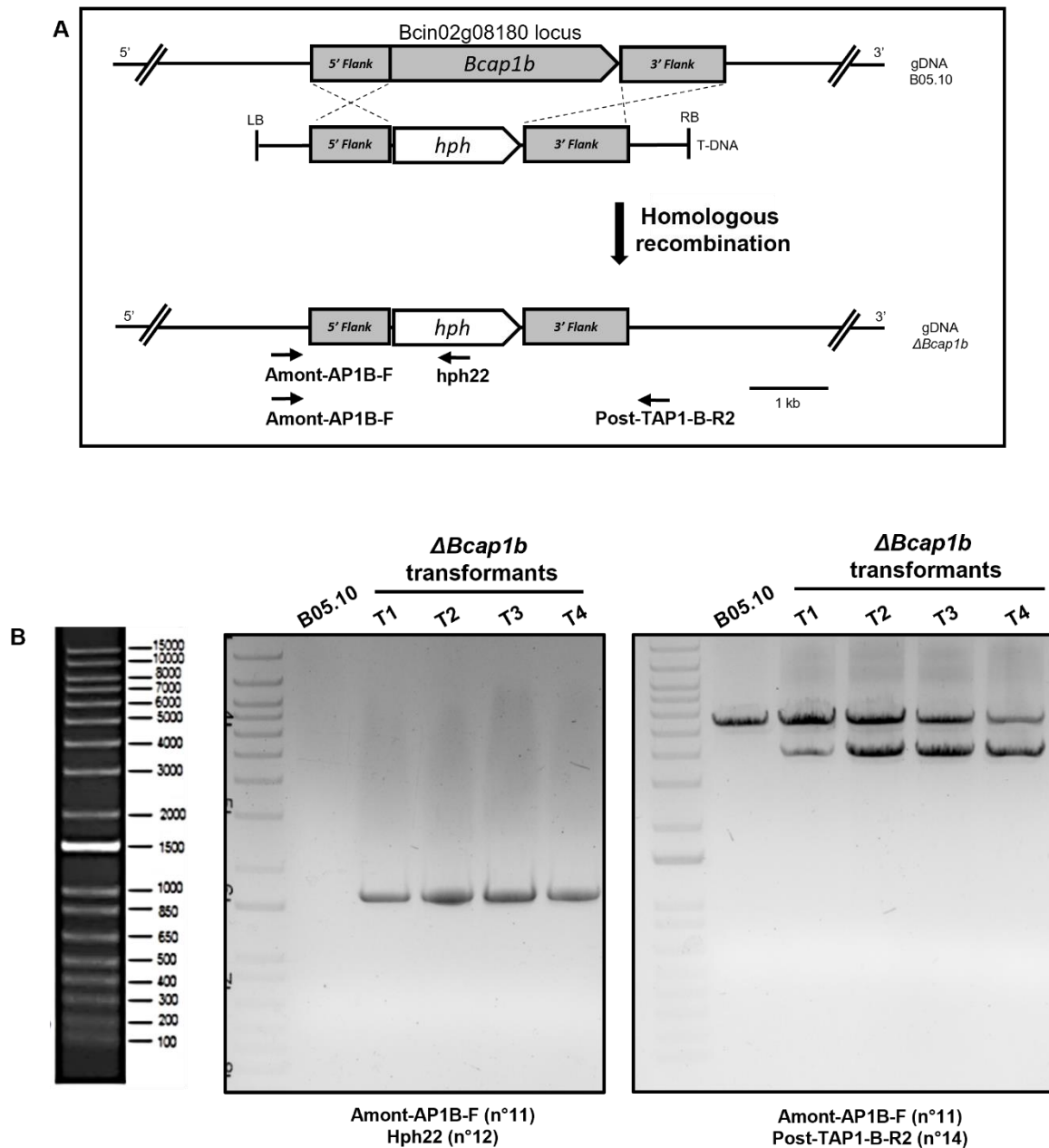
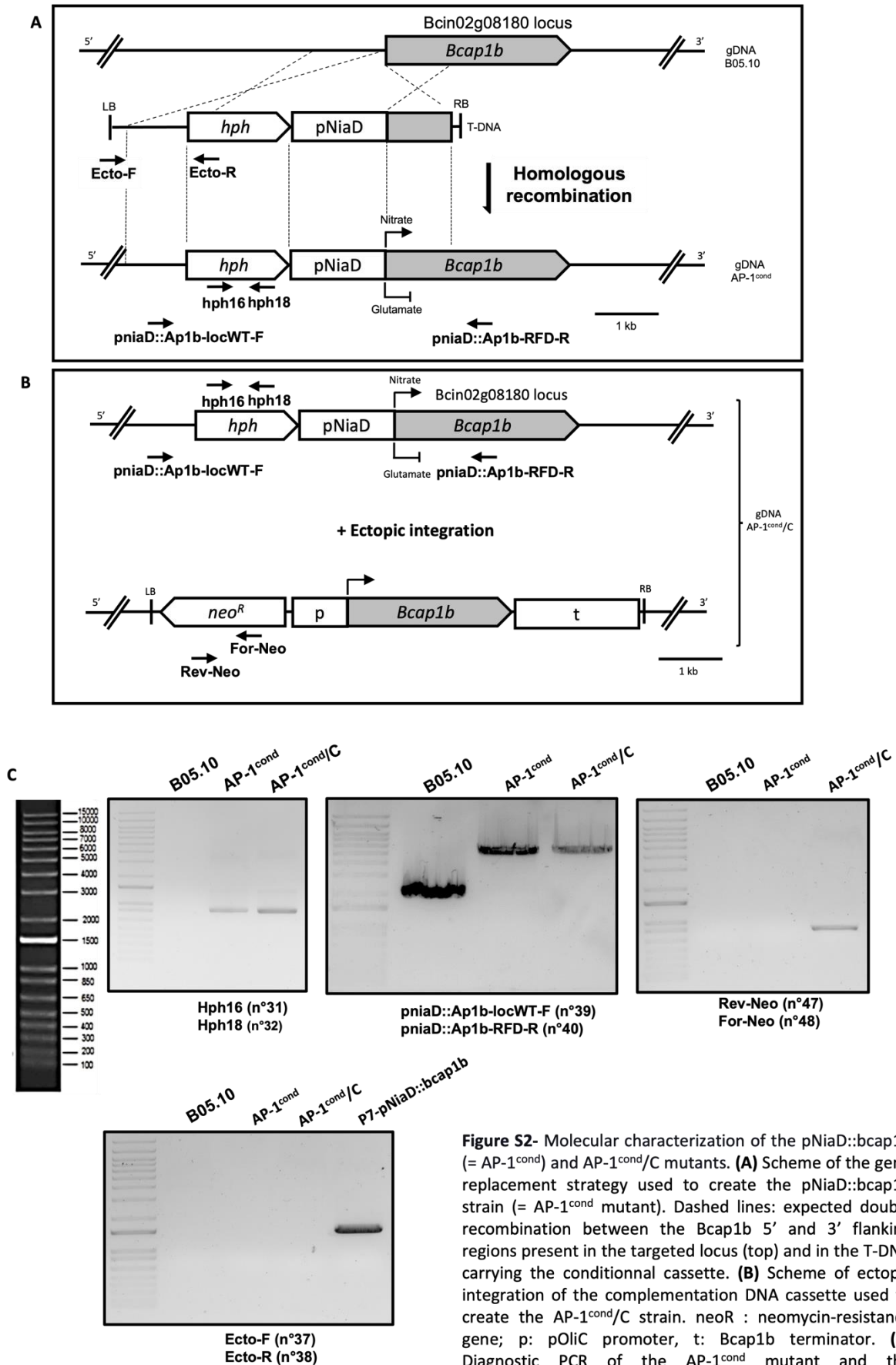


Figure S1- Identification of *Bcap1b* null mutants. **(A)** Scheme of the gene replacement strategy used to create $\Delta Bcap1b$ mutants. Dashed lines: expected double recombination between the *Bcap1b* 5' and 3' flanking regions present in the targeted locus (top) and in the *A. tumefaciens* T-DNA carrying the conditional cassette. **(B)** Diagnostic PCR of $\Delta Bcap1b$ transformants. Primers used are indicated at the bottom of gel images and as arrows in (A).



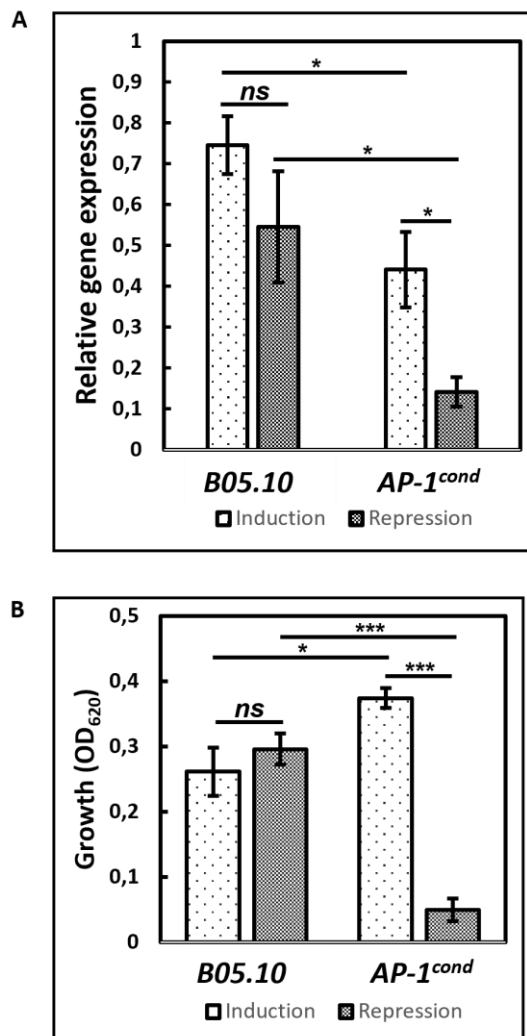


Figure S3- (A) Comparative *Bcap1b* expression patterns of the B05.10 strain and the AP-1^{cond} mutant under inducible and repressible conditions. For *Bcap1b* expression, mycelia were first grown for 4 days in liquid minimal medium and then transferred to either inducible (NaNO₃ 2 g.l⁻¹) or repressible conditions (glutamate 3 g.l⁻¹) for 45 min. All experiments were conducted with at least three biological replicates per condition. Data of each strain were treated independently. **(B)** Growth (OD₆₂₀) of B05.10 and AP-1^{cond} strains under inducible and repressible conditions in liquid minimal medium at 7 dpi. Conidia were grown in TPP microplates at 21°C. Student t-test, * *p*-value < 0.05, ** *p*-value < 0.01, *** *p*-value < 0.001.

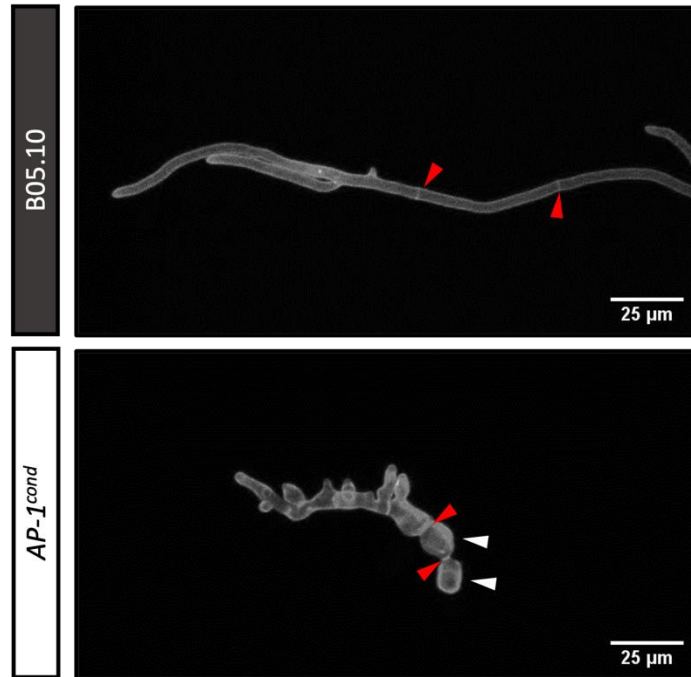


Figure S4 - The *AP-1^{cond}* mutant shows abnormal morphological traits - Confocal microscopy of hypha after 48h of growth under repressible conditions. The cell wall was stained with aniline blue. Image acquisition was carried out using a 40x objective under 405 nm laser excitation. Septa are indicated with red arrows and hyphal swelling with white arrows.

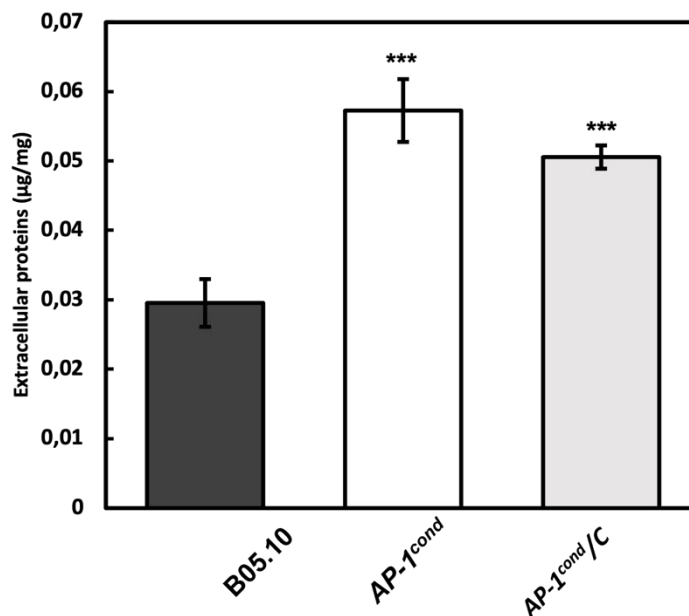


Figure S5- Quantification of extracellular proteins in minimal liquid medium (inducible condition) after three days of culture.

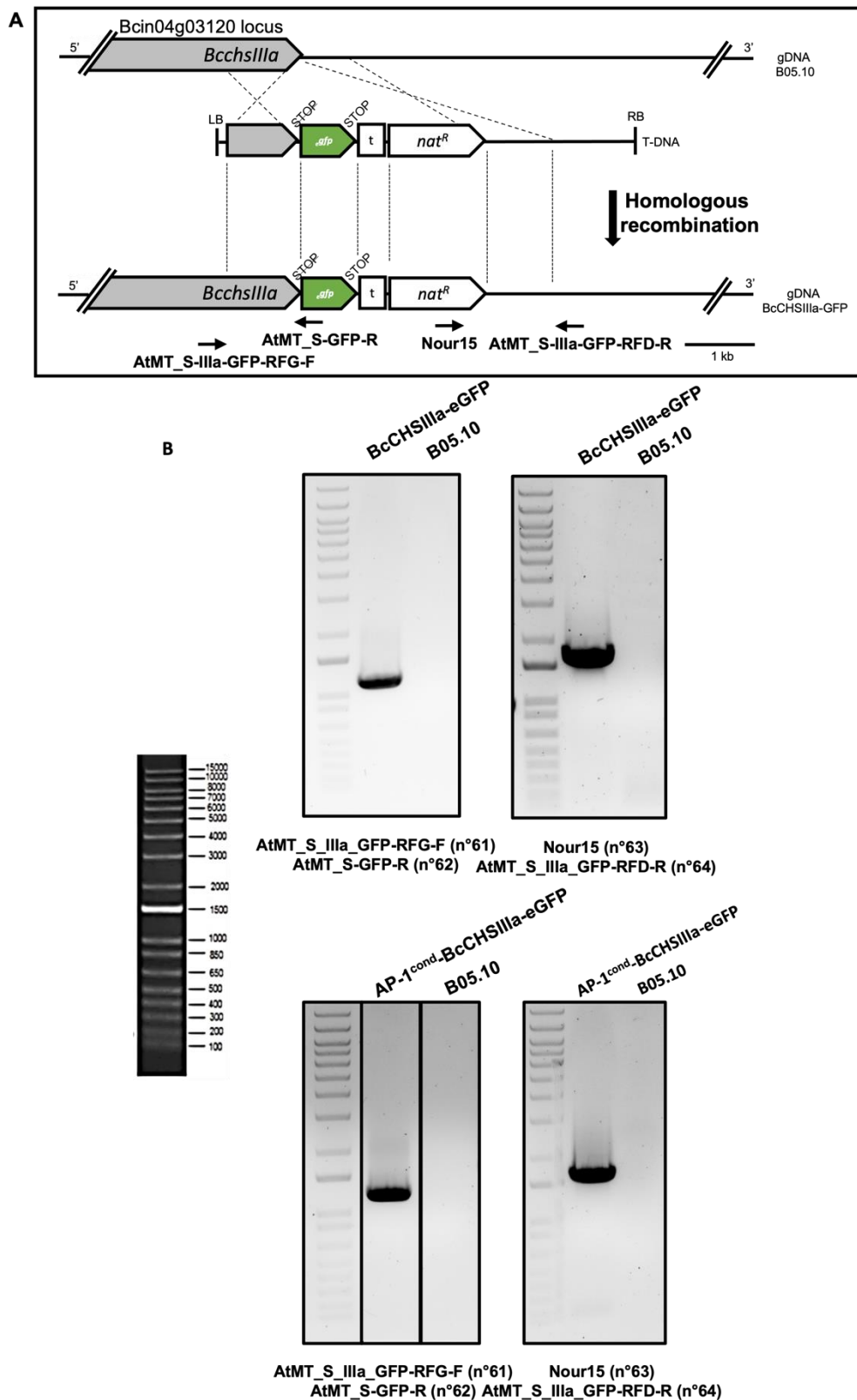


Figure S6- Molecular characterizations of the BcCHSIIIa-eGFP and AP-1^{cond}-BcCHSIIIa-eGFP strains **(A)** Scheme of the gene replacement strategy used to create the BcCHSIIIa-eGFP strain. Dashed lines: expected double recombination between the BcchsIIIa 5' and 3' flanking regions present in the targeted locus (top) and in the *A. tumefaciens* T-DNA carrying the translationnal-fusion cassette. **(B)** Diagnostic PCR of the BcCHSIIIa-eGFP and AP-1^{cond}-BcCHSIIIa-eGFP strains. Primers used are indicated at the bottom of gel images and as arrows in (A).

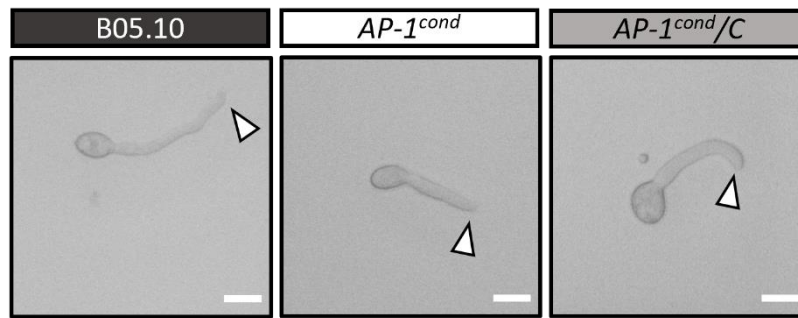


Figure S7 - The *AP-1^{cond}* mutant shows no defect in appressorium formation *in-vitro*
 Light microscopy of hypha after 6h of growth in liquid minimal medium (inducible condition). Appresoria are shown with white arrows. Scale bar = 20 μ m

6.2 Appendix S1

Experimental procedures

Construction of the $\Delta Bcap1b$ transformants, AP-1^{cond} mutant and the complemented strain AP-1^{cond}/C

Knock-out transformants and knock-in mutants were constructed using a gene replacement strategy. Genetic cassettes were constructed by double-joint PCR (Yu, et al., 2004). All primers used are listed in Table S1.

$\Delta Bcap1b$

For $\Delta Bcap1b$ construction (Fig. S1A), three DNA fragments were first amplified by PCR. The 5' flanking region of *bcap1b* (983 pb – fragment A), and the 3' flanking region of *bcap1b* (1316 pb – fragment C) were amplified from *Botrytis cinerea* genomic DNA (50 ng), using the primer pairs 1/2, and 5/6 respectively, while the hygromycine resistance cassette *hph* (1363 pb – fragment B) was amplified from P7-SDH vector using primer pair 3/4. Primer 2 contained a sequence homologous to the 5' end of the *hph* fragment for efficient fusion between fragments A and B, and primer 5 contained a sequence homologous to the 3' end of *hph* fragment for efficient fusion between fragments B and C. Purified A, B and C fragments were combined and amplified together to form the ABC fragment using primer pair 7/8 to form the $\Delta Bcap1b$ cassette. Primers 7 and 8 were flanked with *Bam*HI and *Eco*RI restriction sites, respectively. The gene replacement cassette $\Delta Bcap1b$ and the p7 vector were digested with *Bam*HI and *Eco*RI, at 37°C for 1h30. Ligation was carried out 4h at 25°C, using the T4 DNA Ligase to produce the p7- $\Delta Bcap1b$ plasmid. *E. coli* chemicomptent cells (OneShot™ TOP10, Invitrogen) were transformed with the ligation mixture and selected on LB-agar plates supplemented with kanamycin (50 µg.ml⁻¹). Plasmids were collected from *E. coli*, screened by restriction enzyme digestion (*Hind*III, 37°C) and then verified by sequencing. *Agrobacterium tumefaciens* mediated transformation (*At*MT) was used for the transformation of *Botrytis cinerea* using the protocol described by: (Rolland, Jobic, Fevre, & Burel, 2003). Basically, *Agrobacterium tumefaciens* (LBA1126) was transformed with p7- $\Delta Bcap1b$ and selected on kanamycin (50 µg.ml⁻¹) and spectinomycin (250 µg.ml⁻¹). *A. tumefaciens* containing p7- $\Delta Bcap1b$ were cultured with *B. cinerea* conidia on cellophane-covered agar plates for 2 days, 21°C. Then, cellophane sheets were transferred to selective media (Tanaka medium, hygromycin B – 70 µg.ml⁻¹) to select *B. cinerea* transformants for 5-7 days at 21°C.

Diagnostic PCR was performed to confirm that hygromycin-B-resistant transformants carried *hph* using primer pair 9/10. Homologous recombination was also detected by

diagnostic PCR on hygromycin B-resistant transformants using primer pairs 11/12 (left flanking region Fig. S1B left) and 13/14, respectively. Transformants with additional (i.e. ectopic) integration of the T-DNA were detected by PCR using the primer pairs 15/16 and eliminated. We tried to obtain homokaryotic lines of transformants by several rounds of single-spore isolation on culture medium containing hygromycin-B (70 $\mu\text{g}.\text{ml}^{-1}$). However, we were unable to obtain homokaryotic lines even after 5 round of single-spore isolation: presence of parental locus was detected using primer pair 11/14 (parental locus: 5.1 kb; mutated locus: 3.8 kb – Fig. S1B right).

The pNiaD::bcap1b strain / AP-1^{cond} mutant

For the construction of the AP-1^{cond} mutant (Fig. S2.A), four DNA fragments were first amplified. The 5' flanking region of *bcap1b* (1008 bp, fragment A), the *niaD* promoter (1475 pb, fragment B), and the 3' flanking region of *bcap1b* corresponding to the 5' end of *bcap1b* coding sequence (1022 pb, fragment D) were amplified from *Botrytis cinerea* genomic DNA (50 ng), using the primer pairs 17/18, 21/22 and 23/24 respectively. The *hph* fragment (C) containing the hygromycine-phosphotransferase gene under the control of the *TrpC* promoter was amplified from the p7-SDH vector using primer pair 19/20. Primer 2 contained a sequence homologous to the *hph* fragment for efficient fusion between fragments A and B. Purified A and B fragments were combined and amplified together to form the AB fragment using primer pair 25/26. The CD fragment was obtained by combination and amplification of fragments C and D with the use of the primer pair 27/28. Primer 26 contained a sequence homologous to the CD fragment for efficient fusion between fragments AB and CD, using primer pair 29/30. Primers 29 and 30 were flanked with *Bam*HI and *Sbf*I restriction sites, respectively.

The gene replacement cassette *pBcap1b-hph-pNiaD::bcap1b* and the p7 vector were digested with *Bam*HI and *Sbf*I, at 37°C for 1h30. Ligation was carried out 4h at 25°C, using the T4 DNA Ligase to produce the p7-*pNiaD::bcap1b* plasmid. *E. coli* chemicomptent cells (OneShot™ TOP10, Invitrogen) were transformed with the ligation mixture and selected on LB-agar plates supplemented with kanamycin (50 $\mu\text{g}.\text{ml}^{-1}$). Plasmids were collected from *E. coli*, screened by restriction enzyme digestion (*Hind*III, 37°C) and then verified by sequencing.

Agrobacterium tumefaciens mediated transformation (AtMT) was used for the transformation of *Botrytis cinerea*. *Agrobacterium tumefaciens* (LBA1126) was transformed with p7-*pNiaD::bcap1b* and selected on kanamycin (50 $\mu\text{g}.\text{ml}^{-1}$) and

spectinomycin (250 µg.ml⁻¹). *A. tumefaciens* containing p7- *pNiaD::bcap1b* were cultured with *B. cinerea* conidia on cellophane-covered agar plates for 2 days, 21°C. Then, cellophane sheets were transferred to selective media (Tanaka medium, hygromycin B – 70 µg.ml⁻¹) to select *B. cinerea* transformants for 5-7 days at 21°C.

Diagnostic PCR was performed to confirm that hygromycin-B-resistant transformants carried *hph* using primer pair 31/32 (884 pb, Fig. S2C left). Homologous recombination was also detected by diagnostic PCR on hygromycin B-resistant transformants using primer pairs 33/34 and 35/36, respectively. Transformants with additional (i.e. ectopic) integration of the T-DNA were detected by PCR using the primer pairs 37/38 (1.5 kb, Fig. S2C bottom left) Fig and eliminated.

Homokaryotic lines of transformants were obtained by several rounds of single-spore isolation on MMII minimal medium (2 g/L, NaNO₃) containing hygromycin-B (70 µg.ml⁻¹). Absence of *Bcap1b* parental locus and detection of *pNiaD::bcap1b* insertion at the targeted locus was verified by PCR and performed using primers pair 39/40 (parental locus: 2 kb; *pNiaD::bcap1b* insertion: 5 kb – Fig. S2C middle).

AP-1^{cond}/C

For complementation of the AP-1^{cond} mutant (Fig. S1.B), the *p7-nptii-pOliC-bcap1b* vector was constructed. The *nptii* gene confers resistance to Geneticin G418, and *bcap1b* is under the control of the strong promoter *pOliC* from *A. nidulans*. The construction of *p7-nptii-pOliC-bcap1b* vector followed a similar pattern to that of p7- *pNiaD::bcap1b*. The *pOliC::bcap1b* cassette was also constructed by double-joint PCR. Two fragments were first amplified to construct the *pOliC::bcap1b-term* cassette. The *OliC* promoter (900 bp, fragment A') was amplified from pBht2 (Mullins, et al., 2001) using primer pair 41/42. The *bcap1b* coding sequence and terminator (4500 bp, fragment B') were amplified from *Botrytis cinerea* genomic DNA (50 ng), using the primer pair 43/44. Primer 42 contained a sequence homologous to fragment B' for efficient fusion between fragments A' and B'. Purified A' and B' fragments were combined and amplified together to form the A'B' fragment (*pOliC::bcap1b* cassette) using primer pair 45/46. Primers 45/46 were flanked with 21 bp overlap sequences for *In Vivo Assembly* (García-Nafria, Watson, & Greger, 2016), IVA cloning in the *p7-nptII* vector. Plasmids were collected from *E. coli*, screened by restriction enzyme digestion (*PvuI*, 37°C) and verified by sequencing.

A. tumefaciens transformed with *p7-nptii-pOliC-bcap1b* vector were used for *AtMT* of the AP-1^{cond} mutant to produce the complemented strain *Bcap1_C*. *B. cinerea* transformants were selected using Geneticin G418 (150 µg.ml⁻¹). Diagnostic PCR was performed to

confirm that geneticin-resistant transformants carried *nptii^R* using primer pair 47/48 (Fig. S2C right). The absence of the parental locus (i.e. *bcap1b* under the control of its native promoter) was verified by PCR using primers 39/40 (Fig. S2C middle).

Construction of the BcCHSIIIa-GFP and AP-1^{cond}-BcCHSIIIa-GFP strains

To produce the BcCHSIIIa-eGFP mutant, eGFP was combined to the C-terminal end of BcCHSIIIa using a gene replacement strategy (Fig. S6). The genetic cassette *Bcchs3a-gfp-tniaD-nat^R-3UTR-term* was also produced by double-joint PCR. *nat^R* includes the *nat1* gene under the control of the *OliC* promoter and confers resistance to nourseothricin.

The 5' flanking region of *bcchs3a* (3' end of *bcchs3a* coding sequence excluding stop codon, 1031 bp, fragment A") and the 3' flanking region of *bcchs3a* (*bcchs3a* 3'UTR and terminator region, 924 pb, fragment C"), were amplified from *Botrytis cinerea* genomic DNA (50 ng), using primer pairs 51/52, and 55/56, respectively (Table S1). The *gfp-tniaD-nat^R* fragment (fragment B', 2494 bp) was amplified from the p7-BcCHSVa-GFP vector using primer pair 53/54. Primer 52 contained a sequence homologous to fragment B" for efficient fusion between fragments A" and B", while primer 55 was flanked with a sequence homologous to fragment B" to initiate the fusion between fragment B" and C". The A"B"C" fragment was amplified using primer pair 57/58 to produce the *Bcchs3a-gfp-tniaD-nat^R-3UTR-term* cassette. Primers 57 and 58 were flanked with 21 bp overlap sequences for IVA cloning in the *p7* vector to produce *p7-BcCHSIIIa-eGFP*. Plasmids were collected from *E. coli*, screened by restriction enzyme digestion (*EcoRI*, 37°C) and then verified by sequencing.

A. tumefaciens transformed with *p7-BcCHSIIIa-eGFP* vector were used for *AtMT* of the parental strain B05.10, and the AP-1^{cond} mutant to produce *BcCHSIIIa-eGFP* and *AP-1^{cond}-BcCHSIIIa-eGFP* strains. *B. cinerea* transformants were selected using nourseothricin (70 µg.ml⁻¹).

Diagnostic PCR was performed to confirm that nourseothricin-resistant transformants carried *nat^R* using primer pair 59/60 (Fig. S6). Homologous recombination was also detected by diagnostic PCR on nourseothricin -resistant transformants using primer pairs 61/62 and 63/64 (Fig. S6).

References

- García-Nafría, j., Watson, J. F., & Greger, I. H. (2016). IVA cloning: A single-tube universal cloning system exploiting bacterial In Vivo Assembly. *Scientific Reports*, 6(1), 27459. doi:10.1038/srep27459
- Mullins, E., Chen, X., Romaine, P., Raina, R., Geiser, D., & Kang, S. (2001). Agrobacterium - Mediated Transformation of *Fusarium oxysporum*: An Efficient Tool for Insertional Mutagenesis and Gene Transfer. *Phytopathology*®, 91(2), 173-180. doi:10.1094/PHYTO.2001.91.2.173
- Rolland, S., Jobic, C., Fevre, M., & Burel, C. (2003). Agrobacterium-mediated transformation of *Botrytis cinerea*, simple purification of monokaryotic transformants and rapid conidia-based identification of the transfer-DNA host genomic DNA flanking sequences. *Current Genetics*, 44(3), 164-171. doi:10.1007/s00294-003-0438-8
- Yu, J.-H., Hamari, Z., Han, K.-H., Seo, J.-A., Reyes-Domínguez, Y., & Scazzocchio, C. (2004). Double-joint PCR: a PCR-based molecular tool for gene manipulations in filamentous fungi. *Fungal Genetics and Biology*, 41(11), 973-981. doi:10.1016/j.fgb.2004.08.001

6.3 Table S1

Number	Name	Sequence (5' - 3')	Used for	
Primers used for <i>Δbcap1b</i> cassette construction and gene replacement analysis				
1		ATCCATGCTGGACTCCCAA	Gene knockout	
2		CCAAAAATGCTCCTCAATACAGTTAGATCTTCAAAGAACAGGGACCAG	Gene knockout	5' <i>Bcap1b</i> amplicon = A
3		AACTGATATTGAAGGACATTTTTGG	Gene knockout	
4		CTATTCCTTGCCCTGGAC	Gene knockout	<i>hph</i> amplicon = B
5		GTCCGAGGCAAGGAATAGATGTGAGGGATGGTAATAAGTAG	Gene knockout	
6		CTTGAAGCTGTAGTTGAAGGG	Gene knockout	3' <i>Bcap1b</i> amplicon = C
7		ATCGCTGGATCTCCCAAGTGTACACGCCG	Gene knockout	
8		TTATCAGAATTCGGTTGGTCTGAGTTCGGAT	Gene knockout	Amplification of the fused ABC cassette
9	<i>hph16</i>	TTTCAGTCTGATGTAGGAGG	Diagnostic PCR for mutated strain	
10	<i>hph18</i>	GAGTACTTCTACACAGCCATCG	Diagnostic PCR for mutated strain	Hygromycin(+) screening
11	Amont-AP1B-F	GATTGTTTGGCCGAGTTC	Diagnostic PCR for mutated strain	
12	<i>hph22</i>	TTCTACATCGAAGCTGAAAGC	Diagnostic PCR for mutated strain	Left flanking region
13	<i>hph16</i>	TTTCAGTCTGATGTAGGAGG	Diagnostic PCR for mutated strain	
14	Post-TAP1-B-Loc-R2	GAACCTGTGAACGCTAGAT	Diagnostic PCR for mutated strain	Right flanking region
15	Ecto-F	GTGGAATTGTAGCGGATAACAATT	Diagnostic PCR for mutated strain	
16	Ecto-R	AACTTTTCGATCAGAACTTCTCGAC	Diagnostic PCR for mutated strain	Ectopic integration (Left Border)
Parental locus: Amont-AP1B-F and Post-TAP1-B-Loc-R2				
Primers used for construction of the conditionnal cassette, <i>pNiaD::bcap1b</i> and gene replacement analysis of the AP-1^{cond} mutant				
17		ATCCATGCTGGACTCCCAA	Gene knockin	
18		CCAAAAATGCTCCTCAATACAGTTAGATCTTCAAAGAACAGGGACCAG	Gene knockin	5' <i>Bcap1b</i> amplicon = A
19		AACTGATATTGAAGGACATTTTTGG	Gene knockin	
20		GGTTGATGTTACTGACATCTAGTCTAT	Gene knockin	<i>hph</i> amplicon = B
21		TTACACAGGAAACAGCTGAAT	Gene knockin	
22		CGCTTCTAAAGGACTCGCGGTTGGAATATGTAGGAAACCAG	Gene knockin	<i>pNiaD</i> amplicon = C
23		GCGAGTCTTTCAAGGCG	Gene knockin	
24		GACTCCTTAATATCGAAGCCTG	Gene knockin	<i>Bcap1b</i> amplicon = D
25		TGCCGACTCCCAAGTGT	Gene knockin	
26		GCTCGAATTCAGCTTTCTCTGGTGTGATGACTGACATCTAGTCTATCC	Gene knockin	Fusion 5' <i>Bcap1b-hph</i> amplicon (=AB) with <i>pNiaD::Bcap1b</i> amplicon (=CD)
27		AGGAAACAGCTGAATTCGAGC	Gene knockin	
28		TATCCGAAGCTGATAATCTGC	Gene knockin	
29		ATCGCTGGATCCACTCCCAAGTGTACACGC	Gene knockin	5' <i>Bcap1b-hph-pNiaD::Bcap1b</i> amplicon (=ABCD)
30		tactaaCCTGAGGCGCTGATAATCTGCGCAGAGTAG	Gene knockin	
31	=9 - <i>hph16</i>	TTTCAGTCTGATGTAGGAGG	Diagnostic PCR for mutated strain	
32	=10 - <i>hph18</i>	GAGTACTTCTACACAGCCATCG	Diagnostic PCR for mutated strain	Hygromycin(+) screening
33		TGGGCAAGCATTCTCTGCC	Diagnostic PCR for mutated strain	
34		TAGCTCCAGCAGCCAAAAA	Diagnostic PCR for mutated strain	Left flanking region integration
35		ACGAATGTACCAAGTGGGGAAG	Diagnostic PCR for mutated strain	
36		TGCATCTGATCTCTCGGC	Diagnostic PCR for mutated strain	Right flanking region integration
37	=15 - Ecto-F	GTGGAATTGTAGCGGATAACAATT	Diagnostic PCR for mutated strain	
38	=16 - Ecto-R	AACTTTTCGATCAGAACTTCTCGAC	Diagnostic PCR for mutated strain	Ectopic integration (Left Border)
39	<i>pNiaD::Ap1b-loc</i> -WT-F	GATTCACATCTGAAAGCACGATGCG	Diagnostic PCR for mutated strain	
40	<i>pNiaD::Ap1b-RFD</i> -R	=20	Diagnostic PCR for mutated strain	<i>Bcap1b</i> parental locus and detection of <i>pNiaD::bcap1b</i> insertion
Primers used for complementation cassette AP-1^{cond}/C (=pOII::bcap1b) construct and integration analysis				
41		ACGTTGTAAACACGCGCCA	Complementation of AP-1 ^{cond}	
42		ACTTTAATCCTATTACCGCATGATGATGATGATGAGT	Complementation of AP-1 ^{cond}	<i>pOII</i> amplicon = A'
43		ATGGCGGTAGATAGGATTAAGGT	Complementation of AP-1 ^{cond}	
44		CTCTTTCCAGGCACTCAITCTA	Complementation of AP-1 ^{cond}	<i>Bcap1b-term</i> amplicon = B'
45		GTCGTTTCCGCTTTCAGTTTAAAGCAGCGCCAGTGCCA	Complementation of AP-1 ^{cond}	
46		CCTGTCAACACTGATGATTTACATTCATCTAGTCCCGATGATG	Complementation of AP-1 ^{cond}	<i>pOII::Bcap1b-term</i> amplicon = A'B'
47	For-Néo	ATGATTGAACAAGATGGATTGCAG	Diagnostic PCR for complemented strain	
48	Rev-Néo	TCAGAAGACTGCTCAAGAAG	Diagnostic PCR for complemented strain	G418(+)/neomycin screening
49	=25		Diagnostic PCR for complemented strain	
50	=20		Diagnostic PCR for complemented strain	<i>Bcap1b</i> parental locus
Name				
Sequence (5' - 3')				
Used for				
Primers used for <i>Bcchs3a::eGFP</i> translational fusion and gene replacement analysis				
51		TCTTGTGCTACCCCTACTGCT	Gene knockin	
52		CCTCACCCTGGAAACCATCTCCTCCCTCCACGCTCTCAGAACGACACATC	Gene knockin	3' CDS <i>Bcchs3a</i> amplicon = A"
53		ATGGTTCCAAAGGTTGAGG	Gene knockin	
54		CCTTAGAGTATGATGATATAAGTCTTGTTCAGGGCAGGGCATG	Gene knockin	<i>eGFP-tNiaD-NatR</i> amplicon = B"
55		ACAAGACTTATATCATACACTCTAGAAGG	Gene knockin	
56		CAGTAGGATTTTGGTTGCTGAC	Gene knockin	3' UTR <i>Bcchs3a-term</i> amplicon = C"
57		CGAATTCAGCTCGGTACCCCTGCTTCGGACACTACTGCC	Gene knockin	
58		GTCGACTTAGAGGATCCCTGACGCTTGGCCGAAAGATAT	Gene knockin	3' CDS <i>Bcchs3a-eGFP-tNiaD-NatR-3'UTR-Bcchs3a-term</i> = A"B"C"
59		GCTGGAAAGCCAGGATAGAATA	Diagnostic PCR for mutated strain	
60		GCAGGCGATGCTCATGAGAG	Diagnostic PCR for mutated strain	Nourseotheticin(+) screening
61	AtMT_S-IIIa-GFP-RFG-F	TCAGTTGGTTCATGTTATCTTCTCT	Diagnostic PCR for mutated strain	
62	AtMT_S-GFP-R	GGACATTGCAGGGATACTT	Diagnostic PCR for mutated strain	Left flanking region integration
63	Nour15	CCATGACCACCTTTCAGCACA	Diagnostic PCR for mutated strain	
64	AtMT_S-IIIa-GFP-RFD-R	ATAGGAACCTGAGAAGTGAATAGCTCC	Diagnostic PCR for mutated strain	Right flanking region integration
Primers used for qRT-PCR analysis				
65	qPCR- <i>bcap1b</i> -5-F	GAGACATTTGTGGCCAAAGT	qRT-PCR	
66	qPCR- <i>bcap1b</i> -3-R	TGAATAGCGCGCTGTGGA	qRT-PCR	

6.4 Table S2

Classification and relative quantification of B05.10 and AP-1^{cond} secreted proteins with a predicted signal peptide and no transmembrane domain.

Accession	Abundance Ratio: (Mutant) / (Control)	Functional annotation	Usual name	CAZY	InterPro domain	EC number	Enz. Activity	References
Bcin01p00800.1	0.04	Oxidoreduction	Bclcc8	AA1	IPR001117: Multicopper oxidase, type 1	EC 1.10.3.2	Laccase	1
Bcin01p00930.2	40,986	Other metabolisms	Bcfcpr2		IPR001179: Peptidyl-prolyl cis-trans isomerase,	EC:5.2.1.8	peptidylprolyl isomerase	
Bcin01p01760.1	0.119	FCWE		GH18	IPR013781: Glycoside hydrolase	EC:3.2.1.14	Chitinase	
Bcin01p02320.1	0.009	Lipid metabolism			IPR002642: Lysophospholipase	EC:3.1.1.5	lysophospholipase	
Bcin01p02460.1	14,104	Other CAZY		CBM63	IPR009009: RlpA-like double-psi beta-barrel domain	None	Expansin	
Bcin01p02690.1	0.012	Protein degradation			IPR008758: Peptidase S28	EC 3.4.14.2	Dipeptidyl-peptidase II	10
Bcin01p04530.1	0.083	Metabolism			IPR000073: Alpha/beta hydrolase	None	None	
Bcin01p05680.1	0.002	Other CAZY		GH47	IPR001382: Glycoside hydrolase, family 47	EC 3.2.1.11	mannosidase	
Bcin01p05720.2	0.19	FCWE			IPR011330: Glycoside hydrolase/deacetylase, beta/alpha-barrel	None	None	
Bcin01p06010.1	0.046	FCWE	Bccrh1	GH16	IPR000757: Glycoside hydrolase, family 16	EC 3.2.1.73	Beta-glucanase	2
Bcin01p06060.1	0.015	Unknown			None	None	None	1
Bcin01p06210.1	0.007	Other Metabolisms			IPR001563: Peptidase S10	None	None	
Bcin01p06250.1	0.021	Lipid metabolism			IPR016035: Acyl transferase/acyl hydrolase/lysophospholipase	EC:3.1.1.5	lysophospholipase	
Bcin01p06900.1	0.003	Other Metabolisms			IPR009486: Purine nucleoside permease	None	None	
Bcin01p07210.1	0.014	Other CAZY		GH92	IPR005887: Alpha-1,2-mannosidase, putative	None	None	
Bcin01p07530.1	0.009	Other CAZY		GH125	IPR008313: Uncharacterised conserved protein UCP028846	None	None	
Bcin01p08110.1	0.016	PCWDE-Hemicellulose		GH27, CBM13	IPR000111: Glycoside hydrolase, clan GH-D	EC:3.2.1.22	alpha-galactosidase	10
Bcin01p08910.1	0.06	PCWDE-Hemicellulose		CE16	IPR001087: Lipase, GDSL	None	None	10
Bcin01p11160.1	0.025	PCWDE-Pectin		GH28	IPR000743: Glycoside hydrolase, family 28	EC:3.2.1.67	Exopolylacturonase	10
Bcin01p11220.1	5,918	FCWE		GH17	None	EC:3.2.1.39	glucan endo-1,3-beta-D-glucosidase	1
Bcin01p11300.1	5,138	Unknown			IPR018466: Ser-Thr-rich glycosyl-phosphatidyl-inositol-anchored membra	None	None	
Bcin02p00210.1	0.038	Lipid metabolism			IPR002018: Carboxylesterase, type B	EC:3.1.1.7	acetylcholinesterase	
Bcin02p00280.1	0.004	Oxidoreduction			IPR006094: FAD linked oxidase	None	None	1
Bcin02p00420.2	0.095	PCWDE-Hemicellulose		GH3	None	EC:3.2.1.37	xylan 1,4-beta-xylosidase	
Bcin02p02410.1	16,435	FCWE		GH128	IPR013781: Glycoside hydrolase, catalytic domain	None	None	10
Bcin02p03090.1	0.035	Other CAZY		GH1	IPR001360: Glycoside hydrolase, family 1	None	none	
Bcin02p04090.1	0.008	FCWE		GH16	IPR013320: Concnavalin A-like lectin/glucanase	None	None	
Bcin02p04290.1	0.022	PCWDE-Pectin		PL7	IPR013320: Concnavalin A-like lectin/glucanase, subgroup	None	None	
Bcin02p04350.1	3,616	Unknown			None	None	None	

Bcin02p04400.1	11,286	Unknown			IPR002889: Carbohydrate-binding WSC	None	None	None	None
Bcin02p04550.1	0,09	Unknown			None	None	None	None	None
Bcin02p05630.1	0,006	FCWE	Bcylsm1	CBM50		0	None	None	Comptons et al. (unpublished)
Bcin02p06940.1	0,011	FCWE	Bcgsa1	GH72, CBM43	IPR004886: Glucanosyltransferase GAS1	EC:2.4.1.-	1,3-beta-glucanosyltransferase GAS1	5	
Bcin02p07080.1	0,052	Other CAZY		AA3		0	EC:1.1.99.1 choline dehydrogenase	1	
Bcin02p07700.1	0,027	PCWDE-Pectin	Bcara1	GH43	IPR006710: Glycoside hydrolase, family 43	EC:3.2.1.99	arabinan endo-1,5-alpha-L-arabinosidase	3	
Bcin02p08230.1	0,013	Lipid metabolism			IPR002018: Carboxylesterase, type B	EC:3.1.1.8	cholinesterase		
Bcin02p08380.1	12,879	PCWDE-HP		GH93	IPR011040: Sialidases	None	None		
Bcin02p08590.1	0,03	Protein degradation	Bcap2		IPR001461: Aspartic peptidase	EC:3.4.23.2	Endopeptidase A	8	
Bcin02p09380.1	5,587	Other Metabolisms			IPR013658: SMP-30/Gluconolactonase/LRE-like region	EC:3.1.1.17	gluconolactonase		
Bcin03p00280.1	25,837	PCWDE-Pectin		PL1	IPR002022: Pectate lyase/Amb allergen	EC:4.2.2.10	pectin lyase	10	
Bcin03p00380.1	0,004	Oxidoreduction			IPR006094: FAD linked oxidase, N-terminal	None	None	1	
Bcin03p01250.1	0,032	Unknown			None	None	None	0	
Bcin03p01540.1	0,01	Oxidoreduction		AA3	IPR000172: Glucose-methanol-choline oxidoreductase, N-terminal	EC:1.1.99.1	choline dehydrogenase	1	
Bcin03p01580.1	0,056	Lipid metabolism			IPR002018: Carboxylesterase, type B	None	None		
Bcin03p01600.1	0,012	Other CAZY		GHnc	None	None	None		
Bcin03p02710.1	0,005	PCWDE-Hemicellulose		GH27	IPR000111: Glycoside hydrolase, clan GH-D	EC:3.2.1.22	alpha-galactosidase		
Bcin03p02970.1	0,024	FCWE	Bcoda3	CBM18, CE4	IPR001002: Chitin-binding, type 1	EC 3.5.1.10	Chitin deacetylase	10	
Bcin03p03480.1	0,227	PCWDE-Hemicellulose	BcXyn10A	CBM1_GH10	IPR001000: Glycoside hydrolase, family 10	EC 3.2.1.8	Endo-1,4-beta-xylanase	10	
Bcin03p03830.1	0,167	PCWDE-Pectin	Bcpme2	CE8	IPR000070: Pectinesterase, catalytic	EC 3.1.1.11	Pectinesterase	10	
Bcin03p04010.1	0,005	PCWDE-Cellulose	Bccel5A	GH5	IPR001547: Glycoside hydrolase, family 5	EC:3.2.1.4	cellulase; endoglucanase	4	
Bcin03p04730.1	0,043	Lipid metabolism			IPR002018: Carboxylesterase, type B	EC:3.1.1.8	Acting on ester bonds		
Bcin03p05060.1	0,034	PCWDE-Pectin		CE8	IPR000070: Pectinesterase, catalytic	None	None	10	
Bcin03p05600.2	0,05	Lipid metabolism			IPR007312: Phosphoesterase	EC 3.1.4.3	Phospholipase C	10	
Bcin03p05820.1	106,871	PCWDE-Pectin		PL1	IPR002022: Pectate lyase/Amb allergen	EC:4.2.2.2	Pectate lyase		
Bcin03p07320.1	0,013	Other Metabolisms			IPR001568: Ribonuclease T2-like	None	None		
Bcin03p07360.1	70,019	PCWDE-Pectin		PL1	IPR011050: Pectin lyase fold/virulence factor	EC:4.2.2.10	pectin lyase		
Bcin03p08710.1	0,116	Other CAZY		GH3	IPR001764: Glycoside hydrolase, family 3, N-terminal	EC:3.2.1.21	beta-glucosidase		
Bcin04p01310.1	0,025	Other CAZY		GHnc	None	None	None	10	
Bcin04p02310.1	0,01	Other Metabolisms			IPR009486: Purine nucleoside permease	None	None		

Bcin04p05020.1	0,008	Unknown	Bcf1p1	IPR00782: FAS1 domain	None	None	1
Bcin04p06150.1	0,05	FCWE	GH76	IPR005198: Glycoside hydrolase, family 76	None	None	5
Bcin04p06190.1	0,052	Lipid metabolism		IPR002018: Carboxylesterase, type B	EC:3.1.1.1 / carboxylesterase		
Bcin04p06990.1	16,042	PCWDE-HP	GH43	IPR006710: Glycoside hydrolase, family 43	EC:3.2.1.99 endo- α -1,5-arabinase		
Bcin05p01510.1	0,004	Unknown		None	None	None	10
Bcin05p02520.1	0,125	PCWDE-Pectin	Bcpex1,PGX	IPR000743: Glycoside hydrolase, family 28	EC:3.2.1.67 Exopolysaccharuronase		10
Bcin05p03460.1	61,548	Protein degradation		IPR022742: Serine aminopeptidase	None	None	
Bcin05p04010.1	0,01	Unknown		None	None	None	
Bcin05p05830.1	0,163	Protein degradation		IPR030400: Sedolisin domain	EC:3.4.14.9 Tripeptidyl-peptidase I		
Bcin06p00960.1	0,065	Unknown		IPR023703: Membrane-bound lytic murein transglycosylase F	None	None	
Bcin06p01010.1	0,073	Protein degradation		IPR000209: Peptidase S8/S53 domain	EC:3.4.14.9 tripeptidyl-peptidase I		
Bcin06p01580.1	0,121	PCWDE-Pectin	GH79	IPR017853: Glycoside hydrolase, superfamily	None	None	
Bcin06p01630.1	0,044	PCWDE-Pectin	GH79	IPR017853: Glycoside hydrolase, superfamily	None	None	
Bcin06p02140.1	0,111	PCWDE-Pectin	GH28	IPR000743: Glycoside hydrolase, family 28	EC:3.2.1.67 exo-polygalacturonase		
Bcin06p02510.1	0,01	Protein degradation		IPR001563: Peptidase S10, serine carboxypeptidase	EC:3.4.16.6 carboxypeptidase D		1
Bcin06p03070.1	0,025	Protein degradation		IPR000209: Peptidase S8/S53 domain	EC:3.4.14.9 Tripeptidyl-peptidase I		
Bcin06p04830.1	0,043	FCWE	GH5	IPR001547: Glycoside hydrolase, family 5	None	None	
Bcin06p05050.1	87,21	Other CAZY	AA13,CBM20	IPR002044: Carbohydrate binding module family 20	EC:1.14.99.1ytic starch monoxygenase		
Bcin06p05200.1	0,022	Metabolism		IPR000560: Histidine phosphatase superfamily, clade-2	None	None	
Bcin06p06580.1	0,067	PCWDE-Pectin	GH78	IPR008928: Six-hairpin glycosidase-like	None	None	
Bcin06p06670.1	0,001	Unknown		None	None	None	
Bcin06p07020.1	0,182	Lipid metabolism		IPR002018: Carboxylesterase, type B	EC:3.1.1.7 acetylcholinesterase		
Bcin06p07150.1	93,176	Oxidoreduction		IPR006094: FAD linked oxidase, N-terminal	None	None	10
Bcin07p01720.1	0,186	Protein degradation		IPR001375: Peptidase S9, prolyl oligopeptidase, catalytic domain	EC:3.4.19.1 Acylaminoacyl-peptidase		
Bcin07p02730.1	0,04	FCWE	GH55	IPR012334: Pectin lyase fold	EC:3.2.1.58 glucan 1,3-beta-glucosidase		
Bcin07p02940.1	4,852	Unknown		IPR006652: Keich repeat type 1	None	None	10
Bcin07p03770.1	0,012	FCWE	GH16	IPR013320: Concanavalin A-like lectin/glucanase, subgroup	None	None	
Bcin07p04000.1	0,026	Other CAZY	GH92	IPR005887: Alpha-1,2-mannosidase, putative	None	none	10
Bcin07p04370.1	0,003	Protein degradation		IPR029045: ClpP/crotonase-like domain	EC:3.4.21. None		1
Bcin07p05440.1	0,041	Unknown		None	None	None	

Bcin07p06780.1	0,395	Oxidoreduction	Bccc9	AA1	IPR001117: Multicopper oxidase, type 1	EC 1.10.3.2 Laccase	9
Bcin07p06950.1	0,024	Other Metabolisms			IPR001910: Inosine/uridine-preferring nucleoside hydrolase domain	None	
Bcin07p07080.1	28,857	Other Metabolisms	Bchap2		IPR016274: Histidine acid phosphatase, eukaryotic	EC:3.1.3.2 acid phosphatase	
Bcin08p00150.1	0,027	Unknown			IPR000909: Phospholipase C, phosphatidylinositol-specific, X domain	EC:4.6.1.13 phosphatidylinositol diacylglycerol-lyase	
Bcin08p00280.1	0,002	Protein degradation			IPR001563: Peptidase S10, serine carboxypeptidase	EC 3.4.16.5 Carboxypeptidase Y	1
Bcin08p00400.1	18,985	Unknown			None	None	
Bcin08p00720.1	0,012	Protein degradation	Bcap14		IPR001461: Aspartic peptidase	EC 3.4.23.2 Endopeptidase A	8
Bcin08p00890.1	0,016	PCWDE-HP		GH51	None	EC 3.2.1.55 α -Arabinofuranosidases	10
Bcin08p00910.1	3,931	FCWE	Bcbg12	GH17	IPR000490: Glycoside hydrolase, family 17	EC 3.2.1.58 Exo-1,3-beta-glucanase	
Bcin08p00950.1	0,231	PCWDE-Hemicellulose		CE16	IPR001087: Lipase, GDSL	None	10
Bcin08p01020.1	0,269	Protein degradation			IPR000209: Peptidase S8/S53 domain	EC 3.4.14.9 Tripeptidyl-peptidase I	1
Bcin08p01140.1	5,044	FCWE			IPR021054: Cell wall galactomannoprotein	None	
Bcin08p02120.1	0,077	PCWDE-Hemicellulose		GH27,CBM35	IPR002241: Glycoside hydrolase, family 27	EC:3.2.1.22 Alpha-galactosidase	10
Bcin08p02380.1	48,13	Other Metabolisms			IPR005788: Disulphide isomerase	EC:5.3.4.1 protein disulfide-isomerase	
Bcin08p02990.3	31,322	Protein degradation	Bcser2		IPR000209: Peptidase S8/S53 domain	EC:3.4.21.4 peptidase beta	6
Bcin08p03760.1	0,024	Protein degradation	Bcap10		IPR001461: Aspartic peptidase	None	8
Bcin08p03820.1	28,344	PCWDE-Pectin		PL1	IPR002022: Pectate lyase/Amb allergen	EC 4.2.2.10 Pectin lyase	
Bcin08p05000.1	0,054	Oxidoreduction			IPR010424: Ethanolamine utilisation EutQ	None	
Bcin08p05870.1	0,024	PCWDE-Hemicellulose		GH95	IPR008928: Six-hairpin glycosidase-like	EC 3.2.1.51 Alpha-L-fucosidase	10
Bcin08p06110.1	7,422	FCWE		GH76	IPR005198: Glycoside hydrolase, family 76	EC 3.2.1.10 Mannan endo-1,6- α -mannosidase	1
Bcin08p06900.1	0,009	Unknown			IPR003609: Apple-like	None	
Bcin09p00450.1	0,055	Lipid metabolism			IPR002018: Carboxylesterase, type B	None	
Bcin09p00460.1	0,081	Unknown	Bcibp		None	None	
Bcin09p00620.1	9,631	FCWE	Bcda4		IPR002509: Polysaccharide deacetylase	EC 3.5.1.10 Chitin deacetylase	10
Bcin09p00770.1	0,01	Unknown			IPR011042: Six-bladed beta-propeller, TolB-like	EC:3.1.1.17 gluconolactonase	
Bcin09p01150.2	5,937	Other CAZY		GH131,CBM1	IPR000254: Cellulose-binding domain, fungal	None	
Bcin09p03430.1	0,009	Other Metabolisms			IPR000120: Amidase	EC:3.5.1.4 amidase	
Bcin09p03700.1	485,497	Unknown			None	None	
Bcin09p04020.1	0,136	Other CAZY		CEnc	IPR013831: SGNH hydrolase-type esterase domain	none	10
Bcin09p04230.1	8,927	Unknown			None	None	1

Bcin09p04440.1	0,011	PCWDE-HP	GH51	IPR010720: Alpha-L-arabinofuranosidase	EC 3.2.1.55 α -Arabinofuranosidases	10
Bcin09p04570.1	0,059	Other CAZY	AA3	IPR000172: Glucose-methanol-choline oxidoreductase, N-terminal	none	10
Bcin09p04790.1	0,146	PCWDE-Hemicellulose	GH39	IPR000514: Glycoside hydrolase, family 39	none	10
Bcin09p05250.1	0,141	Unknown		None	None	10
Bcin10p00850.1	11,603	Other Metabolisms		IPR006094: FAD linked oxidase, N-terminal	None	None
Bcin10p01020.1	80,661	Unknown		None	None	None
Bcin10p01080.1	0,011	Oxidoreduction	AA3	IPR000172: Glucose-methanol-choline oxidoreductase, N-terminal	EC 1.1.1.-.- Glucose-MeOH-choline oxidoreductase	10
Bcin10p01510.1	0,024	Unknown		None	None	10
Bcin10p01610.1	0,049	PCWDE-HP	GH43	IPR006710: Glycoside hydrolase, family 43	None	10
Bcin10p01890.1	0,014	Protein degradation		IPR002029: Peptidase S8/S53 domain	EC 3.4.14.9 Tripeptidyl-peptidase I	1
Bcin10p02180.1	0,073	Unknown	BcCFEM1	IPR008427: Extracellular membrane protein, CFEM domain	None	None
Bcin10p02560.1	0,08	Oxidoreduction	Bcprd7	IPR000028: Chloroperoxidase	None	None
Bcin10p03450.1	19,293	Unknown		IPR021851: Protein of unknown function DUF3455	None	10
Bcin10p04320.1	0,123	Protein degradation	Bcqp4	IPR001563: Peptidase S10, serine carboxypeptidase	EC:3.4.16.5 carboxypeptidase C	
Bcin10p04330.1	0,007	Protein degradation		IPR001563: Peptidase S10, serine carboxypeptidase	None	10
Bcin10p05630.1	0,136	Other CAZY	GH3	IPR001764: Glycoside hydrolase, family 3, N-terminal	EC 3.2.1.21 Beta-glucosidase	10
Bcin10p05700.1	0,132	Unknown		None	None	None
Bcin10p05710.1	0,004	Other Metabolisms	GH32	IPR013320: Concanavalin A-like lectin/glucanase, subgroup	EC:3.2.1.26 invertase	10
Bcin10p06130.1	0,023	PCWDE-Pectin	GH28	IPR000743: Glycoside hydrolase, family 28	EC:3.2.1.67 exo-polygalacturonase	10
Bcin11p00010.1	0,037	Other CAZY	GH1	IPR001360: Glycoside hydrolase, family 1	None	None
Bcin11p01370.1	6,811	FCWE	GH55	IPR011050: Pectin lyase fold/virulence factor	EC:3.2.1.58 glucan 1,3-beta-glucosidase	
Bcin11p06400.1	0,015	Unknown		None	None	10
Bcin11p06440.1	0,004	PCWDE-Hemicellulose	GH31	IPR000322: Glycoside hydrolase, family 31	EC:3.2.1.20 alpha-glucosidase	1
Bcin12p00180.1	0,041	Protein degradation	Bcap9	IPR001461: Aspartic peptidase	EC 3.4.23.1. Aspergillopepsin I	8
Bcin12p00300.1	0,074	PCWDE-HP	GH35	IPR001944: Glycoside hydrolase, family 35	EC 3.2.1.23 β -Galactosidases	
Bcin12p01270.1	0,061	Protein degradation		IPR001461: Aspartic peptidase	None	None
Bcin12p01520.1	41,87	Oxidoreduction	Bego2	IPR009880: Glyoxal oxidase, N-terminal	EC 1.1.3.9 Galactose oxidase	10
Bcin12p02040.1	0,002	Protein degradation	Bcap8	IPR001461: Aspartic peptidase	EC 3.4.23.2 Polyporopepsin	8
Bcin12p03270.1	22,575	Protein degradation		IPR007484: Peptidase M28	EC:3.4.11.1 bacterial leucyl aminopeptidase	
Bcin12p04530.1	0,044	PCWDE-Pectin	GH28	IPR000743: Glycoside hydrolase, family 28	EC:3.2.1.67 exo-polygalacturonase	

Bcin12p04640.1	0,051	Oxidoreduction			IPR006094: FAD linked oxidase, N-terminal	None	None	10
Bcin12p06120.1	0,009	Unknown		GH131	None	None	None	
Bcin12p06330.1	0,003	FCWE			IPR000420: Yeast PIR protein repeat	None	None	
Bcin12p06360.1	0,061	Lipid metabolism			IPR002018: Carboxylesterase, type B	None	None	
Bcin12p06770.1	4,933	Unknown			IPR011042: Six-bladed beta-propeller, TolB-like	None	None	10
Bcin13p00040.1	28,179	Unknown			IPR011024: Gamma-crystallin-related	None	None	
Bcin13p00300.1	34,406	Unknown			None	None	None	
Bcin13p00380.1	27,014	Unknown			None	None	None	10
Bcin13p00600.1	22,241	Unknown			None	None	None	
Bcin13p02010.1	40,16	Oxidoreduction			IPR008972: Cupredoxin	None	None	
Bcin13p02330.1	0,058	FCWE		GH72	IPR004886: Glucanoyltransferase	EC:2.4.1.- 1,3-beta-glucanoyltransferase GASS	None	10
Bcin13p05110.1	0,067	Other CAZY		GH13	IPR006047: Glycosyl hydrolase, family 13	EC:3.2.1.1 alpha-amylase	None	
Bcin14p00610.5	0,021	PCWDE-Pectin	Bcpg2, BcPGA2	GH28	IPR000743: Glycoside hydrolase, family 28	EC 3.2.1.15 Polygalacturonase	None	7
Bcin14p00760.1	0,033	Other Metabolisms			IPR002828: phosphatase/nucleotidase	None	None	10
Bcin14p00810.1	0,012	Unknown			IPR027372: Phytase-like domain	None	None	1
Bcin14p00850.1	33,345	PCWDE-Pectin	Bcpg1, BcPGA1	GH28	IPR000743: Glycoside hydrolase, family 28	EC 3.2.1.15 Polygalacturonase	None	8
Bcin14p02510.1	0,002	Oxidoreduction	BcIcc2	AA1	IPR001117: Multicopper oxidase, type 1	None	None	9
Bcin14p03140.1	72,668	Other Metabolisms			IPR000026: Guanine-specific ribonuclease N1/T1	None	None	
Bcin14p03970.1	11,878	FCWE		GH72	IPR004886: Glucanoyltransferase	EC:2.4.1.- 1,3-beta-glucanoyltransferase GASS	None	1
Bcin14p04560.1	0,051	Other CAZY		CEnc	IPR013830: SGNH hydrolase-type esterase domain	None	None	
Bcin14p05500.1	0,02	Oxidoreduction	Bcgod1	AA3	IPR000172: Glucose-methanol-choline oxidoreductase, N-terminal	None	None	
Bcin14p05530.1	11,262	Protein degradation	Bczps1		IPR024079: Metallopeptidase, catalytic domain	None	None	
Bcin14p05570.1	0,02	Oxidoreduction			IPR002227: Tyrosinase copper-binding domain	EC:1.14.18. tyrosinase	None	
Bcin15p00130.1	9,422	Cuticle degradation		CE5	IPR000675: Cutinase	EC 3.1.1.72. Acetylxylylan esterase	None	1
Bcin15p00170.1	30,504	Unknown			IPR011044: Quinoprotein amine dehydrogenase, beta chain-like	None	None	
Bcin15p01030.1	0,065	PCWDE-HP		CE1, CBM1	IPR010126: Esterase, PHB depolymerase	EC 3.1.1.73 Feruloyl esterase	None	10
Bcin15p01050.1	0,088	Protein degradation	Bcape3		IPR003137: Protease-associated domain, PA	EC:3.4.11.1 aminopeptidase Y	None	10
Bcin15p03150.1	0,007	Protein degradation			IPR000209: Peptidase S8/S53 domain	EC 3.4.14.9 Tripeptidyl-peptidase I	None	1
Bcin15p04670.2	0,059	Protein degradation	Bcser8		IPR000209: Peptidase S8/S53 domain	EC 3.4.14.9 Tripeptidyl-peptidase I	None	1
Bcin15p05030.1	0,012	PCWDE-Pectin		GH28	IPR000743: Glycoside hydrolase, family 28	None	None	

Bcin16p00080.1	0,284	Oxidoreduction		IPR006094: FAD linked oxidase, N-terminal	None	None
Bcin16p01590.1	0,011	FCWE	GH18,CBM1	IPR000254: Cellulose-binding domain, fungal	None	None
Bcin16p02130.1	0,001	Unknown		IPR002018: Carboxylesterase, type B	None	None
Bcin16p02490.1	0,008	Lipid metabolism		IPR000073: Alpha/beta hydrolase fold-1	None	1
Bcin16p02560.1	0,046	Other Metabolisms		IPR008928: Six-hairpin glycosidase-like	None	10
Bcin16p03950.1	0,055	PCWDE-Cellulose	GH7	IPR001722: Glycoside hydrolase, family 7	None	None
Bcin16p04210.1	0,016	Oxidoreduction	Bcd11	IPR000627: Intradiol ring-cleavage dioxygenase, C-terminal	EC 3.2.1.91 Cellulose 1,4-beta-cellobiosidase	10
Bcin16p05195.1	15,426	Unknown		IPR008914: Phosphatidylethanolamine-binding protein PEBP	EC 1.13.11. Dioxigenase	10

References

1. Choquer M, Rasclé C, Gonçalves I, de Vallée A, Ribot C, Loisel E, Smilevski P, Ferria J, Savadogo M, Souibgui E, Gagey MJ, Dupuy JW, Rollins JA, Marcato R, Nours C, Bruel C, Pousseeau N. The infection cushion of *Botrytis cinerea*: a fungal 'weapon' of plant-biomass. *Env Microbiol.* 2021; 23(4):2293-2314
2. Bi K, Scalschi L, Jaiswal N, Mengsite T, Fried R, Belen Sanz A, Arroyo J, Zhu W, Masrati G, Sharon A. The *Botrytis cinerea* Crh1 transglycosylase is a cytoplasmic effector triggering plant cell death and defense response. *Nat comm.* 2021 April;12(2166)
3. Nafisi M, Stranne M, Zhang L, van Kan JAL, Sakuragi Y. The endo-arabinanase BcAra1 is a novel host-specific virulence factor of the necrotic fungal phytopathogen *Botrytis cinerea*. *Mol Plant Microbe Interact.* 2014; 27: 781–792.
4. Espino JJ, Brito N, Noda J, González C. *Botrytis cinerea* endo- β -1,4-glucanase Cel5A is expressed during infection but is not required for pathogenesis. *Physiol Mol Plant Pathol.* 2005;66: 213–221
5. Patel PK, Free SJ. The genetics and biochemistry of cell wall structure and synthesis in *Neurospora crassa*, a model filamentous fungus. *Front Microbiol.* 2019; 10: 2294
6. Liu W, Xie J, Fu Y, Jiang D, Chen T, Cheng J. The Subtilisin-Like Protease Bcser2 Affects the Sclerotial Formation, Conidiation and Virulence of *Botrytis cinerea*. *Int J Mol Sci.* 2020;21(2):603
7. Kars I, Krooshof GH, Wageùakers L, Joosten R, Benen JAE, Van Kan JAL. Necrotizing activity of five *Botrytis cinerea* endopolygalacturonases produced in *Pichia pastoris*. *The Plant Journal.* 2005 June;43(2):213-225
8. ten Have, Mulder W, Visser J, van Kan JA. The endopolygalacturonase gene Bcpg1 is required for full virulence of *Botrytis cinerea*. *MPMI.* 1998; 11(10):1009-1016
9. Siegmund U, Viefhues A. Reactive oxygen species in the *Botrytis* – host interaction. In *Botrytis – host interaction. The fungus, the pathogen and its management in agricultural systems*, Fillingier, S., and Elad, Y. (eds). Cham: Springer International Publishing, pp. 269–289. 2016
10. Souibgui E, Bruel C, Choquer M, de Vallée A, Dierckx C, Dupuy JW, Latorse MP, Rasclé C, Pousseeau N. Clathrin is important for virulence factor delivery in the necrotrophic fungus *Botrytis cinerea*. *Front Plant Sci.* 2021

Part 2. Preliminary-work: Identification of putative proteins interacting with the clathrin adaptor AP-1

1	<i>Introduction</i>	136
2	<i>Results and discussion</i>	137
2.1	Construction of the BcAPM1:3×HA strain and validation of the immunoprecipitation technique	137
2.2	Identification of proteins involved in vesicular trafficking potentially interacting with AP-1	137
2.3	Identification of putative AP-1 transmembrane cargos	139
2.4	Identification of putative AP-1 soluble cargos	143
2.5	Limitations of the immunocapture-based method and perspectives ...	143
3	<i>Materials and methods</i>	147
3.1	Strains and culture conditions	147
3.2	Molecular biology	147
3.3	Transformation of <i>Botrytis cinerea</i>	147
3.4	Immunoprecipitation.....	147
3.5	SDS-PAGE and western blot	148
3.6	Sample preparation for proteomics.....	148
3.7	Mass spectrometry analysis	148
3.8	Database search and results processing.....	149
3.9	Label-Free Quantitative Data Analysis.....	149
4	<i>References</i>	150
5	<i>Supplementary data</i>	153

1 Introduction

During the biogenesis process of clathrin-coated vesicles (CCVs) at the Golgi apparatus, the AP-1 complex loads transmembrane cargo proteins into CCVs¹. Three of the four subunits of the AP-1 complex are involved in cargos sorting. The μ 1-subunit recognizes the tyrosine motif Yxx[FILMV] located in cytoplasmic ends or loops of transmembrane proteins², while the hemicomplex γ 1- σ 1 sorts transmembrane proteins by recognizing the di-leucine motif [DE]xxx[LI] in cytoplasmic domains of transmembrane cargos³. The fourth subunit: β , is involved in clathrin recruitment.

In animals, AP-1 sorts several transmembrane cargos like the immunoglobulin receptor^{4,5}, low-density lipoprotein receptor⁶, the transferrin receptor⁷, the mannose-6-phosphate receptor⁸, E-cadherin, ephrin receptor and the interleukin-6 signal transducer^{9,10}, and the HIV-Nef protein¹¹. In the protist pathogen *Toxoplasma gondii*, AP-1 interacts with the sortilin-like receptor (SORTLR) which is likely involved in the loading of soluble cargos such as proteins associated with the secretory organelle: microneme¹². In the parasite *Trypanosoma cruzi*, AP-1 is probably required for the loading of the soluble protease cruzipain¹³, a secreted protein involved in nutrition, cellular differentiation of the parasite, and virulence^{14,15}. Indeed, Moreira et al.¹⁶, demonstrated that the secretion of cruzipain was blocked in AP-1Y knock-out mutants, and cruzipain was enriched in AP-1 interactome¹³. In the yeast *S. cerevisiae*, AP-1 interacts with the chitin synthase Chs3p¹⁷. The discovery of these AP-1 related cargos was performed using various techniques such as immunoprecipitation and confocal microscopy.

We have previously demonstrated that the AP-1 complex plays a major role in two important biological processes in *B. cinerea*: 1) AP-1 is involved in the secretion of enzymes implicated in the infectious process, and 2) the complex participates in fungal polarized growth of the fungus via the establishment/maintenance of the fungal cell-wall.

To enlighten the role of AP-1 in the biology of the necrotrophic fungus *B. cinerea*, we aimed at identifying the proteins interacting with the AP-1 μ -subunit. The goal was to identify three different classes of proteins: 1) cytosolic proteins involved in the AP-1/clathrin machinery, 2) transmembrane cargos selected by AP-1, and 3) secreted soluble cargos. To do so, we added a human influenza hemagglutinin (HA) epitope to the AP-1 μ -subunit and performed immunoprecipitation to collect the interacting proteins. The collected proteins were then identified by mass spectrometry.

Here, we propose a short list of putative AP-1 cargos that remain to be validated by other techniques such as tandem-affinity purification and co-localization experiments.

2 Results and discussion

2.1 Construction of the BcAPM1:3×HA strain and validation of the immunoprecipitation technique

To construct the BcAPM1:3×HA strain, we created a genetic cassette where *Bcapm1* is placed under the control of the strong constitutive promoter *pOliC* (Fig. 1A). We inserted the GGG-3×HA-GGG tag at a specific site on the BcAPM1 protein sequence to prevent the addition of the tag from disrupting the AP-1 complex. The tag was inserted just after the 229th amino acid of BcAPM1 (Bcin04p03770 - ²²⁶TRGK^{A230}; Fig. 1B). In epithelial cells, the insertion of the HA-epitope at this site does not interfere with the incorporation of μ 1-HA into AP-1 complexes¹⁸, and this site has also been used to introduce 3×HA tag in *Arabidopsis thaliana*¹⁹. The BcAPM1:3×HA strain was obtained by *Agrobacterium tumefaciens* mediated transformation of the parental strain B05.10 with the pBht2-pOliC::BcAPM1:3×HA vector, and the BcAPM1:3×HA strain did not display any obvious defect (growth, conidiation, virulence) (data not shown).

To validate the immunoprecipitation technique, we first verified that, BcAPM1:3×HA was present among eluted proteins by western-blot (Fig. 2A ,2B). Then, we ensured that the immunocapture-based method successfully enriched proteins by SDS-PAGE. Indeed, when eluted proteins from the three biological replicates were deposited on a SDS-PAGE gel before trypsin digestion of in-gel proteins, we confirmed that the three BcAPM1:3×HA elutions enriched a lot more proteins when compared to the migration profiles of eluted proteins from the control B05.10 strain (Fig 2C).

2.2 Identification of proteins involved in vesicular trafficking potentially interacting with AP-1

We focused our analysis on 209 proteins detected in three independent biological replicates, with a minimum of two unique and specific peptide, which displayed the same trend three times and were enriched at least ten times (abundance ratio > 10, abundance ratio *p*-value < 0.4; Fig. 3). Among these proteins, seven proteins were related to vesicular trafficking (Table 1). Three of the four subunits of the AP-1 protein complex were detected (σ 1, β 1 and γ 1) proving the efficacy of the immunocapture method. BcAPM1 (μ 1) was found in the dataset but was not significantly enriched (BcAPM1 – Ratio: 15.7, *p*-value: 0.88). The variant μ chain μ 2/Bcapm2 of AP-1R, an AP-1 Related complex dispensable for many clathrin dependent sorting events in yeast²⁰, was also significantly enriched. Interestingly, the ARF GTPase ARL1 was significantly enriched in our dataset (BcARL1–

Ratio: 23.4, p -value: 0.20). This protein recruits AP-1 to the Golgi apparatus and immature secretory granules of salivary glands in *D. melanogaster*²¹. Thus, AP-1 might also be recruited by ARL1 in *B. cinerea*. The three other detected proteins involved in vesicular trafficking included SAR1, an ARF GTPase and component of the coat of COPII-vesicles; Bcin14p04530.1 a putative COP-1 coatomer protein subunit involved in anterograde trafficking between the Golgi apparatus and the Endoplasmic Reticulum (ER); and VPS74, a Golgi PI4K effector. Surprisingly, clathrin light chain and clathrin heavy chains were not significantly enriched in our dataset. We noticed that BcCHC1 was detected with a ratio of 5.6, but with a p -value of 0.47. BcCLC was not detected. Other cytosolic proteins known to interact with AP-1 such as the ADP-ribosylation factor ARF1 (Bcin11p04620.1) were not significantly enriched. Thus, our results suggests that our immunocapture conditions might not be appropriate for the collection of a complete and transient AP-1/Clathrin complex. Moreover, it has been previously described that AP-1 associates with clathrin via clathrin boxes localized in the β -subunit of AP-1 in the filamentous fungus *A. nidulans*²². A clathrin box ⁶²⁹LLDID⁶³³ is also present in the β -subunit of AP-1 of *B. cinerea*²³.

2.3 Identification of putative AP-1 transmembrane cargos

Our second objective was to identify putative transmembrane cargos interacting with AP-1. To identify these putative cargos, we selected the proteins enriched in the dataset and predicted to have at least one transmembrane domain using the transmembrane domain prediction program TMHMM. Twenty-eight transmembrane proteins were identified (Table 2). Nine of them had a predicted tyrosine motif Yxx[FILMV] which is known to be recognized by the AP-1 μ -subunit for sorting of specific transmembrane cargos². Most of these proteins had unknown functions and were predicted to localize at the mitochondrion (prediction by DeepLoc software v1.0, likelihood > 0.6). Only one protein (Bcin16p00820.1) had a predicted di-leucine motif recognized by the hemicomplex γ 1- σ 1 for cargo sorting. This protein is a mitochondrial ABC transporter. Even if these proteins are enriched and possess AP-1 related sorting signals, the possibility that they could be AP-1 cargos is very unlikely. Indeed, no AP-1 dependent traffic between the Golgi apparatus and the mitochondrion has been described so far.

The protein UBX3 was significantly enriched (Abundance ratio: 185, p -value: 0.01). This protein is known to interact with clathrin via a W-box²⁴. However, it is localized at the plasma membrane and is involved in clathrin-mediated endocytosis in the yeast *S. cerevisiae*²⁴. No role of UBX3 in the biogenesis of AP-1/clathrin vesicles has been described

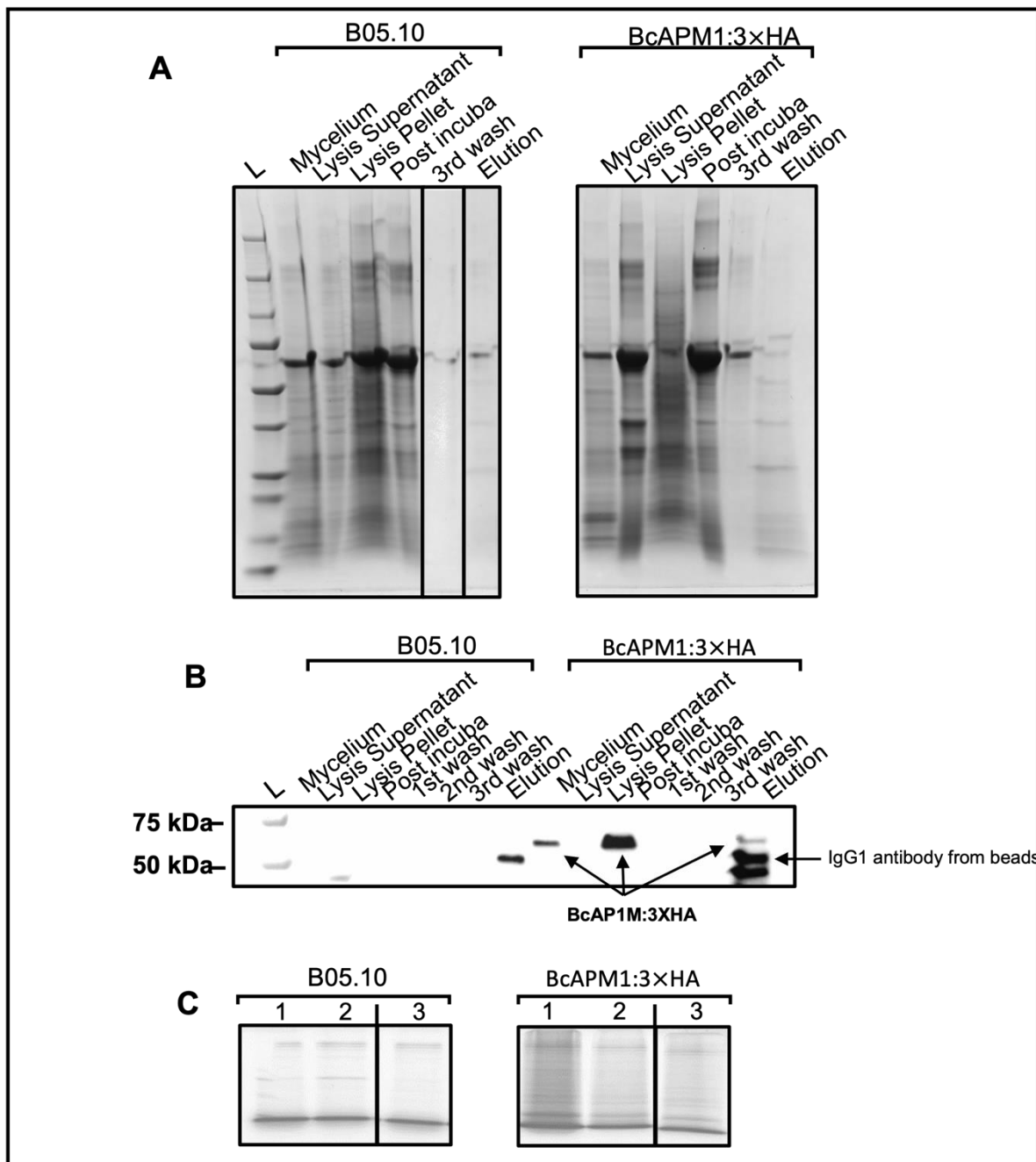


Figure 2 – Development of the immunoprecipitation of BcAPM1:3xHA

(A) SDS-PAGE gel of proteins from different immunoprecipitation steps: crude mycelium extract (Mycelium), proteins extracted with the lysis buffer (lysis supernatant), proteins not extracted with the lysis buffer (lysis pellet), proteins present after overnight incubation of extracted proteins with anti-HA magnetic-beads (Post incubation), proteins remaining in the third wash waste (3rd wash), proteins eluted (elution). **(B)** Detection of BcAPM1:3xHA (54.3 kDa) using an anti-HA antibody on proteins from the different immunoprecipitation steps. IgG1 heavy chain protein from magnetic-beads was also detected (50 kDa) in eluted proteins. **(C)** SDS-PAGE gel of eluted proteins after anti-HA immunoprecipitation on the parental strain and the BcAPM1:3xHA strain from three biological replicates.

so far. It would be interesting to study the role of this protein in *B. cinerea* and determine if BcUbx3 (Bcin09p06820.1) is involved in the biogenesis process of AP-1/Clathrin vesicles. We were surprised to find a high enrichment of ER-exit proteins such as the soluble cargo receptor Erv29 (Table 3). In *N. crassa*, Erv29 is involved in the secretion process of the cellobiohydrolase CBH-2²⁵. We also found Erv25 significantly enriched in our dataset, a protein which associates with Emp24 to form p24, a complex found in COPII-vesicles involved in soluble cargo sorting at the ER in *S. cerevisiae*^{26,27} and *S. sclerotiorum*²⁸. In *N. crassa*, Emp24 is involved in the secretion of the cellobiohydrolase CBH-1 and is localized at early Golgi compartments. Starr *et al.*²⁵ proposed that “Emp24 could be involved in transporting proteins in anterograde fashion past the early Golgi”. Interestingly, one of the other proteins composing the p24 complex, BcErv25, has a predicted tyrosine motif (Table 3) and could directly interact with BcAPM1 via this motif. It might be a co-incidence, but it would be interesting to determine if BcErv25 interacts with AP-1 through co-localization and tandem-affinity purification approaches and discover a potential new function of AP-1 in filamentous fungi.

Another interesting protein found in the dataset is YEA4, an uridine diphosphate-N-acetylglucosamine (UDP-GlcNAc) required for cell wall chitin synthesis in *S. cerevisiae*²⁹. In the yeast, this protein is localized at the ER and its specific role in chitin synthesis is not clear. Indeed, Roy, *et al.* mentioned that: “the present hypothesis on chitin synthesis does not refer any requirements of UDP-Glc-NAc transporter in the ER during its biosynthetic process”. Even if the mechanism by which this protein is involved in chitin synthesis remains to be discovered, the possibility that AP-1 could be involved in the sorting of this proteins is intriguing. Indeed, we previously observed a severe chitin defect in the AP-1 mutant. It would be interesting to localize this protein in *B. cinerea*, determine if it localizes at the ER and/or at other sub-cellular localizations, and figure if AP-1 is indeed involved in the sorting of this protein by tandem affinity purification.

Among the putative AP-1 transmembrane cargos found in our dataset, we expected to find at least one chitin synthase. Indeed, in the first part of this chapter, we have found that AP-1 is important for chitin synthesis, likely via a role of AP-1 in the traffic of the chitin synthase BcCHSIIIa. This protein was detected in the dataset but not significantly enriched (Abundance ratio: 7.9, *p*-value: 0.61); and so did the class V chitin synthase BcCHSVa (Abundance ratio: 10.8, *p*-value: 0.98). Even if BcCHSIIIa was not significantly enriched, we cannot conclude that the chitin synthase BcCHSIIIa is not an AP-1 cargo. Indeed, we did not identify any common transmembrane cargo known to be an AP-1 cargo in other organisms (e.g., Mannose-6-phosphate receptor BcMr11, or transferrin receptor

ortholog Bcin11p01930.1), nor did we identify transmembrane cargos predicted to localize at the endosome or the plasma membrane. Thus, our present work, which is still preliminary, and a first attempt, requires more development/improvement for the identification of known AP-1 transmembrane cargos.

2.4 Identification of putative AP-1 soluble cargos

As our previous work highlighted the importance of AP-1 in the secretion of soluble hydrolytic enzymes, our third objective was to identify putative AP-1 soluble cargos. To do this, we selected significantly enriched proteins which were predicted to contain a signal-peptide (SignalP v5.0) and predicted to localize at the extracellular medium (DeepLoc v1.0, likelihood > 0.6). The laccase (multicopper oxidase) BcLCC2, a protease (Bcin08p00280.2 – carboxypeptidase Y), and a protein of unknown function (Bcin06p06670.1) were significantly enriched (Table 3 and Fig. 3). Interestingly, the laccase BcLCC2 was highly down-accumulated in the mutant exoproteome (500- fold), and so did the protease Bcin08p00280.2 (500-fold) and the protein of unknown function Bcin06p06670.1 (1000-fold). Thus, our results are in agreement with the secretion defect observed for these secreted proteins. Therefore, AP-1 could be involved in the loading process of these hydrolytic enzymes. We expected to enrich more secreted proteins as the AP-1 mutant displays a severe secretion defect. Seven other proteins possessing a signal-peptide and predicted to be secreted were found in our dataset but they were not significantly enriched (Table S2). Thus, we still need to identify other secretory cargos as well as soluble cargo receptors interacting with AP-1 to fully unravel the role of AP-1 in the sorting of soluble cargo receptors.

2.5 Limitations of the immunocapture-based method and perspectives

In this study, our aim was to identify proteins interacting with the AP-1 μ -subunit to detect membrane and soluble cargos transported by AP-1/Clathrin vesicles. We also aimed to detect cytosolic proteins potentially involved in the biogenesis of these vesicles, a first in filamentous fungi.

Proteins interacting with BcAPM1:3 \times HA were identified by mass-spectrometry. Reassuringly, and as mentioned earlier, most of the AP-1 complex proteins were detected in the dataset we generated. The β -subunit, for example, was amongst the most enriched proteins. However, no clathrin heavy chain -which is a protein known to interact with the

Table 3 – Potential membrane cargo proteins identified in dataset

Predicted di-leucine motifs [DE]xxx [LL] and tyrosine motifs Yxx [FILMV] were predicted using elm.org
Transmembrane domains (TMD) were predicted with TMHMM.

Accession	Usual name	[DE]xxx[LL]	Yxx[FILMV]	Localisation	TMD	<i>S. cerevisiae</i>	ortholog	Description
Bcin09p06820.1				NA	1	UBX3		Claithrin-binding protein with a role in endocytosis; localizes to clathrin-coated vesicles
Bcin02p06660.1	Bcho1			Endoplasmic reticulum	6	CHO1		Phosphatidylserine synthase, functions in phospholipid biosynthesis
Bcin14p03400.1	Bcev25	X		Endoplasmic reticulum		ERV25		Member of the p24 family involved in ER to Golgi transport
Bcin10p03790.1		X		NA	2	-		Protein of unknown function
Bcin04p04040.1	Bcyea4			Endoplasmic reticulum	10	YEA4		Uridine diphosphate-N-acetylglucosamine (UDP-GlcNAc) transporter; required for cell wall chitin synthesis
Bcin01p07930.1				NA	3			Autophagy-related protein 33
Bcin06p06590.1	BcFr1			NA	12	-		Sugar/inositol transporter
Bcin08p01350.1		X		NA	2	-		Protein of unknown function
Bcin01p10340.1	Bcyc1			Mitochondrion	1	CYT1		Cytochrome c1; component of the mitochondrial respiratory chain
Bcin14p02380.1		X		Plastid	1	-		Protein of unknown function
Bcin06p05950.1	Bcev46			NA	2	ERV46		Protein localized to COPII-coated vesicles; involved in the membrane fusion stage of transport
Bcin07p05580.1				Endoplasmic reticulum	1	-		Putative protein of unknown function
Bcin08p02900.1				Peroxisome	2	-		Peroxisome membrane protein
Bcin14p02240.1		X		Mitochondrion	1	-		Protein of unknown function
Bcin02p04020.1	Bcmm10	X		Golgi apparatus	1	MNN10		Subunit of a Golgi mannosyltransferase complex
Bcin05p05070.1	Bctim50	X		Mitochondrion	1	TIM50		Essential component of the TIM23 complex
Bcin02p04240.1				Endoplasmic reticulum	7	ELO1 ELO3 ELO2		Elongase I, medium-chain acyl elongase
Bcin06p07240.1	Bccrc1			Mitochondrion	2	CRC1		Mitochondrial inner membrane carnitine transporter
Bcin12p06400.1	Bcbot3			Endoplasmic reticulum	2	-		Cytochrome p450
Bcin11p01670.1		X		Mitochondrion	1	-		Protein of unknown function
Bcin15p01350.1	Bcsey1			Endoplasmic reticulum	1	SEY1		Dynammin-like GTPase that mediates homotypic ER fusion
Bcin11p04180.1	Bcev29			NA	8	ERV29		Protein localized to COPII-coated vesicles; involved in vesicle formation and incorporation of specific secretory cargo
Bcin16p00820.1		X		Mitochondrion	6	MDL1 MDL2		Mitochondrial inner membrane half-type ABC transporter
Bcin01p10560.1	Bcpam17		X	Mitochondrion	2	PAM17		Constituent of the TIM23 complex
Bcin02p03080.1		X		Mitochondrion	3	SDH3 SHH3		Subunit of succinate dehydrogenase and of TIM22 translocase
Bcin02p07550.1				NA	1	-		Protein with CBS domain (IPR000644)
Bcin15p04150.1				Mitochondrion	1	-		Dihydroorotate dehydrogenase involved in the biosynthesis of co-factors
Bcin12p02810.1				Golgi apparatus	1	ANP1		Subunit of the alpha-1,6 mannosyltransferase complex; type II membrane protein; has a role in retention of glycosyltransferases in the Golgi; involved in osmotic sensitivity
Bcin04p05010.1	Bctsc13			Endoplasmic reticulum	4	TSC13		Enoyl reductase; catalyzes last step in each cycle of very long chain fatty acid elongation

AP-1 β -subunit was significantly enriched. Moreover, no transmembrane cargo previously identified as AP-1 cargos in other organisms could be found in our proteomic dataset. The absence in our dataset of enriched transmembrane cargo proteins known to interact with AP-1 can be due to suboptimal immunocapture conditions. Indeed, it can be difficult to solubilize some transmembrane (TM) proteins. Thus, the possibility that we have missed the identification of known AP-1 transmembrane cargos because of TM protein solubilization issues is likely. In the future, we could optimize the immunoprecipitation method by testing wide array of lysis buffers with different detergents to solubilize complex TM proteins. It would also be interesting to increase the ionic strength of the lysis and the wash buffers to capture more specific interacting proteins. Another explanation for the lack of identification of known AP-1 transmembrane cargos could lie in the low amount of trypsin digestion sites in many TM proteins, which makes the identification of membrane proteins difficult by mass-spectrometry³⁰.

Interestingly, even if the immunoprecipitation conditions might not have been optimal for the identification of membrane cargos, we successfully identified putative soluble cargos (summarized in Fig. 4). Indeed, the detection of the laccase BcLCC2, as well as the protease Bcin08p00280.2 is promising and consistent with the secretion defect of oxidoreduction related proteins, and proteases, observed in the AP-1 mutant. Moreover, the AP-1 complex could also be involved in the secretion of proteins of unknown functions such as the protein Bcin06p06670.1. This protein was down-regulated in four non-pathogenic *AtMT* mutants from the BotBank collection³¹ which suggests that this protein could be involved in virulence. We still need to validate that AP-1 is involved in the loading of these soluble cargos via other approaches such as co-localization and tandem-affinity purification techniques, and yeast-two-hybrid.

Finally, crossing our data with a clathrin-heavy chain interactome would have strengthened our results. We have tried to perform immunoprecipitation of clathrin interactants with the BcCHC:3 \times HA strain but we did not manage to find the conditions required to detect BcCHC:3 \times HA in the lysis buffer (data not shown). Indeed, BcCHC:3 \times HA was detected in crude mycelia protein extract, which confirmed the production of the chimeric protein, but we did not manage to detect BcCHC:3 \times HA among the proteins solubilized by a wide range of lysis buffers.

Thus, this work is still preliminary, and we still need to identify transmembrane cargos undergoing the AP-1/Clathrin pathway. Their identification would bring new understanding of general secretion mechanisms in fungi and could also permit the

identification of new antifungal targets. Another way of identifying AP-1 cargos could be to isolate intracellular vesicles from the parental strain, clathrin and AP-1 mutants and perform comparative proteomics on isolated secretory vesicles. This last technique is very challenging from a technical perspective, and to our knowledge, has never been successfully performed in filamentous fungi.

Table 2 – Secreted proteins enriched in dataset

Accession	Usual name	Localization	SP	<i>S. cerevisiae</i> ortholog	Description
Bcin06p06670.1		Extracellular	Yes	-	Protein of unknown function
Bcin14p02510.1	Bclcc2	Extracellular	Yes	-	Secreted multicopper oxidase
Bcin08p00280.1		Extracellular	Yes	-	Secreted protease

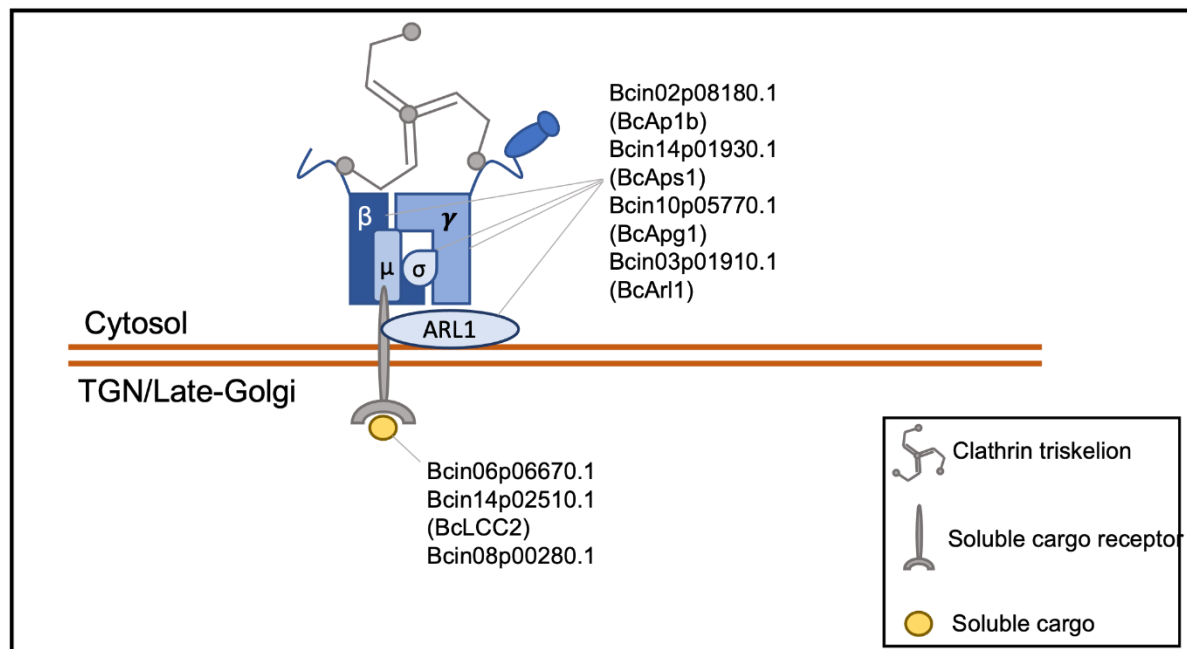


Figure 4 – AP-1 is involved in soluble cargo loading in *B. cinerea*

Our data suggest that AP-1 is a conserved heterotetrameric complex in *B. cinerea*, involved in the loading of soluble cargos such as the protease of unknown function Bcin06p06670.1, the laccase BcLCC2, and the protease Bcin08p00280.1. Proteins thought to interact with AP-1 and not enriched or identified in the interactome are represented in grey.

3 Materials and methods

3.1 Strains and culture conditions

Botrytis cinerea strain B05.10 [teleomorph *Botryotinia fuckeliana* (de Bary) Whetzel] and BcAPM1:3×HA strains were used as for all experiments. Conidia were collected after 11 days of culture on Malt Sporulation medium at 21°C under near-UV light. Spores were suspended in water and then counted using Thoma cell counting chambers and stored on ice before use or suspended in H₂O + glycerol (20%) for conservation at -80°C. All following experiments were carried using spores from 11-day-old cultures.

For submerged liquid cultures, conidia were inoculated (1.10^5 conidia.ml⁻¹) in Potato Dextrose Broth for 72h, at 21°C, under agitation (110 rpm).

3.2 Molecular biology

BcAPM1:3×HA cassette was constructed *in-silico*. The GGG-3×HA-GGG tag was inserted just after the 229 amino acid of BcAPM1 (Bcin04p03770.1 - ²²⁶TRGK^{A230}), as previously performed in epithelial cells¹⁸ and *Arabidopsis thaliana*¹⁹ – (Fig. 1B). BcAPM1:3×HA was placed under the control of the strong constitutive promoter pOliC; tNiaD was used as terminator. The BcAPM1:3×HA cassette was then synthesized and cloned by GenScript in a pUC57-Mini plasmid to produce BcAPM1:3×HA_pUC57-Mini. Then, we amplified the BcAPM1:3×HA cassette from BcAPM1:3×HA_pUC57-Mini using primer pair P1/P2 (Supplementary Table S1) and performed IVA cloning³² in a pBht2 vector pre-digested by *Sma*I to produce pBht2-BcAPM1:3×HA (Fig. S1).

3.3 Transformation of *Botrytis cinerea*

Agrobacterium tumefaciens transformed with pBht2- BcAPM1:3×HA was used to transform *B. cinerea* strain B05.10 as described by Rolland *et al.*, 2003³³. *B. cinerea* transformants were selected using hygromycin B (70 µg.ml⁻¹).

3.4 Immunoprecipitation

Mycelia from 3-day-old cultures were collected using 40 µm cell strainers before deep-freezing in liquid nitrogen and storage at -80°C. Mycelia were ground in liquid nitrogen using a mortar and pestle for 5 min. To perform protein extraction, 1 ml of lysis buffer (Tris-HCl pH 8, NaCl 75 mM, EDTA 2 mM, BSA 0.1%, NP-40 0.65%, SDS 0.005%, plus 13 µl of protease inhibitor cocktail from Sigma) was added to 1 ml of ground mycelia, placed on a wheel for agitation (15 rpm, 30 min, 4°C), and centrifuged at (18 000g, 10 min, 4°C). Anti-HA magnetic beads (Pierce) were washed twice with the lysis buffer before adding 1 ml of the extracted proteins (~700 µg) to 25 µl of beads. Proteins were incubated with the beads on the wheel (10 rpm) for 16h at +4°C. After incubation, the beads were washed five times with the wash buffer (Tris-HCl pH 8, NaCl 75 mM, EDTA 2 mM, NP-40 0.65%, SDS 0.005%, plus 13 µl of protease inhibitor cocktail) and eluted in 60 µL of Laemmli 1X (Tris-HCl 50 mM, pH 6.8, SDS 2%, Saccharose 5%, Bromophenol Blue 0.02%) and boiled for 8 min, 98°C. The parental strain was used as a negative control. Four biological replicates were performed.

3.5 SDS-PAGE and western blot

Collected fractions from different immunoprecipitation steps were boiled in Laemmli 5X buffer for 8 min at 98°C, and then centrifuged at 18 000g for 10 min at +4°C. Supernatants were loaded on tris-glycine polyacrylamide gels (BioRad). Gels were colored using Coomassie blue or subjected to western-blot. For western-blotting, the primary anti-HA antibody (Sigma H9658) was used at 1:20 000 in Tris-Buffer Tween 20 0,1%. The secondary antibody (Sigma A9044) was used at 1:80 000. BcAPM1-3HA was detected using the Clarity™ Western ECL revelation kit (BioRad) and ChemiDoc (BioRad).

3.6 Sample preparation for proteomics

Four independent biological replicates were used to perform co-immunoprecipitation (Co-IP) of the AP-1 protein and its interactants, and control conditions for these enrichments. Samples were sent to the proteomic platform (Plateforme Protéome, Université de Bordeaux) for subsequent treatment. Proteins were loaded on a 10% acrylamide SDS-PAGE gel and proteins were visualized by Colloidal Blue staining. Migration was stopped when samples had just entered the resolving gel and the unresolved region of the gel was cut into only one segment. Each SDS-PAGE band was cut into 1 mm x 1 mm gel pieces. Gel pieces were destained in 25 mM ammonium bicarbonate (NH_4HCO_3), 50% Acetonitrile (ACN) and shrunk in ACN for 10 min. After ACN removal, gel pieces were dried at room temperature. Proteins were first reduced in 10 mM dithiothreitol, 100 mM NH_4HCO_3 for 60 min at 56°C then alkylated in 100 mM iodoacetamide, 100 mM NH_4HCO_3 for 60 min at room temperature and shrunk in ACN for 10 min. After ACN removal, gel pieces were rehydrated with 50 mM NH_4HCO_3 for 10 min at room temperature. Before protein digestion, gel pieces were shrunk in ACN for 10 min and dried at room temperature. Proteins were digested by incubating each gel slice with 10 ng/ μL of trypsin (V5111, Promega) in 40 mM NH_4HCO_3 , rehydrated at 4°C for 10 min, and finally incubated overnight at 37°C. The resulting peptides were extracted from the gel by three steps: a first incubation in 40 mM NH_4HCO_3 for 15 min at room temperature and two incubations in 47.5% ACN, 5% formic acid for 15 min at room temperature. The three collected extractions were pooled with the initial digestion supernatant, dried in a SpeedVac, and resuspended with 40 μL of 0.1% formic acid.

3.7 Mass spectrometry analysis

NanoLC-MS/MS analysis were performed using an Ultimate 3000 RSLC Nano-UPHLC system (Thermo Scientific, USA) coupled to a nanospray Orbitrap Fusion™ Lumos™ Tribrid™ Mass Spectrometer (Thermo Fisher Scientific, California, USA). Each peptide extracts were loaded on a 300 μm ID x 5 mm PepMap C₁₈ precolumn (Thermo Scientific, USA) at a flow rate of 10 $\mu\text{L}/\text{min}$. After a 3 min desalting step, peptides were separated on a 50 cm EasySpray column (75 μm ID, 2 μm C₁₈ beads, 100 Å pore size, ES903, Thermo Fisher Scientific) with a 4-40% linear gradient of solvent B (0.1% formic acid in 80% ACN) in 55 min. The separation flow rate was set at 300 nL/min.

The mass spectrometer operated in positive ion mode at a 1.9 kV needle voltage. Data was acquired using Xcalibur 4.4 software in a data-dependent mode. MS scans (m/z 375-1500) were recorded at a resolution of $R = 120000$ (@ m/z 200), a standard AGC target and an injection time in automatic mode, followed by a top speed duty cycle of up to 3 seconds for MS/MS acquisition. Precursor ions (2 to 7 charge states) were isolated in the quadrupole with a mass window of 1.6 Th and fragmented with HCD@28% normalized collision energy. MS/MS data was acquired in the Orbitrap cell with a resolution of $R=30000$ (@ m/z 200), a standard AGC target and a maximum injection time in automatic mode. Selected precursors were excluded for 60 seconds.

3.8 Database search and results processing

Protein identification and Label-Free Quantification (LFQ) were done in Proteome Discoverer 2.5. MS Amanda 2.0, Sequest HT and Mascot 2.5 algorithms were used for protein identification in batch mode by searching against a ENSEMBL *Botrytis cinerea* ASL83294v1 database (13749 entries, release 53). Two missed enzyme cleavages were allowed for the trypsin. Mass tolerances in MS and MS/MS were set to 10 ppm and 0.02 Da. Oxidation (M) and acetylation (K) were searched as dynamic modifications and carbamidomethylation (C) as static modification. Peptide validation was performed using Percolator algorithm³⁴ and only “high confidence” peptides were retained corresponding to a 1% false discovery rate at peptide level.

3.9 Label-Free Quantitative Data Analysis

Minora feature detector node (Label Free Quantification) was used along with the feature mapper and precursor ions quantifier. The quantification parameters were selected as follows: (1) Unique peptides (2) Precursor abundance based on intensity (3) Normalization mode: no normalization was applied (4) Protein abundance calculation: summed abundances (5) Protein ratio calculation: pairwise ratio based (6) Imputation mode: Low abundance resampling and (7) Hypothesis test: t-test (background based). Quantitative data were considered for master proteins, quantified by a minimum of 2 unique peptides, a fold changes above 10 and an abundance ratio (for each biological replicate) seen 3 times with the same trend, with an abundance ratio p -value < 0.4 .

4 References

1. Robinson, M. S. Adaptable adaptors for coated vesicles. *Trends in Cell Biology* **14**, 167–174 (2004).
2. Collawn, J. F., Kuhn, L. A., Liu, L. F., Tainer, J. A. & Trowbridge, I. S. Transplanted LDL and mannose-6-phosphate receptor internalization signals promote high-efficiency endocytosis of the transferrin receptor. *The EMBO Journal* **10**, 3247–3253 (1991).
3. Janvier, K. *et al.* Recognition of dileucine-based sorting signals from HIV-1 Nef and LIMP-II by the AP-1 γ - σ 1 and AP-3 δ - σ 3 hemicomplexes. *Journal of Cell Biology* **163**, 1281–1290 (2003).
4. Casanova, E. & Mostov, K. E. An Autonomous Signal for Basolateral Sorting in the Cytoplasmic Domain of the Polymeric Immunoglobulin Receptor. 11.
5. Aroeti, B., Kosen, P. A., Kuntz, I. D., Cohen, F. E. & Mostov, K. E. Mutational and secondary structural analysis of the basolateral sorting signal of the polymeric immunoglobulin receptor. *Journal of Cell Biology* **123**, 1149–1160 (1993).
6. Matter, K., Hunziker, W. & Mellman, I. Basolateral sorting of LDL receptor in MDCK cells: The cytoplasmic domain contains two tyrosine-dependent targeting determinants. *Cell* **71**, 741–753 (1992).
7. Odorizzi, G. & Trowbridge, I. S. Structural Requirements for Basolateral Sorting of the Human Transferrin Receptor in the Biosynthetic and Endocytic Pathways of Madin-Darby Canine Kidney Cells. *Journal of Cell Biology* **137**, 1255–1264 (1997).
8. Stöckli, J. & Rohrer, J. The Palmitoyltransferase of the Cation-dependent Mannose 6-Phosphate Receptor Cycles between the Plasma Membrane and Endosomes. *MBoC* **15**, 2617–2626 (2004).
9. Takahashi, D. *et al.* The Epithelia-Specific Membrane Trafficking Factor AP-1B Controls Gut Immune Homeostasis in Mice. *Gastroenterology* **141**, 621–632 (2011).
10. Hase, K. *et al.* AP-1B-Mediated Protein Sorting Regulates Polarity and Proliferation of Intestinal Epithelial Cells in Mice. *Gastroenterology* **145**, 625–635 (2013).
11. Craig, H. M., Reddy, T. R., Riggs, N. L., Dao, P. P. & Guatelli, J. C. Interactions of HIV-1 Nef with the μ Subunits of Adaptor Protein Complexes 1, 2, and 3: Role of the Dileucine-Based Sorting Motif. *Virology* **271**, 9–17 (2000).
12. Venugopal, K. *et al.* Dual role of the *Toxoplasma gondii* clathrin adaptor AP1 in the sorting of rhoptry and microneme proteins and in parasite division. *PLoS Pathog* **13**, e1006331 (2017).
13. Kalb, L. C. *et al.* Conservation and divergence within the clathrin interactome of *Trypanosoma cruzi*. *Sci Rep* **6**, 31212 (2016).
14. Urbina, J. A. Chemotherapy of Chagas Disease. **8**, 287–295 (2002).
15. Branquinha, M. H. *et al.* Cruzipain: An Update on its Potential as Chemotherapy Target against the Human Pathogen *Trypanosoma cruzi*. *CMC* **22**, 2225–2235 (2015).
16. Moreira, C. M. do N. *et al.* Knockout of the gamma subunit of the AP-1 adaptor complex in the human parasite *Trypanosoma cruzi* impairs infectivity and differentiation and prevents the maturation and targeting of the major protease cruzipain. *PLoS ONE* **12**, e0179615 (2017).
17. Starr, T. L., Pagant, S., Wang, C.-W. & Schekman, R. Sorting Signals That Mediate Traffic of Chitin Synthase III between the TGN/Endosomes and to the Plasma Membrane in Yeast. *PLoS One* **7**, (2012).
18. Fölsch, H., Pypaert, M., Schu, P. & Mellman, I. Distribution and Function of AP-1 Clathrin Adaptor Complexes in Polarized Epithelial Cells. *The Journal of Cell Biology* **152**,

595–606 (2001).

19. Park, M. *et al.* Arabidopsis -adaptin subunit AP1M of adaptor protein complex 1 mediates late secretory and vacuolar traffic and is required for growth. *Proceedings of the National Academy of Sciences* **110**, 10318–10323 (2013).
20. Stepp, J. D., Pellicena-Palle, A., Hamilton, S. & Kirchhausen, T. A Late Golgi Sorting Function for *Saccharomyces cerevisiae* Apmlp, but not for Apm2p, a Second Yeast Clathrin AP Medium Chain-related Protein. *Molecular Biology of the Cell* **6**, 18 (1995).
21. Torres, I. L., Rosa-Ferreira, C. & Munro, S. The Arf family G protein Arl1 is required for secretory granule biogenesis in *Drosophila*. *Journal of Cell Science* jcs.122028 (2014) doi:10.1242/jcs.122028.
22. Martzoukou, O., Diallinas, G. & Amillis, S. Secretory Vesicle Polar Sorting, Endosome Recycling and Cytoskeleton Organization Require the AP-1 Complex in *Aspergillus nidulans*. *Genetics* **209**, 1121–1138 (2018).
23. Souibgui, E. Rôle de la clathrine dans le processus infectieux du champignon phytopathogène *Botrytis cinerea*. (Université Claude Bernard Lyon 1, 2017).
24. Farrell, K. B., Grossman, C. & Di Pietro, S. M. New Regulators of Clathrin-Mediated Endocytosis Identified in *Saccharomyces cerevisiae* by Systematic Quantitative Fluorescence Microscopy. *Genetics* **201**, 1061–1070 (2015).
25. Starr, T. L., Gonçalves, A. P., Meshgin, N. & Glass, N. L. The major cellulases CBH-1 and CBH-2 of *Neurospora crassa* rely on distinct ER cargo adaptors for efficient ER-exit: Fungal cellulase ER cargo adaptors. *Molecular Microbiology* **107**, 229–248 (2018).
26. Schimmöller, F. *et al.* The absence of Emp24p, a component of ER-derived COPII-coated vesicles, causes a defect in transport of selected proteins to the Golgi. *The EMBO Journal* **14**, 1329–1339 (1995).
27. Castillon, G. A. *et al.* The yeast p24 complex regulates GPI-anchored protein transport and quality control by monitoring anchor remodeling. *MBoC* **22**, 2924–2936 (2011).
28. Xie, C. *et al.* Early Secretory Pathway-Associated Proteins SsEmp24 and SsErv25 Are Involved in Morphogenesis and Pathogenicity in a Filamentous Phytopathogenic Fungus. *mBio* **12**, e03173-21 (2021).
29. Roy, S. K., Chiba, Y., Takeuchi, M. & Jigami, Y. Characterization of Yeast Yea4p, a Uridine Diphosphate-N-acetylglucosamine Transporter Localized in the Endoplasmic Reticulum and Required for Chitin Synthesis. *Journal of Biological Chemistry* **275**, 13580–13587 (2000).
30. Carroll, J., Altman, M. C., Fearnley, I. M. & Walker, J. E. Identification of membrane proteins by tandem mass spectrometry of protein ions. *Proc. Natl. Acad. Sci. U.S.A.* **104**, 14330–14335 (2007).
31. de Vallée, A. *et al.* A Similar Secretome Disturbance as a Hallmark of Non-pathogenic *Botrytis cinerea* ATMT-Mutants? *Front. Microbiol.* **10**, (2019).
32. García-Nafria, J., Watson, J. F. & Greger, I. H. IVA cloning: A single-tube universal cloning system exploiting bacterial In Vivo Assembly. *Sci Rep* **6**, 27459 (2016).
33. Rolland, S., Jobic, C., Fèvre, M. & Bruel, C. Agrobacterium -mediated transformation of *Botrytis cinerea*, simple purification of monokaryotic transformants and rapid conidia-based identification of the transfer-DNA host genomic DNA flanking sequences. *Current Genetics* **44**, 164–171 (2003).
34. Käll, L., Canterbury, J. D., Weston, J., Noble, W. S. & MacCoss, M. J. Semi-supervised learning for peptide identification from shotgun proteomics datasets. *Nat Methods* **4**, 923–925 (2007).

5 Supplementary data

Table S1 – Primers used in this study

P1	k7-Ap1m- 3HA_IVAPBht2-F	CGAATTCGAGCTCGGTACCCGCTTATTAACCGCGGTGCA
P2	k7-Ap1m- 3HA_IVAPBht2-R	GTCGACTCTAGAGGATCCCCATAGATACAGGCATTGGATTAATAATTGTTG

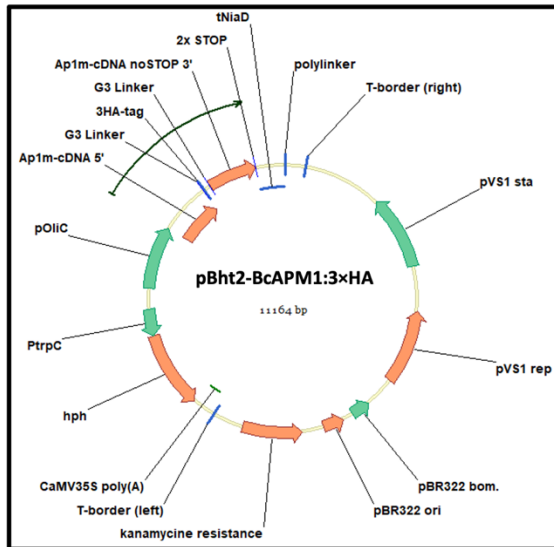


Figure S1 – Plasmid-map of the pBht2-BcAPM1:3xHA vector

Table S2 – Other proteins predicted to be secreted and containing a predicted signal peptide

Accession	Usual name	Localisation	SP	<i>S. cerevisiae</i> ortholog	Description	Abundance Ratio: (AP-1) / (Control)	Abundance Ratio P-Value: (AP-1) / (Control)
Bcin01p05720.2		Extracellular	Oui	*		3.111	0,147998077
Bcin03p01540.1		Extracellular	Oui	*		16,8	0,57922109
Bcin03p06740.1		Extracellular	Oui	YLR179C	Protein of unknown function	3,579	0,273722985
Bcin05p05900.1	Bcap5	Extracellular	Oui		Aspartic peptidase	22,096	0,63611614
Bcin12p02040.1	Bcap8	Extracellular	Oui		Aspartic peptidase	26,374	0,465395371
Bcin12p03270.1		Extracellular	Oui	YDR415C	Putative aminopeptidase	17,093	0,6980053431
Bcin15p02380.1	Bcap1	Extracellular	Oui		Peptidase	8,892	0,68916572

Table S3 – List of proteins identified by mass spectrometry

SP: Signal Peptide – TMD : Transmembrane domain - GO: Gene ontology

Accession	Usual name	Predicted localisation	SP	TMD	GO Biological process	Ratio: (AP-1) / (Control)	Ratio P-Value: (AP-1) / (Control)
Bcin01.p00160.1	Bcboa17	Mitochondrion			0 obsolete oxidation-reduction process, obsolete pathogenesis	10.657	0.812801648
Bcin01.p00170.1		Endoplasmic reticulum			12 amino acid transport, transmembrane transport, organic substance transport	5.566	0.598719374
Bcin01.p00350.1		Endoplasmic reticulum			2 lipid biosynthetic process, ergosterol biosynthetic process, cellular lipid metabolic process	14.185	0.528284518
Bcin01.p00360.1	Bcerg1	Peroxisome			3 sterol biosynthetic process	10.624	0.763378984
Bcin01.p00370.1	Bcprf1	Cytoplasm			0 cytoplasm, actin filament polymerization, negative regulation of actin filament polymerization,	15.217	0.472811081
Bcin01.p00440.1	Bcfas2	Peroxisome			0 long-chain fatty acid biosynthetic process, fatty acid biosynthetic process, metabolic process,	47.837	0.233556773
Bcin01.p00450.2		Peroxisome			0 fatty acid biosynthetic process, organic substance metabolic process, cellular metabolic process,	50.042	0.164382702
Bcin01.p00510.1	Bcarp5	Nucleus			0 chromatin remodelling, nucleosome mobilization	10.906	0.894382328
Bcin01.p00550.1	Bcsas1	Golgi apparatus			0 NA	11.187	0.92283224
Bcin01.p00630.1		Mitochondrion			2 cellular process, magnesium ion transport, magnesium ion export from mitochondrion	8.21	0.754298135
Bcin01.p00660.1	Bente1	Endoplasmic reticulum			3 lipid catabolic process, lipid metabolic process, phosphatidylcholine catabolic process	7.895	0.919387786
Bcin01.p00980.1		Cytoplasm			0 translation, rRNA export from nucleus, positive regulation of translational fidelity	96.073	0.06343881
Bcin01.p01040.1	Bcutp4	Nucleus			0 NA	4.657	0.33843184
Bcin01.p01500.1	Bcbna4	Mitochondrion			1 quinolinate biosynthetic process, tryptophan catabolic process	21.419	0.426978732
Bcin01.p01530.1	Bccdc40	Nucleus			0 mRNA splicing, via spliceosome	2.872	0.126738305
Bcin01.p01710.1		Golgi apparatus			0 endosomal vesicle fusion	11.568	0.854402582
Bcin01.p01720.1	Bemic60	Mitochondrion			1 NA	6.895	0.769834657
Bcin01.p01800.1		Cytoplasm			0 translation	16.54	0.833487186
Bcin01.p01970.1		Nucleus			0 NA	13.121	0.801422019
Bcin01.p02000.1	Bcrac	Cell membrane			0 small GTPase mediated signal transduction	16.628	0.752709089
Bcin01.p02050.1		Cytoplasm			0 translational initiation	20.721	0.485582507
Bcin01.p02060.1		Golgi apparatus	1 4		cellular response to oxidative stress	6.515	0.852303442
Bcin01.p02060.2		Golgi apparatus	1 4		cellular response to oxidative stress	6.515	0.852303442
Bcin01.p02070.1		Mitochondrion			0 protein insertion into mitochondrial inner membrane from matrix	7.548	0.67862628
Bcin01.p02090.2	Bcade1	Cytoplasm			0 de novo IMP biosynthetic process, purine nucleotide biosynthetic process,	26.301	0.194208005
Bcin01.p02160.1	Bcsla2	Cytoplasm			0 endocytosis, cellular process, actin cortical patch assembly, actin filament organization	12.54	0.959897949
Bcin01.p02310.1	Bcpmt1	Endoplasmic reticulum			12 protein O-linked glycosylation, protein glycosylation, protein O-linked mannosylation	5.34	0.431809488
Bcin01.p02640.1	Bche12	Cytoplasm			0 rescue of stalled ribosome, protein ubiquitination	6.742	0.832678447
Bcin01.p02670.1	Bccct2	Cytoplasm			0 protein folding	18.318	0.738847935
Bcin01.p02680.1	Bcppt1	Cytoplasm			0 translational initiation, formation of cytoplasmic translation initiation complex, translation	35.962	0.362274688
Bcin01.p02790.1	Bcdga1,BcdGAT2	Endoplasmic reticulum			1 NA	11.277	0.697880392
Bcin01.p02880.1		Cytoplasm			0 NA	15.175	0.915453926
Bcin01.p03000.1	Bcipp1	Cytoplasm			0 phosphate-containing compound metabolic process	14.487	0.948731089
Bcin01.p03220.1	Bcnoip14	Nucleus			0 ribosome biogenesis	9.821	0.863398692
Bcin01.p03270.1		Peroxisome			0 NA	70.599	0.09443338
Bcin01.p03440.1		Cytoplasm			0 valyl-tRNA aminoacylation, tRNA aminoacylation for protein translation, translation	51.686	0.204989513
Bcin01.p03500.1		Endoplasmic reticulum			1 lipid transport, endoplasmic reticulum-plasma membrane tethering	20.487	0.69830259
Bcin01.p03640.1	Bcugp1	Cytoplasm			0 UDP-glucose metabolic process, glycogen biosynthetic process, trehalose biosynthetic process	8.78	0.681211745
Bcin01.p03830.1	Bcsod3	Mitochondrion			0 superoxide metabolic process, removal of superoxide radicals	11.308	0.863045504

Bcin01p04050.1	Bcpn01	Nucleus	0 endonucleolytic cleavage in ITS1 to separate SSU-rRNA from 5.8S rRNA	5.369	0.730269697
Bcin01p04340.1	BcmE3	Cytoplasm	0 methionine biosynthetic process, sulfate assimilation, sulfur amino acid metabolic process	59.022	0.19459864
Bcin01p04440.2	Bcarp9	Cytoplasm	0 NA	25.26	0.472647629
Bcin01p04710.1	Bcnop7	Nucleus	0 maturation of LSU-rRNA from trichosteric rRNA transcript (SSU-rRNA, 5.8S rRNA, LSU-rRNA)	7.612	0.5307327
Bcin01p04800.1	Bcsam50	Mitochondrion	0 NA	3.867	0.681552201
Bcin01p04890.1		Endoplasmic reticulum	0 obsolete pathogenesis	12.175	0.631058833
Bcin01p04900.1	gstII	Cytoplasm	0 glutathione metabolic process	14.002	0.794160985
Bcin01p04980.1	Bcsdh2_SdhB	Mitochondrion	0 tricarboxylic acid cycle, electron transport chain	12.691	0.908664533
Bcin01p05120.1		Plastid	4 lipid metabolic process	13.755	0.872878162
Bcin01p05130.1	BcmrpI25	Mitochondrion	0 NA	41.465	0.225789045
Bcin01p05360.1	BbrfC2	Nucleus	0 DNA replication, DNA replication checkpoint signaling	15.229	0.495223354
Bcin01p05380.1		Nucleus	0 NA	10.054	0.777350838
Bcin01p05390.1		Nucleus	0 NA	124.865	0.107962028
Bcin01p05400.1	Bcrd1	Peroxisome	0 ribosome biogenesis, RNA processing	17.598	0.296311226
Bcin01p05430.1	Bcfrs2	Cytoplasm	0 phenylalanyl-tRNA aminoacylation, tRNA aminoacylation, translation	16.386	0.596069732
Bcin01p05480.1	Bcsc66	Endoplasmic reticulum	1 posttranslational protein targeting to membrane, translocation	14.369	0.683043101
Bcin01p05550.1	Bccpa2	Mitochondrion	0 nitrogen compound metabolic process	6.422	0.63621133
Bcin01p05590.1		Nucleus	0 translation, translational initiation, cytoplasmic translational initiation	21.232	0.671839637
Bcin01p05650.1	Bcmgm101	Mitochondrion	0 DNA repair, mitochondrial genome maintenance	6.354	0.610877093
Bcin01p05720.2		Extracellular	1 0 carbohydrate metabolic process, carbohydrate metabolic process	3.111	0.147998077
Bcin01p05740.1		Mitochondrion	0 NA	11.423	0.662525368
Bcin01p06220.1		Nucleus	0 nucleocytoplasmic transport, protein transport, nucleocytoplasmic transport, protein transport	3.678	0.217563729
Bcin01p06320.1	Bcpol30	Nucleus	0 regulation of DNA replication, DNA replication, regulation of catalytic activity, mitotic cell cycle	3.098	0.734789465
Bcin01p06450.3	Bcenol1_BcEnol-1	Cytoplasm	0 glycolytic process, glycolytic process, glycolytic process	14.792	0.935077981
Bcin01p06450.2	Bcenol1_BcEnol-1	Cytoplasm	0 glycolytic process, glycolytic process, glycolytic process	14.792	0.935077981
Bcin01p06460.1	Bcprt4_BcPIO6	Cytoplasm	0 protein catabolic process, nucleotide-excision repair, ubiquitin-dependent ERAD pathway,	12.286	0.943546552
Bcin01p06470.1		Cytoplasm	1 UDP-N-acetylglucosamine biosynthetic process, glutamine metabolic process	13.107	0.974281437
Bcin01p06550.2	Bchir1	Nucleus	0 chromatin organization, transcription, DNA-templated, regulation of transcription	3.587	0.612464955
Bcin01p06550.1		Mitochondrion	0 translation	7.047	0.536174802
Bcin01p06800.1		Mitochondrion	0 aromatic amino acid family biosynthetic process, chorismate biosynthetic process	16.794	0.448206374
Bcin01p06930.2	BccarA	Mitochondrion	0 de novo pyrimidine nucleobase biosynthetic process, glutamine metabolic process	8.006	0.721184167
Bcin01p07240.1	Bchgh1	Cytoplasm	0 chaperone-mediated protein folding	10.875	0.960508717
Bcin01p07460.1	Bcidh1	Mitochondrion	0 tricarboxylic acid cycle	67.221	0.13047599
Bcin01p07490.1		Mitochondrion	0 NA	28.157	0.428114315
Bcin01p07510.1	BceerJ5	Endoplasmic reticulum	1 NA	14.191	0.966310978
Bcin01p07610.1		Cytoplasm	0 negative regulation of transcription, DNA-templated	5.059	0.361361038
Bcin01p07830.1	Bcpam16	Mitochondrion	0 protein import into mitochondrial matrix, protein transport	8.006	0.93042959
Bcin01p07830.2	Bcpam16	Mitochondrion	0 protein import into mitochondrial matrix, protein transport	8.026	0.93042959
Bcin01p07930.1		Plastid	3 NA	37.545	0.097542342
Bcin01p08030.1	Bcegm20	Cytoplasm	0 regulation of translational elongation, positive regulation of autophagy	10.572	0.830730779

Bcin01.p08040.1	Bctuba	Cytoplasm			0 microtubule-based process, cytoskeleton organization	37,309	0.33888628
Bcin01.p08150.2		Cytoplasm			0 NA	25,965	0.38811655
Bcin01.p08320.1	Bcne1	Endoplasmic reticulum	1		1 protein folding	10,191	0.79233568
Bcin01.p08400.1		Endoplasmic reticulum	1		3 protein N-linked glycosylation, protein glycosylation	9,653	0.97086219
Bcin01.p08500.1	Bcym1	Mitochondrion			0 ethanol metabolic process	6,136	0.82192626
Bcin01.p08520.1	Bcprx4	Cytoplasm			0 cellular oxidant detoxification, cellular response to oxidative stress	17,559	0.77232325
Bcin01.p08660.1		Mitochondrion			1 NA	14,32	0.63874269
Bcin01.p08780.1		Cytoplasm			0 aromatic amino acid family biosynthetic process, biosynthetic process	15,164	0.65702438
Bcin01.p08850.1	Bcmr1	Peroxisome			0 cellular metabolic process, cellular biosynthetic process	12,494	0.63208254
Bcin01.p09100.1		Cytoplasm			0 trehalose biosynthetic process, trehalose metabolic process	4,46	0.27362492
Bcin01.p09120.1	Bcpn10	Cytoplasm			0 proteolysis involved in cellular protein catabolic process	19,576	0.33793802
Bcin01.p09310.1		Cytoplasm			0 NA	20,847	0.69513037
Bcin01.p09320.1		Endoplasmic reticulum			8 calcium ion transport, ion transport, calcium ion transmembrane transport	21,536	0.56541472
Bcin01.p09350.1		Cytoplasm			0 translation	25,15	0.55945267
Bcin01.p09360.1	Bccp1	Mitochondrion			1 cellular response to oxidative stress, response to oxidative stress, cellular oxidant detoxification	17,708	0.60949157
Bcin01.p09500.1	Bcst4	Cytoplasm			0 phosphatidylinositol-mediated signaling, phosphatidylinositol phosphate biosynthetic process	8,193	0.95612471
Bcin01.p09530.1		Mitochondrion			0 NA	52,493	0.20114428
Bcin01.p09550.1		Mitochondrion			1 de novo pyrimidine nucleobase biosynthetic process, pyrimidine nucleotide biosynthetic process	8,004	0.83467861
Bcin01.p09560.1		Cytoplasm			0 formation of cytoplasmic translation initiation complex, cellular process, translation	41,036	0.18977366
Bcin01.p09580.2		Peroxisome			0 de novo IMP biosynthetic process, purine nucleotide biosynthetic process	12,465	0.94762762
Bcin01.p09610.1	Bcsmb1	Nucleus			0 NA	3,342	0.86504531
Bcin01.p09620.1		Nucleus			0 translation	5,314	0.375981107
Bcin01.p09650.1	Bczwf1	Cytoplasm			0 glucose metabolic process, pentose-phosphate shunt, carbohydrate metabolic process	6,041	0.44472796
Bcin01.p09660.1		Mitochondrion			0 translation	5,408	0.384783212
Bcin01.p09780.3		Cytoplasm			0 NA	6,615	0.50089435
Bcin01.p09780.1		Cytoplasm			0 NA	6,615	0.50089435
Bcin01.p09780.2		Cytoplasm			0 NA	6,615	0.50089435
Bcin01.p09800.1	Bcutp23	Nucleus			0 rRNA processing, ribosome biogenesis	5,467	0.366735948
Bcin01.p09810.1		Golgi apparatus			4 NA	3,074	0.141347687
Bcin01.p09940.1	Bcchl1	Cytoplasm			0 intracellular protein transport, vesicle-mediated transport	5,527	0.471882767
Bcin01.p09950.1		Cytoplasm			0 gluconeogenesis, pyruvate metabolic process, small molecule biosynthetic process	13,571	0.99457729
Bcin01.p10100.1	Bcpic7	Cytoplasm			0 glycolytic process, phosphorylation, glycolytic process, phosphorylation	8,398	0.64821086
Bcin01.p10150.1	Bcpsd	Cytoplasm			0 phospholipid biosynthetic process	67,922	0.077322658
Bcin01.p10330.1		Cytoplasm			0 aromatic amino acid family biosynthetic process, biosynthetic process	3,657	0.83300982
Bcin01.p10340.1	Bccy1	Mitochondrion			1 electron transport chain, mitochondrial electron transport, ubiquinol to cytochrome c	47,633	0.181810475
Bcin01.p10350.1		Nucleus			0 NA	21,371	0.462261011
Bcin01.p10480.1	Bcrrs1	Nucleus			0 ribosome biogenesis	50,773	0.21219652
Bcin01.p10490.1	Bcrsm23,BcPIO16	Mitochondrion			0 mitochondrial translation	17,369	0.81515405
Bcin01.p10520.1		Cytoplasm			0 proteolysis	8,484	0.68619688
Bcin01.p10540.1		Nucleus			0 maturation of 5S rRNA from tricistronic rRNA transcript (5S rRNA, 5.8S rRNA, LSU rRNA)	36,23	0.242017419

Bcin01p10560.1	Bcpam17	Mitochondrion	2 protein transport, protein import into mitochondrial matrix	24.497	0.357698702
Bcin01p10610.1	Bbcm7	Nucleus	0 DNA replication initiation, DNA replication, DNA duplex unwinding, cell cycle	9.206	0.982928917
Bcin01p10660.1	Bbsec13	Nucleus	0 mRNA transport, positive regulation of TORC1 signaling, COP1-coated vesicle budding	7.754	0.703032257
Bcin01p10690.1	Bbbrm1	Nucleus	0 mitotic chromosome condensation, cell division, cell cycle, chromosome condensation	12.441	0.734387749
Bcin01p10980.1	Bbcprn2	Nucleus	0 regulation of protein catabolic process, regulation of catalytic activity	8.676	0.757698218
Bcin01p11230.1		Mitochondrion	1 NA	10.866	0.880362325
Bcin01p11450.1	Bbcnps7	Cytoplasm	0 NA	6.659	0.738133077
Bcin01p11460.1		Plastid	7 NA	7.03	0.773173117
Bcin01p11490.1		Mitochondrion	0 methylation	26.099	0.501160702
Bcin01p11520.1		Cytoplasm	0 NA	16.775	0.364079883
Bcin01p11530.1		Peroxisome	0 NA	46.096	0.231787789
Bcin01p11550.1	Bcpgs5	Cytoplasm	0 methylation, fatty acid biosynthetic process, metabolic process	9.265	0.718765715
Bcin02p00013.1		Mitochondrion	1 NA	8.434	0.653534724
Bcin02p00014.1		Peroxisome	0 NA	19.47	0.808879971
Bcin02p00120.1		Mitochondrion	0 cysteinyl-tRNA aminoacylation, tRNA aminoacylation for protein translation, translation	3.274	0.42194006
Bcin02p00230.1		Cytoplasm	0 NA	35.453	0.363803684
Bcin02p00240.1		Endoplasmic reticulum	3 obsolete pathogenesis	10.889	0.9418879
Bcin02p00460.1		Endoplasmic reticulum	1 obsolete pathogenesis	13.555	0.852473834
Bcin02p00900.1		Cytoplasm	0 microtubule-based process, cytoskeleton organization	17.689	0.801340487
Bcin02p01010.1		Peroxisome	0 NA	19.851	0.71880673
Bcin02p01020.1		Cytoplasm	0 NA	18.08	0.538235657
Bcin02p01300.1	Bcrism27	Mitochondrion	0 NA	17.237	0.565172467
Bcin02p01360.1	Bceord2	Endoplasmic reticulum	5 protein retention in ER lumen, protein transport	9.262	0.741925909
Bcin02p01370.1		Mitochondrion	0 ATP synthesis coupled electron transport	4.534	0.463251084
Bcin02p01390.1	Bcnp1	Cytoplasm	0 NA	20.239	0.705212289
Bcin02p01610.3	Bcndc3	Peroxisome	0 NA	9.949	0.985942033
Bcin02p01790.1	Bctub8	Cytoplasm	0 microtubule-based process, cytoskeleton organization	20.978	0.680227137
Bcin02p01830.1	Bccgr1	Nucleus	0 rRNA processing, ribosome biogenesis	6.905	0.907462182
Bcin02p01920.1	Bccct4	Cytoplasm	0 protein folding	13.523	0.99786382
Bcin02p01930.1	Bcprt1	Nucleus	0 protein catabolic process, positive regulation of cellular process	7.031	0.534759788
Bcin02p01980.1	Bcpmt4	Endoplasmic reticulum	11 protein O-linked glycosylation, protein glycosylation, protein O-linked mannosylation	12.855	0.960330675
Bcin02p02240.1	Bcstt3	Endoplasmic reticulum	13 protein glycosylation	15.376	0.906526628
Bcin02p02250.1		Mitochondrion	0 ATP synthesis coupled proton transport, ion transport, ATP biosynthetic process	29.508	0.312617438
Bcin02p02350.1	Bcprp7	Mitochondrion	0 translation	5.263	0.37298982
Bcin02p02520.1	Bcqr2	Mitochondrion	0 NA	14.761	0.936175314
Bcin02p02540.1	Bcggc1	Mitochondrion	0 cellular process, mitochondrial genome maintenance, guanine nucleotide transport	20.424	0.688790487
Bcin02p02630.1	Bcdnm1	Cytoplasm	0 mitochondrial inheritance, mitochondrial fission, mitochondrial organization	7.501	0.575720785
Bcin02p02700.1		Extracellular	1 NA	200.659	0.003079572
Bcin02p02740.1	Bcylm2	Mitochondrion	0 cellular process	40.668	0.289986028
Bcin02p02750.1		Mitochondrion	0 citrate metabolic process	19.265	0.76674785

Bcin02p02890.1	Bcnic96	Nucleus	0 nucleocytoplasmic transport	7.007	0.693381713
Bcin02p03080.1		Mitochondrion	3 tricarboxylic acid cycle, electron transport chain	25.692	0.362487192
Bcin02p03160.1		Mitochondrion	0 mitochondrial translation, RNA processing, RNA phosphodiester bond hydrolysis	37.297	0.319503989
Bcin02p03300.1	Bctra1	Cytoplasm	0 histone acetylation, phosphorylation, chromatin organization	6.941	0.613794691
Bcin02p03320.1	Bchap2	Nucleus	0 regulation of transcription, DNA-templated	5.157	0.450921986
Bcin02p03490.1	Bcyc63	Cytoplasm	0 transsulfuration	17.416	0.378070476
Bcin02p03530.1		Cytoplasm	1 0 translational elongation, cytoplasmic translational elongation	27.765	0.194453548
Bcin02p03540.1	Bcrps15	Cytoplasm	0 translation, rRNA export from nucleus	7.023	0.534055584
Bcin02p03580.1	Bcnop12	Nucleus	0 ribosome biogenesis	17.992	0.789342567
Bcin02p03780.2	Bcpex6	Nucleus	0 NA	5.094	0.959225756
Bcin02p03780.1	Bcpex6	Nucleus	0 NA	5.094	0.959225756
Bcin02p03830.1	Bctaf6	Cytoplasm	0 DNA-templated transcription, initiation	9.194	0.964170392
Bcin02p03880.1		Nucleus	0 rRNA processing, ribosome biogenesis	30.085	0.389175535
Bcin02p03930.1	Bcowa1	Mitochondrion	3 establishment of protein localization to membrane	17.72	0.492840619
Bcin02p04020.1	Bcmnn10	Golgi apparatus	1 cell wall mannoprotein biosynthetic process, division septum assembly	26.694	0.251982627
Bcin02p04190.1	Bcnsa2	Nucleus	0 rRNA processing, ribosome biogenesis	17.036	0.828318068
Bcin02p04200.1	Bcmrpl49	Mitochondrion	0 NA	4.683	0.337370781
Bcin02p04220.1		Cytoplasm	0 translation	271.721	0.004615388
Bcin02p04240.1		Endoplasmic reticulum	7 fatty acid biosynthetic process, lipid metabolic process, fatty acid metabolic process	33.449	0.254504569
Bcin02p04510.1		Cytoplasm	0 cellular response to oxidative stress	27.038	0.486573545
Bcin02p04870.1		Nucleus	0 nucleosome assembly	89.612	0.074353407
Bcin02p04900.1		Nucleus	0 base-excision repair, DNA replication, DNA replication, removal of RNA primer, DNA repair	12.537	0.620336624
Bcin02p05070.1	Bcsfb3	Nucleus	0 endoplasmic reticulum to Golgi vesicle-mediated transport, intracellular protein transport	2.919	0.486571212
Bcin02p05140.1	Bcrpl28	Cytoplasm	0 translation	6.299	0.469642984
Bcin02p05160.1	Bcycs4	Nucleus	0 chromosome condensation, mitotic cell cycle, mitotic chromosome condensation, cell division	12.592	0.921407977
Bcin02p05260.1		Cytoplasm	0 intracellular protein transport, vesicle-mediated transport, protein transport	17.123	0.62596889
Bcin02p05270.1	Bckre5	Endoplasmic reticulum	1 0 protein glycosylation, organic substance metabolic process, cellular process, UDP-glucosylation	12.83	0.441813152
Bcin02p05460.2		Nucleus	0 regulation of transcription, DNA-templated, regulation of transcription by RNA polymerase II	8.107	0.732243225
Bcin02p05870.1		Peroxisome	0 NA	10.057	0.904433206
Bcin02p05920.1	Bcaeo1	Mitochondrion	0 tricarboxylic acid cycle, mitochondrial genome maintenance	20.02	0.712824749
Bcin02p05950.1	Bcrpn9	Cytoplasm	0 NA	7.032	0.534850718
Bcin02p05960.1		Mitochondrion	0 NA	6.289	0.500904093
Bcin02p06050.1		Cytoplasm	0 translation	21.05	0.677763696
Bcin02p06070.1	Bcrps31	Cytoplasm	0 translation	16.798	0.841018525
Bcin02p06170.1	Bcsmc4	Nucleus	0 chromosome organization, cell division, chromosome segregation, mitotic cell cycle	20.398	0.699698988
Bcin02p06240.1		Mitochondrion	0 NA	3.107	0.19894337
Bcin02p06270.3		Cytoplasm	0 glucose catabolic process, glycolytic process, glucose catabolic process, glycolytic process	16.96	0.68572764
Bcin02p06320.1		Cell membrane	12 transmembrane transport, cellular process	3.372	0.533668678
Bcin02p06400.1		Mitochondrion	0 cell redox homeostasis	13.362	0.877910772
Bcin02p06440.2		Nucleus	0 NA	15.359	0.759204277

Bcin02p06480.1	Bcutp22	Nucleus	0 rRNA processing, ribosome biogenesis	8,179	0.632697371
Bcin02p06500.1		Cytoplasm	0 regulation of translational initiation, formation of cytoplasmic translation initiation complex	26,599	0.231619728
Bcin02p06580.1		Cytoplasm	0 NA	22,293	0.639565472
Bcin02p06650.1	Begar1	Nucleus	0 rRNA processing, pseudouridine synthesis, ribosome biogenesis, snRNA pseudouridine synthesis	3,621	0.242070258
Bcin02p06660.1	Bccho1	Endoplasmic reticulum	6 phospholipid biosynthetic process, phosphatidylethanolamine biosynthetic process	80,052	0.015547338
Bcin02p06790.1		Nucleus	0 NA	5,226	0.398413
Bcin02p06810.1		Mitochondrion	0 mitochondrial electron transport, MADH to ubiquinone	2,109	0.14151828
Bcin02p06900.1	Bcrps20	Cytoplasm	0 translation	23,409	0.69593202
Bcin02p06930.1		Cell membrane	17 (1->3)-beta-D-glucan biosynthetic process	9,163	0.712531241
Bcin02p06950.1		Mitochondrion	0 transmembrane transport, cellular process	9,429	0.791157309
Bcin02p07150.1		Cytoplasm	0 protein folding	19,298	0.777091866
Bcin02p07410.1	Bcpep1	Cytoplasm	0 protein import into nucleus, protein transport	12,81	0.714539653
Bcin02p07550.1		Endoplasmic reticulum	1 NA	27,658	0.368253521
Bcin02p07560.1	Bcmrp4	Mitochondrion	0 translation	14,25	0.759503991
Bcin02p07590.1		Nucleus	0 DNA repair, DNA replication, DNA biosynthetic process	4,289	0.779301054
Bcin02p07710.1		Nucleus	0 translational initiation, translation, regulation of translation	23,999	0.569911362
Bcin02p07990.1	Bcrrp14	Nucleus	0 NA	14,226	0.811751467
Bcin02p08000.1	Bcops74	Golgi apparatus	0 protein localization to Golgi apparatus	17,596	0.321621516
Bcin02p08090.1	Bccmk2	Cytoplasm	0 protein phosphorylation, negative regulation of transcription by RNA polymerase II	5,029	0.763146672
Bcin02p08110.1	Bcutp6	Nucleus	0 maturation of 5S rRNA from tricistronic rRNA transcript (5S rRNA, 5.8S rRNA, LSU-rRNA)	3,356	0.39959622
Bcin02p08170.4	Bmp1	Cytoplasm	0 protein phosphorylation, phosphorylation, MAPK cascade, protein phosphorylation	12,862	0.901814718
Bcin02p08180.1		Golgi apparatus	0 protein transport, intracellular protein transport, vesicle-mediated transport	236,852	0.009959198
Bcin02p08260.1		Cytoplasm	0 formation of cytoplasmic translation initiation complex, translation, translational initiation	22,496	0.633369135
Bcin02p08270.1		Mitochondrion	0 translation	9,051	0.984795326
Bcin02p08280.1	Bcswi1	Nucleus	1 NA	15,979	0.539542517
Bcin02p08330.1		Nucleus	0 endoplasmic reticulum to Golgi vesicle-mediated transport, intracellular protein transport	9,258	0.716287689
Bcin02p08340.1	Bctps1	Cytoplasm	0 trehalose biosynthetic process, trehalose biosynthetic process, ascospore formation	3,066	0.325074058
Bcin02p08400.2		Nucleus	0 protein ubiquitination, protein ubiquitination, meiosis I	25,984	0.216259227
Bcin02p08400.1		Nucleus	0 protein ubiquitination, protein ubiquitination, meiosis I	25,994	0.216259227
Bcin02p08420.1	Bctma16	Nucleus	0 NA	20,739	0.488510459
Bcin02p08460.1		Mitochondrion	0 transmembrane transport, cellular process	11,159	0.953061023
Bcin02p08540.1	Bcnoip56	Nucleus	0 ribosome biogenesis, rRNA processing	21,465	0.694642331
Bcin02p08590.1	Bcap2	Lysosome/Vacuole	1 proteolysis	19,833	0.597513783
Bcin02p08600.1	Bcshn2	Cytoplasm	0 tetrahydrofolate interconversion, glycine biosynthetic process from serine	18,512	0.798995334
Bcin02p08630.1		Nucleus	0 NA	10,461	0.94652363
Bcin02p08670.1	Bcgcd6	Cytoplasm	0 GDP-mannose biosynthetic process, biosynthetic process, regulation of catalytic activity	17,911	0.575923313
Bcin02p08690.1	Bcrlt3	Cytoplasm	0 protein catabolic process, positive regulation of cellular process	23,019	0.617077495
Bcin03p000590.1	Bcrlps5	Cytoplasm	0 translation, rRNA export from nucleus	25,349	0.554448345
Bcin03p00770.1		Plastid	0 NA	9,619	0.816108125
Bcin03p00790.1		Cytoplasm	0 NA	16,093	0.871531739

Bcin03p00870.1	Bczf1	Nucleus	0 transcription, DNA-templated, regulation of transcription, DNA-templated	14,039	0.8362444
Bcin03p01010.1		Mitochondrion	2 transmembrane transport, mitochondrial ADP transmembrane transport	16,529	0.851670872
Bcin03p01030.1	Bcmir1	Mitochondrion	0 transmembrane transport, mitochondrial phosphate ion transmembrane transport	13,04	0.970442794
Bcin03p01090.1	Bcnop16	Nucleus	0 rRNA processing, ribosome biogenesis, ribosomal large subunit biogenesis	26,008	0.517224682
Bcin03p01520.2		Peroxisome	0 NA	54,988	0.189649453
Bcin03p01540.1		Extracellular	1	68.9	0.57922109
Bcin03p01560.1		Cytoplasm	0 NA	35,368	0.365011288
Bcin03p01820.1		Cytoplasm	0 translation	37,791	0.333000887
Bcin03p01890.1	Bcslp1	Cytoplasm	0 protein ubiquitination, ubiquitin-dependent protein catabolic process	38,247	0.149720653
Bcin03p01900.1		Mitochondrion	0 translation	8,594	0.668371685
Bcin03p01910.1	Bcan1	Golgi apparatus	0 protein targeting to vacuole, endocytosis, vesicle-mediated transport, macroautophagy	23,476	0.201805677
Bcin03p01920.1	Bccat5	Peroxisome	0 response to oxidative stress, alkaloid metabolic process, hydrogen peroxide catabolic process	21,041	0.52912589
Bcin03p02170.1		Mitochondrion	1 proteolysis, signal peptide processing, protein import into mitochondrial matrix	18,663	0.672979385
Bcin03p02310.1	Bccse1	Nucleus	0 intracellular protein transport, protein export from nucleus	5,886	0.418875746
Bcin03p02320.1		Cytoplasm	2 formation of cytoplasmic translation initiation complex, translation,	20,329	0.702046288
Bcin03p02530.1		Cytoplasm	0 translation	21,795	0.654192411
Bcin03p02620.1	Bcepe3	Cytoplasm	0 intracellular protein transport, vesicle-mediated transport	21,179	0.227776109
Bcin03p02680.1	Bcsup45	Cytoplasm	0 translational termination, translation	56,977	0.176965363
Bcin03p02790.1	Bcsec61	Endoplasmic reticulum	10 protein transport, SRP-dependent cotranslational protein targeting to membrane, translocation	11,686	0.888774087
Bcin03p02930.1	Bccla4	Cytoplasm	0 protein phosphorylation, response to pheromone, cellular process	19,348	0.529647656
Bcin03p02940.1		Mitochondrion	0 glycyL-tRNA aminoacylation, tRNA aminoacylation for protein translation	5,997	0.79857049
Bcin03p02940.2		Mitochondrion	0 glycyL-tRNA aminoacylation, tRNA aminoacylation for protein translation	5,997	0.79857049
Bcin03p02950.1	Bcrpf1	Nucleus	0 rRNA processing, ribosome biogenesis	7,673	0.78657049
Bcin03p03060.1	bcdh	Cytoplasm	0 nucleotide-sugar metabolic process, small molecule metabolic process	12,694	0.807315587
Bcin03p03060.2	bcdh	Cytoplasm	0 nucleotide-sugar metabolic process, small molecule metabolic process	12,694	0.793530955
Bcin03p03130.1		Nucleus	0 mRNA cis splicing, via spliceosome, mRNA splicing, via spliceosome	6,107	0.450888188
Bcin03p03230.1	Bcsas10	Nucleus	0 NA	28,75	0.342638244
Bcin03p03360.1		Cytoplasm	0 pentose-phosphate shunt, carbohydrate metabolic process	16,681	0.844458117
Bcin03p03380.1		Cytoplasm	0 gene silencing by RNA, nucleic acid phosphodiester bond hydrolysis	14,404	0.954559621
Bcin03p03380.2		Cytoplasm	0 gene silencing by RNA, nucleic acid phosphodiester bond hydrolysis	14,404	0.954559621
Bcin03p03420.2		Cytoplasm	0 regulation of catalytic activity, regulation of catalytic activity	2,597	0.106549474
Bcin03p03420.1		Cytoplasm	0 regulation of catalytic activity, regulation of catalytic activity	2,597	0.106549474
Bcin03p03620.1		Cytoplasm	0 translation	79,145	0.095504746
Bcin03p03660.1	Bcyme2	Mitochondrion	1 mitochondrial genome maintenance, mRNA processing	4,812	0.844408971
Bcin03p03890.1		Nucleus	0 NA	31,278	0.279008379
Bcin03p04120.1		Nucleus	0 mRNA processing	14,459	0.904770362
Bcin03p04130.1	Bcpet127	Mitochondrion	0 mitochondrial RNA metabolic process	13,636	0.839584151
Bcin03p04160.1		Nucleus	0 mRNA transport, ribosomal large subunit biogenesis, ribosome biogenesis	14,737	0.717028787
Bcin03p04610.1	Bcsec65	Nucleus	0 SRP-dependent cotranslational protein targeting to membrane	11,576	0.612927932
Bcin03p04800.1		Cytoplasm	1 protein polyubiquitination	9,479	0.958335392

Bcin03p04810.1	Cytoplasm		0 mRNA transport, regulation of translation, mRNA processing	7.196	0.626101519
Bcin03p04840.1	Mitochondrion	Bcrsm7	0 translation	10.486	0.89398872
Bcin03p04950.1	Nucleus		0 mRNA transport, nucleocytoplasmic transport, protein transport	5.899	0.789652896
Bcin03p05100.1	Endoplasmic reticulum		5 NA	5.847	0.516587119
Bcin03p05210.1	Mitochondrion		0 NA	7.902	0.69767176
Bcin03p05220.1	Nucleus	Bcutp14	0 rRNA processing	20.854	0.202715752
Bcin03p05250.1	Nucleus		0 histone acetylation, regulation of transcription, DNA-templated	34.691	0.125048652
Bcin03p05350.1	Peroxisome	Bcchr1	0 threonine metabolic process, threonine biosynthetic process, phosphorylation	13.854	0.363210388
Bcin03p05360.1	Nucleus		0 NA	6.796	0.752793698
Bcin03p05480.1	Cytoplasm		0 NA	18.901	0.751442711
Bcin03p05790.1	Nucleus	Bcrpa49	0 transcription, DNA-templated	6.944	0.730085399
Bcin03p05850.1	Endoplasmic reticulum	Bcrrer1	4 cellular process, localization	4.824	0.51206743
Bcin03p05860.1	Nucleus	Bcpaf1	0 histone modification, transcription elongation from RNA polymerase II promoter	5.06	0.351478915
Bcin03p05960.1	Cytoplasm	Bcgst25	0 glutathione metabolic process, translational elongation, translation	30.86	0.437153306
Bcin03p05970.1	Mitochondrion	Bcmrps9	0 translation	6.333	0.471792378
Bcin03p06080.1	Cytoplasm	Bcmvo2	0 NA	7.903	0.581088298
Bcin03p06170.1	Cytoplasm		0 translation	17.897	0.736181975
Bcin03p06180.1	Cytoplasm		0 L-serine biosynthetic process	15.494	0.684645655
Bcin03p06200.1	Cytoplasm		0 riboflavin biosynthetic process	13.564	0.99872731
Bcin03p06210.1	Nucleus	Bcellf1	0 NA	7.859	0.92378227
Bcin03p06230.1	Nucleus		3 regulation of sister chromatid cohesion	7.249	0.919008511
Bcin03p06250.1	Cytoplasm	Bces1	0 seryl-tRNA aminoacylation, tRNA aminoacylation for protein translation	28.134	0.49042577
Bcin03p06300.1	Cytoplasm	Bcsec15	0 vesicle docking involved in exocytosis, intracellular protein transport	8.81	0.973908138
Bcin03p06390.1	Cytoplasm	Bcpsa1	0 GDP-mannose biosynthetic process, biosynthetic process	10.914	0.837361588
Bcin03p06520.1	Cytoplasm		0 carbon utilization, carbon utilization	7.83	0.98305981
Bcin03p06530.1	Cytoplasm		0 ribosome biogenesis, rRNA processing	3.673	0.217018435
Bcin03p06600.1	Cytoplasm		0 NA	107.158	0.050770914
Bcin03p06670.1	Cytoplasm		0 NA	5.475	0.925767085
Bcin03p06740.1	Extracellular		1	3.579	0.273722985
Bcin03p06860.1	Mitochondrion	Bcmrp123	0 translation	5.578	0.44681715
Bcin03p06940.1	Cytoplasm	Bcnp1	0 translational initiation, formation of cytoplasmic translation initiation complex	44.516	0.261323754
Bcin03p06970.1	Cytoplasm		0 translation	50.597	0.213403857
Bcin03p06990.1	Cytoplasm		0 translation	16.64	0.763743224
Bcin03p07080.2	Nucleus		0 nuclear-transcribed mRNA catabolic process, nonsense-mediated decay	54.824	0.188804145
Bcin03p07080.1	Nucleus		0 nuclear-transcribed mRNA catabolic process, nonsense-mediated decay	54.824	0.188804145
Bcin03p07100.1	Golgi apparatus		1 NA	4.035	0.525272844
Bcin03p07110.1	Mitochondrion		0 translation	16.224	0.965483588
Bcin03p07120.1	Cytoplasm	Bcrps12	0 translation	21.005	0.817485746
Bcin03p07200.1	Nucleus		0 rRNA processing, ribosome biogenesis	9.378	0.72739488
Bcin03p07210.1	Mitochondrion		1 NA	11.518	0.802898514

Bcin03p07240.1	Bctuf1	Mitochondrion			0 translational elongation, translation, mitochondrial translation	7.278	0.556468835
Bcin03p07450.1	Bcbm12	Nucleus			0 methylation, rRNA methylation	31.645	0.265872843
Bcin03p07460.1	Bcpr125	Cytoplasm			0 translation	20.937	0.695957087
Bcin03p07580.1		Mitochondrion			0 translational termination	23.611	0.238964737
Bcin03p07630.1		Cytoplasm			0 maturation of LSU-rRNA from trichostonic rRNA transcript (SSU-rRNA, 5.8S rRNA, LSU-rRNA)	9.798	0.759871114
Bcin03p07720.1	Bcrpa135	Nucleus			0 transcription, DNA-templated, transcription by RNA polymerase I	5.986	0.778282191
Bcin03p07920.1	Bcnam9	Mitochondrion			0 translation	24.196	0.584289754
Bcin03p07940.1	Bcmrp13	Mitochondrion			0 RNA processing, rRNA catabolic process, RNA phosphodiester bond hydrolysis	10.481	0.807619887
Bcin03p07950.1	Bcmcm3	Nucleus			0 DNA replication initiation, DNA replication, DNA duplex unwinding	11.53	0.681821386
Bcin03p07980.1	Bcsmv2	Cytoplasm			0 actin filament organization, cytoskeleton organization, cell morphogenesis	58.4	0.167650196
Bcin03p08100.1	Bcbm2	Peroxisome			0 NA	9.707	0.681281244
Bcin03p08110.1	Bcsdcd1	Cytoplasm			0 melanin metabolic process	4.847	0.840123848
Bcin03p08260.1		Endoplasmic reticulum	1	1	NA	7.360	0.74113018
Bcin03p08370.1		Mitochondrion			0 mitochondrial electron transport, ubiquinol to cytochrome c, aerobic respiration	7.435	0.820468789
Bcin03p08380.1		Nucleus			0 ubiquitin-dependent protein catabolic process via the N-end rule pathway	7.443	0.783717359
Bcin03p09000.2		Cytoplasm			0 mitotic cytokinesis, septin ring assembly, septin ring disassembly	26.795	0.449435592
Bcin03p09000.3		Cytoplasm			0 mitotic cytokinesis, septin ring assembly, septin ring disassembly	26.795	0.449435592
Bcin03p09280.1	Bclys9	Cytoplasm			0 NA	9.38	0.820784884
Bcin03p09290.1		Endoplasmic reticulum	4	1	0 cellular process, response to stress	6.812	0.940273058
Bcin03p09318.1		Cytoplasm			0 NA	37.037	0.219289702
Bcin04p00070.1	Bcmrp124	Mitochondrion			0 translation	7.674	0.615800151
Bcin04p00520.1		Cytoplasm			0 NA	5.415	0.430061239
Bcin04p00530.1	Bgcgn1	Cytoplasm			0 positive regulation of kinase activity, regulation of translation	9.815	0.759885578
Bcin04p00540.1		Mitochondrion			0 translation	5.377	0.38200872
Bcin04p00570.1	Bcprx1	Nucleus			0 cellular response to oxidative stress, cellular oxidant detoxification	93.139	0.069623023
Bcin04p00760.1	Bcfaa2	Peroxisome			0 long-chain fatty acid metabolic process, fatty acid beta-oxidation	12.426	0.916948582
Bcin04p00810.1		Cytoplasm			0 NA	12.239	0.646226803
Bcin04p01180.1		Cytoplasm			0 translation	4.65	0.309845973
Bcin04p01270.1		Mitochondrion			2 transmembrane transport, cellular process	5.854	0.933508714
Bcin04p01290.1		Golgi apparatus		1	NA	16.423	0.772200347
Bcin04p01660.1	Bcdug1	Mitochondrion			0 organic substance metabolic process, proteolysis	4.881	0.464164569
Bcin04p01690.1	Bcdhp3	Nucleus			0 endonucleolytic cleavage in ITS1 upstream of 5.8S rRNA	22.819	0.48841746
Bcin04p01770.1		Endoplasmic reticulum		5	mRNA transport, protein transport	16.592	0.701058158
Bcin04p01780.1	Bcaach1	Cytoplasm			0 propionate metabolic process, methylcitrate cycle, acetate metabolic process	31.3	0.409381384
Bcin04p01950.1		Nucleus			0 RNA catabolic process	9.587	0.867198676
Bcin04p01960.1		Cytoplasm		2	intracellular signal transduction	17.023	0.828818389
Bcin04p02090.1	Bcufd2	Cytoplasm			0 ubiquitin-dependent ERAD pathway, ubiquitin-dependent protein catabolic process	11.791	0.76385309
Bcin04p02090.2	Bcufd2	Cytoplasm			0 ubiquitin-dependent ERAD pathway, ubiquitin-dependent protein catabolic process	11.791	0.76385309
Bcin04p02100.1		Endoplasmic reticulum		1	NA	2.717	0.58214475
Bcin04p02150.1	Bcrsm25	Mitochondrion			0 NA	7.141	0.793468858

Bcin04p02200.1	Bcif6	Mitochondrion	0 branched-chain amino acid biosynthetic process, isoleucine biosynthetic process	17.308	0.484813651
Bcin04p02740.1		Mitochondrion	0 translation	11.389	0.899264591
Bcin04p02750.1	Bcho1	Cell membrane	0 small GTPase mediated signal transduction	27.139	0.512075426
Bcin04p02960.1	Bcaim22	Mitochondrion	0 protein lipoylation, cellular protein modification process	7.983	0.976670984
Bcin04p03020.1	Bcnop15	Nucleus	0 NA	6.695	0.504697914
Bcin04p03030.1	Bctif34	Nucleus	0 formation of cytoplasmic translation initiation complex, translation, translational initiation	32.25	0.411309191
Bcin04p03040.1		Mitochondrion	0 tetrahydrofolate interconversion, one-carbon metabolic process	35.699	0.360767489
Bcin04p03060.1	Bctrp5	Cytoplasm	0 tryptophan biosynthetic process, tryptophan metabolic process	7.274	0.797989025
Bcin04p03100.1	Bcliv5	Mitochondrion	0 branched-chain amino acid biosynthetic process, isoleucine biosynthetic process	24.213	0.583039667
Bcin04p03120.1	BcChSIIla	Cell membrane	7 cell wall organization, chitin biosynthetic process, conidium formation	7.949	0.613665263
Bcin04p03140.1	Bcras2	Cell membrane	0 signal transduction	37.007	0.264639083
Bcin04p03190.1		Cytoplasm	0 NA	24.02	0.431130192
Bcin04p03400.1	Bcmpp10	Nucleus	0 rRNA processing, ribosome biogenesis	34.243	0.234463049
Bcin04p03420.1	Bcnp133	Nucleus	0 nucleocytoplasmic transport	10.572	0.900294201
Bcin04p03440.1		Endoplasmic reticulum	1 NA	16.916	0.597734022
Bcin04p03490.1		Nucleus	0 GDP-mannose biosynthetic process, regulation of transcription, DNA-templated	3.46	0.345217517
Bcin04p03490.2		Nucleus	0 GDP-mannose biosynthetic process, regulation of transcription, DNA-templated	3.46	0.345217517
Bcin04p03490.3		Nucleus	0 GDP-mannose biosynthetic process, regulation of transcription, DNA-templated	3.46	0.345217517
Bcin04p03580.1	Bcgus1	Cytoplasm	0 glutamyl-tRNA aminoacylation, tRNA aminoacylation	22.749	0.624662092
Bcin04p03590.1	Bcmrp11	Mitochondrion	0 NA	10.207	0.626963863
Bcin04p03660.1	Bcvma1	Mitochondrion	0 ATP metabolic process, proton transmembrane transport, ion transport	19.926	0.559372123
Bcin04p03690.1	Bcvps1	Cytoplasm	0 NA	4.638	0.310624228
Bcin04p03770.1	Bcapm1	Cytoplasm	0 intracellular protein transport, vesicle-mediated transport, protein transport, Golgi to endosome	15.777	0.88831133
Bcin04p03870.1	Bcsp54	Cytoplasm	0 SRP-dependent cotranslational protein targeting to membrane, protein targeting to ER	22.692	0.547989336
Bcin04p04040.1	Bcyea4	Endoplasmic reticulum	10 transmembrane transport, carbohydrate transport	37.071	0.094307696
Bcin04p04260.1		Cytoplasm	0 methionyl-tRNA aminoacylation, tRNA aminoacylation for protein translation, translation	64.661	0.139149748
Bcin04p04290.1		Cytoplasm	0 translational elongation	12.558	0.627745517
Bcin04p04490.1		Cytoplasm	0 asparagine biosynthetic process, glutamine metabolic process	9.6	0.740739692
Bcin04p04770.2	Bcarg8	Mitochondrion	0 arginine metabolic process, arginine biosynthetic process, arginine metabolic process	6.867	0.880969762
Bcin04p04770.1	Bcarg8	Mitochondrion	0 arginine metabolic process, arginine biosynthetic process, arginine metabolic process	6.867	0.880969762
Bcin04p04800.1	Bcbm1	Peroxisome	0 NA	3.032	0.158009689
Bcin04p04820.1	Bcvma2	Lysosome/Vacuole	0 ATP metabolic process, proton transmembrane transport, ion transport	27.904	0.493284116
Bcin04p05000.1	BcppoA90	Mitochondrion	1 response to oxidative stress, cellular oxidant detoxification	8.795	0.685735883
Bcin04p05010.1	Bctsc13	Endoplasmic reticulum	4 lipid metabolic process	33.069	0.396991733
Bcin04p05050.2		Nucleus	0 protein ubiquitination, protein ubiquitination, protein ubiquitination	7.742	0.674003656
Bcin04p05050.1		Nucleus	0 protein ubiquitination, protein ubiquitination, protein ubiquitination	7.742	0.674003656
Bcin04p05060.1		Cytoplasm	0 ribonucleoside monophosphate biosynthetic process, nucleotide biosynthetic process	19.099	0.481631649
Bcin04p05070.1		Cytoplasm	0 translation	26.809	0.51981914
Bcin04p05190.1		Cytoplasm	0 translation	24.127	0.58615662
Bcin04p05250.1		Mitochondrion	1 NA	4.35	0.530500909

Bcin04p05260.1	Bccdc60	Cytoplasm	0 leucyl-tRNA aminoacylation, tRNA aminoacylation for protein translation, translation	11.273	0.861320555
Bcin04p05440.1		Cytoplasm	0 translation	34.809	0.379026519
Bcin04p05510.1		Nucleus	0 NA	17.812	0.796690553
Bcin04p05630.1	Beste7	Cytoplasm	0 protein phosphorylation	16.355	0.858516739
Bcin04p05680.1	Bchfd1	Mitochondrion	0 cellular aldehyde metabolic process	9.586	0.867124504
Bcin04p05730.1		Mitochondrion	1 NA	9.807	0.98411048
Bcin04p05740.1	Bcapm2	Cytoplasm	0 intracellular protein transport, vesicle-mediated transport, protein transport	20.394	0.326279703
Bcin04p05790.1	Bcmprl8	Mitochondrion	0 translation	22.065	0.562407482
Bcin04p05810.1		Nucleus	0 translational initiation, formation of cytoplasmic translation initiation complex, translation	38.695	0.269898934
Bcin04p05920.1	Bccdc10, BcSep4	Cytoplasm	0 NA	17.764	0.798660081
Bcin04p05930.1		Mitochondrion	0 translation	5.367	0.381603342
Bcin04p06140.1		Peroxisome	2 proline biosynthetic process	7.634	0.746087245
Bcin04p06210.1		Nucleus	0 regulation of transcription, DNA-templated, regulation of transcription by RNA polymerase II	9.686	0.946664455
Bcin04p06290.1	Bcptc5	Mitochondrion	1 protein dephosphorylation, peptidyl-serine dephosphorylation	13.473	0.538581731
Bcin04p06300.2	Bcrqc1	Cytoplasm	0 NA	4.031	0.711274045
Bcin04p06400.1	Begut2	Mitochondrion	1 glycerol-3-phosphate metabolic process, organic substance metabolic process	24.151	0.586468845
Bcin04p06450.2		Cytoplasm	0 NA	6.634	0.659217256
Bcin04p06450.1		Cytoplasm	0 NA	8.504	0.659217256
Bcin04p06570.1	Bcmet6	Cytoplasm	0 methylation, methionine biosynthetic process, cellular amino acid biosynthetic process	182.163	0.014098001
Bcin04p06740.1		Cytoplasm	0 DNA replication, metabolic process	23.517	0.602901891
Bcin04p06890.1		Cytoplasm	0 NA	9.427	0.99475876
Bcin05p00010.1		Cytoplasm	0 NA	22.897	0.56235343
Bcin05p00080.1	Bcpre1	Cytoplasm	0 proteolysis involved in cellular protein catabolic process	2.863	0.302818971
Bcin05p00090.1		Cytoplasm	0 translation, translational initiation, cytoplasmic translational initiation	30.772	0.438743984
Bcin05p00180.1		Cytoplasm	0 NA	301.701	0.003371895
Bcin05p00480.1		Cytoplasm	0 adenine salvage, purine ribonucleoside salvage, nucleoside metabolic process, AMP salvage	4.687	0.721054711
Bcin05p00580.1		Peroxisome	0 NA	10.323	0.917973117
Bcin05p00840.1	Bcops13	Golgi apparatus	0 protein transport, protein retention in Golgi apparatus, late endosome to vacuole transport	10.886	0.832086192
Bcin05p00940.1		Endoplasmic reticulum	2 NA	2.769	0.231511658
Bcin05p00960.1	BcmaK11	Nucleus	0 NA	6.327	0.557583123
Bcin05p01030.1		Cytoplasm	0 NA	10.076	0.590312558
Bcin05p01140.1	Bcatp20	Mitochondrion	0 ATP synthesis coupled proton transport, ion transport	67.432	0.128584742
Bcin05p01240.1		Cell membrane	0 NA	5.503	0.614647657
Bcin05p01260.1		Cytoplasm	0 NA	6.673	0.520764335
Bcin05p01420.1	Bcrpo21	Nucleus	0 transcription by RNA polymerase II, transcription, DNA-templated, translation synthesis	10.597	0.884380772
Bcin05p01490.1	Bcutp11	Nucleus	0 rRNA processing	26.015	0.403888812
Bcin05p01520.1		Endoplasmic reticulum	1 carbohydrate metabolic process	15.78	0.69639509
Bcin05p01530.1		Endoplasmic reticulum	7 NA	11.909	0.90520865
Bcin05p01550.1		Cytoplasm	0 D-xylose catabolic process, carbohydrate metabolic process, D-xylose metabolic process	16.867	0.613019714
Bcin05p01620.1		Cell membrane	0 dephosphorylation	7.278	0.818861085

Bcin05p01700.1	Bchrd3	Endoplasmic reticulum	1	1	NA	7.401	0.94622002
Bcin05p01740.1		Cytoplasm			NA	10.187	0.690088374
Bcin05p01760.2		Nucleus			NA	65.425	0.076942865
Bcin05p02050.1	Bcalo1	Peroxisome			NA	7.685	0.88956459
Bcin05p02170.1	Bcstu2	Cytoplasm			0	14.943	0.926946696
Bcin05p02250.1	Bcdus3	Nucleus			0	5.827	0.975567823
Bcin05p02330.1	Bcnan1	Nucleus			0	4.059	0.253510884
Bcin05p02400.1	Bcrfz2	Mitochondrion			3	5.270	0.363875284
Bcin05p02470.1		Cytoplasm			0	7.488	0.850101016
Bcin05p02580.1		Mitochondrion			0	70.146	0.120427034
Bcin05p02590.1	Bcrpd3	Nucleus			0	6.788	0.751842249
Bcin05p02600.1		Cytoplasm			0	18.212	0.620928982
Bcin05p02640.1		Mitochondrion			1	6.686	0.641179354
Bcin05p02880.1	Bcrpn6	Cytoplasm			0	5.9	0.50884139
Bcin05p02910.1	Bcsor1	Nucleus			0	10.119	0.974967733
Bcin05p02910.1	Bccc3	Cytoplasm			0	26.996	0.472672202
Bcin05p03000.1	Bcala1	Cytoplasm			0	14.605	0.77382916
Bcin05p03030.1	Bcyps8	Cytoplasm			0	6.041	0.521365556
Bcin05p03230.1		Cytoplasm			0	19.455	0.733081781
Bcin05p03270.1		Mitochondrion			1	24.794	0.568815131
Bcin05p03300.1		Cytoplasm			0	6.894	0.769844458
Bcin05p03430.1	Bcktl12	Cytoplasm			0	7.946	0.540546484
Bcin05p03640.1	Bcapl3	Cytoplasm			0	9.275	0.88424252
Bcin05p03730.1		Mitochondrion			0	30.256	0.311385088
Bcin05p03750.1	Bccha1	Peroxisome			0	4.830	0.426939922
Bcin05p03790.1	Bcyme1	Mitochondrion			1	10.364	0.7788916
Bcin05p03830.1	Bcrpep	Endoplasmic reticulum			6	10.119	0.8081839
Bcin05p04060.1		Nucleus			0	32.584	0.407466757
Bcin05p04170.1	Bcnoc2	Nucleus			1	5.801	0.447788674
Bcin05p04420.1	Bcmas1	Mitochondrion			0	44.172	0.26457424
Bcin05p04850.2		Nucleus			0	8.376	0.792224164
Bcin05p05070.1	Bctim50	Mitochondrion			1	35.584	0.252148782
Bcin05p05100.1		Mitochondrion			0	9.586	0.92049498
Bcin05p05250.1	Bctaf9	Nucleus			0	8.655	0.62828804
Bcin05p05400.1		Cytoplasm			0	3.011	0.154934373
Bcin05p05460.1	Bcdst1	Nucleus			0	24.262	0.381454267
Bcin05p05700.1	Bcsec18	Cytoplasm			0	12.155	0.67434871
Bcin05p05740.1	Bcspb4	Nucleus			0	5.431	0.693104181
Bcin05p05790.1	Bcnop58	Nucleus			0	11.377	0.945211935
Bcin05p05810.1		Mitochondrion			0	8.633	0.669537285

Bcin05p05820.1		Cytoplasm		0 translation, ribosomal small subunit assembly	21.093	0.676711098
Bcin05p05900.1	Bcap5	Extracellular	1	0 proteolysis	22.086	0.63811614
Bcin05p05960.1		Mitochondrion		0 biosynthetic process	9.163	0.967852986
Bcin05p06070.1	Bcrpl38	Cytoplasm		0 translation	40.07	0.305918819
Bcin05p06130.1		Cytoplasm		0 translation	49.463	0.221244396
Bcin05p06320.1	Bcp1	Mitochondrion		0 protein peptidyl-prolyl isomerization, protein folding, protein peptidyl-prolyl isomerization	7.889	0.608984656
Bcin05p06410.1	Bcmsb1	Cytoplasm		0 NA	6.026	0.81291263
Bcin05p06430.1		Cytoplasm		0 de novo IMP biosynthetic process, biosynthetic process, one-carbon metabolic process	7.795	0.600763483
Bcin05p06730.1		Cytoplasm		0 tryptophan biosynthetic process, tryptophan metabolic process, glutamine metabolic process	5.434	0.446290478
Bcin05p06800.1	Bcrok1	Nucleus		0 maturation of SSU-rRNA	10.09	0.86026292
Bcin05p06880.1		Cytoplasm		0 protein phosphorylation, protein phosphorylation	7.334	0.944271451
Bcin05p06880.2		Cytoplasm		0 protein phosphorylation, protein phosphorylation	7.334	0.944271451
Bcin05p07050.1		Nucleus		0 NA	15.608	0.453007187
Bcin05p07060.1	Bcdld1	Mitochondrion		0 NA	18.833	0.68808273
Bcin05p07200.1		Cytoplasm		0 NA	9.403	0.991947781
Bcin05p07290.1		Lysosome/Vacuole		6 cation transport, transmembrane transport, cation transmembrane transport	3.077	0.509442144
Bcin05p07420.1	Bcsnu114	Nucleus		0 RNA splicing, mRNA processing	5.273	0.389451472
Bcin05p07440.1	Bckre33	Nucleus		0 ncRNA processing, rRNA metabolic process, rRNA modification	6.367	0.534803652
Bcin05p07450.1		Cytoplasm		0 NA	22.782	0.333831051
Bcin05p07460.1	Bcsmx2	Cytoplasm		0 spliceosomal snRNP assembly, mRNA processing, RNA splicing, mRNA splicing, via spliceosome	3.617	0.372621401
Bcin05p07500.1		Mitochondrion		0 NA	20.163	0.68155638
Bcin05p07640.1		Endoplasmic reticulum		1 obsolete pathogenesis	11.743	0.881778007
Bcin05p07670.1		Mitochondrion		0 NA	4.509	0.334659523
Bcin05p07900.1	Bcklp3	Cytoplasm		0 microtubule-based movement	11.903	0.643839689
Bcin05p08070.1		Cytoplasm		0 rRNA processing, translation	12.796	0.91003362
Bcin06p00380.1		Cytoplasm		0 translation	5.905	0.42626259
Bcin06p00610.1		Cytoplasm		0 NA	17.781	0.602554706
Bcin06p00700.1	Bcrsm22	Mitochondrion		0 methylation, translation	3.983	0.331462535
Bcin06p00790.1	Bcprs1	Cytoplasm		0 ribonucleoside monophosphate biosynthetic process, nucleotide biosynthetic process	15.909	0.880165959
Bcin06p00800.1		Peroxisome		0 inositol phosphate dephosphorylation, phosphatidylinositol phosphate biosynthetic process	2.473	0.190881985
Bcin06p01050.1		Nucleus		0 regulation of transcription, DNA-templated	6.513	0.726425532
Bcin06p01100.1	Bcmrp2	Mitochondrion		0 translation	6.489	0.732710853
Bcin06p01270.1	Bcmrps8	Mitochondrion		0 translation	54.574	0.186251938
Bcin06p01700.1	Bcmsy1	Mitochondrion		0 tyrosyl-rRNA aminoacylation, rRNA aminoacylation for protein translation, translation	7.051	0.908675329
Bcin06p01840.1		Nucleus		0 NA	32.013	0.416981872
Bcin06p01920.1		Nucleus		0 NA	9.005	0.881418428
Bcin06p02010.1		Mitochondrion	1	NA	10.625	0.929481783
Bcin06p02030.1		Peroxisome		0 NA	18.997	0.518700719
Bcin06p02110.1		Plastid		0 NA	13.513	0.739012767
Bcin06p02120.1	Bcsec21	Cytoplasm		0 intracellular protein transport, vesicle-mediated transport, protein transport	6.627	0.73246147

Bcin06p02220.1	Cytoplasm	0 protein dephosphorylation	2,925	0.129653724
Bcin06p02300.1	Cytoplasm	0 lysine biosynthetic process	20,618	0.653270042
Bcin06p02340.1	Plastid	0 NA	41,492	0.290607767
Bcin06p02350.1	Nucleus	0 ribosomal large subunit export from nucleus, regulation of ribosomal subunit export from nucleus	12,27	0.948119878
Bcin06p02380.1	Cytoplasm	0 NA	41,959	0.285819949
Bcin06p02390.1	Nucleus	0 NA	8,34	0.958743139
Bcin06p02430.1	Cytoplasm	0 biosynthetic process	21,628	0.596817547
Bcin06p02610.1	Cytoplasm	0 protein deneddylation	13,055	0.82905765
Bcin06p02870.3	Cytoplasm	0 protein phosphorylation, protein phosphorylation, protein phosphorylation	11,59	0.650300561
Bcin06p02870.1	Cytoplasm	0 protein phosphorylation, protein phosphorylation, protein phosphorylation	36,668	0.201052613
Bcin06p02890.1	Nucleus	0 translation	9,806	0.759007143
Bcin06p02930.1	Nucleus	0 NA	11,557	0.561834231
Bcin06p02940.1	Nucleus	0 NA	10,685	0.849687773
Bcin06p02950.1	Nucleus	0 NA	24,147	0.44237833
Bcin06p03110.1	Nucleus	0 regulation of transcription, DNA-templated, regulation of transcription by RNA polymerase II	6,295	0.859711942
Bcin06p03220.1	Golgi apparatus	1 NA	17,892	0.696952724
Bcin06p03290.1	Nucleus	0 rRNA processing	12,713	0.620844637
Bcin06p03350.1	Cytoplasm	0 translation	14,191	0.967372168
Bcin06p03360.1	Cytoplasm	0 NA	9,36	0.901564675
Bcin06p03370.1	Mitochondrion	0 mitochondrial phosphate ion transmembrane transport, endosome to Golgi, protein transport, intracellular protein transport	2,559	0.248482623
Bcin06p03460.1	Cytoplasm	0 retrograde transport, endosome to Golgi, protein transport, intracellular protein transport	23,59	0.459852381
Bcin06p03480.1	Nucleus	0 protein deneddylation	15,144	0.500445637
Bcin06p03610.1	Endoplasmic reticulum	15 transmembrane transport, oligopeptide transmembrane transport	2,292	0.19379907
Bcin06p04940.1	Mitochondrion	0 heme biosynthetic process, porphyrin-containing compound biosynthetic process	9,964	0.765562256
Bcin06p04160.1	Peroxisome	0 NA	11,824	0.69813595
Bcin06p04900.1	Cytoplasm	0 inositol phosphate dephosphorylation, phosphatidylinositol phosphate biosynthetic process	8,548	0.326483183
Bcin06p04940.1	Peroxisome	0 obsolete oxidation-reduction process	15,821	0.884190046
Bcin06p04980.1	Nucleus	2 coenzyme A biosynthetic process, coenzyme A biosynthetic process	7,852	0.993543264
Bcin06p05030.2	Nucleus	2 coenzyme A biosynthetic process, coenzyme A biosynthetic process	7,852	0.993543264
Bcin06p05030.1	Cytoplasm	0 phosphorylation, phosphorylation	7,023	0.909751004
Bcin06p05040.1	Cytoplasm	0 phosphorylation, phosphorylation	7,023	0.909751004
Bcin06p05140.1	Nucleus	0 rRNA processing	6,079	0.5033967
Bcin06p05140.1	Cell membrane	4 NA	23,546	0.49055963
Bcin06p05380.1	Cytoplasm	0 microtubule-based movement	11,649	0.885781449
Bcin06p05520.1	Cytoplasm	0 protein phosphorylation, plasma membrane organization	6,367	0.474927675
Bcin06p05570.1	Mitochondrion	4 NA	8,707	0.505782071
Bcin06p05720.1	Mitochondrion	1 NA	8,964	0.955622987
Bcin06p05860.1	Mitochondrion	0 translation	13,573	0.99375947
Bcin06p05950.1	Endoplasmic reticulum	2 cellular process, endoplasmic reticulum to Golgi vesicle-mediated transport	36,035	0.216085103
Bcin06p06280.1	Mitochondrion	0 response to heat, protein folding, response to heat, protein folding, 'de novo' protein folding	36,911	0.34400814

Bcin06p06330.1	Bcrpp0	Cytoplasm		0 ribosome biogenesis, ribosomal large subunit assembly, cytoplasmic translation	9.001	0.70308293
Bcin06p06360.1	Bcsm2	Nucleus		0 NA	20.192	0.23993837
Bcin06p06440.1	Bchs1	Cytoplasm		0 NA	15.692	0.86174032
Bcin06p06550.1		Nucleus		1 rRNA processing	2.703	0.143025812
Bcin06p06560.1	Bcarc35	Nucleus		0 actin filament polymerization, Arp2/3 complex-mediated actin nucleation	2.465	0.19702746
Bcin06p06570.1	Bchh155	Nucleus		1 spliceosomal complex assembly	7.348	0.837815981
Bcin06p06590.1	Bcfrt1	Lysosome/Vacuole		12 transmembrane transport	28.805	0.130175154
Bcin06p06610.1	Bcutp13	Nucleus		0 rRNA processing	5.803	0.64689452
Bcin06p06640.1	Bcrgd2	Cytoplasm		0 intracellular signal transduction, signal transduction, regulation of catalytic activity	5.55	0.945371113
Bcin06p06670.1		Extracellular	1	0 NA	86.39	0.068410544
Bcin06p06690.1	Boym1	Nucleus		0 maturation of LSU-rRNA from tricistronic rRNA transcript (SSU-rRNA, 5.8S rRNA, LSU-rRNA)	3.15	0.158721459
Bcin06p07090.1		Mitochondrion		0 NA	81.742	0.150329209
Bcin06p07180.1		Plastid		0 NA	5.415	0.197878649
Bcin06p07240.1	Bccrc1	Mitochondrion		2 cellular process	31.41	0.2578202865
Bcin06p07280.1	Bcbfr1	Cytoplasm		0 NA	19.741	0.722718057
Bcin07p001120.1	Bcdhh1	Cytoplasm		0 mRNA transport, regulation of translation, mRNA processing	18.135	0.783550001
Bcin07p001130.1	Bcpr1	Nucleus		0 DNA replication, synthesis of RNA primer, DNA replication	24.897	0.29007814
Bcin07p00240.1		Mitochondrion		0 NA	12.14	0.755028816
Bcin07p00300.1		Peroxisome		0 iron ion homeostasis	2.842	0.311485075
Bcin07p00440.1	Bcrpn3	Nucleus		0 regulation of protein catabolic process, regulation of catalytic activity	14.552	0.948004362
Bcin07p00530.1		Cytoplasm		0 NA	4.303	0.628172935
Bcin07p00720.1	Bpk3, BcATG1	Cytoplasm		0 autophagy, protein phosphorylation, protein transport, phosphorylation	11.765	0.480229394
Bcin07p00730.1		Plastid		0 L-proline biosynthetic process, ornithine metabolic process	23.418	0.453491438
Bcin07p00830.1	Besws2	Mitochondrion		0 translation	66.658	0.075390348
Bcin07p00940.1	Bctps2	Cytoplasm		0 trehalose biosynthetic process, trehalose metabolic process, trehalose biosynthetic process	8.739	0.905386464
Bcin07p00940.2	Bctps2	Cytoplasm		0 trehalose biosynthetic process, trehalose metabolic process, trehalose biosynthetic process	8.739	0.905386464
Bcin07p01150.1		Cytoplasm		0 translation	2.901	0.15045699
Bcin07p01210.1	Bcflm12	Cytoplasm		0 translation, translational initiation	10.796	0.829392117
Bcin07p01260.1	Bcrsp68	Cytoplasm		0 SRP-dependent cotranslational protein targeting to membrane	8.421	0.65252467
Bcin07p01290.1		Cytoplasm		0 NA	6.216	0.921985638
Bcin07p01290.2		Cytoplasm		0 NA	6.216	0.921985638
Bcin07p01320.1		Nucleus		0 NA	53.473	0.128192386
Bcin07p01390.1	Bcst1	Cytoplasm		0 cell division, cell cycle	5.523	0.883029695
Bcin07p01430.1	Bseec62	Endoplasmic reticulum		2 protein transport	8.333	0.630080793
Bcin07p01510.1	Bdisb6	Cytoplasm		0 phosphorylation, phosphatidylinositol phosphate biosynthetic process	9.059	0.96972318
Bcin07p01540.1		Cytoplasm		0 translation	7.254	0.563001613
Bcin07p01580.1	Bcnog1	Nucleus		0 ribosome biogenesis, ribosomal subunit export from nucleus, rRNA processing	16.496	0.853594947
Bcin07p01620.1	Bcrpp8	Nucleus		0 methylation, rRNA processing	7.073	0.912573233
Bcin07p01710.1	Bcphb2	Mitochondrion		0 NA	38.175	0.397904626
Bcin07p01800.1		Nucleus		0 NA	16.854	0.689023733

Bcin07p01810.1	Bcrmsp1	Mitochondrion	1	protein targeting to mitochondrion, protein hexamerization	12.472	0.650680933
Bcin07p01890.1		Mitochondrion	0	acetyl-CoA biosynthetic process from pyruvate, pseudohyphal growth	4.362	0.293673048
Bcin07p02150.1	Bchtz1	Nucleus	0	chromatin organization, chromatin remodelling	11.151	0.853254595
Bcin07p02270.1		Cytoplasm	0	NA	12.296	0.747575123
Bcin07p02320.1	Bcpho88	Endoplasmic reticulum	2	protein targeting to ER	15.731	0.557933468
Bcin07p02370.1		Peroxisome	0	NA	22.919	0.818977138
Bcin07p02570.1	Bcrtg2	Peroxisome	0	NA	7.339	0.934159542
Bcin07p02580.1		Nucleus	0	NA	6.235	0.989862823
Bcin07p02600.1		Nucleus	0	NA	21.116	0.487108387
Bcin07p02610.1		Cytoplasm	0	pentose-phosphate shunt, D-gluconate metabolic process	6.073	0.447684883
Bcin07p02610.2		Cytoplasm	0	pentose-phosphate shunt, D-gluconate metabolic process	6.073	0.447684883
Bcin07p02640.2		Peroxisome	0	phosphorylation, phosphorylation	32.45	0.27563282
Bcin07p02820.1	Bcmet12	Cytoplasm	0	methionine metabolic process, tetrahydrofolate interconversion	14.622	0.457342577
Bcin07p03000.2		Peroxisome	5	cellular process, cellular process	3.855	0.84718206
Bcin07p03060.1		Plastid	0	NA	6.57	0.961607354
Bcin07p03080.1		Cytoplasm	0	proteolysis	20.991	0.303211794
Bcin07p03160.1	Bcaps2	Cytoplasm	0	clathrin-dependent endocytosis, protein transport, intracellular protein transport	3.487	0.344144133
Bcin07p03390.1	Bctop2	Nucleus	0	DNA topological change, DNA metabolic process, meiosis I cell cycle process	10.233	0.914669888
Bcin07p03490.1	Bcsm1	Nucleus	0	NA	11.291	0.858592219
Bcin07p03810.1		Mitochondrion	0	arginyl-tRNA aminoacylation, tRNA aminoacylation for protein translation, translation	15.636	0.768784408
Bcin07p03950.1	Bcdhp9	Nucleus	0	rRNA processing, ribosome biogenesis	20.096	0.507107421
Bcin07p04130.1		Peroxisome	0	fatty acid beta-oxidation, cellular process	3.765	0.225943798
Bcin07p04280.1	Bcdh2	Mitochondrion	0	tricarboxylic acid cycle	54.07	0.1876878
Bcin07p04430.2	Bcsst2	Cytoplasm	0	intracellular signal transduction, negative regulation of signal transduction	10.692	0.839634795
Bcin07p04430.1	Bcsst2	Cytoplasm	0	intracellular signal transduction, negative regulation of signal transduction	10.692	0.839634795
Bcin07p04500.2		Nucleus	0	cellular process, protein peptidyl-prolyl isomerization, cellular process	24.083	0.587342206
Bcin07p04500.1		Nucleus	0	cellular process, protein peptidyl-prolyl isomerization, cellular process	24.093	0.587342206
Bcin07p04610.2		Nucleus	0	cellular process, protein peptidyl-prolyl isomerization, cellular process	24.083	0.587342206
Bcin07p04620.1	Bccap2	Cytoplasm	0	barbed-end actin filament capping, actin cytoskeleton organization, filamentous growth	19.546	0.69726297
Bcin07p04650.1	Bcgr1	Cytoplasm	0	regulation of transcription by RNA polymerase II	4.098	0.255161713
Bcin07p04690.1	Bcatp3	Mitochondrion	0	ATP synthesis coupled proton transport, ion transport, ATP biosynthetic process	11.598	0.985989695
Bcin07p04700.1	Bctop1	Nucleus	0	DNA topological change, regulation of mitotic recombination	8.827	0.877511657
Bcin07p04730.1	Bccmk1	Cytoplasm	0	protein phosphorylation, protein phosphorylation	14.449	0.902209823
Bcin07p04900.1		Endoplasmic reticulum	1	NA	10.827	0.83148344
Bcin07p05050.1		Nucleus	0	DNA repair, chromatin organization, cellular response to DNA damage stimulus	8.473	0.656715174
Bcin07p05090.1		Golgi apparatus	0	NA	16.514	0.537475506
Bcin07p05110.1	Bcnop2	Nucleus	0	RNA methylation, ribosome biogenesis, RNA processing, methylation	17.39	0.775672135
Bcin07p05470.1		Cytoplasm	0	NA	6.374	0.475536036
Bcin07p05560.1		Lysosome/Vacuole	0 1	NA	8.121	0.915562487

Bcin07p05560.2	Lysosome/Vacuole	0 1	NA	8.121	0.915562487
Bcin07p05580.1	Endoplasmic reticulum		1 ERAD pathway, endoplasmic reticulum calcium ion homeostasis	49.221	0.223144282
Bcin07p05670.1	Nucleus		0 ribosome assembly, ribosome biogenesis	11.835	0.88938785
Bcin07p05700.1	Mitochondrion		0 NA	6.685	0.929410537
Bcin07p05720.4	Nucleus		0 protein deubiquitination, ubiquitin-dependent protein catabolic process, proteolysis	18.516	0.696254842
Bcin07p05720.1	Nucleus		0 protein deubiquitination, ubiquitin-dependent protein catabolic process, proteolysis	18.516	0.696254842
Bcin07p05720.2	Nucleus		0 protein deubiquitination, ubiquitin-dependent protein catabolic process, proteolysis	18.516	0.696254842
Bcin07p05720.3	Nucleus		0 protein deubiquitination, ubiquitin-dependent protein catabolic process, proteolysis	18.516	0.696254842
Bcin07p05750.1	Mitochondrion		2 NA	15.122	0.918030762
Bcin07p05770.2	Endoplasmic reticulum		3 NA	6.499	0.998819082
Bcin07p05890.1	Cytoplasm		0 CTP biosynthetic process, pyrimidine nucleotide biosynthetic process	9.902	0.650154376
Bcin07p06060.1	Mitochondrion		0 obsolete oxidation-reduction process	17.115	0.39908871
Bcin07p06100.1	Cytoplasm		0 NA	3.966	0.415083034
Bcin07p06110.1	Peroxisome		0 NA	8.723	0.921563502
Bcin07p06140.1	Plastid		0 response to heat, protein folding, response to heat, protein folding	8.63	0.930333398
Bcin07p06160.1	Mitochondrion		0 protein quality control for misfolded or incompletely synthesized proteins	5.242	0.677898568
Bcin07p06220.1	Mitochondrion		0 protein folding	3.794	0.261232123
Bcin07p06230.1	Cytoplasm		0 formation of cytoplasmic translation initiation complex, translation, translational initiation	31.791	0.386263752
Bcin07p06280.1	Nucleus		0 chromosome organization, chromosome condensation, cell division, chromosome segregation	16.55	0.787286602
Bcin07p06310.1	Endoplasmic reticulum		5 unsaturated fatty acid biosynthetic process, lipid metabolic process, fatty acid metabolic process	23.2	0.547547204
Bcin07p06360.3	Cytoplasm		0 methionine metabolic process, tetrahydrofolate interconversion, methionine metabolic process	7.681	0.893263838
Bcin07p06370.2	Nucleus	0 2	transcription, DNA-templated	16.994	0.511780314
Bcin07p06370.1	Nucleus	0 2	transcription, DNA-templated	16.994	0.511780314
Bcin07p06390.1	Mitochondrion		0 translation	4.308	0.265525947
Bcin07p06400.1	Cytoplasm		0 small GTPase mediated signal transduction, protein transport, regulation of catalytic activity	16.599	0.759002096
Bcin07p06550.1	Cytoplasm		0 leucine biosynthetic process, cellular amino acid biosynthetic process	4.288	0.534536559
Bcin07p06580.1	Nucleus		0 rRNA processing, ribosome biogenesis	13.949	0.978790158
Bcin07p06650.1	Cytoplasm		0 NA	2.382	0.31104833
Bcin07p06960.2	Cytoplasm		0 fatty acid biosynthetic process, malonyl-CoA biosynthetic process, metabolic process	16.5	0.709172149
Bcin07p07060.1	Golgi apparatus		1 NA	5.444	0.388381208
Bcin08p00090.1	Mitochondrion		0 NA	8.649	0.939271243
Bcin08p00280.1	Extracellular	1	0 proteolysis	35.593	0.361988544
Bcin08p00460.2	Nucleus		0 DNA replication, synthesis of RNA primer, DNA replication, DNA replication	6.095	0.814079494
Bcin08p00590.1	Mitochondrion		0 translation	41.522	0.260001986
Bcin08p00620.1	Mitochondrion		0 translation	33.599	0.39138526
Bcin08p00630.1	Nucleus		0 ribosome biogenesis	11.335	0.730226599
Bcin08p00660.1	Nucleus		0 DNA repair, mRNA splicing, via spliceosome, protein ubiquitination	19.699	0.521319414
Bcin08p00760.1	Cytoplasm		0 translation	5.919	0.43324721
Bcin08p00810.1	Cytoplasm		0 cellular metabolic process, organonitrogen compound biosynthetic process	23.415	0.450030163
Bcin08p01110.1	Cytoplasm		0 positive regulation of translational elongation, translation	77.472	0.098568482

Bcin08p01270.5		Nucleus		0 NA		31.748	0.296900693
Bcin08p01270.4		Nucleus		0 NA		31.748	0.296900693
Bcin08p01270.3		Nucleus		0 NA		31.748	0.296900693
Bcin08p01270.1		Nucleus		0 NA		31.748	0.296900693
Bcin08p01350.1		Cell membrane		2 NA		48.89	0.140620819
Bcin08p01370.1		Nucleus		0 SRP-dependent cotranslational protein targeting to membrane		3.083	0.296370193
Bcin08p01420.1	Bcgb1	Nucleus		0 signal transduction, signal transduction		3.2	0.150146103
Bcin08p01420.2	Bcgb1	Nucleus		0 signal transduction, signal transduction		3.2	0.150146103
Bcin08p01540.1		Peroxisome		0 steroid biosynthetic process, methylation, sterol biosynthetic process		11.234	0.913725953
Bcin08p01550.1		Cytoplasm		0 NA		19.345	0.59800313
Bcin08p01710.2		Cytoplasm		0 NA		11.494	0.550249025
Bcin08p01710.1		Cytoplasm		0 NA		11.494	0.550249025
Bcin08p01710.3		Cytoplasm		0 NA		11.494	0.550249025
Bcin08p01740.1	Brrg1	Cytoplasm		0 phosphorelay signal transduction system, phosphorelay signal transduction system		13.172	0.47555989
Bcin08p01740.2	Brrg1	Cytoplasm		0 phosphorelay signal transduction system, phosphorelay signal transduction system		13.172	0.47555989
Bcin08p02230.1		Endoplasmic reticulum		1 NA		10.037	0.818470809
Bcin08p02270.1		Peroxisome		0 peroxisome fission		4.684	0.885640733
Bcin08p02290.3		Mitochondrion		4 NA		20.266	0.704222741
Bcin08p02490.1	Bcrlp32	Cytoplasm		0 translation		10.779	0.828179837
Bcin08p02500.1	Bcodj1	Mitochondrion		0 response to heat, protein folding		14.765	0.935973178
Bcin08p02520.2	Bcrrl1	Cytoplasm		0 proteolysis, proteolysis, proteolysis		16.27	0.494129533
Bcin08p02540.1	Bcdml4	Nucleus		0 DNA biosynthetic process, DNA ligation involved in DNA repair, DNA recombination		6.171	0.793750328
Bcin08p02600.1	Bcedc3	Cytoplasm		0 NA		2.78	0.1341838
Bcin08p02620.1	Bcpub1	Nucleus		0 NA		40.434	0.192197028
Bcin08p02620.1	Bcpub1	Nucleus		0 NA		40.434	0.192197028
Bcin08p02770.1		Cytoplasm		0 NA		57.196	0.081465683
Bcin08p02840.1	Bcwbp1	Endoplasmic reticulum	1	1 protein N-linked glycosylation via asparagine, protein glycosylation		15.889	0.797648838
Bcin08p02900.1		Peroxisome		2 peroxisome organization		24.92	0.23194037
Bcin08p02950.1		Mitochondrion		0 NA		7.342	0.561981977
Bcin08p02980.1	Bcbph1	Cytoplasm		0 NA		7.09	0.785973242
Bcin08p03020.1		Endoplasmic reticulum		2 endoplasmic reticulum tubular network organization		6.511	0.965250672
Bcin08p03170.1	Bcehd3	Mitochondrion		0 valine catabolic process		16.375	0.702844784
Bcin08p03200.1	Bcoyl6	Mitochondrion		0 translation, translation		8.935	0.693315651
Bcin08p03210.1	Bcmrp135	Mitochondrion		0 NA		23.549	0.602017917
Bcin08p03360.1		Cytoplasm		0 ubiquitin-dependent protein catabolic process, transcription-coupled nucleotide-excision repair		6.82	0.57981191
Bcin08p03470.1	Bcemc1	Endoplasmic reticulum	1	1 NA		13.568	0.526852094
Bcin08p03530.1		Cytoplasm		0 translation		8.385	0.64957943
Bcin08p03630.1		Endoplasmic reticulum		7 ceramide biosynthetic process, plasma membrane organization		4.374	0.461474107
Bcin08p03700.1	Bccdc48	Cytoplasm		0 regulation of cellular process, cellular protein localization		15.162	0.916052635
Bcin08p03710.1	Bcnde2	Mitochondrion		0 NADH oxidation		11.749	0.862160307

Bcin08p03780.1	Cytoplasm	0 intracellular signal transduction, regulation of catalytic activity	9.046	0.17208019
Bcin08p03790.1	Endoplasmic reticulum	6 fatty acid biosynthetic process, lipid metabolic process, fatty acid metabolic process	3.373	0.31017567
Bcin08p04080.1	Mitochondrion	0 NA	26.33	0.19893084
Bcin08p04150.1	Nucleus	0 rRNA processing, mRNA processing, RNA processing	11.279	0.86175533
Bcin08p04170.1	Nucleus	0 NA	3.909	0.687162704
Bcin08p04200.1	Cytoplasm	0 NA	6.844	0.91775146
Bcin08p04270.1	Nucleus	0 rRNA methylation, methylation, rRNA processing, rRNA methylation	13.1	0.973889591
Bcin08p04360.1	Cytoplasm	0 phosphatidylinositol-mediated signaling	2.904	0.958625388
Bcin08p04380.1	Mitochondrion	5 lipid homeostasis	3.951	0.476291905
Bcin08p04420.1	Cytoplasm	0 nucleotide metabolic process, inosine salvage, dephosphorylation	6.26	0.801050514
Bcin08p04450.2	Mitochondrion	0 mitochondrial translation, translation, glutamyl-tRNAIn biosynthesis via transamidation	2.656	0.512527633
Bcin08p04450.1	Mitochondrion	0 mitochondrial translation, translation, glutamyl-tRNAIn biosynthesis via transamidation	2.659	0.512527633
Bcin08p04450.3	Mitochondrion	0 mitochondrial translation, translation, glutamyl-tRNAIn biosynthesis via transamidation	2.656	0.512527633
Bcin08p04480.1	Mitochondrion	0 fatty acid biosynthetic process, aerobic respiration	14.254	0.68975993
Bcin08p04500.1	Mitochondrion	0 NA	36.292	0.28179744
Bcin08p04540.1	Mitochondrion	0 acetyl-CoA biosynthetic process from pyruvate	4.839	0.348462186
Bcin08p04730.1	Cytoplasm	0 carbohydrate metabolic process, dephosphorylation	22.387	0.567816257
Bcin08p04830.1	Nucleus	0 NA	10.754	0.829482644
Bcin08p04840.1	Endoplasmic reticulum	7 lipid metabolic process	3.848	0.351019786
Bcin08p05050.1	Mitochondrion	0 NA	10.162	0.980201115
Bcin08p05060.1	Cytoplasm	0 NA	12.02	0.765271103
Bcin08p05120.1	Mitochondrion	0 translation	61.194	0.120363616
Bcin08p05160.1	Nucleus	0 intracellular protein transport	8.601	0.944822384
Bcin08p05200.1	Endoplasmic reticulum	1 obsolete pathogenesis	11.615	0.942967779
Bcin08p05220.1	Cytoplasm	0 gluconeogenesis, glycolytic process, gluconeogenesis, glycolytic process	10.095	0.819222618
Bcin08p05240.1	Nucleus	0 mRNA splicing, via spliceosome	10.085	0.819222618
Bcin08p05250.1	Nucleus	0 ribosomal large subunit assembly, ribosome biogenesis	12.72	0.973553988
Bcin08p05290.1	Golgi apparatus	1 protein glycosylation, mannosylation	17.088	0.684208513
Bcin08p05410.1	Cytoplasm	0 RNA catabolic process	12.46	0.936181521
Bcin08p05770.1	Nucleus	0 protein import into nucleus, protein transport, protein import into nucleus, protein transport	5.322	0.508034275
Bcin08p05800.1	Mitochondrion	0 aspartyl-tRNA aminoacylation, tRNA aminoacylation for protein translation, translation	19.849	0.51884182
Bcin08p05830.1	Cytoplasm	0 regulation of translation	8.712	0.67582517
Bcin08p05890.1	Nucleus	0 ribosome biogenesis, ribosomal large subunit biogenesis	5.267	0.696939843
Bcin08p05920.1	Mitochondrion	0 mitochondrion inheritance, mitochondrial genome maintenance, mitochondrion organization	8.613	0.80835053
Bcin08p06040.1	Mitochondrion	1 transmembrane transport, cellular process	7.102	0.541027126
Bcin08p06300.1	Cytoplasm	0 fructose 6-phosphate metabolic process, glycolytic process, metabolic process, phosphorylation	12.867	0.960373473
Bcin08p06400.1	Endoplasmic reticulum	4 NA	33.998	0.385262008
Bcin08p06410.1	Endoplasmic reticulum	0 GPI anchor biosynthetic process	4.043	0.702339853
Bcin08p06450.1	Cytoplasm	0 NA	7.955	0.859583486
			11.798	0.177855386

Bcin08p06600.1		Nucleus		0 spliceosomal snRNP assembly, RNA processing, mRNA processing, RNA splicing	3.271	0.261274314
Bcin08p06700.1	Bchh1	Cytoplasm		0 protein folding, cellular response to heat	7.048	0.78010145
Bcin08p06750.1	Bctf2	Nucleus		0 transcription initiation from RNA polymerase II promoter	5.46	0.451415719
Bcin08p07040.2		Cytoplasm		0 obsolete pathogenesis, obsolete pathogenesis, obsolete pathogenesis	12.35	0.638138118
Bcin08p07060.1	Bcgp16	Endoplasmic reticulum	1	1 attachment of GPI anchor to protein	29.346	0.122811784
Bcin09p00080.1	Bcmf1	Cell membrane		0 NA	5.288	0.8898851
Bcin09p00240.1	Bcubp3	Nucleus		0 protein deubiquitination, ubiquitin-dependent protein catabolic process, proteolysis	12.604	0.63020916
Bcin09p00250.1		Endoplasmic reticulum	10	10 sterol biosynthetic process, lipid metabolic process, steroid biosynthetic process	16.853	0.51088577
Bcin09p00280.2		Extracellular		0 NA	4.053	0.40959853
Bcin09p00540.1		Mitochondrion		0 NA	4.07	0.70402889
Bcin09p00550.1	Bcc13	Mitochondrion		0 tricarboxylic acid cycle, propionate catabolic process, 2-methylcitrate cycle	21.712	0.501733686
Bcin09p00870.1	Bcnew1	Cytoplasm		0 chromatin remodeling, regulation of translational termination, gene expression	24.59	0.573847596
Bcin09p00980.1		Mitochondrion		0 isocitrate metabolic process, tricarboxylic acid cycle	8.74	0.843648153
Bcin09p01080.1		Nucleus		0 RNA splicing, nuclear-transcribed mRNA catabolic process, nonsense-mediated decay	10.829	0.565984642
Bcin09p01240.1		Cytoplasm		0 lipid catabolic process	5.521	0.387261888
Bcin09p01310.1	Bctre1	Cytoplasm		0 trehalose catabolic process, trehalose metabolic process, carbohydrate metabolic process	16.5	0.35024027
Bcin09p01340.1		Mitochondrion		0 translation	16.492	0.85115262
Bcin09p01460.2		Mitochondrion		0 NA	9.967	0.96300274
Bcin09p01520.1	Bcefr3	Cytoplasm		0 protein localization to plasma membrane, protein localization to plasma membrane	6.732	0.88808089
Bcin09p01820.1		Cytoplasm		0 NA	22.563	0.416562357
Bcin09p01820.2		Cytoplasm		0 NA	22.563	0.416562357
Bcin09p02000.1	Bch17	Cytoplasm		0 glutamine metabolic process, histidine biosynthetic process, metabolic process	11.719	0.788952729
Bcin09p02020.1		Cytoplasm		0 protein phosphorylation, phosphorylation	7.022	0.943250865
Bcin09p02100.1	Bcarg5	Mitochondrion		0 arginine biosynthetic process, metabolic process, cellular amino acid biosynthetic process	16.448	0.852875949
Bcin09p02170.1	Bcdim1	Nucleus		0 rRNA processing, rRNA modification, methylation	9.727	0.81804579
Bcin09p02190.1	Bcutp7	Nucleus		0 endonucleolytic cleavage in ITS1 to separate SSU-rRNA from 5.8S rRNA	16.681	0.835656583
Bcin09p02210.1	Bcade12	Cytoplasm		0 purine nucleotide biosynthetic process, 'de novo' AMP biosynthetic process	7.857	0.855041231
Bcin09p02370.1	Bcwr1	Cytoplasm		0 tryptophanyl-tRNA aminoacylation, tRNA aminoacylation for protein translation, translation	30.289	0.447427783
Bcin09p02390.2	Bmp3	Cytoplasm		0 protein phosphorylation, phosphorylation, MAPK cascade, cell wall integrity MAPK cascade	20.827	0.616267389
Bcin09p02420.1		Mitochondrion	1	1 intracellular protein transport, protein transmembrane transport	26.185	0.534097884
Bcin09p02490.1		Cytoplasm		0 translation	5.254	0.370167623
Bcin09p02680.1		Cytoplasm		0 carbohydrate metabolic process, oligosaccharide metabolic process	6.448	0.557735555
Bcin09p02810.1	Bcrpb3	Cytoplasm		0 transcription, DNA-templated	4.716	0.414334016
Bcin09p02860.1	Bcrvb1	Nucleus		0 DNA repair, chromatin organization, cellular response to DNA damage stimulus	14.191	0.965801417
Bcin09p03410.1	Bcsub2	Nucleus		0 mRNA splicing, via spliceosome, transcription-coupled nucleotide-excision repair	16.542	0.851030415
Bcin09p03550.1		Cytoplasm		0 translation	20.228	0.705553822
Bcin09p03870.1		Mitochondrion		0 NA	25.313	0.485250384
Bcin09p04160.1		Cytoplasm		0 NA	14.849	0.809887671
Bcin09p04650.1	Bcrsm18	Mitochondrion		0 translation	21.858	0.64844174
Bcin09p04660.1		Nucleus		0 rRNA processing, ribosomal small subunit biogenesis	11.539	0.967428213

Bcin09p04950.1	Cytoplasm	0 translation	43.972	0.26626565
Bcin09p05030.1	Nucleus	0 SRP-dependent cotranslational protein targeting to membrane, intracellular protein transport	16.502	0.698375988
Bcin09p05060.1	Mitochondrion	1 NA	3.906	0.739286298
Bcin09p05590.1	Cytoplasm	0 translation	16.107	0.796714773
Bcin09p05600.1	Cytoplasm	0 NA	3.102	0.163330039
Bcin09p05650.1	Mitochondrion	0 NA	6.413	0.715715987
Bcin09p05760.2	Cytoplasm	0 translational elongation, translation, translational elongation, translation	5.795	0.420753952
Bcin09p05840.1	Cytoplasm	0 lipid transport	10.827	0.838238245
Bcin09p06110.1	Cytoplasm	0 tricarboxylic acid cycle, glyoxylate cycle	13.383	0.747789122
Bcin09p06180.1	Cell membrane	10 phospholipid transport, lipid translocation, phospholipid transport, lipid translocation	7.372	0.841194426
Bcin09p06180.2	Cell membrane	10 phospholipid transport, lipid translocation, phospholipid transport, lipid translocation	7.372	0.841194426
Bcin09p06410.1	Cytoplasm	0 leucine biosynthetic process, carboxylic acid metabolic process	17.229	0.289363915
Bcin09p06480.1	Cytoplasm	0 NA	16.118	0.870335401
Bcin09p06820.1	Cytoplasm	1 NA	154.524	0.013624822
Bcin09p07030.1	Cytoplasm	0 UDP-N-acetylglucosamine biosynthetic process	14.627	0.672224681
Bcin10p00020.1	Lysosome/Vacuole	13 transmembrane transport, cellular process	5.103	0.779402696
Bcin10p00030.1	Cytoplasm	0 NA	14.228	0.963862282
Bcin10p00040.1	Cytoplasm	3 methylation, fatty acid biosynthetic process, metabolic process	3.473	0.197988757
Bcin10p00060.1	Mitochondrion	0 NA	6.915	0.52440811
Bcin10p00300.1	Cytoplasm	0 protein folding	12.896	0.961503512
Bcin10p00560.1	Lysosome/Vacuole	7 NA	15.664	0.56396954
Bcin10p00650.1	Boyf1	14 transmembrane transport, glutathione metabolic process, response to metal ion	7.827	0.885941888
Bcin10p00750.1	Bcms15	0 mRNA splicing, via spliceosome, cellular process, mRNA processing, RNA splicing	17.19	0.394510134
Bcin10p00920.1	Bcbmt5	0 NA	12.97	0.63942264
Bcin10p00930.1	Bcaos1	0 cellular protein modification process, cellular metabolic process, protein sumoylation	8.193	0.913473692
Bcin10p01030.1	Bcpnx9	0 cellular oxidant detoxification	46.621	0.234052514
Bcin10p01050.2	Nucleus	0 NA	14.472	0.828879655
Bcin10p01050.1	Nucleus	0 NA	14.472	0.828879655
Bcin10p01180.1	Bcarb1	0 ribosomal small subunit export from nucleus, ribosome biogenesis	65.594	0.138372335
Bcin10p01380.1	Cytoplasm	0 NA	13.594	0.498970989
Bcin10p01520.1	Bcelp3	0 cellular process, tRNA processing	8.47	0.866038165
Bcin10p01530.1	Mitochondrion	0 tricarboxylic acid cycle	3.821	0.2398734
Bcin10p01550.1	Cell membrane	9 transmembrane transport	11.127	0.73811981
Bcin10p02060.1	Cytoplasm	0 NA	10.789	0.733119802
Bcin10p02220.1	Endoplasmic reticulum	2 lipid catabolic process, lipid metabolic process, triglyceride metabolic process	4.994	0.984125785
Bcin10p02230.1	Bcsar1	0 intracellular protein transport, vesicle-mediated transport, protein transport	66.282	0.064104123
Bcin10p02290.1	Bcape4	0 proteolysis	50.343	0.03344078
Bcin10p02410.1	Bcefg1	0 rRNA processing	6.995	0.531562092
Bcin10p02660.1	Mitochondrion	0 NA	16.052	0.417926461
Bcin10p02810.1	Nucleus	0 NA	8.434	0.767940647

Bc1n10p02960.1		Endoplasmic reticulum		3	NA	5.441	0.60233501
Bc1n10p03090.1	Bchem1	Mitochondrion	0 tetrapyrrole biosynthetic process, biosynthetic process			3.571	0.41228928
Bc1n10p03250.1		Cytoplasm	0 NA			5.715	0.421348193
Bc1n10p03260.1	Bchut1	Golgi apparatus	10 transmembrane transport, carbohydrate transport, UDP-glucose transmembrane transport			6.581	0.725943185
Bc1n10p03400.1	Bcrg1	Cytoplasm	0 cytoplasmic translation, positive regulation of cellular response to amino acid starvation			29.894	0.455098136
Bc1n10p03430.1		Nucleus	0 regulation of transcription, DNA-templated, regulation of cellular process			9.871	0.764041718
Bc1n10p03440.1	Bcctr9	Nucleus	0 histone modification, regulation of transcription, DNA-templated			4.847	0.330914336
Bc1n10p03470.1		Cytoplasm	0 vesicle-mediated transport			10.872	0.597514684
Bc1n10p03630.1	Bccli1	Cytoplasm	0 intracellular distribution of mitochondria, organelle organization, mitochondrion organization			16.468	0.774047703
Bc1n10p03790.1		Endoplasmic reticulum	2 NA			56.907	0.056716851
Bc1n10p03820.1	Bcrg1	Cytoplasm	0 formation of cytoplasmic translation initiation complex, translation, translational initiation			54.554	0.189579527
Bc1n10p03900.1		Mitochondrion	0 DNA recombination, mitochondrial genome maintenance			29.207	0.381542793
Bc1n10p03910.1	Bchsp104	Cytoplasm	0 protein refolding, protein unfolding, cellular heat acclimation			14.381	0.834516133
Bc1n10p03930.1		Cytoplasm	0 protein dephosphorylation, DNA replication checkpoint signaling			8.755	0.67921023
Bc1n10p03930.2		Cytoplasm	0 protein dephosphorylation, DNA replication checkpoint signaling			8.795	0.67921023
Bc1n10p03950.1	Bcstp10	Nucleus	0 rRNA processing, ribosome biogenesis			8.622	0.792356353
Bc1n10p03970.1	Bsec63	Endoplasmic reticulum	3 posttranslational protein targeting to membrane, translocation, protein transport			9.654	0.731145746
Bc1n10p04050.1	Bcds1	Nucleus	0 ribosome biogenesis, ribosomal large subunit assembly, rRNA processing			6.263	0.501829888
Bc1n10p04110.1	Bcpap1	Nucleus	0 mRNA processing, RNA polyadenylation, RNA 3'-end processing, cellular process			6.819	0.885400194
Bc1n10p04130.1	Bcfsf1	Mitochondrion	4 ion transport, amino acid transport, transmembrane transport, ion transmembrane transport			11.353	0.875468732
Bc1n10p04140.1		Nucleus	0 protein phosphorylation			5.654	0.770474502
Bc1n10p04220.1	Bctma19, BcPIC6	Cytoplasm	0 translation			8.013	0.61902249
Bc1n10p04290.1		Cytoplasm	0 translation			67.152	0.130562757
Bc1n10p04300.1		Cytoplasm	0 translation			58.544	0.169934251
Bc1n10p04480.1		Endoplasmic reticulum	1 NA			7.137	0.920989223
Bc1n10p04550.1	Bcnop1	Nucleus	0 methylation, rRNA processing			24.676	0.566442388
Bc1n10p04580.1		Cytoplasm	0 COPII-coated vesicle budding, intracellular protein transport			3.719	0.221479982
Bc1n10p04610.1		Cytoplasm	0 translation			36.413	0.378654175
Bc1n10p04680.1	Bcopp2	Nucleus	0 RNA phosphodiester bond hydrolysis, exonucleolytic, mRNA catabolic process			103.119	0.058964044
Bc1n10p05000.1		Nucleus	0 NA			7.038	0.90379833
Bc1n10p05050.1	Bcprt2	Nucleus	0 protein catabolic process, positive regulation of cellular process			16.538	0.597595231
Bc1n10p05280.3		Endoplasmic reticulum	7 sterol biosynthetic process, lipid metabolic process, steroid biosynthetic process			5.823	0.433755502
Bc1n10p05310.1	Bcleu2	Cytoplasm	0 leucine biosynthetic process, cellular amino acid biosynthetic process			13.036	0.705672407
Bc1n10p05400.1	Bcprd3	Cytoplasm	0 regulation of translation, mitotic spindle assembly checkpoint signaling			10.321	0.92882126
Bc1n10p05430.1	Bcrps3	Mitochondrion	0 translation, ribosomal small subunit export from nucleus, cytoplasmic translation			26.505	0.388312729
Bc1n10p05460.1	Bcret2	Cytoplasm	0 retrograde vesicle-mediated transport, Golgi to endoplasmic reticulum, protein transport			27.246	0.509704109
Bc1n10p05510.1	Bcsmc1	Nucleus	0 mitotic sister chromatid cohesion, chromosome organization, cell division			26.476	0.463164547
Bc1n10p05640.1	Bcbim1	Cytoplasm	0 cell division, cell cycle, cellular component organization			2.292	0.104190187
Bc1n10p05740.1	Bcmdj2	Mitochondrion	0 NA			14.292	0.907247004
						13.909	0.691988178

Bcin1p005770.1	Cytoplasm		0	intracellular protein transport, vesicle-mediated transport, protein transport	53.772	0.19393427
Bcin1p005950.2	Nucleus	Bcpac1, BcpacC	0	NA	7.401	0.96297236
Bcin1p005950.1	Nucleus	Bcpac1, BcpacC	0	NA	7.401	0.96297236
Bcin1p005980.1	Endoplasmic reticulum		4	NA	4.1	0.50203813
Bcin1p006020.1	Nucleus		0	regulation of transcription, DNA-templated, regulation of transcription, DNA-templated	4.469	0.324512697
Bcin1p006020.2	Nucleus		0	regulation of transcription, DNA-templated, regulation of transcription, DNA-templated	4.469	0.324512697
Bcin1p001170.1	Lysosome/Vacuole	Bcvma5	0	proton transmembrane transport, ion transport	13.178	0.890055432
Bcin1p00330.1	Cytoplasm	Bceerg13	0	isoprenoid biosynthetic process, sterol biosynthetic process	15.997	0.875951903
Bcin1p00500.1	Endoplasmic reticulum	Bcopl3	5	methylation, phosphatidylcholine biosynthetic process, lipid metabolic process	21.062	0.521809025
Bcin1p00750.1	Cytoplasm		0	NA	27.655	0.247874649
Bcin1p00830.1	Mitochondrion		0	NA	15.918	0.8790598
Bcin1p00980.1	Cytoplasm	Bcesy1	0	protein phosphorylation	10.001	0.608113187
Bcin1p00990.1	Mitochondrion		1	transmembrane transport, cellular process	26.69	0.449157242
Bcin1p01040.1	Nucleus		0	NA	2.493	0.204654892
Bcin1p01190.1	Peroxisome		0	NA	10.519	0.941409698
Bcin1p01630.1	Nucleus		0	organic substance transport, nitrogen compound transport	2.699	0.409813637
Bcin1p01670.1	Mitochondrion		1	NA	31.165	0.303715493
Bcin1p01750.1	Nucleus	Bcprp31	0	mRNA splicing, via spliceosome, spliceosomal tri-snRNP complex assembly, mRNA processing	21.695	0.598534979
Bcin1p01830.1	Peroxisome	Bcdpm1	0	protein glycosylation, mannosylation	16.929	0.794002125
Bcin1p01950.1	Cytoplasm		0	NA	3.761	0.696969894
Bcin1p02110.1	Nucleus	Bchmt1	0	peptidyl-arginine methylation, methylation, mRNA export from nucleus	26.891	0.541138391
Bcin1p02130.1	Cytoplasm	Bcpom1	0	UDP-N-acetylglucosamine biosynthetic process, carbohydrate metabolic process	3.748	0.373285379
Bcin1p02220.1	Nucleus	Bcds3	0	RNA phosphodiester bond hydrolysis	5.896	0.431214593
Bcin1p02250.1	Nucleus	Bcnug1	0	ribosomal large subunit export from nucleus	14.178	0.969487507
Bcin1p02330.1	Cytoplasm	Bcsec26	0	intracellular protein transport, vesicle-mediated transport, protein transport	10.493	0.809424269
Bcin1p02490.1	Cytoplasm		0	carbohydrate metabolic process, organic substance metabolic process	6.504	0.571849588
Bcin1p02610.1	Cytoplasm		0	NA	26.899	0.517510583
Bcin1p02630.1	Cytoplasm		0	NA	16.588	0.770204253
Bcin1p02670.1	Peroxisome		0	NA	43.002	0.275468543
Bcin1p02700.1	Peroxisome	Bcpls4	2	methylation, fatty acid biosynthetic process, metabolic process	16.141	0.597339721
Bcin1p02730.1	Cytoplasm	BcPIO5	0	NA	29.336	0.465008412
Bcin1p03040.1	Mitochondrion		0	branched-chain amino acid biosynthetic process, isoleucine biosynthetic process	2.981	0.262868633
Bcin1p03090.1	Cytoplasm	Bcfba1	0	glycolytic process, carbohydrate metabolic process, gluconeogenesis	99.092	0.08019413
Bcin1p03100.1	Mitochondrion		0	translation	52.644	0.179477005
Bcin1p03130.1	Nucleus		1	rRNA processing, ribosome biogenesis	3.722	0.22177974
Bcin1p03140.1	Nucleus	Bcrrp3	0	rRNA processing, ribosome biogenesis, maturation of 5S rRNA from tricistronic rRNA transcript	26.527	0.35333971
Bcin1p03280.1	Nucleus		0	maturation of LSU-rRNA From tricistronic rRNA Transcript (SSU-rRNA, 5.8S rRNA, LSU-rRNA)	6.236	0.462763407
Bcin1p03320.1	Mitochondrion		0	NA	5.404	0.384549832
Bcin1p03520.1	Cytoplasm		0	S-adenosylmethionine biosynthetic process, one-carbon metabolic process	19.404	0.734947352
Bcin1p03560.1	Cytoplasm	Bos4, BcOS4	0	protein phosphorylation, stress-activated MAPK cascade, phosphorylation	9.899	0.989922543

Bc1n1p03740.1	Bcrl11	Cytoplasm		0 NA		19,094	0.746223733
Bc1n1p03750.2	Bcchd1	Nucleus	0 chromatin remodeling, chromatin remodeling			8,05	0.624929598
Bc1n1p03750.1	Bcchd1	Nucleus	0 chromatin remodeling, chromatin remodeling			8,05	0.624929598
Bc1n1p04180.1	Bceev29	Golgi apparatus		8 NA		20,622	0.313026305
Bc1n1p04200.1		Mitochondrion		2 NA		11,014	0.731059051
Bc1n1p04250.1		Mitochondrion		0 NA		11,454	0.599888016
Bc1n1p04260.1	Bcatp10	Mitochondrion		0 NA		22,315	0.286186579
Bc1n1p04420.1	Bcefb1	Cytoplasm	0 translational elongation, translation			11,445	0.936270095
Bc1n1p04610.2	Bcemp24	Endoplasmic reticulum	1 protein retention in ER lumen, endoplasmic reticulum to Golgi vesicle-mediated transport	1		16,99	0.416929461
Bc1n1p04610.1	Bcemp24	Endoplasmic reticulum	1 protein retention in ER lumen, endoplasmic reticulum to Golgi vesicle-mediated transport	1		16,99	0.416929461
Bc1n1p04620.1		Golgi apparatus		0 NA		8,242	0.637939643
Bc1n1p04650.1		Mitochondrion	0 ribosome biogenesis			9,789	0.634562694
Bc1n1p04740.1	Bcrlr11	Mitochondrion	0 tRNA splicing, via endonucleolytic cleavage and ligation, tRNA processing, phosphorylation			6,922	0.784251554
Bc1n1p04840.1	Bcrlm2	Mitochondrion	0 translation, mitochondrial translation			9,262	0.73117868
Bc1n1p05080.1		Cytoplasm		0 1 NA		5,747	0.737426367
Bc1n1p05080.2		Cytoplasm		0 1 NA		5,747	0.737426367
Bc1n1p05130.1	Bcckb1	Cytoplasm	0 protein phosphorylation, phosphorylation, septum digestion after cytokinesis			21,439	0.68515131
Bc1n1p05160.1	Bcsah1	Cytoplasm	0 one-carbon metabolic process, triglyceride metabolic process			3,618	0.211785184
Bc1n1p05170.1		Cytoplasm	0 formation of cytoplasmic translation initiation complex, translation, translational initiation			18,264	0.681381583
Bc1n1p05210.1	Bcnat1	Cytoplasm		0 NA		19,415	0.734560321
Bc1n1p05220.1		Nucleus	0 regulation of transcription, DNA-templated			11,091	0.862859525
Bc1n1p05570.1	Bcmic26	Mitochondrion	2 cristae formation			7,879	0.608919859
Bc1n1p05580.1	Bccty1	Cytoplasm	0 tyrosyl-tRNA aminoacylation, tRNA aminoacylation for protein translation, translation			15,975	0.69113947
Bc1n1p05610.1	Bcpze2	Cytoplasm	0 proteolysis involved in cellular protein catabolic process			4,014	0.514831316
Bc1n1p05700.1	Bcbwk	Cytoplasm	0 cellular glucose homeostasis, glycolytic process, carbohydrate metabolic process, phosphorylation			21,275	0.670433974
Bc1n1p05710.1	Bcoost1	Endoplasmic reticulum	1 protein glycosylation	1		28,476	0.483279685
Bc1n1p05760.1	Bcmmc4	Cytoplasm	0 DNA replication initiation, DNA replication, DNA duplex unwinding			20	0.404531287
Bc1n1p05870.1	Bcsnf5	Nucleus	0 chromatin remodeling, regulation of transcription, DNA-templated			16,388	0.454677932
Bc1n1p05900.1		Cytoplasm	0 translation			34,611	0.375931095
Bc1n1p05920.1		Cytoplasm	0 translation			11,697	0.878617062
Bc1n1p06020.1	Bcprt5	Cytoplasm	0 protein catabolic process, positive regulation of cellular process			20,698	0.562112298
Bc1n1p06110.2	BcSCH9,BPK2	Cytoplasm	0 protein phosphorylation, phosphorylation, protein phosphorylation, phosphorylation			9,877	0.968729681
Bc1n1p06110.3	BcSCH9,BPK2	Cytoplasm	0 protein phosphorylation, phosphorylation, protein phosphorylation, phosphorylation			9,877	0.968729681
Bc1n1p06110.1	BcSCH9,BPK2	Cytoplasm	0 protein phosphorylation, phosphorylation, protein phosphorylation, phosphorylation			9,877	0.968729681
Bc1n1p06240.1	Bcpqk1	Cytoplasm	0 glycolytic process, phosphorylation			23,37	0.462551985
Bc1n1p06300.1		Peroxisome		0 NA		3,303	0.308211482
Bc1n12p001140.2		Cytoplasm	0 nitrogen compound metabolic process, nitrogen compound metabolic process			4,241	0.867771751
Bc1n12p001140.1		Cytoplasm	0 nitrogen compound metabolic process, nitrogen compound metabolic process			4,241	0.867771751
Bc1n12p00310.1	Bcmrps12	Mitochondrion		0 translation		63,967	0.615036367
Bc1n12p00330.1	Bcpat1	Lysosome/Vacuole	0 deadenylation-dependent decapping of nuclear-transcribed mRNA			23,318	0.525161175

Bcim12p00420.1	Bcemd3	Nucleus	0 protein transport, ribosomal large subunit export from nucleus	8.899	0.889730123
Bcim12p00710.1	Cytoplasm	Peroxisome	0 organonitrogen compound biosynthetic process, cellular biosynthetic process	30.807	0.16890851
Bcim12p00740.1	Peroxisome	Peroxisome	0 obsolete oxidation-reduction process	48.364	0.128627397
Bcim12p00830.1	Mitochondrion	Peroxisome	0 NA	9.087	0.974353689
Bcim12p01020.1	Bcoah	Peroxisome	1 NA	27.805	0.453033036
Bcim12p01040.1	Bcbms1	Nucleus	0 ribosome biogenesis	5.414	0.40750987
Bcim12p01050.2	Peroxisome	Peroxisome	0 NA	9.226	0.602420669
Bcim12p01230.1	Nucleus	Nucleus	0 transcription, DNA-templated, regulation of transcription, DNA-templated	3.012	0.821358884
Bcim12p01300.1	Cytoplasm	Endoplasmic reticulum	0 translation	23.254	0.610349728
Bcim12p01450.1	Endoplasmic reticulum	Nucleus	2 obsolete oxidation-reduction process	11.453	0.859054047
Bcim12p01790.1	Bcspo1	Nucleus	0 NA	10.869	0.84719428
Bcim12p01810.1	Bcdp10	Nucleus	0 rRNA processing, ribosome biogenesis	19.819	0.720035659
Bcim12p01840.1	Endoplasmic reticulum	Endoplasmic reticulum	1 NA	3.169	0.28724684
Bcim12p01960.1	Cytoplasm	Peroxisome	0 antibiotic biosynthetic process	20.809	0.468157603
Bcim12p02000.1	Begcn3	Peroxisome	0 cellular metabolic process, translation, translational initiation	8.082	0.978717888
Bcim12p02040.1	Bcap8	Extracellular	1 0 proteolysis	28.374	0.485385371
Bcim12p02450.1	Bcbio2	Mitochondrion	0 biotin biosynthetic process	18.255	0.742738075
Bcim12p02600.1	Peroxisome	Peroxisome	0 NA	16.304	0.596334155
Bcim12p02640.1	Bcap11	Golgi apparatus	0 protein transport, intracellular protein transport, vesicle-mediated transport	13.194	0.710542082
Bcim12p02760.1	Bcrpb8	Cytoplasm	0 transcription, DNA-templated, transcription by RNA polymerase I	3.483	0.333842803
Bcim12p02810.1	Golgi apparatus	Golgi apparatus	1 NA	26.108	0.38554125
Bcim12p03150.1	Bcrpn1	Endoplasmic reticulum	0 regulation of protein catabolic process, regulation of catalytic activity	11.287	0.862276375
Bcim12p03180.1	Bccpr1	Endoplasmic reticulum	1 ergosterol biosynthetic process, sterol biosynthetic process, lipid metabolic process	20.541	0.565282593
Bcim12p03270.1	Extracellular	Extracellular	1 0 proteolysis	17.093	0.669053431
Bcim12p03480.1	Bccho2	Endoplasmic reticulum	11 methylation, phospholipid metabolic process, phosphatidylcholine biosynthetic process	16.242	0.454861797
Bcim12p03700.1	Bcnde1	Mitochondrion	1 NADH oxidation	8.978	0.934774036
Bcim12p03770.1	Bcnop53	Nucleus	0 ribosomal large subunit assembly, ribosome biogenesis	46.594	0.243542936
Bcim12p03880.1	Bcpp2Ac	Cytoplasm	0 protein dephosphorylation	10.641	0.882445989
Bcim12p03890.1	Nucleus	Nucleus	0 exocytosis, protein transport	5.802	0.789837294
Bcim12p03900.1	Bctom20	Mitochondrion	1 intracellular protein transport, protein targeting, tRNA import into mitochondrion	16.465	0.795698052
Bcim12p03910.1	Bcdyn1	Cytoplasm	1 microtubule-based movement	3.138	0.454738014
Bcim12p03940.1	Cytoplasm	Mitochondrion	1 protein phosphorylation, protein phosphorylation	27.332	0.188033888
Bcim12p03950.1	Bcmrp19	Mitochondrion	0 translation	32.159	0.41451908
Bcim12p04380.1	Nucleus	Cytoplasm	0 translation, translational elongation, gene expression, cytoplasmic translation	60.005	0.159884715
Bcim12p04450.1	Bccef1	Nucleus	0 RNA splicing, mRNA processing	39.829	0.308617903
Bcim12p04560.1	Bcgst24	Cytoplasm	0 NA	15.388	0.75934814
Bcim12p04650.1	Bcrip1	Mitochondrion	0 electron transport chain, proton transmembrane transport, mitochondrial electron transport	26.156	0.644931581
Bcim12p04660.1	Bctcp1	Cytoplasm	0 protein folding	29.011	0.472379163
Bcim12p04670.1	Cytoplasm	Cytoplasm	0 tRNA aminoacylation for protein translation, poly-tRNA aminoacylation	45.169	0.25552818
Bcim12p04680.1	Bcpkc1	Cytoplasm	0 fungal-type cell wall biogenesis, intracellular signal transduction, protein phosphorylation	10.595	0.815540773

Bcin12p04690.1	Mitochondrion	0 NA	3,355	0.493559932
Bcin12p04860.1	Cytoplasm	0 de novo' UMP biosynthetic process, 'de novo' pyrimidine nucleobase biosynthetic process	7,871	0.607868977
Bcin12p05000.1	Cytoplasm	0 aromatic amino acid family biosynthetic process, chorismate metabolic process	3,891	0.755563845
Bcin12p05100.1	Nucleus	0 mRNA processing, RNA processing, mRNA splicing, via spliceosome	2,386	0.184686551
Bcin12p05190.1	Mitochondrion	0 NA	12,515	0.718155501
Bcin12p05210.1	Mitochondrion	0 malate metabolic process, carboxylic acid metabolic process, tricarboxylic acid cycle	28,647	0.458928571
Bcin12p05290.1	Cytoplasm	0 tRNA aminoacylation, tRNA aminoacylation for protein translation, translation	19,826	0.719845336
Bcin12p05370.1	Cell membrane	6 conidium formation	10,764	0.986241682
Bcin12p05550.1	Cytoplasm	0 cellular amino acid metabolic process, biosynthetic process	4,18	0.386352687
Bcin12p05760.1	Cell membrane	0 signal transduction	10,324	0.907841183
Bcin12p05985.1	Cytoplasm	0 NA	4,011	0.52797814
Bcin12p06020.1	Endoplasmic reticulum	10 proton export across plasma membrane, ion transport	18,849	0.837529309
Bcin12p06180.1	Peroxisome	0 nitrogen compound metabolic process, cyanide catabolic process, cellular process	14,214	0.84533375
Bcin12p06370.1	Endoplasmic reticulum	1 obsolete pathogenesis	8,18	0.915941309
Bcin12p06380.1	Endoplasmic reticulum	1 obsolete pathogenesis	6,06	0.446617529
Bcin12p06400.1	Endoplasmic reticulum	2 obsolete pathogenesis	31,999	0.264156665
Bcin12p06450.1	Mitochondrion	0 translation	3,889	0.227818674
Bcin12p06550.1	NA	0 rRNA processing, nucleic acid phosphodiester bond hydrolysis, ribosomal large subunit assembly	20,218	0.498133007
Bcin12p06740.1	NA	0 DNA replication initiation, DNA replication, DNA duplex unwinding, cell cycle	4,566	0.749801427
Bcin13p00020.1	NA	0 NA	19,851	0.442572259
Bcin13p00120.1	NA	0 NA	6,38	0.522192327
Bcin13p00480.1	Cytoplasm	0 mitotic sister chromatid cohesion, cell division	9,213	0.83888563
Bcin13p00540.1	Nucleus	0 chromatin remodeling	6,43	0.843408857
Bcin13p00550.1	Nucleus	0 NA	50,198	0.21678945
Bcin13p00680.1	Nucleus	0 NA	12,44	0.719770287
Bcin13p00680.2	Nucleus	0 NA	12,44	0.719770287
Bcin13p00700.1	Endoplasmic reticulum	1 NA	63,28	0.145575835
Bcin13p00750.1	Nucleus	0 mRNA splicing, via spliceosome, spliceosomal complex assembly, response to xenobiotic stimulus	9,847	0.580397981
Bcin13p00790.1	Mitochondrion	0 NA	18,222	0.624743733
Bcin13p00830.1	Cytoplasm	0 translation	9,122	0.707852232
Bcin13p00910.1	Mitochondrion	0 mitochondrial translation	13,331	0.874487637
Bcin13p00960.1	Endoplasmic reticulum	1 karyogamy involved in conjugation with cellular fusion,	189,622	0.018603025
Bcin13p00980.1	Cytoplasm	0 regulation of translation, translational elongation, regulation of translation	11,275	0.694913905
Bcin13p00980.2	Cytoplasm	0 regulation of translation, translational elongation, regulation of translation	11,275	0.694913905
Bcin13p01010.1	Peroxisome	0 NA	13,824	0.55510112
Bcin13p01280.1	Mitochondrion	0 translation	12,267	0.761728489
Bcin13p01310.1	Nucleus	0 NA	16,62	0.728973786
Bcin13p01340.2	Cytoplasm	0 protein ubiquitination, protein ubiquitination, protein ubiquitination, protein ubiquitination	9,059	0.962010865
Bcin13p01340.3	Cytoplasm	0 protein ubiquitination, protein ubiquitination, protein ubiquitination, protein ubiquitination	9,056	0.962010865
Bcin13p01340.4	Cytoplasm	0 protein ubiquitination, protein ubiquitination, protein ubiquitination, protein ubiquitination	9,059	0.962010865

Bcin13p01350.1	Mitochondrion	0 electron transport chain	6.022	0.905638603
Bcin13p01390.3	Bcufd4	0 protein ubiquitination, protein ubiquitination, protein ubiquitination	9.701	0.751567748
Bcin13p01390.1	Bcufd4	0 protein ubiquitination, protein ubiquitination, protein ubiquitination	9.701	0.751567748
Bcin13p01450.1	Nucleus	0 NA	22.798	0.624685125
Bcin13p01630.1	Cytoplasm	0 regulation of catalytic activity, positive regulation of mitotic metaphase/anaphase transition	25.599	0.548952225
Bcin13p01650.1	Nucleus	0 NA	5.671	0.936565803
Bcin13p01740.1	Mitochondrion	0 translation	40.572	0.189180548
Bcin13p02240.1	Cytoplasm	0 protein import into nucleus, intracellular protein transport	13.545	0.861858613
Bcin13p02430.1	Cytoplasm	0 NA	8.618	0.666262394
Bcin13p02440.1	Cytoplasm	0 lipid metabolic process, lipid metabolic process	12.326	0.92868988
Bcin13p02620.1	Cytoplasm	0 NA	16.78	0.759647983
Bcin13p02650.1	Cytoplasm	0 protein folding	11.775	0.967793847
Bcin13p02830.1	Nucleus	0 RNA splicing, spliceosomal complex disassembly	23.644	0.588570029
Bcin13p03450.1	Cytoplasm	0 sulfate assimilation	6.473	0.62350276
Bcin13p03600.1	Cytoplasm	0 translation	47.894	0.232881522
Bcin13p03730.1	Cytoplasm	0 NA	23.103	0.468762246
Bcin13p03790.1	Mitochondrion	0 NA	6.59	0.622435129
Bcin13p03850.1	Nucleus	0 NA	8.967	0.880584988
Bcin13p03860.1	Nucleus	0 methylation, RNA methylation, tRNA processing, tRNA nucleoside ribose methylation	32.841	0.253878717
Bcin13p03990.1	Cytoplasm	0 NA	120.324	0.033081579
Bcin13p04000.1	Mitochondrion	0 NA	16.161	0.575958733
Bcin13p04010.1	Mitochondrion	0 NA	10.967	0.949526063
Bcin13p04380.1	Nucleus	0 transcription, DNA-templated	46.812	0.040653122
Bcin13p04390.1	Nucleus	0 mRNA splicing, via spliceosome, mRNA processing, RNA splicing, mRNA cis splicing	12.632	0.870643481
Bcin13p04410.1	Nucleus	0 NA	9.071	0.703936934
Bcin13p04430.1	Peroxisome	0 aromatic amino acid family biosynthetic process, chorismate biosynthetic process	5.029	0.824627885
Bcin13p04540.1	Cytoplasm	0 isoleucyl-tRNA aminoacylation, tRNA aminoacylation for protein translation, translation	8.492	0.657435904
Bcin13p04650.1	Nucleus	0 NA	14.723	0.739538457
Bcin13p04800.1	Nucleus	0 NA	17.719	0.538153196
Bcin13p05220.1	Cytoplasm	0 NA	24.965	0.516790658
Bcin13p05240.1	Nucleus	0 NA	32.446	0.438724659
Bcin13p05370.1	Cytoplasm	0 GDP-mannose biosynthetic process, biosynthetic process	28.944	0.473718232
Bcin13p05530.1	Cytoplasm	0 actin filament organization, Arp2/3 complex-mediated actin nucleation	8.814	0.693861196
Bcin13p05550.1	Nucleus	0 nucleotide-excision repair, regulation of transcription, DNA-templated	14.288	0.538108402
Bcin13p05580.1	Cytoplasm	0 NA	13.021	0.996989594
Bcin13p05610.1	Cytoplasm	0 barbed-end actin filament capping, actin filament organization	16.034	0.702738184
Bcin14p00470.1	Nucleus	0 DNA replication initiation, DNA replication, negative regulation of DNA helicase activity	11.598	0.986838601
Bcin14p00840.1	Mitochondrion	1 NA	13.591	0.830448072
Bcin14p00960.1	Nucleus	0 rRNA processing, ribosome biogenesis	7.274	0.550665072
Bcin14p01030.1	Cytoplasm	0 ethanol oxidation, organic substance metabolic process, small molecule metabolic process	9.629	0.759826303

Bcin14p01230.1				10 phospholipid transport, lipid translocation		7.372	0.841198426
Bcin14p01380.1	Bcaif1	Mitochondrion	0	0 NA		10.84	0.74329737
Bcin14p01590.1	Bcrpb2	Nucleus	0	0 transcription, DNA-templated, transcription by RNA polymerase II		11.959	0.90791468
Bcin14p01710.1		Cytoplasm	0	0 NA		20.02	0.298264742
Bcin14p01740.2		Cytoplasm	0	0 polyamine biosynthetic process, polyamine metabolic process, cellular process		6.04	0.722079208
Bcin14p01800.1	Berf5	Cytoplasm	0	0 DNA replication, DNA strand elongation involved in DNA replication		19.761	0.473510894
Bcin14p01930.1	Bcaps1	Cytoplasm	0	0 protein transport, intracellular protein transport, vesicle-mediated transport, protein transport		69.463	0.125938702
Bcin14p01980.1		Peroxisome	0	0 NA		35.077	0.369168437
Bcin14p02160.1	Bcmrp19	Mitochondrion	0	0 translation		24.302	0.591464211
Bcin14p02240.1		Mitochondrion	1	1 cellular process		20.572	0.246451197
Bcin14p02330.1	Bcrp7	Nucleus	0	0 NA		12.009	0.959946394
Bcin14p02380.1		Plastid	1	1 NA		37.814	0.195641467
Bcin14p02480.1	Bceuv41	Lysosome/Vacuole	0	0 cellular process		9.25	0.731031685
Bcin14p02510.1	Bclcc2	Extracellular	1	0 NA		31.994	0.255412339
Bcin14p02520.1	Bcimp4	Nucleus	0	0 rRNA processing, ribosome biogenesis, ribosomal small subunit biogenesis		4.759	0.321673674
Bcin14p02530.1	Bcnam7	Cytoplasm	0	0 nuclear-transcribed mRNA catabolic process, nonsense-mediated decay		7.309	0.850527709
Bcin14p02580.1		Cytoplasm	0	0 NA		8.817	0.949962022
Bcin14p02650.1		Cytoplasm	0	0 NA		8.883	0.771442654
Bcin14p02680.1		Cytoplasm	0	0 translation		55.943	0.180514694
Bcin14p02720.1	Bcnf1	Mitochondrion	0	0 [2Fe-2S] cluster assembly, iron-sulfur cluster assembly, tRNA wobble uridine modification		8.92	0.798125098
Bcin14p02830.1	Bcrpl3	Cytoplasm	0	0 translation		21.866	0.651663502
Bcin14p02920.1	Bcmrp16	Mitochondrion	0	0 translation, mitochondrial translation		8.452	0.650309662
Bcin14p03010.1	Bcgb1	Nucleus	0	0 invasive growth in response to glucose limitation, positive regulation of protein phosphorylation		13.559	0.99872731
Bcin14p03040.1	Bctb4	Cytoplasm	0	0 microtubule nucleation, microtubule-based process, cytoplasmic microtubule organization		22.207	0.26428875
Bcin14p03100.1	Bcdhp5	Cytoplasm	0	0 mRNA export from nucleus, tRNA export from nucleus, translational termination		14.457	0.857447408
Bcin14p03270.1		Lysosome/Vacuole	5	5 NA		9.476	0.910897
Bcin14p03400.1	Bceuv25	Endoplasmic reticulum	1	1 endoplasmic reticulum to Golgi vesicle-mediated transport		77.296	0.025509694
Bcin14p03460.1		Nucleus	0	0 NA		10.489	0.902930557
Bcin14p03500.1	Bcsu3	Nucleus	0	0 translational initiation, translation, translational initiation, translation		7.532	0.57841852
Bcin14p03500.2	Bcsu3	Nucleus	0	0 translational initiation, translation, translational initiation, translation		7.532	0.57841852
Bcin14p03790.1	Bcdpl1	Mitochondrion	1	1 carboxylic acid metabolic process		14.325	0.926558218
Bcin14p03800.1	Bcmnn11	Golgi apparatus	1	1 glycoprotein metabolic process		22.773	0.439675708
Bcin14p03890.1		Cytoplasm	0	0 phosphorylation, protein phosphorylation		14.694	0.690463917
Bcin14p04100.1		Cytoplasm	0	0 translation		4.351	0.262728377
Bcin14p04120.1		Cytoplasm	0	0 NA		4.896	0.84032742
Bcin14p04140.2	Bcnu2	Nucleus	0	0 intracellular transport, intracellular transport		8.902	0.796631978
Bcin14p04140.1	Bcnu2	Nucleus	0	0 intracellular transport, intracellular transport		8.902	0.796631978
Bcin14p04230.1	Bcrpl5	Cytoplasm	0	0 translation, ribosomal large subunit assembly		49.52	0.226338915
Bcin14p04390.1		Golgi apparatus	1	6 retrograde vesicle-mediated transport, Golgi to endoplasmic reticulum		7.905	0.700036362
Bcin14p04440.1		Mitochondrion	0	0 NA		10.814	0.865913297

Bcim14p04520.1	Cytoplasm	0 retrograde vesicle-mediated transport, Golgi to endoplasmic reticulum, protein transport	27.445	0.361636926
Bcim14p04580.1	Cytoplasm	0 NA	32.302	0.412112581
Bcim14p04590.1	Nucleus	0 NA	34.684	0.374361416
Bcim14p04650.1	Nucleus	0 endoplasmic reticulum to Golgi vesicle-mediated transport, vesicle-mediated transport	7.844	0.88589146
Bcim14p04710.1	Nucleus	0 nuclear-transcribed mRNA catabolic process, mRNA processing	2.231	0.823842789
Bcim14p04790.1	Cytoplasm	0 translation	3.827	0.184251903
Bcim14p04810.1	Mitochondrion	0 NA	65.02	0.014460732
Bcim14p04850.1	Nucleus	0 ribosome biogenesis	4.481	0.338984465
Bcim14p04860.1	Mitochondrion	1 mitochondrial electron transport, ubiquinol to cytochrome c	10.267	0.806155987
Bcim14p04870.1	Mitochondrion	0 mitochondrial inheritance, protein folding, inner mitochondrial membrane organization	51.096	0.210215985
Bcim14p05110.1	Nucleus	0 NA	13.243	0.898561254
Bcim14p05160.1	Plastid	0 translation	15.293	0.789191687
Bcim14p05400.1	Cytoplasm	0 carboxylic acid metabolic process, lysine biosynthetic process via aminoadipic acid	32.315	0.362559601
Bcim15p00140.1	Peroxisome	0 NA	19.372	0.534179692
Bcim15p00190.1	Endoplasmic reticulum	2 NA	3.661	0.28591057
Bcim15p00310.1	Mitochondrion	1 sterol biosynthetic process	9.949	0.794578308
Bcim15p00320.1	Cytoplasm	0 NA	8.54	0.739000989
Bcim15p00360.1	Nucleus	0 ubiquitin-dependent protein catabolic process	46.29	0.245974477
Bcim15p00370.1	Nucleus	0 NA	3.834	0.823519832
Bcim15p00590.1	Cytoplasm	0 NA	4.699	0.563062101
Bcim15p00600.1	Mitochondrion	0 translation	32.402	0.278495693
Bcim15p00670.1	Mitochondrion	0 transmembrane transport, cellular process	13.129	0.509065443
Bcim15p00820.1	Bcalm24	0 NA	7.007	0.504822128
Bcim15p00870.1	Cytoplasm	0 protein folding	20.597	0.893229649
Bcim15p01020.1	Cytoplasm	0 NA	7.949	0.703145697
Bcim15p01020.2	Cytoplasm	0 NA	7.946	0.703145697
Bcim15p01120.1	Mitochondrion	0 ATP metabolic process, proton transmembrane transport	15.493	0.899874104
Bcim15p01180.1	Mitochondrion	0 tricarboxylic acid cycle, electron transport chain, cellular respiration	16.37	0.774283167
Bcim15p01240.1	Nucleus	0 regulation of catalytic activity, negative regulation of exit from mitosis	13.982	0.534961919
Bcim15p01270.1	Nucleus	0 NA	8.234	0.882297026
Bcim15p01290.1	Mitochondrion	0 NA	5.118	0.533944671
Bcim15p01350.1	Endoplasmic reticulum	1 endoplasmic reticulum organization, endoplasmic reticulum membrane fusion	27.689	0.311484544
Bcim15p01380.1	Mitochondrion	0 tricarboxylic acid cycle, succinyl-CoA metabolic process	20.277	0.705234925
Bcim15p01440.1	Nucleus	0 histone modification, transcription elongation from RNA polymerase II promoter	8.439	0.912900834
Bcim15p01490.1	Cell membrane	5 sterol metabolic process	16.05	0.921617252
Bcim15p01500.1	Cytoplasm	0 signal transduction, regulation of catalytic activity, regulation of cellular process	7.298	0.871482418
Bcim15p01550.1	Nucleus	0 ribosomal large subunit assembly, rRNA processing, maturation of LSU-rRNA	4.412	0.28962137
Bcim15p02080.1	Mitochondrion	0 ATP metabolic process, proton transmembrane transport	11.439	0.872175797
Bcim15p02090.1	Cytoplasm	0 glycogen biosynthetic process, carbohydrate metabolic process, glycogen biosynthetic process	7.715	0.871407757
Bcim15p02110.1	Mitochondrion	1 mitochondrial electron transport, cytochrome c to oxygen	4.133	0.299002817

Bcin15p02120.1	Cytoplasm			0 glucose metabolic process, glycolytic process	223.468	0.00097814
Bcin15p02270.1	Cytoplasm			0 glycogen biosynthetic process	11.243	0.85944621
Bcin15p02380.1	Extracellular	1		0 proteolysis	8.802	0.88916572
Bcin15p02460.3	Cytoplasm			0 glutamine metabolic process, nitrogen compound metabolic process	11.678	0.90033207
Bcin15p02550.1	Cytoplasm			0 NA	4.955	0.536575134
Bcin15p02610.1	Cytoplasm			0 mitotic cytokinesis, septin ring assembly, maintenance of cell polarity	41.881	0.286505843
Bcin15p02620.1	Nucleus			0 rRNA processing	8.148	0.743625595
Bcin15p02700.1	Nucleus			0 nucleotide-excision repair, transcription initiation from RNA polymerase II promoter	8.029	0.777972842
Bcin15p02730.1	Mitochondrion			0 NA	3.624	0.832357788
Bcin15p02860.1	Mitochondrion			0 translation	8.802	0.882891459
Bcin15p02890.1	Nucleus			0 mitotic chromosome condensation, cell division, cell cycle, chromosome condensation	5.981	0.543949949
Bcin15p02960.1	Nucleus			0 NA	5.645	0.731081185
Bcin15p02990.1	Cytoplasm			0 DNA replication initiation, DNA replication, DNA duplex unwinding	10.962	0.834541084
Bcin15p03020.1	Nucleus			0 protein phosphorylation, protein phosphorylation	9.057	0.816000482
Bcin15p03350.1	Nucleus			0 RNA phosphodiester bond hydrolysis, endonucleolytic	8.574	0.924579854
Bcin15p03420.1	Endoplasmic reticulum		10	protein O-linked glycosylation, protein glycosylation, protein O-linked mannosylation	15.537	0.877338313
Bcin15p03540.1	Nucleus			0 NA	11.612	0.883378628
Bcin15p03580.1	Cytoplasm			0 protein phosphorylation, stress-activated MAPK cascade, phosphorylation	14.483	0.850459365
Bcin15p03600.1	Cytoplasm			0 ubiquitin-dependent protein catabolic process	5.687	0.473652096
Bcin15p03620.1	Cytoplasm			0 carbohydrate metabolic process	16.365	0.859305025
Bcin15p03900.1	Nucleus			0 NA	8.887	0.887438888
Bcin15p03930.1	Endoplasmic reticulum		4	NA	13.096	0.873000567
Bcin15p03980.1	Cytoplasm			0 NA	5.674	0.724488367
Bcin15p04150.1	Mitochondrion			1 'de novo' pyrimidine nucleobase biosynthetic process, 'de novo' UMP biosynthetic process	20.215	0.385487693
Bcin15p04200.1	Mitochondrion			1 mitochondrial electron transport, ubiquinol to cytochrome c	21.099	0.634765673
Bcin15p04350.2	Endoplasmic reticulum			0 obsolete pathogenesis, obsolete pathogenesis, obsolete pathogenesis	3.877	0.472897488
Bcin15p04370.1	Cytoplasm			0 dephosphorylation	32.714	0.137725638
Bcin15p04420.1	Cytoplasm			0 mitotic actomyosin contractile ring assembly	6.422	0.822513122
Bcin15p04490.1	Cytoplasm			0 formation of cytoplasmic translation initiation complex, cap-dependent translational initiation	29.763	0.457216929
Bcin15p04610.1	Mitochondrion			0 NA	22.272	0.288531184
Bcin15p04630.1	Nucleus			0 NA	26.005	0.362325694
Bcin15p04630.2	Nucleus			0 NA	26.005	0.362325694
Bcin15p04980.1	Cytoplasm			0 protein phosphorylation, phosphorylation, protein phosphorylation, phosphorylation	36.356	0.32594472
Bcin15p04990.1	Nucleus			0 regulation of transcription by RNA polymerase II, regulation of histone acetylation	7.074	0.87580006
Bcin15p05010.2	Mitochondrion			0 translation, translation	8.528	0.85944959
Bcin15p05230.1	Mitochondrion		1	protein import into mitochondrial matrix, protein transport	6.889	0.774414759
Bcin15p05330.1	Mitochondrion			0 cardiolipin biosynthetic process, CDP-diacylglycerol biosynthetic process, lipid metabolic process	8.474	0.875829427
Bcin15p05330.2	Mitochondrion			0 cardiolipin biosynthetic process, CDP-diacylglycerol biosynthetic process, lipid metabolic process	9.474	0.875829427
Bcin15p05380.1	Peroxisome			0 NA	3.052	0.158679668
Bcin15p05550.1	Endoplasmic reticulum		1	fatty acid elongation, lipid metabolic process, fatty acid metabolic process	7.119	0.54428349

Bcin15p05560.1	Cytoplasm		0 nucleocytoplasmic transport	8.044	0.468657055
Bcin15p05610.1	Cytoplasm		0 intracellular protein transport, vesicle-mediated transport, protein transport	9.402	0.780374857
Bcin15p00160.1	Mitochondrion		8 heme A biosynthetic process	9.51	0.91529437
Bcin15p00430.1	Cytoplasm		0 lysyl-tRNA aminoacylation, tRNA aminoacylation for protein translation	30.685	0.442186484
Bcin15p00490.1	Cytoplasm		0 protein phosphorylation, negative regulation of transcription by RNA polymerase II	35.603	0.361702517
Bcin15p00630.1	Cytoplasm		0 gluconeogenesis	14.318	0.857719185
Bcin15p00710.1	Cytoplasm		0 translational termination, nuclear-transcribed mRNA catabolic process	12.257	0.923838749
Bcin15p00820.1	Mitochondrion		6 transmembrane transport	28.219	0.330130101
Bcin15p00870.1	Mitochondrion		1 NA	11.548	0.873248448
Bcin15p00960.1	Cytoplasm		0 NA	7.637	0.743070854
Bcin15p01170.1	Endoplasmic reticulum	1	1 NA	13.616	0.902945523
Bcin15p01350.1	Nucleus		0 translational initiation, translation, formation of cytoplasmic translation initiation complex	20.837	0.684840814
Bcin15p01450.1	Mitochondrion		4 proteolysis	6.841	0.921913674
Bcin15p01530.1	Endoplasmic reticulum		2 NA	22.665	0.439000129
Bcin15p01640.1	Cytoplasm		0 protein folding	22.88	0.620313204
Bcin15p01660.1	Cytoplasm		2 NA	15.961	0.383530789
Bcin15p01970.1	Endoplasmic reticulum		16 GPI anchor biosynthetic process	23.009	0.464918475
Bcin15p01990.1	Cytoplasm		0 cell wall biogenesis	12.626	0.495746349
Bcin15p02020.1	Cytoplasm		0 NA	22.022	0.646653555
Bcin15p02280.1	Nucleus		0 NA	6.795	0.744910805
Bcin15p02310.1	Nucleus		0 DNA replication, DNA biosynthetic process	6.728	0.737671273
Bcin15p02360.1	Cytoplasm		0 NA	40.987	0.087948749
Bcin15p03080.2	Nucleus		0 NA	6.409	0.828791954
Bcin15p03080.5	Nucleus		0 NA	6.409	0.828791954
Bcin15p03080.3	Nucleus		0 NA	6.409	0.828791954
Bcin15p03080.1	Nucleus		0 NA	6.409	0.828791954
Bcin15p03080.6	Nucleus		0 NA	6.409	0.828791954
Bcin15p03130.1	Cytoplasm		0 cytoplasmic translation, positive regulation of cellular response to amino acid starvation	9.837	0.62612708
Bcin15p03280.1	Golgi apparatus		9 phospholipid transport, lipid translocation	7.554	0.886980288
Bcin15p03390.1	Nucleus		0 NA	42.96	0.104188974
Bcin15p03490.1	Nucleus		0 transcription initiation from RNA polymerase II promoter, regulation of transcription	7.41	0.638286792
Bcin15p03500.1	Peroxisome		0 cysteine biosynthetic process from serine, cysteine biosynthetic process via cystathionine	18.823	0.598470845
Bcin15p03660.1	Nucleus		0 SRP-dependent cotranslational protein targeting to membrane	24.376	0.579486258
Bcin15p03720.1	Mitochondrion		0 translation	31.914	0.332388877
Bcin15p03930.1	Cytoplasm		0 NA	16.726	0.411356736
Bcin15p04240.1	Mitochondrion		0 translation	18.659	0.763042268
Bcin15p04320.1	Nucleus		0 mRNA transport, mRNA cis splicing, via spliceosome, RNA metabolic process	4.177	0.421578776
Bcin15p04330.2	Cytoplasm		0 protein phosphorylation, protein phosphorylation, SREBP signaling pathway	14.789	0.935746431
Bcin15p04340.1	Mitochondrion		0 protein import into mitochondrial matrix, transmembrane transport, protein transport	10.565	0.726212974
Bcin15p04350.2	Cytoplasm		0 fructose 2,6-bisphosphate metabolic process, fructose metabolic process	5.941	0.611838551

Bcin16p04640.2	Bcfdh1	Mitochondrion			0 formate catabolic process, formate catabolic process	25.265	0.35578799
Bcin16p04640.1	Bcfdh1	Mitochondrion			0 formate catabolic process, formate catabolic process	25.265	0.35578799
Bcin16p04730.1	Bcser1	Cytoplasm			0 L-serine biosynthetic process, serine family amino acid biosynthetic process	7.94	0.613276572
Bcin16p04750.1		Nucleus			0 NA	73.889	0.109131599
Bcin16p04800.8		Cytoplasm			0 malate metabolic process, carboxylic acid metabolic process, tricarboxylic acid cycle	22.333	0.597804777
Bcin16p04800.4		Cytoplasm			0 malate metabolic process, carboxylic acid metabolic process, tricarboxylic acid cycle	22.333	0.597804777
Bcin16p04810.1		Cytoplasm			0 translation	109.625	0.04609841

Chapter 2 – Strategies to isolate fungal secretory vesicles

1	<i>Introduction</i>	189
2	<i>Results</i>	192
2.1	Enrichment of intracellular vesicles by Size-Exclusion Chromatography	192
2.2	Enrichment of intracellular vesicles by density-gradient centrifugation.....	194
2.1	Proposed isolation procedure for the isolation of BcCHSIIIa-GFP SVs	198
3	<i>Discussion</i>	202
3.1	Size exclusion chromatography is not suitable for IVs isolation.....	202
3.2	IVs can be enriched using density-gradient centrifugation	202
3.3	Immuno-isolation is a promising technique for SVs isolation but needs further improvements.....	203
4	<i>Materials and methods</i>	205
4.1	Culture media	205
4.2	Strains and culture conditions.....	205
4.3	Cell fractionation	205
4.4	Size-exclusion chromatography.....	206
4.5	Density gradient.....	206
4.6	SDS-PAGE and western blots	206
4.7	Detection of pectin-hydrolase activity	207
4.8	Transmission electron microscopy.....	207
5	<i>Supplementary data</i>	208
6	<i>References</i>	210

1 Introduction

Secretory vesicles (SVs) have been observed at the hyphal tip of filamentous fungi decades ago. In 1957, Girbardt¹ was the first to name this organized structure “Spitzenkörper” which accumulates secretory vesicles (SVs) at the hyphal tip. SVs play major roles in fungal growth, and fungal nutrition. In filamentous fungi, hyphal tip growth relies on the fusion of SVs with the apical plasma membrane. Apical extension also depends on the correct delivery of fungal cell wall biosynthesis enzymes like the β -1,3 glucan synthase and chitin synthases, which are transported by SVs². SVs likely transport hydrolytic enzymes essential for fungal nutrition. Indeed, the amylase *amyB* was found at the hyphal tip in *Aspergillus oryzae*³ and *Fusarium odoratissimum*⁴.

In many filamentous fungi, the Spitzenkörper is stratified and accumulates two distinct classes of SVs that can be distinguished by their sizes and densities: micro and macro-vesicles. Micro-vesicles, sometimes referred as chitosomes, have a diameter of 30 to 40 nm, a relatively low buoyant density ($d = 1.14$)⁵⁻⁷ and transport chitin synthases in the filamentous fungus *Neurospora crassa*^{2,8,9}. Macro-vesicles, on the other hand, are twice bigger than microvesicles: they have a diameter of 70 to 100 nm¹⁰ and a high buoyant density ($d = 1.24$)⁷. In *N. crassa*, macrovesicles are associated with the glucan synthase FKS1¹¹. Despite their crucial role in fungal biology almost nothing is known about the content of these secretory vesicles.

To our knowledge, there are no report of a SVs proteomic-catalogue in filamentous fungi. One of the aims of the thesis was to investigate different approaches to purify putative secretory vesicles, and obtain the first SVs protein content in a filamentous fungus.

There are only a few techniques reported for the enrichment of secretory vesicles in fungi. In the yeast *Saccharomyces cerevisiae* SVs have been enriched using differential centrifugation followed by either size-exclusion chromatography (SEC) or density gradient centrifugation. When using SEC, SVs are enriched according to their size¹². When performing density gradient centrifugations, SVs are enriched according to their densities¹³. Another technique based on immuno-isolation can be used to isolate SVs¹⁴. This technique is based on the isolation of SVs transporting a specific protein epitope (bait) which is recognized by a specific antibody. Contrary to SEC and density-gradient

centrifugation, this technique has the advantage to be far more specific and can be used to specifically isolate a subset of SVs.

It is important to visualize the differences between IVs and SVs: IVs regroup SVs and other intracellular vesicles (COPI and COPII vesicles, etc.), while SVs represent a subset of intracellular vesicles. For examples, micro- and macro-vesicles are SVs, and SVs are IVs. However, IVs are not necessarily SVs (Fig. 1).

Our first objective was to enrich IVs from *Botrytis cinerea*. To do so, we first tested the two different approaches already described in *S. cerevisiae*: SEC and density gradient centrifugation.

Then, we have proposed a procedure for the isolation of a subset of fungal SVs from IVs. This approach is based on the use of density gradient centrifugation combined with the immuno-isolation of vesicles.

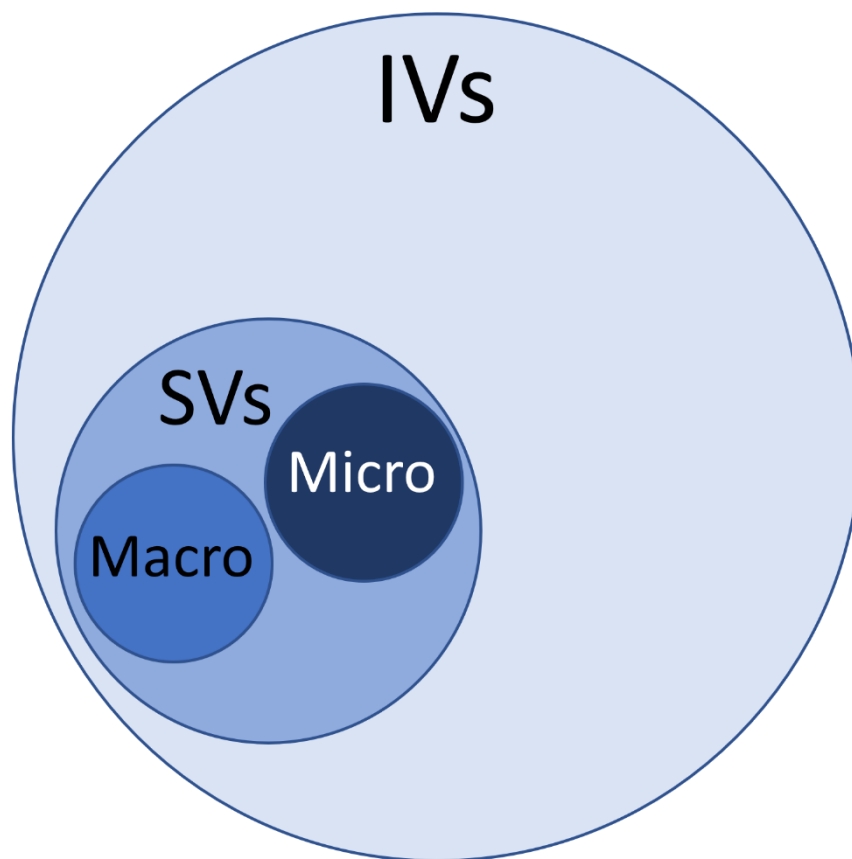


Figure 1 – Schematic representation of intracellular-vesicles in filamentous fungi

Intracellular vesicles (IVs) regroup vesicles of different functions, including secretory vesicles (SVs). In filamentous fungi, macro- and micro-vesicles constitute the majority of secreted vesicles.

2 Results

2.1 Enrichment of intracellular vesicles by Size-Exclusion Chromatography

To enrich fungal IVs from the complex mixture produced by mycelia grinding, we first tried to enrich small IVs (diameter < 55 nm) using size-exclusion chromatography. Mycelia were obtained from 3-days old Potato Dextrose Broth liquid culture (21°C, 110 rpm), inoculated with conidia. After several differential centrifugations to remove cellular debris and organelles such as nucleus and mitochondria, the microsomal pellet (P3) obtained from a 100 000g high-speed centrifugation was resuspended in an osmotic buffer to preserve vesicles integrity. The resuspended pellet was then injected in Sephacryl S-500 HR column connected to the Fast-Protein-Liquid-Chromatography (FPLC) AKTA pure (Fig. 2A). This column was chosen for its theoretical exclusion limit of 55 nm which was appropriate to enrich small IVs. The elution profile (chromatogram) of free-proteins and proteins transported by vesicles was detected using a 280 nm UV detector. Three independent experiments were performed, and a similar elution profile was obtained for each experiment (Fig 2B). Indeed, the chromatogram was characterized by two peaks. The first peak (pA) had a retention volume of $V_r(pA) = 39.81 \pm 0.12$ mL (Fig. 2C), and corresponded to the dead volume of the column. Therefore, particles obtained from pA fractions did not interact with the Sephacryl matrix. The second peak (pB) was characterized by a retention volume $V_r(pB) = 56.94 \pm 0.67$ mL. Particles obtained in this fraction interacted with the matrix and were therefore eluted after pA particles. Particles obtained in pB fractions were characterized with a retention factor of $K_r(pB) = (V_r(pB) - V_r(pA)) / V_r(pA) = 0.43 \pm 0.02$. These results suggest that the SEC-method is very reproducible.

To determine if pA and pB fractions contained vesicles, we performed electron microscopy on the collected samples. The pA fraction contained numerous membranes particles which were very uneven in form and shape. A few particles resembling α -glycogen particles¹⁵ could also be observed in transmission-electron micrographs (TEM) (Fig. 2D). On the other hand, particles collected in the pB fraction, which resembled β -glycogen particles¹⁶ had a very uniform shape and size (Fig. 2D). The presence of glycogen in these fractions was confirmed using a lugol test: when applying lugol on the fractions, the lugol solution turned brown (data not shown).

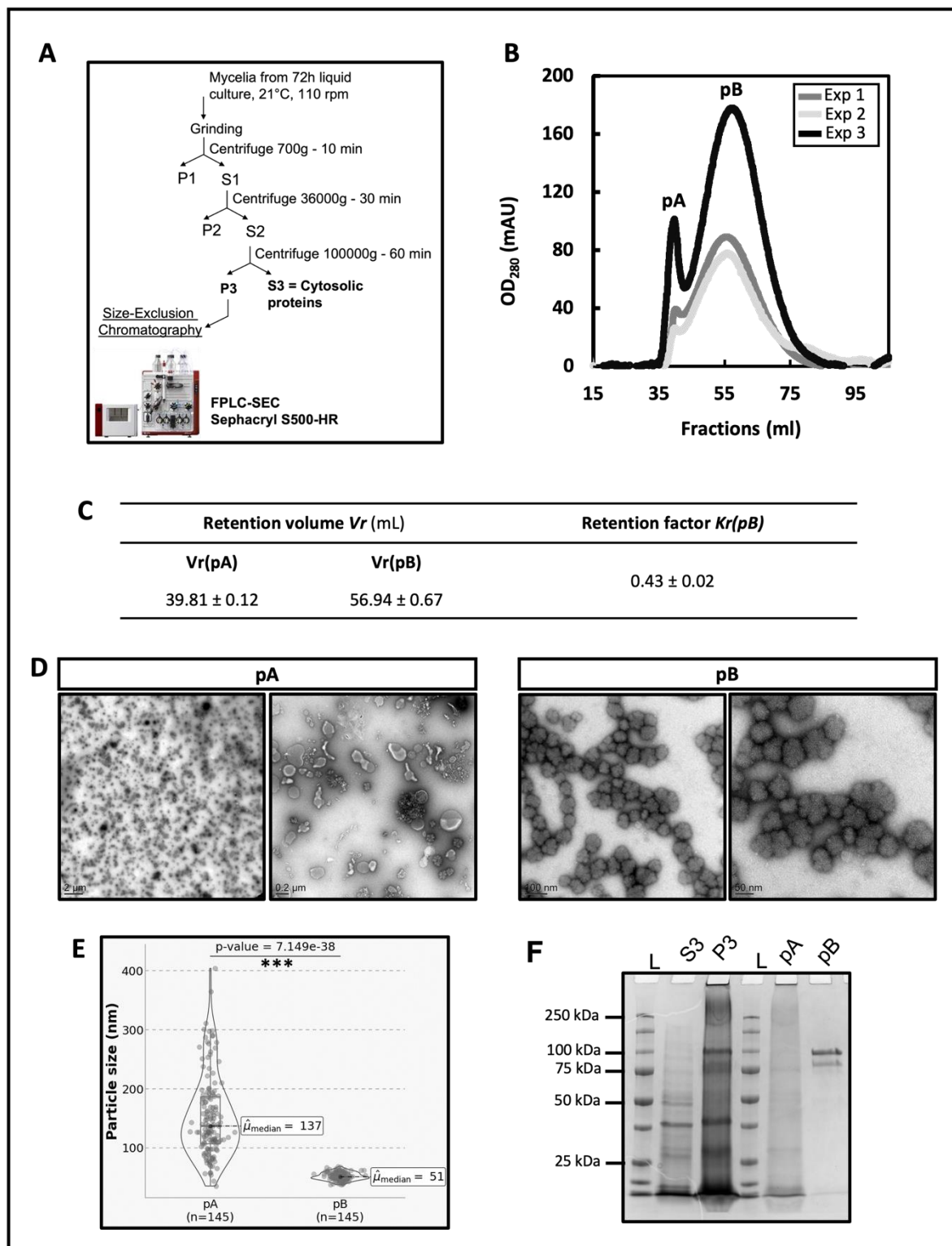


Figure 2 – Enrichment of intracellular vesicles by Size Exclusion Chromatography

(A) Size exclusion-chromatography (SEC) procedure for the enrichment of intracellular vesicles. **(B)** The protein elution profile shows two peaks (pA and pB), based on three independent experiments. pA particles are first eluted because their diameter is too large? to interact with the internal matrix, while smaller pB particles interact with the matrix and are later eluted. **(C)** Table showing retention volume V_r and the retention factor K_r . $V_r(pA)$ corresponds to the column void volume. pB particles are associated with a mean retention factor of 0.43. **(D)** Electron micrographs of SEC isolated pA and pB particles. **(E)** Particles diameter from both fraction: pA and pB. pA particles have a median diameter of 137 nm while the median diameter of pB particles is 51 nm. Student T-test, *** p -value < 0.001. **(F)** Protein profile profile of fractions from: 100 000xg supernatant (S3) and pellet (P3) and SEC peaks pA and pB.

Next, we measured particles diameter from TEM pictures using ImageJ software to determine if the column had indeed an exclusion limit of 55 nm. Particles obtained from the pA fraction had a median diameter of 137 nm (Fig. 2E) but the diameter of enriched particles was extremely irregular. Indeed, some particles had a diameter as high as 400 nm while others were rather small (58 nm). On the contrary, particles from pB fraction displayed a very regular diameter, with a median diameter of 51 nm.

These observations confirm the predicted exclusion limit (55 nm) of the Sephacryl S-500 HR column. This result also supports, the idea that this column can be used to enrich vesicles with a diameter smaller than 55 nm.

At the same time, the protein content of the different fractions were isolated was investigated using SDS-PAGE. The microsomal pellet P3 displayed a high number of proteins (Fig. 2F). Most of the proteins enriched in the microsomal pellet were not found in the cytosol fraction (S3), suggesting that the microsomal pellet was not contaminated with a high number of cytosolic proteins. Among pA and pB fractions isolated after SEC, pA had a greater diversity of proteins when compared to the pB fraction. Indeed, two proteins were mainly detected in the pB fraction. This low diversity of proteins together with the morphological aspects of pB particles, suggest that pB fraction was only made of α -glycogen particles. Thus, the SEC-method failed to enrich a specific subset of IVs from ground mycelia of *Botrytis cinerea*.

2.2 Enrichment of intracellular vesicles by density-gradient centrifugation

In a second time, we tried to enrich IVs using another technology based on density gradient centrifugation. Considering the literature, the isolation of synaptic vesicles¹⁷ or secretory lysosomes from lymphocytes¹⁸ was based on the use of iodixanol gradients. We adapted this protocol to the fungal material. The microsomal pellet (P3) obtained by cell fractionation was then deposited in the bottom of an iodixanol gradient (5%, 16%, 25%, 25% and 50% of iodixanol – equal volumes), and centrifuged for an hour at +4°C (Fig. 3A). Clear interphases could be observed on the iodixanol gradient after high-speed centrifugation (100 000g) (Fig. 3B). Thicker interphases were observed for the 16/25% iodixanol gradient interphase (I16/25%) and the I25/50% interphase, which corresponded to particles with the following densities: 1.12 to 1.16 for I16/25%, and 1.16 to 1.27 for

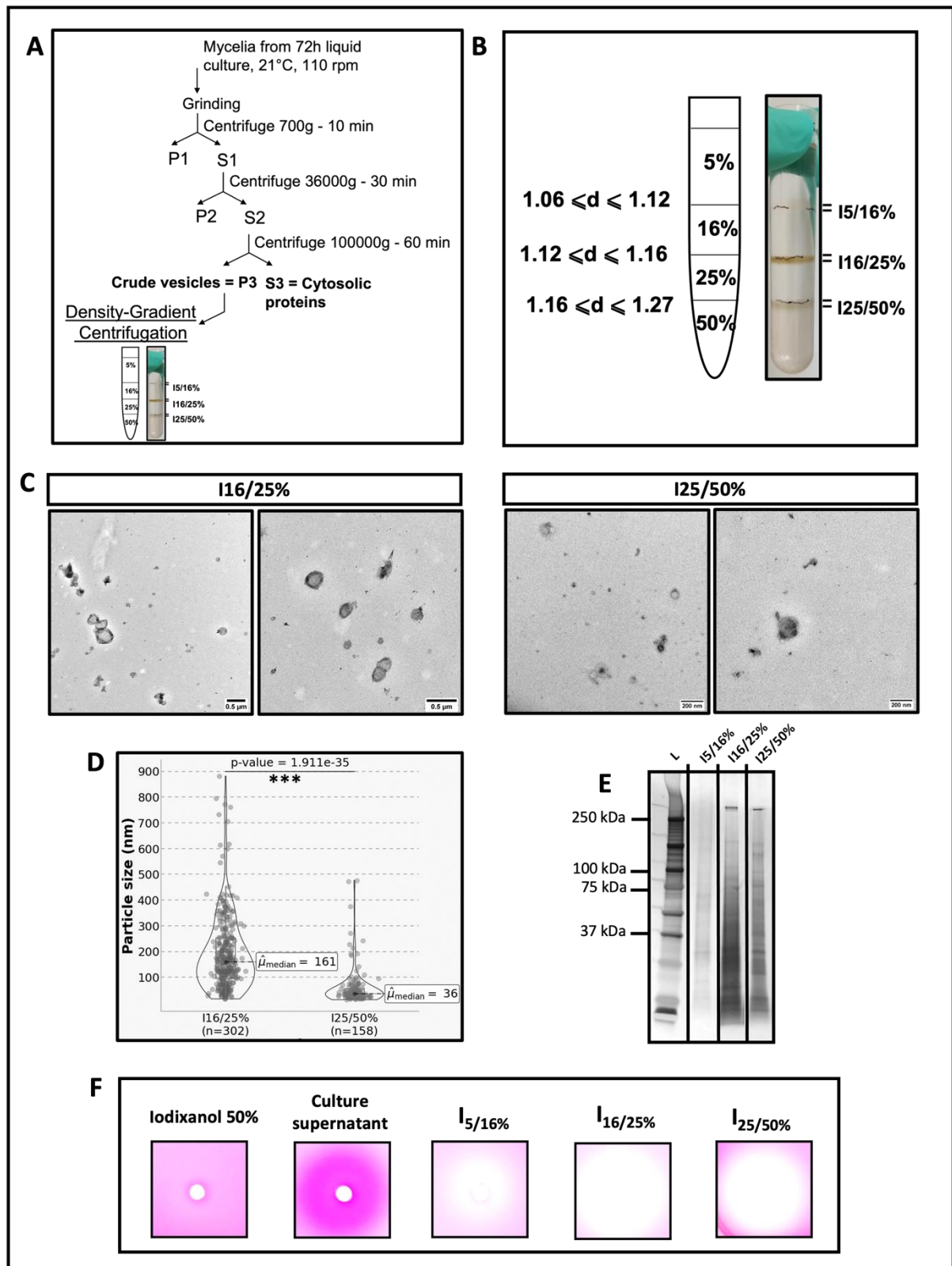


Figure 3 – Enrichment of intracellular vesicles by density gradient centrifugation

(A) Density-gradient centrifugation (DC) procedure for the enrichment of intracellular vesicles. (B) Intracellular vesicles were enriched using a 5%, 16%, 25%, and 50% discontinuous iodixanol gradient. (C) Electron micrographs of DC-enriched intracellular vesicles from the 16-25% interphase ($I_{16/25\%}$) and the 25-50% interphase ($I_{25/50\%}$). (D) Particles diameter of vesicles from $I_{16/25\%}$ and $I_{25/50\%}$ interphases. Median diameter of $I_{16/25\%}$ vesicles: 160 nm; $I_{25/50\%}$ vesicles: 36 nm. (E) Protein profile of fractions from: $I_{5/16\%}$, $I_{16/25\%}$ and $I_{25/50\%}$ interphases. (F) Presence of pectinase (white halo) and pectin-methyl esterase (pink halo) in DC-fractions was detected with radial gel diffusion.

I25/50%. This result suggested that the gradient was kept discontinuous during the high-speed centrifugation and produced interphases with concentrated particles.

To determine if the interphases contained IVs, we observed interphases I16/25% and I25/50% using a transmission electron microscope. Interphase I5/16% was not observed because no intracellular vesicles are known to have a density ranging from 1.06 to 1.12. Interphase I16/25% contained vesicles, heterogenous in size (Fig. 3C). Interphase I25/50% also contained vesicles, but they seemed much more uniform in size (Fig. 3C and 3D). Thus, our observations demonstrate that the density-gradient is suitable for the isolation of IVs.

Next, we wanted to know if the interphases were enriched in vesicles of a particular size. To do so, we measured vesicles diameter with ImageJ. The median vesicle diameter found in Interphase I16/25% was 161 nm and varied greatly between 40 nm and 800 nm (Fig. 3D). On the other hand, vesicles from the I25/50% interphase were a lot smaller (median diameter of 36 nm), and more homogenous in size. These results indicate that the density-gradient method can be used to isolate IVs and enrich a subpopulation of small IVs (36 nm) but with high densities ($1.16 \leq d \leq 1.27$).

To investigate the protein content of the vesicles enriched in I16/25% and I25/50% interphases, samples were denatured and loaded on a polyacrylamide-gel. Interphase I5/16% accumulated a rather small numbers of proteins when compared to the migration profile obtained for I16/25% and I25/50% interphases (Fig. 3). Moreover, only a fraction of proteins found in the I25/50% interphase was also detected in the I16/25% interphase. Thus, this result suggests that the density-gradient method can be used to enrich different subsets of IVs, which differ in size and densities and might also differ in protein content. Performing a proteomic catalogue on the different interphases could confirm these preliminary results.

Next, we determined if some of the enriched IVs transported hydrolytic enzymes. To do so, we checked the presence of pectin-hydrolase and pectin-methyl esterase, two easily detectable enzymatic activities. We deposited the culture medium in which the mycelia had grown, and samples from each interphase on pectin-agar plates to detect the activities of secreted pectin-hydrolase and pectin-methyl esterase. Pectin-hydrolase (white halo) was detected in each interphase, and a stronger activity was observed in the I16/25%.

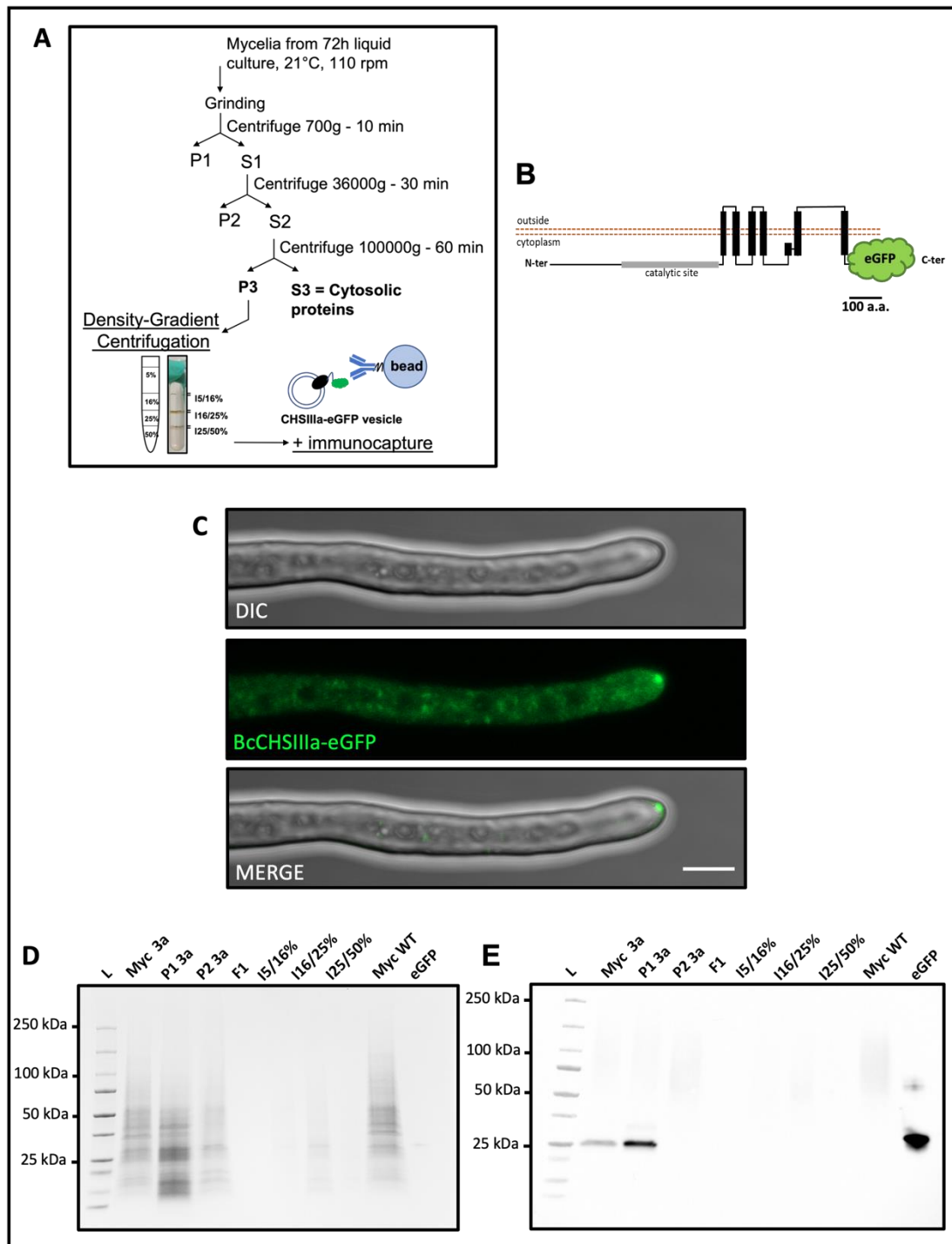


Figure 4 – Purification of BcCHSIIIa vesicles

(A) Purification strategy of BcCHSIIIa-vesicles **(B)** Prediction of the topology of the chimeric Class III Chitin synthase BcCHSIIIa-eGFP. **(C)** Subcellular localization of BcCHSIIIa-eGFP. Images are maximum intensity projections from z-stacks. DIC = Differential Interference Contrast; Scale bar = 5 μ m. BcCHSIIIa-eGFP vesicles were purified using the previously described discontinuous gradient method. **(D)** Protein profile of the crude mycelium extract (Myc 3a), 1000xg and 36000xg pellets (P1 3a and P2 3a), the first fraction from the top of the density gradient (F1), interphases 5-16%, 16-25%, and 25-50% (I_{5-16%}, I_{16-25%}, I_{25-50%}) and the ladder (L). **(E)** Anti-eGFP western-blot. Crude extract from the parental strain (Myc WT) mycelium was used as a negative control. Recombinant eGFP (27 kDa) was used as a positive control.

interphase (Fig. 3F). However, no pectin-methyl esterase activity (fuchsia halo) could be detected in the interphases. This result strongly suggests that the enriched IVs transport secreted hydrolytic enzymes such as pectin-hydrolases and that some of the enriched IVs could be SVs. Overall, our work demonstrates that the density-gradient is a powerful method for the enrichment of IVs.

2.1 Proposed isolation procedure for the isolation of BcCHSIIIa-GFP SVs

The successful enrichment of fungal IVs by density-gradient centrifugation enabled us to focus on an isolation procedure of SVs. Our strategy was to use the green-fluorescent protein GFP fused to a transmembrane protein localized at the Spitzenkörper as a bait for immuno-isolation of secretory vesicles from the enriched IVs. Indeed, the plan was to expose the vesicles enriched in the I16/25% and I25/50% interphases to beads coated with anti-eGFP antibodies (Fig. 4A). The class IIIa chitin synthase CHSIIIa was chosen as a bait to isolate CHSIIIa-eGFP SVs. Indeed, the localization of this transmembrane enzyme has been previously determined in *N. crassa*: the class III chitin synthase localizes at the Spitzenkörper.

To verify that the class III chitin synthase also localizes at the Spitzenkörper in *B. cinerea*, we first had to produce the chimeric protein by fusing eGFP to BcCHSIIIa. Topology prediction predicted that the C-terminus region was localized in the cytoplasm¹⁹. As it was predicted to be extra-vesicular, we fused the eGFP to this region of the protein to use CHSIIIa-eGFP as a bait (Fig. 4B). Then, we introduced the BcCHSIIIa-eGFP genetic cassette at the BcCHSIIIa locus to place the chimeric construct under the control of the native promoter.

Once we obtained the BcCHSIIIa-eGFP mutant, we observed the localization of the chimeric protein using a confocal microscope. BcCHSIIIa-eGFP accumulated at the hyphal tip, in a structure resembling the Spitzenkörper, where SVs accumulate (Fig. 4C). This result comforted the use of BcCHSIIIa as a marker of SVs and its use as a bait for SVs isolation.

Next, we performed enrichment of IVs originating from the BcCHSIIIa-eGFP strain as previously described. Our aim was to detect BcCHSIIIa-eGFP in one or more interphases

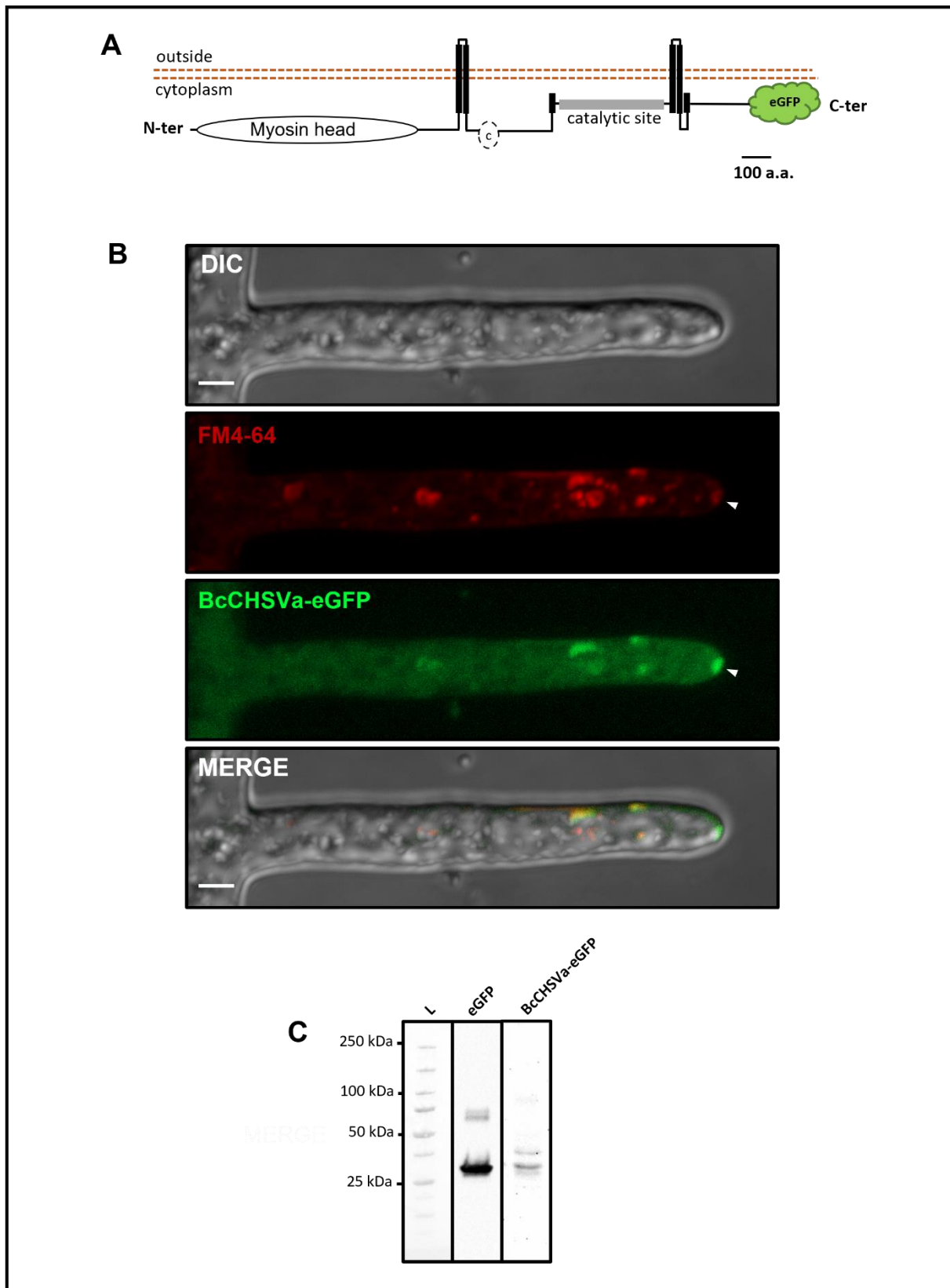


Figure 5 – BcCHSVa-eGFP localizes at the Spitzenkörper but is not detected by western blot
(A) Topology of the chimeric Class Va Chitin synthase BcCHSVa-eGFP; c: cytochrome b5-like helme/steroid binding domain. **(B)** Subcellular localization of endogenously tagged BcCHSVa-eGFP. FM4-64 was used to stain the endomembrane system, including the Spitzenkörper (white arrowhead). Images are maximum intensity projections from z-stacks. DIC = Differential Interference Contrast; Scale bar = 2 μ m. **(C)** Detection of BcCHSVa-eGFP using anti-eGFP antibody. eGFP protein was used as a positive control.

to determine which interphase would be the most appropriate for immuno-isolation. However, no chimeric protein (130 kDa) could be observed when we performed the western-blot (Fig. 4D and 4E). The chimeric protein was not even found in crude mycelia: only cleaved eGFP (27 kDa) was detected in crude mycelia and pellet P1 samples. This result compromised the use of BcCHSIIIa-eGFP as a bait for the immuno-isolation of SVs. Indeed, it is crucial to detect the bait by western-blot to develop the immuno-isolation procedure. Consequently, we tried to use another chitin synthase as a bait for SVs isolation and chose the class Va chitin synthase (BcCHSVa). This protein was chosen because it has fewer transmembrane domains than BcCHSIIIa¹⁹ (4 vs 6), and also localizes at the Spitzenkörper (Fig. 5A, B). However, no chimeric protein (233 kDa) was detected when performing western-blot (Fig. 5C).

In the laboratory, Matthieu Blandenet, a *Ph.D.* student who studied the role of putative polysaccharide synthases in *B. cinerea*, has recently discovered that another transmembrane protein, the GT2 glycosyl-transferase (BcGTa - Bcin04p06040.1 ; 88 kDa – Fig. 6A) fused to 3HA-mNeonGreen also localizes at the Spitzenkörper in *B. cinerea* (Fig. 6B). Thus, we had another protein, smaller than the chitin synthases BcCHSIIIa and BcCHSVa that could potentially be used as a bait to capture secretory vesicles. Therefore, we performed an anti-HA western-blot to determine if we could detect the chimeric protein in crude mycelia. Luckily, we were able to detect the chimeric protein (118 kDa) by anti-HA western-blot on proteins extracted from 24h old mycelium (Fig 6C). Thus, we have finally found a bait for the isolation of SVs. This result enables the development of the immuno-isolation procedure of SVs.

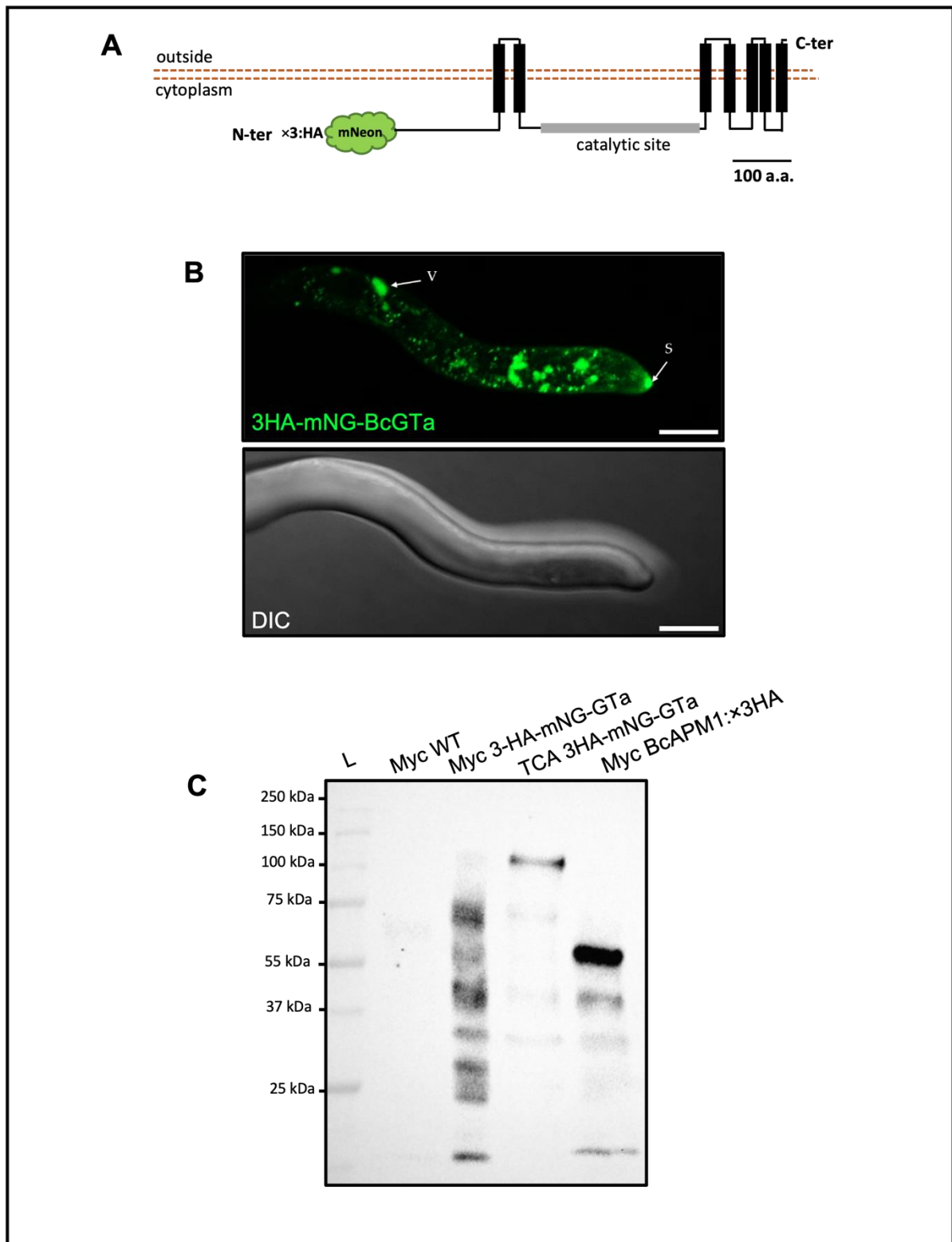


Figure 6 – 3HA-mNG-BcGTa localizes at the Spitzenkörper and is detected by western-blot
(A) Topology of the polysaccharide synthase BcGTa fused to mNeon-Green fluorescent protein **(B)** Subcellular localization of 3HA-mNG-BcGTa (S= Spitzenkörper, V = vacuole). Images are maximum intensity projections from z-stacks. DIC = Differential Interference Contrast; Scale bar = 5 μ m. Pictures were taken by Matthieu Blandenet. **(C)** Detection of 3HA-mNG-BcGTa (118 kDa) using anti-HA antibody. The strain expressing the BcAPM1:x3HA protein (55 kDa) was used as a positive control. Crude mycelium extract from the parental strain (Myc WT) was used as a negative control. Proteins precipitated with trichloroacetic acid (TCA 3HA-mNG-Gta). Ladder (L).

3 Discussion

Fungal SVs are crucial for fungal growth, nutrition, and virulence. However, there is currently no proteomic-catalogue available for SVs in filamentous fungi. Here, we report for the first time in *Botrytis cinerea*, an exploration of the different methods used to enrich IVs and isolate SVs.

3.1 Size exclusion chromatography is not suitable for IVs isolation

To enrich fungal IVs, we first tried size-exclusion chromatography. SEC is a method of choice for the isolation of extracellular vesicles (EVs). This method is fast, it removes protein contaminants, and maintains vesicle structure and content²⁰. Moreover, SEC has recently been used in the plant-pathogen *Fusarium oxysporum* to isolate EVs with great success²¹. When performing SEC in the case of IVs of *B. cinerea*, we obtained two fractions. The first one, as expected, contained contaminants (microsomes, debris...) and these particles were too large in size to enter the matrix pores. On the other hand, the second one which should have enriched small vesicles (< 55 nm) did not. Indeed, no IVs with a diameter smaller than 55 nm could be observed when performing electron microscopy. We first thought that the TEM grids were covered with β -glycogen, hiding IVs. However, only two proteins, likely glycogen-related proteins (dimer of glycogenin isoform-1 78 kDa; dimer of glycogenin isoform-2 110 kDa) were found when we performed SDS-PAGE on this fraction. We could have tried to remove glycogen particles using amylase, but very few proteins were detected using SDS-PAGE, even after long exposition during silver staining. In the yeast *S. cerevisiae*, the Sephacryl S-1000 column, with a larger exclusion limit (400 nm), has been used successfully to enrich IVs²², the authors did not mention any problem related to glycogen particles. Thus, the glycogen issue might be specific to our model *Botrytis cinerea*. This result is not surprising as it has been already described that *B. cinerea* can contain glycogen²³. Therefore, we explored another method to enrich IVs from *Botrytis cinerea*.

3.2 IVs can be enriched using density-gradient centrifugation

Density-gradient centrifugation is a promising technique for IVs isolation. We have used a discontinuous iodixanol gradient centrifugation method to enrich vesicles of specific densities. The idea was to enrich vesicles with low-buoyant densities ($1.12 \leq d \leq 1.16$) in one fraction (interphase 16/25%), and enrich vesicles with high-densities ($1.16 \leq d \leq 1.27$)

in the fraction corresponding to the 25/50% interphase. Indeed, IVs could be found in these two fractions observed with an electron microscope. Thus, the density gradient method is suitable for IVs enrichment in *Botrytis cinerea*. This technique enabled enrichment of a subset of IVs characterized with a small diameter (36 nm) in the interphase I25/50%. Isolated IVs from this interphase have the size of chitosomes^{5,7,24}. However, the predicted density ($1.16 \leq d \leq 1.27$) is more similar to the density described for macrovesicles (70 to 100 nm) in *Neurospora crassa*⁷. This interesting finding may suggest that IVs physical properties might differ in *Botrytis cinerea*. In this fungus, small IVs have high densities, while larger IVs have low densities. The high densities found in enriched small IVs may suggest that they carry more protein cargos than the larger. Fortunately, pectin-hydrolase, an enzyme secreted by *Botrytis cinerea*, was detected in the enriched IVs. This result strongly suggests that secretory vesicles might be found among the enriched IVs. This method, however, is not sufficient to isolate SVs. Indeed, vesicles trafficking between the endoplasmic reticulum and the Golgi apparatus like COPI and COPII vesicles, could also be enriched in IVs interphases using this technique. Therefore, density-gradient centrifugation can be considered as an interesting technique to enrich IVs before performing SVs isolation.

3.3 Immuno-isolation is a promising technique for SVs isolation but needs further improvements

Contrary to SEC or density-gradient centrifugation-based procedures, immuno-isolation is a technique that can be used to isolate vesicles transporting specific protein cargos. The isolation of synaptic vesicles by immuno-isolation can yield exceptional purity²⁵. In fungi, the technique was developed in 1992 to isolate SVs transporting the Guanine nucleotide exchange factor (GEF) for ADP ribosylation factor: Sec7p in *S. cerevisiae*¹⁴. In 2009, researchers from Simons Lab have developed a novel immunoisolation procedure for the isolation of specific subpopulations of post-Golgi secretory vesicles in the yeast^{26,27}. We aimed at reproducing a similar technique in *B. cinerea*, using a different bait.

In our case, we first had to select transmembrane proteins transported by secretory vesicles. We have tried to use two distinct chitin synthases: BcCHSIIIa and BcCHSVa as a bait. Indeed, these proteins localize at the Spitzenkörper in *Neurospora crassa*⁹ and *Aspergillus nidulans*²⁸. Even if we have confirmed that they are also localized at the Spitzenkörper in *B. cinerea*, we encountered several technical issues which hampered the development of the immune-isolation procedure. Indeed, we were not able to detect these

large chimeric proteins by western-blot. This is a major technological lock to develop immuno-isolation. To overcome this difficulty, different parameters were tested: different membranes (PVDF), trichloro-acid protein precipitation, and low temperature heating (37°C). We obtained no convincing result. According to Kaur and Bachhawat²⁹, performing western-blot on membrane proteins has always remained challenging. Fortunately, we have finally found, a potential bait: the glycosyl transferase BcGTa (88 kDa), which is detectable by western-blot. Considering the methodology developed by Simon's Lab^{26,27}, a TEV protease cleavage site between the bait and eGFP or mNeonGreen will be introduced to provide a greater specificity during the elution of immunisolated vesicles. Finally, as proposed by Adrien Hamandjian, it would also be interesting to test the v-SNARE BcSnc (Bcin09p02090.1) as bait to isolate a broad range of secretory vesicles. This work will soon be continued in the lab.

Using gradient-density centrifugation, we developed a methodology to enrich several populations of IVs in *B. cinerea*. This approach will be also performed in the case of AP-1 and clathrin down-expressing strains to perform proteomic along with IVs morphological studies and identify the vesicles and protein cargos undergoing the clathrin/AP-1 pathway. The isolation of secretory vesicles in these different strains will complete the characterization of the mutants and precise the importance of the clathrin machinery in the secretion process in *B. cinerea*.

4 Materials and methods

4.1 Culture media

Four culture media were used: (1) PDB1/4: potato dextrose broth diluted to the fourth. (2) LB: 10g.L⁻¹ bactopectone, NaCl 10 g.L⁻¹, 5g.L⁻¹ yeast extract. (3) LB-NaCl: LB: 10g.L⁻¹ bactopectone, 5g.L⁻¹ yeast extract. (4) Tanaka-N70 [derived from Tanaka-B medium (Ou, 1985)]: agar 15 g.L⁻¹, glucose 10 g.L⁻¹, yeast extract 2 g.L⁻¹, NaNO₃ 2 g.L⁻¹, KH₂PO₄ 2 g.L⁻¹, MgSO₄·7H₂O, 500 mg.L⁻¹, CaCl₂·2H₂O, 100 mg.L⁻¹, FeSO₄·7H₂O 4 mg.L⁻¹, microelements as in Tanaka-B, nourseothricin 70 µg.mL⁻¹, pH 5.5.

4.2 Strains and culture conditions

Botrytis cinerea strain B05.10 [teleomorph *Botryotinia fuckeliana* (de Bary) Whetzel] was used as for all experiments unless otherwise stated. Conidia were collected after 14 days of culture on Malt Sporulation medium at 21°C under near-UV light. Spores were suspended in water and then counted using Thoma cell counting chambers and stored on ice before use or suspended in glycerol (20%) for conservation at -80°C.

For submerged liquid cultures, conidia were inoculated (2.10⁵ conidia.ml⁻¹) in PDB1/4 for 72h, at 21°C, under agitation (110 rpm).

For BcCHSIIIa-eGFP mutant construction, see Chapter 1. eGFP was fused to the C-terminal end of BcCHSVa using a gene replacement strategy (Fig. S1A). The genetic cassette *Bcchs5a3'cds-egfp-tniaD-nat^R-Bcchs5a3'UTR-term* was amplified from the pCR4Blunt-TOPO-CHS5a-GFP plasmid using primers P1 and P2 (Table S1). *nat^R* includes the *nat1* gene placed under the control of the *OliC* promoter and confers resistance to nourseothricin. Primers P1 and P2 were flanked with 21 bp overlap sequences for IVA cloning in the *p7* vector to produce *p7-BcCHSVa-GFP*. Plasmids were collected from *E. coli*, screened by restriction enzyme digestion (*EcoRI*, 37°C) and then verified by sequencing. *A. tumefaciens* transformed with *p7-BcCHSVa-GFP* vector were used for *AtMT* of the parental strain B05.10 to produce *BcCHSVa-GFP*. *B. cinerea* transformants were selected using nourseothricin (70 µg.ml⁻¹). Homologous recombination was detected by diagnostic PCR on nourseothricin resistant transformants using primer pairs S1/S2 and S3/S4.

4.3 Cell fractionation

Three-days-old mycelia from submerged cultures were first filtered using a 100 µm Nylon cloth. All following steps were performed at +4°C unless otherwise stated. Mycelia was

ground by either a bead beater (beads – 1 mm diameter) or by a mortar and pestle under liquid nitrogen. Vesicle buffer (Sigma 7-9 50mM pH 7.4, Sorbitol 1M, NaCl 150 mM, EDTA 10 mM, DTT 1mM) was then added to ground mycelia. Ground mycelia suspension was subjected to several centrifugation steps to remove major contaminants. A 700g spin for 10 min generated pellet P1 and supernatant S1. S1 was centrifuged at 36 000g for 30 min to remove mitochondrion, and generated pellet P2 and supernatant S2. S2 was in turn centrifuged at 100 000g for 1h to generate P3 and S3. P3 corresponded to a mix of intracellular vesicles and microsomes, while S3 contained the cytosol. P3 was overlaid by 1 ml of vesicle buffer and resuspended for downstream processes (Fig. 2A).

4.4 Size-exclusion chromatography

The column HiPrep 16/60 Sephacryl S-500 HR, (dimensions 16x600 mm) was chosen for its exclusion diameter of 55 nm. The column was connected to a Pure Fast Protein Liquid Chromatography system (AKTA). For column equilibration, vesicle buffer was used at a flow rate of 0.5 ml⁻¹.min. Two column volumes were used for column equilibration. Then, a volume of 1 mL of the P3 pellet resuspended in vesicle buffer obtained from cellular fractionation was loaded in the FPLC Chromatography system at a flow rate of 0.5 ml⁻¹.min. Fractions of 1 mL were collected in 48-well deep plates. OD₂₈₀ was recorded for each fraction to establish the protein elution profile.

4.5 Density gradient

Vesicles were fractionated using a discontinuous gradient of OptiPrep™ (D1556 Sigma): 5%, 16%, 25% solutions were prepared in suspension medium 1 (12.25% w/v sorbitol, 1 mM EDTA, 10 mM Tris-HCl, pH 7.4 – 750 mOsm) and the 50% solution was prepared in suspension medium 2 (17.5% w/v sorbitol, 1 mM EDTA, 10 mM Tris-HCl, pH 7.4 – 750 mOsm). Resuspended vesicles were loaded from the bottom with a (1.2 mm) needle and subjected to centrifugation, 100 000g, 1h at +4°C. Fractions of 0.5 mL and 1 mL were collected from the top.

4.6 SDS-PAGE and western blots

Collected fractions were boiled in Laemmli 4X buffer with 8M urea for 8 min at 80°C, and then centrifuged at 18 000g for 10 min at +4°C. Supernatants were loaded in either 10-15% in tris-glycine or tris-acetate polyacrylamide gels (BioRad). Gels were colored using Pierce™ Silver Stain kit (ThermoFisher) or subjected to western-blot. For western-blotting, the primary anti-GFP antibody (abcam ab183734) was used at 1:20 000 in Tris-Buffer Tween 20 0,1%. The secondary antibody (Sigma H0545) was used at 1:80 000.

Protein of interest was detected using the Clarity™ Western ECL revelation kit (BioRad) and ChemiDoc (BioRad)

4.7 Detection of pectin-hydrolase activity

Pectin hydrolases and pectin-methyl-esterases activities were detected using pectoplates³⁰. Pectoplates were prepared with 0.1% (w/v) of apple pectin (Sigma 76282), 1% (w/v) agarose (Fisher Bioreagents BP160), 12.5 mM citric acid and 50 mM Na₂HPO₄, pH 6.5. The gel was cast into 120 mm square petri dishes (50 mL per plate) and steel cork borer were used to produce 4mm diameter wells. 60 µL of culture supernatant, interphases I5/16%, I16/25% and I25/50% were loaded in each well. Iodixanol 50% was used as negative control. Plates were incubated at 30°C for 24 h, and stained with 0.05% (w/v) Ruthenium red for 30 min. The plates were de-stained by several washes of ultrapure water and then photographed.

4.8 Transmission electron microscopy

A volume of 5 µL of isolated vesicles was deposited on a TEM-Copper-Formvar grid (75 meshes) and left decanted for 30 second. Excess liquid was absorbed with Whatman paper and the grid was flipped over a drop of 2% uranyl acetate (UA) for 30 seconds. UA was removed and the grid was washed with distilled water. The grid was then placed into the chamber of a transmission electron microscope JEOL 1400 Flash at the Centre Technologique des Microstructures – Université Claude Bernard Lyon 1.

5 Supplementary data

Table S1 – Primers used in this study

Name	Sequence 5' – 3'	
P1 CHSVa-GFP-IVA-P7-F	CGAATTCGAGCTCGGTACCCGTCGCTGGATTAACCTCAACCG	P7-CHSVa-eGFP construction
P2 CHSVa-GFP-IVA-P7-R	GTCGACTCTAGAGGATCCCCGTACAGATTTGTATATTCACTCATGCT	
S1 CHSVa-GFP-RFG-F	CTAAAGCATTGAAAGTTTGTGGTAG	Diagnostic PCR
S2 CHSVa-GFP-RFG-R	TATTTTAGACGCAGTTCAATGGCAAA	
S3 <i>nour22</i>	CTTCGTGGTCTCTCGTACTCC	
S4 <i>Chs5aVerifRev</i>	GGGTAGAATAAGCAATCATCTGC	

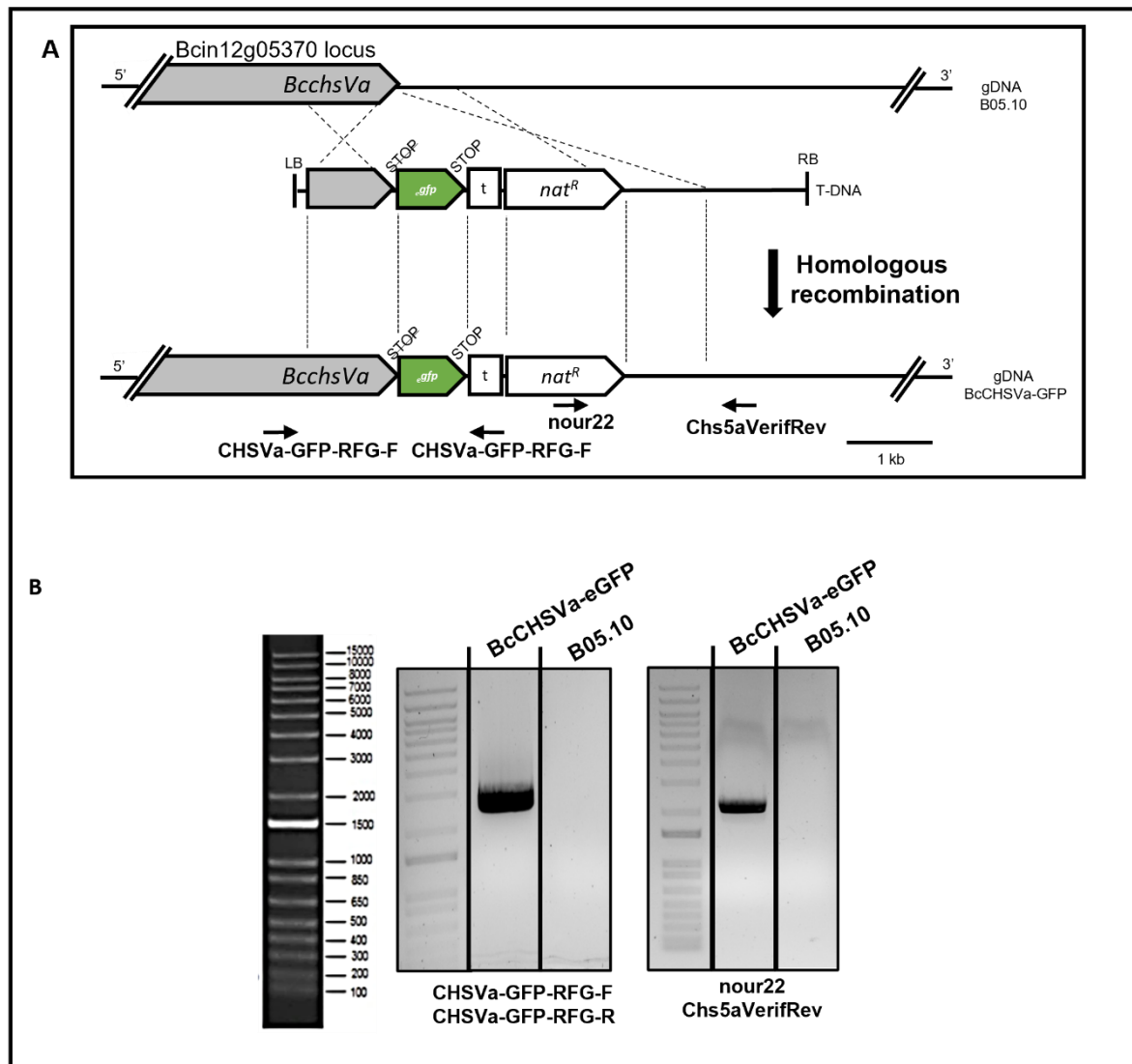


Figure S1 – Molecular characterizations of the BcCHSVa-eGFP strain

(A) Scheme of the gene replacement strategy used to create the BcCHSVa-eGFP strain. Dashed lines: expected double recombination between the *BcchsVa* 5' and 3' flanking regions present in the targeted locus (top) and in the *A. tumefaciens* T-DNA carrying the translationnal-fusion cassette. T: *niaD* terminator, *nat^R*: nourseothricine resistance cassette. (B) Diagnostic PCR of the BcCHSVa-eGFP strain. Primers used are indicated at the bottom of gel images and as arrows in (A).

6 References

1. Girbardt, M. Die Ultrastruktur der Apikalregion von Pilzhyphen. *Protoplasma* **67**, 413–441 (1969).
2. Riquelme, M. & Sánchez-León, E. The Spitzenkörper: a choreographer of fungal growth and morphogenesis. *Current Opinion in Microbiology* **20**, 27–33 (2014).
3. Hayakawa, Y., Ishikawa, E., Shoji, J., Nakano, H. & Kitamoto, K. Septum-directed secretion in the filamentous fungus *Aspergillus oryzae*. *Molecular Microbiology* **81**, 40–55 (2011).
4. Yang, S. *et al.* The exocyst regulates hydrolytic enzyme secretion at hyphal tips and septa in banana Fusarium wilt fungus, *Fusarium odoratissimum*. *Appl Environ Microbiol* (2021) doi:10.1128/AEM.03088-20.
5. Bracker, C., Ruiz-Herrera, J. & Bartnicki-Garcia, S. Structure and transformation of chitin synthase particles (chitosomes) during microfibril synthesis *in vitro*. 4570–4574 (1976).
6. Ruiz-Herrera, J., Lopez-Romero, E. & Bartnicki-García, S. Properties of chitin synthase in isolated chitosomes from yeast cells of *Mucor rouxii*. 3338–3343 (1977).
7. Verdin, J., Bartnicki-Garcia, S. & Riquelme, M. Functional stratification of the Spitzenkörper of *Neurospora crassa*. *Molecular Microbiology* **74**, 1044–1053 (2009).
8. Riquelme, M. *et al.* Spitzenkörper Localization and Intracellular Traffic of Green Fluorescent Protein-Labeled CHS-3 and CHS-6 Chitin Synthases in Living Hyphae of *Neurospora crassa*. *Eukaryot Cell* **6**, 1853–1864 (2007).
9. Sánchez-León, E. *et al.* Traffic of Chitin Synthase 1 (CHS-1) to the Spitzenkörper and Developing Septa in Hyphae of *Neurospora crassa*: Actin Dependence and Evidence of Distinct Microvesicle Populations. *Eukaryotic cell* **10**, 683–95 (2011).
10. Weber, R., Gavin, E., Pitt, W. & Pitt, D. Histochemical and ultrastructural characterization of vacuoles and spherosomes as components of the lytic system in hyphae of the fungus *Botrytis cinerea*. *The Histochemical Journal* **31**, 293–301 (1999).
11. Sánchez-León, E. & Riquelme, M. Live imaging of β -1,3-glucan synthase FKS-1 in *Neurospora crassa* hyphae. *Fungal Genetics and Biology* **82**, 104–107 (2015).
12. Walworth, N. & Novick, P. Purification and characterization of constitutive secretory vesicles from yeast. *The Journal of Cell Biology* **105**, 163–174 (1987).
13. Gurunathan, S., David, D. & Gerst, J. E. Dynamin and clathrin are required for the biogenesis of a distinct class of secretory vesicles in yeast. *EMBO J* **21**, 602–614 (2002).
14. Franzusoff, A., Lauzé, E. & Howell, K. Immuno-isolation of Sec7p-coated transport vesicles from the yeast secretory pathway. *Nature* **6356**, 173–175 (1992).
15. Sullivan, M., Harcourt, B., Xu, P., Forbes, J. & Gilbert, R. Impairment of Liver Glycogen Storage in the db/db Animal Model of Type 2 Diabetes: A Potential Target for Future Therapeutics? *CDT* **16**, 1088–1093 (2015).
16. Sullivan, M. A. *et al.* Nature of α and β Particles in Glycogen Using Molecular Size Distributions. *Biomacromolecules* **11**, 1094–1100 (2010).
17. Yao, J., Kwon, S. E., Gaffaney, J. D., Dunning, F. M. & Chapman, E. R. Uncoupling the roles of synaptotagmin I during endo- and exocytosis of synaptic vesicles. *Nat Neurosci* **15**, 243–249 (2012).
18. Schmidt, H. *et al.* Enrichment and analysis of secretory lysosomes from lymphocyte populations. *BMC Immunol* **10**, 41 (2009).
19. Gonçalves, I. R. *et al.* Genome-wide analyses of chitin synthases identify horizontal gene transfers towards bacteria and allow a robust and unifying classification into fungi. *BMC Evol Biol* **16**, 252 (2016).
20. Monguió-Tortajada, M., Gálvez-Montón, C., Bayes-Genis, A., Roura, S. & Borràs, F. Extracellular vesicle isolation methods: rising impact of size exclusion chromatography. *Cellular and Molecular Life Sciences* 2369–2382 (2019) doi:doi.org/10.1007/s00018-019-03071-y.
21. Garcia-Ceron, D., Dawson, C. S., Faou, P., Bleackley, M. R. & Anderson, M. A. Size-exclusion chromatography allows the isolation of EVs from the filamentous fungal plant

- pathogen *Fusarium oxysporum* f. sp. *vasinfectum* (Fov). *Proteomics* **21**, 2000240 (2021).
22. Harsay, E. & Bretscher, A. Parallel secretory pathways to the cell surface in yeast. *The Journal of Cell Biology* **131**, 297–310 (1995).
 23. Dulermo, T. *et al.* Dynamic carbon transfer during pathogenesis of sunflower by the necrotrophic fungus *Botrytis cinerea* : from plant hexoses to mannitol. *New Phytologist* **183**, 1149–1162 (2009).
 24. Bartnicki-Garcia, S., Bracker, C. E., Reyes, E. & Ruiz-Herrera, J. Isolation of chitosomes from taxonomically diverse fungi and synthesis of chitin microfibrils in Vitro. *Experimental Mycology* **2**, 173–192 (1978).
 25. Takamori, S., Riedel, D. & Jahn, R. Immunoisolation of GABA-Specific Synaptic Vesicles Defines a Functionally Distinct Subset of Synaptic Vesicles. *J. Neurosci.* **20**, 4904–4911 (2000).
 26. Klemm, R. W. *et al.* Segregation of sphingolipids and sterols during formation of secretory vesicles at the trans-Golgi network. *Journal of Cell Biology* **185**, 601–612 (2009).
 27. Surma, M. A., Klose, C., Klemm, R. W., Ejsing, C. S. & Simons, K. Generic Sorting of Raft Lipids into Secretory Vesicles in Yeast. *Traffic* **12**, 1139–1147 (2011).
 28. Fukuda, K. *et al.* Class III Chitin Synthase ChsB of *Aspergillus nidulans* Localizes at the Sites of Polarized Cell Wall Synthesis and Is Required for Conidial Development. *Eukaryot Cell* **8**, 945–956 (2009).
 29. Kaur, J. & Bachhawat, A. K. A modified Western blot protocol for enhanced sensitivity in the detection of a membrane protein. *Analytical Biochemistry* **384**, 348–349 (2009).
 30. Lionetti, V. PECTOPLATE: the simultaneous phenotyping of pectin methylesterases, pectinases, and oligogalacturonides in plants during biotic stresses. *Front. Plant Sci.* **6**, (2015).

Discussion and perspectives

The different roles of the clathrin adaptor AP-1 in <i>B. cinerea</i>	214
AP-1: a role in polar growth	214
AP-1: a role in cell-wall integrity maintenance	215
AP-1: a virulence determinant involved in the formation of penetration structures and the conventional protein secretion of hydrolytic enzymes ..	215
Are the cargos selected by the AP-1/Clathrin machinery involved in virulence and the establishment of the fungal cell wall?	216
Is the AP-1/Clathrin machinery involved in the biogenesis process of a subset of apical secretory vesicles?	218
What could the pursuit of this work bring to the fungal community, and beyond?	219
References	221

Vesicular trafficking has been under-explored in filamentous fungi: so far, only a few studies focused on the role of secretion mechanisms biology and pathogenicity in fungal plant pathogens. In the lab, we have previously identified that clathrin plays a major role in fungal virulence through the delivery of hydrolytic enzymes and virulence factors in the plant-pathogen *B. cinerea*. Additionally, clathrin seems to be more important to the exocytic process than endocytosis¹. In the yeast *S. cerevisiae*, clathrin is involved in the biogenesis process of secretory vesicles². In the fruit fly *D. melanogaster* and in mouse corticotrope tumor cells, clathrin acts in the formation of secretory granules together with the clathrin adaptor AP-1^{3,4}, a heterotetrameric complex involved in cargo selection and clathrin recruitment. In the protist pathogen *Toxoplasma gondii*, AP-1 mediates the biogenesis of the Rhoptry secretory organelle⁵. Finally, in the filamentous fungus *A. nidulans*, AP-1 is thought to sort secretory vesicles⁶. In this work, we aimed at dressing the role of the clathrin adaptor AP-1 in the development, the virulence, and the biogenesis of secretory vesicles in the plant-pathogen and necrotrophic fungus *B. cinerea*.

The different roles of the clathrin adaptor AP-1 in *B. cinerea*

AP-1: a role in polar growth

AP-1 functions are likely essential in *Botrytis cinerea*: we first tried to delete the gene (*bcap1b*) encoding for the AP-1 complex β -subunit which interacts with clathrin, but no homokaryotic strain could be obtained despite numerous attempts. As a result, we tried another approach and placed the *bcap1b* gene under the control of the nitrate reductase promoter to control *bcap1b* gene expression to create the AP-1 mutant. Repressible conditions were too strong and unsuitable for proper phenotyping. Indeed, we observed extremely retarded growth and near lethal morphological defects when adding the repressor (glutamate) to the culture medium. When we placed the mutant in inducible conditions, we observed that *bcap1b* exhibited a level of expression lower than the native promoter. Thus, we used inducible conditions to down-regulate the expression of *bcap1b*, which sufficed to produce significant phenotypes. In these conditions, the AP-1 mutant displayed hyphal swelling, increase hyphal width and hyperseptation which are characteristics of polar growth defects in filamentous fungi. Interestingly, similar results were also obtained in conditional AP-1 mutants in the filamentous fungus *A. nidulans*⁶. Our results strengthen the idea that AP-1 plays an essential role in polarized growth in filamentous fungi, as proposed by Martzoukou *et al.*, in 2018⁶.

AP-1: a role in cell-wall integrity maintenance

An important observation made during this study is perhaps the function of AP-1 in cell-wall integrity maintenance. Indeed, the AP-1 mutant is hypersensitive to cell-wall stresses such as hyperosmotic shock and cell-wall synthase inhibitors, which demonstrates that AP-1 is involved in cell-wall homeostasis. Interestingly, the clathrin mutant underexpressing the clathrin heavy chain encoding gene also displays similar phenotypes⁷, which suggests that the whole AP-1/Clathrin machinery is involved in cell-wall formation or maintenance. More importantly, AP-1 is required for efficient chitin synthesis, likely via a role in the traffic of the chitin synthase BcCHSIIIa. We confirmed that the BcCHSIIIa localizes at the Spitzenkörper in fast growing hyphae and forms a vesicular crescent in slow growing hyphae in the parental strain B05.10. In contrast, in the AP-1 mutant, BcCHSIIIa does not localize at the hyphal apex but accumulates in small puncta beneath the plasma-membrane in sub-apical regions. Thus, the traffic of the BcCHSIIIa is AP-1 dependent in *B. cinerea*. In *A. nidulans*, BcCHSIIIa ortholog ChsB was also mis-localized in AP-1 mutants⁶ which suggests that the role of AP-1 in the class III chitin synthase traffic might be conserved in filamentous fungi. Based on the prediction of tyrosine motifs in the cytoplasmic tail of BcCHSIIIa, we hypothesize that this protein could be a transmembrane cargo sorted by AP-1 during AP-1/Clathrin vesicles biogenesis. Interestingly, in the yeast *S. cerevisiae*, the class IVa chitin synthase Chs3p is an AP-1 transmembrane cargo⁸. Thus AP-1 might be involved in the sorting of several chitin synthase across the fungal kingdom. The assumption that AP-1 could transport several chitin synthases in the same organism could explain why we observed a severe cell wall defect in the AP-1 mutant. More work is still required to address this possibility. The interactome performed on the HA-tagged BcAPM1:3×HA strain, which aimed at addressing this eventuality, did not provide any information on the sorting of the different chitin synthases in *Botrytis*. However, this approach identified YEA4 a transporter of the chitin substrate uridine diphosphate-N-acetylglucosamine. Thus, AP-1 could be involved in the biogenesis process of chitosomes, which are vesicles involved in chitin synthesis.

AP-1: a virulence determinant involved in the formation of penetration structures and the conventional protein secretion of hydrolytic enzymes

Few studies have focused on the role of AP-1 in infectious strategies developed by eukaryotic pathogens: AP-1 is a virulence determinant in the protists *T. cruzi*⁹, *T. gondii*¹⁰ and *Leishmania*¹¹. To our knowledge, there are currently no study on the putative role of AP-1 in virulence mechanisms adopted by pathogenic fungi. In *B. cinerea*, AP-1 seems to

be involved in the plant-penetration mechanism. Indeed, the AP-1 mutant is unable to penetrate onion epidermis and does not produce infection cushions, the last being important for plant-necrosis and plant-tissue maceration¹². Moreover, the virulence defect observed in the AP-1 mutant could also result from the impaired secretion of hydrolytic enzymes. Indeed, in the protist *T. cruzi*, AP-1 gamma is required for the secretion of the protease cruzipain, a protein involved in nutrition, differentiation, and virulence⁹.

In this study, we have also demonstrated that the clathrin adaptor AP-1 is implicated in the secretion process of many secreted enzymes undergoing the conventional secretory pathway. In the AP-1 mutant, the secretion of proteins associated with protein degradation, plant-cell-wall degradation and oxidoreduction proteins is heavily impaired. Similar results were also obtained in the clathrin mutant¹, which confirms the important role of the AP-1/clathrin machinery in conventional protein secretion of hydrolytic enzymes in *B. cinerea*.

In this work, we have identified the essential role of the AP-1/Clathrin machinery in the maintenance of polar growth, and the establishment of functional cell wall and enzyme secretion in *B. cinerea*. We have also demonstrated, for the first time in a pathogenic fungus, that AP-1 is a virulence determinant. From now on, it would be interesting to determine if these AP-1 functions described in *B. cinerea* are conserved in other filamentous fungi and if they can be extended to other eukaryotic pathogens.

Are the cargos selected by the AP-1/Clathrin machinery involved in virulence and the establishment of the fungal cell wall?

During the biogenesis process of AP-1/Clathrin vesicles, AP-1 selects specific protein cargos. Interestingly, in the secretome of the AP-1 mutant, many hydrolytic enzymes were down-accumulated. Moreover, the localization of the chitin synthase BcCHSIIIa also revealed an AP-1 dependent traffic of the chitin synthase in *B. cinerea*. Therefore, we wanted to identify secreted soluble cargos (potential hydrolytic enzymes) and transmembrane cargos (potential cell-wall synthases and cargo receptors) interacting with AP-1. Interestingly, when we performed immunoprecipitation on the BcAPM1:3×HA strain, we found three putative secreted soluble cargos: the laccase BcLCC2, the protease Bcin08p00280.2, and a protein which function remains to be discovered: Bcin06p06670.1. Each of these proteins were strongly down-accumulated in the AP-1 mutant secretome, (more than a 500-fold). This result strongly suggests that AP-1 could be involved in the

sorting of cargo receptors interacting with these soluble cargos. To confirm this hypothesis, we still need to perform tandem-affinity purification and co-localization experiments. To achieve this, we absolutely need to find a new fluorescent marker other than eGFP or mNeonGreen to be able to complete co-localization experiments successfully. In addition to the identification of soluble cargos, we also wished to identify the transmembrane cargos sorted by AP-1. The interactome did not provide a list of any transmembrane cargos known to interact with AP-1 in other organisms. Surprisingly, the protein Erv25, which, with Emp24 forms the p24 complex involved in secretory cargo sorting at the ER¹³⁻¹⁵, possess a predicted tyrosine motif and is significantly enriched in our dataset. In *N. crassa*, its partner Emp24, is thought to transport proteins in anterograde fashion past the early Golgi¹⁶. Thus, AP-1 could sort Erv25 in *B. cinerea*. We still need to test this hypothesis using co-localization, co-immunoprecipitation, and membrane-based two-hybrid system experiments. If the hypothesis were to be validated, it would open a new and undescribed mechanism of AP-1-dependent cargo selection.

The identification of putative AP-1 cargos using interactomics was an interesting yet frustrating approach: no known AP-1 transmembrane cargos could be identified, possibly due to the use of protein solubilization buffer suboptimal for the solubilization of transmembrane proteins. Another way of identifying AP-1 cargos could be to isolate IVs from the parental strain and clathrin and AP-1 mutants and then perform comparative proteomics to determine which are the protein cargos missing in the vesicles isolated from the AP-1 mutant. To do so, we have explored different strategies to enrich fungal intracellular vesicles (IVs) from the parental strain, and clathrin and AP-1 mutants. We have found that density gradient centrifugation is the best suited technique for IVs enrichment, contrary to EVs isolation where size-exclusion chromatography is considered as the most suitable technique.

The aim was, and still is, to perform comparative proteomics, and compare vesicle protein content of the three strains to identify putative clathrin/AP-1 cargos (i.e., the cargos missing in AP-1 and clathrin vesicles, but present in WT vesicles). The proteomic approach will allow us to identify the cargos missing in IVs originating from clathrin and AP-1 mutants. These outputs will be compared to the secretome in order to correlate the vesicle content with the secretion defect observed in these mutants. Altogether, this will strengthen our understanding of the role of the Clathrin/AP-1 machinery in the sorting of

protein cargos. Hopefully, this work could decipher the roles of AP-1 in the establishment of the fungal cell wall and virulence.

Is the AP-1/Clathrin machinery involved in the biogenesis process of a subset of apical secretory vesicles?

At the fungal apex of fast-growing hyphae, micro- and macro-vesicles accumulate and form the Spitzenkörper¹⁷. Despite being important for hyphal elongation, cell-wall formation, and fungal nutrition via the transport of hydrolytic enzymes, their biogenesis process is still poorly described. As previously mentioned, AP-1 and clathrin are involved in the biogenesis process of vesicles in eukaryotes^{2-4,18}. In *B. cinerea*, hyphal growth, chitin synthesis and the secretion of hydrolytic enzymes rely on the AP-1/Clathrin machinery. Based on these results we assume that both AP-1 and clathrin could be involved in the biogenesis process of SVs accumulating at the Spitzenkörper. More precisely, based on the strong chitin defect observed in the AP-1 mutant, we assume that the AP-1/Clathrin machinery could be involved in the biogenesis of vesicles transporting chitin synthases. If the transport of chitin synthases in *B. cinerea* is similar to the one described in *N. crassa*¹⁹, then AP-1 could be involved in the biogenesis of micro-vesicles (30-50nm diameter). Thus, one way of studying the biogenesis process of apical SVs is to isolate SVs from the parental strain and AP-1 and clathrin mutants. The identification of a loss of a subset of SVs, even partial, could be detected by Nanoparticle Tracking Analysis (NTA) on isolated SVs. Indeed, this technique is used to quantify vesicles subpopulations of different sizes²⁰. We have developed a technique to enrich fungal IVs. However, these IVs likely consist of a mix of SVs and other irrelevant IVs such as COPI and COPII vesicles. Thus, we had to isolate/separate SVs from IVs. To do so, we performed an immunoisolation approach. First, we had to find a transmembrane protein transported by SVs and accumulating at the Spk in *B. cinerea* that could be used as a bait for SVs isolation. As no data was available in the literature for *B. cinerea*, we based our work on the findings of Verdin *et al.* (2009), who demonstrated that chitin synthase and glucan synthase proteins are localized at the Spitzenkörper in *N. crassa*. Therefore, we fused eGFP to chitin synthases belonging to different division BcCHSIIIa (division I) and BcCHSVa (division II) to maximize our chances. We also fused eGFP to BcFKS1, a glucan-synthase which is associated with macro-vesicles in *N. crassa*²¹. Luckily all of them localizes at the Spk, even if BcFKS1-eGFP displays weak and unpredictable fluorescence. Unfortunately, we were unable to detect them by western-blot, likely because of their high molecular weight and hydrophobicity. This limitation seriously hampered the quest for isolating SVs as no

immunocapture procedure could be developed. We assumed that the high molecular weight and the high number of transmembrane domains in these proteins compromised their detection by western blot. Luckily, another *Ph.D.* student, Matthieu Blandenet, who studied polysaccharide synthases in *B. cinerea* during his thesis, found that BcGTa (Bcin04p06040.1 ; 88 kDa), a putative cell-wall synthase, accumulated at the Spk²². This protein being smaller than its counterparts (BcCHSIIIa 101 kDa; BcCHSVa 207 kDa), we were able to detect this protein by western blot. Thus, we have finally identified a potential target for the isolation of a specific subset of SVs.

The recent discovery of a transmembrane protein localized at the Spk and detectable by western-blot will permit the development of immunocapture based method to isolate SVs from enriched IVs. A complementary approach could be to use the v-SNARE BcSnc (Bcin09p02090.1) as bait for SVs immunoisolation (collaboration with Adrien Hamandjian).

Another interesting and challenging experiment would be to perform *in-planta* confocal microscopy on the BcCHSIIIa-eGFP strain to determine if *B. cinerea* produces a Spitzenkörper at hyphal apex during plant infection. To our knowledge, the observation of a Spk during plant-infection has not been reported yet. Infection cushions (ICs) being important secretory organs produced by *B. cinerea* during the infection process¹², it would also be relevant to use electron microscopy to visualize intracellular vesicles in ICs, to capture the establishment of vesicular trafficking during host interactions.

What could the pursuit of this work bring to the fungal community, and beyond?

Despite being of significant importance, the description of the molecular processes underlying secretory cargo selection and fungal secretion remain largely unknown. In this work, we have characterized new mechanisms regarding fungal secretion: we have enlightened several roles of the conventional secretion mechanisms in the biology of *B. cinerea*. From now on, we need to find answers to other important questions: what are the other molecular actors driving conventional protein secretion in *B. cinerea*? Do they impact fungal pathogenicity? If so, then how? What about the unconventional secretory pathway? Is there a link between the AP-1/Clathrin machinery and the production of extracellular vesicles? Answering these questions is paramount to decipher fungal secretion(s).

This work could also contribute to the identification of new and promising antifungal targets. Future antifungals could either target unconserved domains of proteins from the AP-1/Clathrin machinery or specific AP-1 cargos. This could enable the development of species-specific fungicides with reduced ecotoxicological impact than currently used antifungals. It could also lead to the development of antifungal medicines. Deciphering secretion mechanisms in fungi could also drive the development of new genetic tools that could boost the industrial bioproduction of enzymes such as lignocellulose-degrading enzymes which are required for biofuel production²³.

References

1. Souibgui, E. *et al.* Clathrin Is Important for Virulence Factors Delivery in the Necrotrophic Fungus *Botrytis cinerea*. *Front. Plant Sci.* **12**, 668937 (2021).
2. Gurunathan, S., David, D. & Gerst, J. E. Dynamin and clathrin are required for the biogenesis of a distinct class of secretory vesicles in yeast. *EMBO J* **21**, 602–614 (2002).
3. Burgess, J. *et al.* AP-1 and clathrin are essential for secretory granule biogenesis in *Drosophila*. 2094–2105 (2011).
4. Bonnemaïson, M. *et al.* AP-1A Controls Secretory Granule Biogenesis and Trafficking of Membrane Secretory Granule Proteins. *Traffic* **15**, 1099–1121 (2014).
5. Ngô, H. M. *et al.* AP-1 in *Toxoplasma gondii* Mediates Biogenesis of the Rhoptry Secretory Organelle from a Post-Golgi Compartment. *Journal of Biological Chemistry* **278**, 5343–5352 (2003).
6. Martzoukou, O., Diallinas, G. & Amillis, S. Secretory vesicle polar sorting, endosome recycling and cytoskeleton organisation require the AP-1 complex in *Aspergillus nidulans*. **209**, 1121–1138 (2018).
7. Souibgui, E. Rôle de la clathrine dans le processus infectieux du champignon phytopathogène *Botrytis cinerea*. (Université Claude Bernard Lyon 1, 2017).
8. Starr, T. L., Pagant, S., Wang, C.-W. & Schekman, R. Sorting Signals That Mediate Traffic of Chitin Synthase III between the TGN/Endosomes and to the Plasma Membrane in Yeast. *PLoS One* **7**, (2012).
9. Moreira, C. M. do N. *et al.* Knockout of the gamma subunit of the AP-1 adaptor complex in the human parasite *Trypanosoma cruzi* impairs infectivity and differentiation and prevents the maturation and targeting of the major protease cruzipain. *PLoS ONE* **12**, e0179615 (2017).
10. Venugopal, K. *et al.* Dual role of the *Toxoplasma gondii* clathrin adaptor AP1 in the sorting of rhoptry and microneme proteins and in parasite division. *PLoS Pathog* **13**, e1006331 (2017).
11. Vince, J. E. *et al.* Leishmania Adaptor Protein-1 Subunits Are Required for Normal Lysosome Traffic, Flagellum Biogenesis, Lipid Homeostasis, and Adaptation to Temperatures Encountered in the Mammalian Host. *Eukaryotic Cell* **7**, 1256–1267 (2008).
12. Choquer, M. *et al.* The infection cushion of *Botrytis cinerea* : a fungal ‘weapon’ of plant-biomass destruction. *Environ Microbiol* **23**, 2293–2314 (2021).
13. Schimmöller, F. *et al.* The absence of Emp24p, a component of ER-derived COPII-coated vesicles, causes a defect in transport of selected proteins to the Golgi. *The EMBO Journal* **14**, 1329–1339 (1995).
14. Castillon, G. A. *et al.* The yeast p24 complex regulates GPI-anchored protein transport and quality control by monitoring yeast anchor remodeling. *MBoC* **22**, 2924–2936 (2011).
15. Xie, C. *et al.* Early Secretory Pathway-Associated Proteins SsEmp24 and SsErv25 Are Involved in Morphogenesis and Pathogenicity in a Filamentous Phytopathogenic Fungus. *mBio* **12**, e03173-21 (2021).
16. Starr, T. L., Gonçalves, A. P., Meshgin, N. & Glass, N. L. The major cellulases CBH-1 and CBH-2 of *Neurospora crassa* rely on distinct ER cargo adaptors for efficient ER-exit: Fungal cellulase ER cargo adaptors. *Molecular Microbiology* **107**, 229–248 (2018).
17. Riquelme, M., Roberson, R. & Sánchez-León, E. 3 hyphal tip growth in filamentous fungi. in *Growth, Differentiation and Sexuality* vol. 1 47–66 (Wendland J., 2016).
18. Borgonovo, B., Ouwendijk, J. & Solimena, M. Biogenesis of secretory granules. *Current Opinion in Cell Biology* **18**, 365–370 (2006).
19. Verdin, J., Bartnicki-Garcia, S. & Riquelme, M. Functional stratification of the Spitzenkörper of *Neurospora crassa*. *Molecular Microbiology* **74**, 1044–1053 (2009).
20. Bachurski, D. *et al.* Extracellular vesicle measurements with nanoparticle tracking analysis – An accuracy and repeatability comparison between NanoSight NS300 and ZetaView. *Journal of Extracellular Vesicles* **8**, 1596016 (2019).
21. Sánchez-León, E. & Riquelme, M. Live imaging of b-1,3-glucan synthase FKS-1 in *Neurospora crassa* hyphae. *Fungal Genetics and Biology* **82**, 104–107 (2015).

22. Blandenet, M. Développement d'un outil génétique pour la création de collections de mutants : application à l'étude de la paroi fongique chez *Botrytis cinerea*. (Université Claude Bernard Lyon 1, 2022).
23. Cairns, T. C., Zheng, X., Zheng, P., Sun, J. & Meyer, V. Turning Inside Out: Filamentous Fungal Secretion and Its Applications in Biotechnology, Agriculture, and the Clinic. *JoF* 7, 535 (2021).

Appendix

Table 1 – Conservation of the proteins involved in the biogenesis of clathrin-coated vesicles in *B. cinerea*

Modified from: SOUIBGUI, Rôle de la clathrine dans le processus infectieux du champignon phytopathogène *Botrytis cinerea*. Thèse Microbiologie. Lyon : UCBL1, 2017, 198 p.

<i>H. sapiens</i>	<i>S. cerevisiae</i>	PFAM Domain	<i>B. cinerea</i> protein
Clathrin (heavy chain)	Chc1	Clathrin_propel (PF01394) Clathrin-link (PF09268) Clathrin_H_link (PF13838) Clathrin (PF00637)	Bcin01g09940.1
	Cle1		
FCHO 1	Syp1	F-BAR (PF00611) Muniscin (PF10291)	Bcin15g04120.1
FCHO 2	-		-
EPS15	Ede1	EH (PF12763)	Bcin02g00910.1
EPS15	Pan1	EH (PF12763)	Bcin05g00930.1
EPS15	End3	EH (PF12763)	Bcin07g03670.1
Epsin 1	Ent1	ENTH (PF01417) UIM (PS50330)	Bcin03g04970.1
Epsin 2	Ent2	ENTH (PF01417) UIM (PS50330)	-
Epsin 3	Ent3	EH (PF12763)	Bcin05g06330.1
Epsin 4	Ent4	ENTH (PF01417)	-
-	Ent5	ANTH (PF07651)	-
Intersectin	-	EH (PF12763) SH3 (PF00018) RHOGEF PH C2	-
CIN85	Sla1	SH3 (PF00018) SHD1 (PF03983)	Bcin02g00850.1
WASP	Las17	WH1 (PF00568) WH2 (PF02205)	Bcin09g06240.1
AP-2 alpa	Apl3	Adaptin_N (PF01602) Alpha_adaptinC2 (PF02883)	Bcin05g03640.1
AP-2 beta 2	Apl1	Adaptin_N (PF01602)	Bcin12g02640.1
AP-2 mu 2	Apm4	Adap_mu (PF00928)	Bcin10g01540.1
AP-2 sigma 2	Aps2	Clat_adaptor_s (PF01217)	Bcin07g03160.1
AP-1 gamma	Apl4	Adaptin_N (PF01602) Alpha_adaptinC2 (PF02883)	Bcin10g05770.1
AP-1 beta1	Apl2	Adaptin_N (PF01602)	Bcin02g08180.1

AP-1 sigma1	Aps1	Clat_adaptor_s (PF01217)	Bcin14g01930.1
AP-1 mu1	Apm1	Clat_adaptor_s (PF01217) Adap_mu (PF00928)	Bcin04g03770.1
AP-3 delta	Apl5	Adaptin_N (PF01602)	Bcin07g00490.1
AP-3 beta3	Apl6	Adaptin_N (PF01602)	Bcin12g04150.1
AP-3 sigma3	Aps3	Clat_adaptor_s (PF01217)	Bcin04g05240.1
AP-3 mu3	Apm3	Adap_mu (PF00928)	Bcin04g05740.1
GGA1	GGA1	VHS (PF00790) GAT (PF03127) Alpha_adaptinC2 (PF02883)	Bcin02g09160.1
GGA2	GGA2	VHS (PF00790) GAT (PF03127) Alpha_adaptinC2 (PF02883)	-
GGA3			-
Stonin	-	Adap_mu (PF00928)	-
NECAP	-	PH	-
HIP1	Sla2	ANTH (PF07651)	Bcin01g02160.1
AP180	YAP1801	ANTH (PF07651)	Bcin01g08430.1
DAB2	-	PTB (PF08416)	-
ARH	-	PTB (PF08416)	-
Numb	-	PTB (PF08416)	-
HRB	Gcs1	ArgGAP (PF01412)	Bcin06g01850.1
β -arrestin	-	Arrestin_N (PF00339) Arrestin_C (PF02752)	-
Amphiphysine	rvs167	N-BAR (PF03114) SH3 (PF00018)	Bcin14g02730.1
SNX9	SNX4	SH3 PX BAR	-
Dynamine		Dynamamin N Dynamamin M PH GED	Bcin02g02630.1
Auxiline	SWA2	PTEN DNAJ	Bcin02g01030.1

Table 2 – Proteins containing the clathrin box consensus sequence in *B. cinerea*

Modified from: SOUIBGUI, Rôle de la clathrine dans le processus infectieux du champignon phytopathogène *Botrytis cinerea*. Thèse Microbiologie. Lyon : UCBL1, 2017, 198 p.

Cellular localisation	<i>H. sapiens</i> protein	<i>S. cerevisiae</i> protein	<i>B. cinerea</i> protein	Clathrin box (<i>B. cinerea</i> protein)
Plasma membrane	AP-2 beta	Apl1	Bcin12g02640.1	-
	AP180	YAP1801	Bcin01g02160.1	-
			Bcin01g08430.1	-
	Epsine	Ent1/2	Bcin03g04970.1	-
Golgi apparatus and endosomes	AP-1 beta	Apl2	Bcin02g08180.1	LLDID 629-633
	GGA1	GGA1	Bcin02g09160.1	LVLLD 83-87
				LIDFD 352-356
	Epsin	Ent3/5	Bcin05g06330.1	LFSFD 292-296
Plasma membrane Golgi apparatus	AP-3 beta	Apl6	Bcin10g01540.1	-
	Amphiphysin	Rvs167	Bcin14g02730.1	LFTLE 208-212



FOLIO ADMINISTRATIF

THESE DE L'INSA LYON, MEMBRE DE L'UNIVERSITE DE LYON

NOM : CALVAR

DATE de SOUTENANCE : 14/12/2022

Prénoms : Glen John

TITRE : Role of the clathrin adaptor AP-1 in the virulence and the biogenesis process of secretory vesicles in the plant-pathogenic fungus *Botrytis cinerea*

NATURE : Doctorat

Numéro d'ordre : 2022ISAL0113

Ecole doctorale : E2M2 - Evolution, Ecosystèmes, Microbiologie, Modélisation

Spécialité : Microbiologie

RESUME :

Plant pathogenic fungi represent an increasing threat to global food security which is increased by climate change. Understanding the mechanisms of pathogenesis is therefore essential to limit the development of fungal diseases in plants. The virulence of these fungi is largely based on the secretion of various proteins capable of degrading the host plant's constituents. Before being released into the extracellular environment, these proteins pass through the endoplasmic reticulum, the Golgi apparatus and sometimes the endosome, and are transported from one cellular compartment to another in intracellular vesicles. Today, the mechanisms of secretion, and more particularly of the biogenesis of these vesicles, are very little studied in fungi, despite being essential for the comprehension of pathogenesis. To better understand these mechanisms, we have created an under-expression mutant of a gene encoding for a subunit of the clathrin adaptor AP-1 in the necrotrophic fungus *Botrytis cinerea*. This adaptor is involved in the biogenesis of secretory granules in *Drosophila* and humans. Characterization of the AP-1 mutant revealed that the complex was involved in polarized growth, fungal cell-wall synthesis, and the secretion of hydrolytic enzymes essential for fungal nutrition and virulence. To better understand the putative role of this adaptor in vesicle biogenesis, we also undertook the enrichment of intracellular vesicles, and we propose a strategy to isolate secretory vesicles. Our study shows for the first time the importance of the clathrin adaptor AP-1 in secretion mechanisms in a plant pathogenic fungus.

MOTS-CLÉS : Vesicular trafficking, Secretion, vesicles, Adaptor-protein 1, AP-1, clathrin, virulence, *Botrytis cinerea*

Laboratoire de recherche : Microbiology, Adaptation and Pathogenesis (MAP)

Directeur de thèse : POUSSEREAU Nathalie

Co-directeur de thèse : RAHBE Yvan

Président de jury : Le Borgne Roland

Directeur de Recherche

CNRS

Composition du jury :

Godiard Laurence

Hahn Matthias

Le Borgne Roland

Zaidman-Rémy Anna

Poussereau Nathalie

Rahbé Yvan

Chargé de Recherche HDR

Professeur des Universités

Directeur de Recherche

Maître de Conférences HDR

Maître de Conférences HDR

Directeur de Recherche

INRAe

TUK

CNRS

INSA Lyon

UCBL1

INRAe

Rapporteuse

Rapporteur

Rapporteur

Examinatrice

Directrice de thèse

Co-directeur de thèse